VNIVERSITAT ⅅ VALÈNCIA

Facultad de Química

Instituto de Ciencia Molecular

Programa de Doctorado en Nanociencia y Nanotecnología

Magnetostructural characterization of compounds based on the highly anisotropic Mn(III) and Re(IV) metal ions

Tesis Doctoral

Carlos Alberto Rojas Dotti

Noviembre de 2019

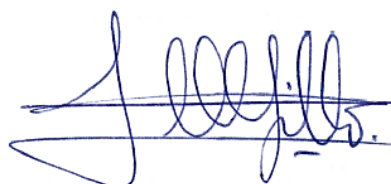Dirigida por los Dres. Francisco Lloret Pastor y Francisco José Martínez Lillo

Francisco Lloret Pastor, Doctor en Química, Catedrático de la Universidad de Valencia, Francisco José Martínez Lillo, Doctor en Química, miembros ellos del Instituto de Ciencia Molecular (ICMol) y del Departamento de Química Inorgánica de la Facultad de Química de la Universidad de Valencia,

CERTIFICAN:

Que el trabajo que presenta Don. Carlos Alberto Rojas Dotti en esta Memoria titulada *"Magnetostructural characterization of compounds based on the highly anisotropic Mn(III) and Re(IV) metal ions"*, en el marco del Programa de Doctorado de Nanociencia y Nanotecnología, ha sido realizado bajo nuestra dirección en el Instituto de Ciencia Molecular y el Departamento de Química Inorgánica de la Universidad de Valencia para optar al título de Doctor en Nanociencia y Nanotecnología. Y para que así conste, firmamos el presente certificado en Paterna a 7 de noviembre de 2019.

Prof. Francisco Lloret Pastor
Director

Dr. Francisco José Martínez Lillo
Director y Tutor

A las dos personas a las que me debo, a mi padre y a mi hermano.

Agradecimientos/Acknowledgments

Pienso en el pibe que hace más de ocho años se aventuraba de su micro-mundo de pueblo lejano y polvareda a Montevideo, que por entonces le era abrumadora y ajena. Pienso en él y en sus cavilaciones imposibles, en sus indecisiones infinitas y en cómo ha llegado hasta aquí, hasta este hoy, hasta este presente alguna vez quimérico que se hace plausible ahora, en este puñado de hojas bien zurcidas. Pienso, y no hace falta mucho pensar para saber que nada de esto hubiera sido posible sin este mar de gente al que le debo tanto y que me acompaña, me sigue acompañando en este derrotero de la academia y de los días.

Siendo que la hora es propicia y el momento es oportuno, he de agradecer, y si he de agradecer no he de comenzar por otra persona que no sea Paco. Y al decir Paco digo también Miguel. Me refiero a esa entidad única e indivisible que han conformado y han sabido sostener a lo largo de los años, que ha sobrevivido a esta jungla confusa de una sociedad que, en cuanto a las relaciones humanas se refiere, todo lo destruye; posiblemente esto sea lo que los vuelve aún más admirables, este algo que, sin la humildad y el tesón que los caracteriza, jamás podrían haber conseguido. A ustedes dos les estaré siempre agradecido; y en mí les agradezco también por cada pasante de un mes, de seis meses, estudiantes de master y doctorado, cada joven de tierras lejanas que han recibido con los brazos abiertos, con la mayor disposición y entrega, como iguales; gracias por las oportunidades que nos han brindado, por haber allanado el camino de nuestro crecimiento y aprendizaje, gracias.

Debo agradecerles, por supuesto, todo lo que me han enseñado, su entera disposición para resolver mis dudas en cuanto se las he planteado y para volcar, generosos en todo, ese caudal inconmensurable de conocimiento que poseen, no solo hacia mi persona, sino hacia cada uno de sus estudiantes. Miguel, siempre atesoraré nuestras charlas de pasillo, café – o esa cosa que nos escupe la máquina de *Delikia* – en mano, discurriendo entre filosofía, política, sátira y liso y llano humor de barrio, sin descuidar el arte, por supuesto; por ello escribo estas líneas escuchando *La Comparsita*; nada que me recuerde más a ti y a Paco que un buen Tango. Y por eso ahora es *Mi Buenos Aires Querido*, para decirte, Paco, que así mismo vivirán en mi memoria tus inigualables disertaciones en la sobremesa de algún bar, de los nitratos y las anécdotas a tu propia filosofía y unas palabras que jamás olvidaré "… me da igual cuanto publicas, si publicas. La gente se afana, y lo importante no es eso. Lo que importa, y lo que a fin de cuentas te quedará cuando todo haya pasado, es lo que has vivido, cómo lo has vivido, y sobre todo, las personas con las que has llegado a compartir."

Si he de seguir agradeciendo, he de seguir indiscutiblemente por José. Recuerdo nuestro primer contacto, vía e-mail, por allá por el 2014. Lejos estaba en aquel momento de imaginar que acabaría trabajando contigo, codo a codo, aquí en Valencia. Aquella primera comunicación que tuvimos resultó de enorme motivación para mí y ese

entusiasmo siguió alimentándome a lo largo de estos años. Por ello gracias, porque sin motivación no somos nada. Agradezco también todo el tiempo que hemos compartido en el laboratorio, instancia que ha resultado sumamente enriquecedora para mí como estudiante, como químico, y como persona. Eres una fuente inagotable de ideas innovadoras. Brindo por ello y por tu carrera como Profesor, a la que sin duda le aguarda un futuro por demás prometedor. Por último, no puedo dejar de agradecerte especialmente la dedicación y sobre todo la paciencia que has puesto en la corrección, versión tras versión, de esta Tesis. Toda esa labor dedicada en estos tiempos tan ajetreados es invaluable. Esta también ha sido una etapa muy importante de aprendizaje para mí.

Gracias de nuevo a los tres, Paco, Miguel y José, por su generosidad, porque en los momentos más difíciles ha sido encomiable.

Rafa, debería de agradecerte por las ideas brillantes que has aportado a lo largo de esta Tesis ¡que vaya si lo han sido! Y a vos, Nico, la paciencia admirable que has tenido y tienes para llevar a cabo las medidas de SQUID, los pedidos, etc., conciliando las exigencias de medio mundo de modo tal que siempre logras satisfacer, más o menos, un poco a todos. Debería agradecerles todo eso, pero no, par de gandules, que para eso les pagan a fin de cuentas. Lo que sin dudas he de agradecer es habérmelos encontrado, porque, reivindicando a esta jungla de la academia, a veces también nos pone de frente con personas inolvidables, de esas por las que vale la pena haber estado en algún sitio, haberse detenido a tomar un café – o un quinto, que si no Nico ni se asoma –. Gracias por alegrar tantas mañanas con esos 'almuerzos' de conversaciones surrealistas entre pinchos de patata, donde poco importa el tema del cual se habla y los hilos conductores no exigen dirección o no conducen a ninguna parte, donde no hay lugar para la memoria a corto plazo, donde cada uno es uno mismo y la risa es la ideología imperante, gracias. De hecho este es buen momento para recordar a Joan, verdadera inspiración para los jueves de Básquet. Sin dudas nuestro mentor en lo referente al deporte de la canasta. Gracias por tus consejos y sentido del humor. Perdón por haberte lesionado de por vida.

Si es por seguir un orden en este absurdo intento de no olvidarme de nadie, he de seguir por mis colegas del *labo*. Primero que nadie Marta, porque has sido una compañera inolvidable, en el trabajo y en la vida, te estaré siempre agradecido y ocuparás un lugar especial en mi memoria. Todo lo demás ya te lo he dicho en persona. Renato, a pesar de ser tan *deselegante*, sé que te caigo bien, por algo juntos hemos sido los orgullosos cofundadores del fracaso más grande de nuestro tiempo, el *Burja-Team.* Siempre habrá un *Pizza & Birra* en alguna esquina para nosotros. Salud por ustedes, dúo fantástico, los quiero. Perucho, bueno debería decir Adrián, pero tú eres Perucho. Te dejo aquí, en el ICMol, como el nuevo experto del renio. Sé que cumplirás con ese rol mucho mejor de lo que yo lo he hecho. Prometo que la próxima vez te haré llegar esos alfajores de cartón, que digo, de galleta de arroz, para celíacos, que no serán los originales, pero también son una delicia – tú créetelo –. Cuídate, chaval, que eres único.

Y a todos los demás que han ido pasando durante este tiempo y sin dudas han sido importantes para mí, tanto en el *labo* como fuera de él. A Lumi, siempre presta para los consejos, a la maravillosa locura de María, reina de las ardillas, a Thais, por nuestras catarsis de diván, a Lucía, la mejor uruguaya de todo el Instituto, recordaré siempre esas charlas al sol, de café y sobremesa en tiempos difíciles. A ustedes, gracias.

También he de dedicar unas líneas a mis amigos y colegas de Uruguay, que siempre han estado ahí cuando he necesitado retornar al paisito para recobrar fuerzas, para ganar impulso, para seguir. Gracias a Nati y Clau, siempre al firme para escucharme, darme hospedaje y consejo y hasta una mano con los interminables trámites, *¡uno para todos y todos para uno!* A Mari y Andrés, por haberme adoptado desde el principio y haberme recibido siempre con la calidez que los caracteriza. A Paula y Diego, y Santiago, amigos entrañables que también me abrieron las puertas de sus casas – sí, me he recorrido Montevideo de casa en casa –. Y más, a Marcos – se me olvidaba que también pase una noche en tu ratonera, gracias –, Gonza, Seba, Ezequiel, que sin tu demencia no me hubiera atrevido a meterme en Inorgánica, Cami, que sin tu demencia ni siquiera hubiera estudiado Inorgánica, Fati, Irma y a los que estoy olvidando, no se ofendan, ya me conocen. A todos ustedes, nos vemos a la vuelta.

Quiero mencionar a dos personas que me quedan fuera de toda posible clasificación, amigos, pero que son de acá y no estrictamente del Labo: Maricarmen, Héctor, son los seres más bonicos que me llevo de aquí. Los quiero.

A mi familia por el apoyo incondicional y por haberme motivado siempre a ir hacia delante, a soñar y a volar. Viejo querido, papá, vuelvo pronto. *Elvi*, hermano ¡la que nos espera! Mamá, fuiste la razón de todo, gracias por haber estado de la manera que lo hiciste mientras te fue posible; te amaré toda la vida.

Por último he de agradecer al hombre sin el cual no estaría aquí, a quien me impulsó, me motivó y veló por mí como pocos durante estos años. A un tipo común, sencillo, callado, casi Onettiano pero más feliz, que prefiere pasar desapercibido y que seguro preferiría que no lo nombrase pero tarde piaste. Tanta distancia y tantos reencuentros, incluso alguna que otra aventura germánica que supimos correr juntos nos han acercado todavía más, y eso me alegra porque nos une, porque significa que esta camaradería, esta suerte de amistad que trasciende el vínculo académico de padre-hijo, perdurará más allá de las fronteras y de las universidades. Por todo y ante todo, gracias Ricardo.

*"Quien se sienta a la orilla de las cosas
resplandece de cosas sin orillas."*

Verano, Ida Vitale

Index

Resumen/Abstract

El presente trabajo de tesis doctoral se recoge en el formato de "compendio de artículos" de acuerdo con el reglamento de depósito, evaluación y defensa de la tesis doctoral de la Universidad de Valencia, ACCUV 266/2011. En cumplimiento de dicha reglamentación, en esta sección se expone un resumen global de la temática, resultados y conclusiones extraídas de los mismos.

El trabajo desarrollado en el marco de esta tesis se encuentra comprendido en el campo del Magnetismo Molecular y la Química de Coordinación. El Magnetismo Molecular ha sido un área de sostenido interés durante los últimos 30 años. La convergencia de múltiples disciplinas, desde la Química y la Física hasta la Biología, ha llevado a un progreso rápido y destacado en esta área debido a la complementariedad, tanto de las técnicas experimentales utilizadas, como de los conocimientos implicados. El objetivo de poder controlar factores como las interacciones y la anisotropía magnéticas ha propiciado la obtención de especies capaces de presentar un mejor desempeño magnético con miras a potenciales futuras aplicaciones tecnológicas en espintrónica y computación cuántica y molecular.

La investigación desarrollada en esta Tesis Doctoral se ha centrado en la caracterización estructural y estudio de propiedades magnéticas de sistemas basados en los iones metálicos Mn(III) y Re(IV). El primero es un ion 3d mientras que el último es un ion metálico 5d. Estos iones metálicos han sido seleccionados a cuenta de que, dados los altos valores de anisotropía y espín que presentan, pueden brindar resultados destacables desde el punto de vista del Magnetismo Molecular.

El estudio, tanto de complejos mononucleares como polinucleares discretos o extendidos en una, dos o tres dimensiones, se ha centrado fundamentalmente en los iones metálicos de la primera serie de transición (metales 3d) y lantánidos (metales 4f). Sin embargo, los iones metálicos de la segunda y tercera series de transición (metales 4d y 5d, respectivamente) se han investigado y desarrollado mucho menos.

La experiencia previa de nuestro grupo, respaldada por decenas de publicaciones destacadas, relacionada con la Química de Coordinación del Re(IV) y el estudio de las propiedades magnéticas de sus compuestos, ha permitido el desarrollo exitoso de los objetivos planteados. Asimismo, ha sido amplia la contribución previa que este equipo ha hecho a la descripción y el entendimiento de los sistemas de moléculas imán conocidos como [Mn_6]s. Entre ellos destacan nada menos que la estructura del primer [Mn_6] reportada en la literatura y un estudio exhaustivo de la correlación magnetostructural de sus propiedades. Todo ello ha sido fundamental para el desarrollo adecuado y la posterior publicación de cada uno de los trabajos presentados en esta Tesis.

Resumen

En este contexto, los principales objetivos de esta Tesis se componen de dos partes:

Centrándonos en los complejos basados en Mn(III), se ha buscado ampliar el conocimiento, mejorar las propiedades y funcionalizar sistemas pertenecientes a la familia de los [Mn$_6$]s. Estos sistemas constituyen una de las familias más sistemáticamente estudiada de imanes moleculares, hecho que hace de los [Mn$_6$]s candidatos prometedores para estudiar su posible funcionalización y aplicación en campos como la espintrónica molecular y la electrónica molecular. Por ello, uno de los principales objetivos de esta Tesis ha sido funcionalizar y posteriormente intentar conectar estas moléculas a nanodispositivos electrónicos.

Por otra parte, a pesar de la cantidad de estructuras de sistemas del tipo [Mn$_6$] reportados, es muy reducido el número de especies catiónicas descritas en la literatura. En consecuencia, hemos considerado que es necesario desarrollar nuevas especies tanto neutras como catiónicas de [Mn$_6$], dado que al incluir nuevos ligandos o contraiones aniónicos se pueden introducir a estos sistemas funcionalidades complementarias, pudiendo obtener así nuevos compuestos multifuncionales.

El otro apartado de la investigación ha sido dedicado a la obtención y el estudio de sistemas basados en Re(IV), con el objetivo de contribuir a una mejor comprensión de los fenómenos de canje magnético, así como para tratar de aproximar estos sistemas a nuevas posibles aplicaciones.

Dada la alta anisotropía magnética que exhibe el ion Re(IV), se esperaba observar resultados interesantes como los revelados previamente por sistemas como el tetranuclear [Ni{ReCl$_4$(ox)}$_3$]$^{4-}$ y los mononucleares [ReX$_4$(ox)]$^{2-}$ (X = Cl, Br), todos ellos complejos aniónicos, el primero siendo un *Single Molecule Magnet* (SMM) y los otros *Single Ion Magnets* (SIMs). En este contexto, con el diseño de sistemas donde las especies mononucleares Re(IV) puedan ser consideradas magnéticamente aisladas, hemos buscado estudiar y ajustar los principales parámetros que definen sus propiedades magnéticas. Para mantener aislados los complejos en estado sólido, se utilizó específicamente un ion inorgánico magnéticamente inactivo como lo es el Zn(II), un ion d^{10}. Además, también se han utilizado otros cationes de diferente naturaleza, diamagnéticos y paramagnéticos, con el objetivo de introducir algunas posibles funciones y modificaciones en las propiedades magnéticas de estos sistemas de interés.

Basándonos en la amplia experiencia de nuestro grupo en esta área de investigación, hemos diseñado y llevado a cabo una metodología de trabajo adecuada, la cual nos ha permitido alcanzar exitosamente los objetivos antes planteados.

Esta metodología, como todo el cuerpo de esta memoria, ha estado conformada por dos ejes fundamentales. Esto es, la síntesis y caracterización de:

1. Sistemas pertenecientes a la familia de los [Mn$_6$]
2. Sistemas basados en el ion Re(IV)

Ambas líneas de trabajo se diferencian fundamentalmente en la etapa de síntesis de los compuestos. Una vez sintetizados los mismos se ha realizado una caracterización primaria mediante espectroscopia infrarroja, análisis elemental de elementos livianos y análisis de emisión de rayos–X mediante microscopía electrónica de barrido. Seguidamente se ha procedido a la caracterización estructural mediante difracción de rayos–X sobre monocristal y, por último, a la determinación de las propiedades magnéticas mediante magnetometría SQUID sobre muestras microcristalinas de los compuestos obtenidos. Una vez obtenida la información estructural y magnética de los sistemas, se ha procedido con el análisis magneto-estructural de los mismos.

En lo que se refiere a la síntesis de los compuestos de la familia de los [Mn$_6$], se han seguido los procedimientos habituales previamente reportados. En primer lugar se ha sintetizado *in situ* el complejo [Mn$_6$] a partir de una sal simple de Mn(II) y salicilamidoxima empleando trietilamina como base. Para ello se ha utilizado etanol como disolvente en todos los casos, a excepción del derivado obtenido empleando dmf (N-N'dimetilformamida) donde el solvente empleado ha sido la propia dimetilformamida. Una vez se ha obtenido el complejo preformado, se han agregado a la mezcla de reacción los nuevos agentes previamente seleccionados para llevar a cabo las diferentes modificaciones estructurales sobre el compuesto (diferentes contraiones, ligandos tipo azoles y ligandos funcionalizados con grupos tioéster respectivamente). Finalmente, en los casos en que ha sido necesario, se ha procedido a la recristalización de los compuestos mediante difusión directa. Para ello se han empleado, según el caso, disolventes como etanol, acetona, dmf y éter.

Por su parte, el trabajo sobre compuestos basados en Re(IV) ha implicado una gama más amplia de desafíos desde el punto de vista sintético. En los trabajos dirigidos exclusivamente al estudio magneto-estructural de los compuestos basados en Re(IV), se parte del precursor mononuclear de Re(IV) preformado {sea este [ReX$_6$]$^{2-}$ o [ReX$_4$(ox)]$^{2-}$ (X = Cl, Br)}, sintetizado según el procedimiento reportado en la literatura.

Aquellos trabajos dedicados al estudio de las propiedades magnéticas de las especies mononucleares [ReX$_6$]$^{2-}$ han implicado procedimientos de metátesis, donde se ha llevado a cabo el intercambio de cationes de una sal apropiada (de potasio o tetrabutilamonio, según el caso específico) del anión, por los cationes de interés, en el medio adecuado (solventes acuosos como los ácidos HX u orgánicos como la dmf). Por su parte, en los trabajos dedicados a especies heteropolinucleares, la síntesis se ha realizado en mezclas apropiadas de solventes orgánicos (isoporpanol, acetonitrilo, nitrometano) mediante la mezcla directa de los correspondientes precursores [ReX$_4$(ox)]$^{2-}$ con sales simples de los iones metálicos 3D [sólo en el trabajo basado en Re(IV) y Cu(II) se han empleado ligandos auxiliares, añadidos en forma directa sobre la mezcla de reacción]. La cristalización de las especies involucradas se ha completado mediante evaporación lenta del disolvente.

Resumen

Finalmente, el trabajo dedicado a la exploración de una nueva ruta de síntesis de especies mononucleares basadas en Re(IV) ha implicado la utilización del precursor $[ReCl_4(MeCN)_2]$ como compuesto de partida. La estrategia de síntesis ha consistido en la sustitución directa de las moléculas de acetonitrilo por diferentes disolventes [dmf y dma (N,N'dimetilacetamida)]. Para ello se ha disuelto el precursor en el disolvente que se desea emplear para la sustitución, se ha procedido al calentamiento de la mezcla y se han probado diferentes tiempos de reacción. La cristalización de los compuestos se ha llevado a cabo mediante difusión directa de éter sobre la mezcla de reacción.

De este modo, la presente tesis se estructura en tres secciones diferentes. La primera de ellas es una sección introductoria, la Sección 0. Allí se expone una breve revisión histórica sobre el Magnetismo Molecular, desde los orígenes mismos de la noción de magnetismo hasta la consolidación de la disciplina. A continuación, se presentan los conceptos de SMM y SIM, donde se ejemplifican los trabajos más relevantes en el desarrollo de este campo, así como aquellos sistemas destacables relacionados directamente con la investigación de esta Tesis. Seguidamente, se presentan los conceptos básicos relacionados con el Magnetismo Molecular, fundamentales para el entendimiento de la materia, tales como magnetización, susceptibilidad magnética, tiempos de relajación, etc. Finalmente se lleva a cabo el desarrollo del tratamiento y la interpretación de los datos obtenidos de las medidas magnéticas aplicando un campo oscilante, comúnmente conocidas como medidas AC (por sus siglas en inglés Alternating Current). Estas medidas son especialmente importantes en lo referente a la caracterización de sistemas que presentan señales fuera de fase, tales como los SMMs o SIMs.

En la segunda sección, Sección A, se introduce brevemente la familia de complejos hexanucleares conocidos comúnmente como [Mn$_6$]s. Estas especies, basadas en el ion metálico Mn(III) y diferentes tipos de oximas y sus derivados, han sido extensamente estudiadas, presentando todas ellas comportamiento de tipo SMM. Aquí se realiza un breve recorrido histórico destacando los resultados más relevantes obtenidos en este contexto.

De las especies de [Mn$_6$] reportadas hasta el momento, la mayoría componen el grupo de compuestos de naturaleza aniónica o neutra. Teniendo en cuenta este hecho, una de las finalidades del trabajo de esta Tesis ha sido la síntesis y caracterización, estructural y magnética, de nuevas especies catiónicas. Esto en el entendido de enriquecer el conocimiento ya existente en lo que se refiere a los sistemas pertenecientes a esta familia.

Así, en el trabajo titulado "*Ferromagnetic Oxime-Based Manganese(III) Single-Molecule Magnets with Dimethylformamide and Pyridine as Terminal Ligands*", dos nuevos miembros de la familia de [Mn$_6$] SMMs de fórmulas $[Mn_6(\mu_3\text{-}O)_2(H_2N\text{-}sao)_6(dmf)_8](ClO_4)_2$

y $[Mn_6(\mu_3\text{-}O)_2(H_2N\text{-}sao)_6(py)_6(EtOH)_2][ReO_4]_2\cdot 4EtOH$, (dmf = N,N'-dimetilformamida, py = piridina, $H_2N\text{-}saoH_2$ = salicilamidoxima) han sido sintetizados y caracterizados estructural y magnéticamente. Ambos compuestos fueron directamente preparados a partir de la desprotonación del ligando $H_2N\text{-}saoH_2$ en presencia de la sal deseada de manganeso y el disolvente coordinante adecuado (dmf y py, respectivamente). El compuesto conteniendo dmf cristaliza en el sistema triclínico con grupo espacial $P\bar{1}$, mientras que el análogo de py cristaliza en el sistema monoclínico con el grupo espacial $P2_1/n$. En el empaquetamiento cristalino de estos compuestos, los aniones $(ClO_4)^-$ y $[ReO_4]^-$ se encuentran entre las unidades catiónicas $[Mn_6]^{2+}$, que están unidas por enlace de hidrógeno a los grupos $-NH_2$ de los ligandos salicilamidoxima. El estudio de las propiedades magnéticas reveló acoplamiento ferromagnético entre los iones metálicos Mn(III) y la aparición de relajación lenta de la magnetización, característica típica del comportamiento de SMM. La naturaleza catiónica de estas especies $[Mn_6]^{2+}$ sugiere que podrían usarse como bloques de construcción adecuados para preparar nuevos materiales magnéticos que exhiban funcionalidades adicionales. Además, la especie conteniendo dmf como ligando terminal presenta el valor de barrera de energía más alto reportado hasta el momento para un compuesto catiónico de la familia de los $[Mn_6]$s.

Sin embargo, no sólo se ha explorado la síntesis y caracterización de nuevos sistemas catiónicos, sino que además se ha buscado profundizar en la obtención y el estudio de compuestos neutros en los cuales pudiesen coexistir funcionalidades complementarias, tales como SMMs que resulten adecuados para estudios de espintrónica y electrónica molecular. Para ello, los sistemas neutros resultan particularmente apropiados ya que se trata de uno de los grupos de especies más estudiadas dentro de la familia de los $[Mn_6]$s.

De este modo, en el trabajo titulado *"Hexanuclear manganese(III) single-molecule magnets based on oxime and azole-type ligands"*, y publicado en un número especial con motivo del 65° aniversario del Prof. Miguel Julve, se han reportado dos nuevos complejos hexanucleares de manganeso (III) de fórmulas $[Mn_6(\mu_3\text{-}O)_2(H_2N\text{-}sao)_6(bta)_2(EtOH)_6]\cdot 2EtOH\cdot 4H_2O$ y $[Mn_6(\mu_3\text{-}O)_2(H_2Nsao)_6(pta)_2(EtOH)_6]\cdot 4EtOH$ (bta = anión 1,2,3-benzotriazolato, pta = anión 5-fenil-tetrazolato), los cuales se han sintetizado y caracterizado estructural y magnéticamente. Ambos compuestos cristalizan en el sistema triclínico con el grupo espacial $P\bar{1}$. En el empaquetamiento cristalino, los complejos adyacentes de $[Mn_6]$ están conectados a través de moléculas de disolvente no coordinantes, que a su vez están unidos mediante enlaces de hidrógeno a átomos de N de los anillos de azol y los grupos $-NH_2$ del ligando salicilamidoxima. El estudio de las propiedades magnéticas, a través de mediciones de susceptibilidad magnética, revelan como interacción predominante un acoplamiento antiferromagnético entre los iones metálicos Mn(III) en ambos compuestos. Las medidas de magnetización a temperatura y campo variable confirmaron la existencia de un estado fundamental de espín de S = 4

para ambos compuestos. Asimismo, la presencia de relajación lenta de la magnetización en ambos indica que es compatible con el comportamiento de SMM.

Finalmente, el trabajo más destacado de la sección dedicada a los sistemas de Mn(III) implicó la funcionalización de sistemas conocidos de [Mn$_6$] con ligandos del tipo tioésteres, proyectando la posibilidad a futuro de su estudio de aplicación a *junction devices*. Este trabajo ha consistido en el diseño y la caracterización estructural y magnética de dichos compuestos. Los resultados obtenidos han sido reportados en el artículo titulado "*Thioester-functionalised and oxime-based hexametallic manganese(III) single-molecule magnets*". Aquí se reportan dos nuevos complejos hexametálicos de Mn(III) de fórmula [Mn$_6$(μ_3-O)$_2$(H$_2$N-sao)$_6$(3-atha)$_2$(EtOH)$_6$]·2EtOH·2H$_2$O y [Mn$_6$(μ_3-O)$_2$(H$_2$N-sao)$_6$(6-atha)$_2$(EtOH)$_6$]· 6EtOH [hatpa = ácido 3-acetilpropiónico, 6-hatha = ácido 6-acetilhexanoico]. Estos compuestos fueron sintetizados mediante el uso de ligandos con grupos funcionales tioéster y carboxilato, y caracterizados magneto-estructuralmente. El primero de ellos cristaliza en el sistema triclínico con grupo espacial *P$\bar{1}$* mientras que el segundo lo hace en el sistema monoclínico con grupo espacial *P2$_1$/c*. El estudio de la susceptibilidad magnética DC y AC revela un comportamiento de SMM para ambos compuestos con estados fundamentales de espín S = 12 y S = 4, respectivamente. Por lo tanto, estos compuestos son nuevos miembros de la familia de moléculas imán [Mn$_6$] basados en oximas y funcionalizados con el grupo tioéster.

En base a los resultados obtenidos, se plantea como una proyección a futuro de este trabajo realizar los estudios de aplicación de estas nuevas moléculas funcionalizadas en dispositivos a escala nanométrica. Asimismo, este trabajo ha abierto las puertas a la posibilidad de funcionalizar sistemas de [Mn$_6$] con un amplio abanico de ligandos como pueden ser tioésteres de cadena alifática larga u otro tipo de moléculas conteniendo azufre.

En vista de lo antes expuesto, podemos afirmar que se ha cumplido en términos generales con los objetivos planteados inicialmente. Se han obtenido nuevas especies catiónicas, una de las cuales representa incluso una mejora en las propiedades magnéticas de esta familia de compuestos. Se ha explorado la síntesis y además se han reportado dos estructuras de compuestos [Mn$_6$] neutros empleando ligandos del tipo azol. Esto abre las puertas al uso de este tipo de ligandos, adecuados en lo que se refiere a la funcionalización de estos sistemas, a los que podrían añadir otras propiedades físicas de luminiscencia, por ejemplo. Asimismo, se han funcionalizado y caracterizado dos nuevos [Mn$_6$], funcionalizados con dos ligandos del tipo tioéster presentando diferentes longitudes de cadena. Este trabajo deja abierta la perspectiva a futuro de explorar el uso de estos compuestos para conectar electrodos en dispositivos a escala nanométrica.

Una vez expuestos los trabajos relativos a los sistemas basados en Mn(III), se desarrolla en esta memoria la tercera y última sección, Sección B, previa a las conclusiones, referida a la investigación llevada a cabo sobre compuestos basados en Re(IV). Aquí se han caracterizado y analizado las propiedades magnéticas de diferentes sales de los aniones $[ReX_6]^{2-}$, donde X = Cl, Br, empleando cationes de diferente naturaleza: moléculas protonables de origen biológico, cationes paramagnéticos, capaces de ordenar los complejos mononucleares en diferentes arreglos de simetría dentro de la estructura cristalina. Estos sistemas exhiben propiedades magnéticas interesantes que se describen a continuación.

En primer lugar, en el trabajo titulado *"Enhancement of Intermolecular Magnetic Exchange through Halogen···Halogen Interactions in Bisadeninium Rhenium(IV) Salts"*, se han sintetizado y caracterizado magneto-estructuralmente dos nuevas sales de Re(IV) de fórmula general $[H_2ade]_2[ReX_6]X_2 \cdot 4H_2O$ [$(H_2ade)^{2+}$ = 9H-adenina-1,7-diinio; X = Cl, Br]. Ambos compuestos son sales isoestructurales que cristalizan en el sistema ortorrómbico con el grupo espacial *Fdd2*. Ambas estructuras cristalinas están conformadas por aniones mononucleares discretas $[ReX_6]^{2-}$ y X y cationes de adenina doblemente protonados. El ion de renio (IV) está hexacoordinado y unido a seis ligandos haluro [X = Cl y Br respectivamente] en una geometría octaédrica. En ambas redes cristalinas se observan interacciones intermoleculares cortas del tipo Re(IV)- X ··· X - Re(IV), así como Re- X ··· H-N(H₂ade) y Re- X ··· H-O_w. Las medidas de susceptibilidad magnética en sendas muestras microcristalinas, en el intervalo de temperatura 2.0–300 K, revelan interacciones intermoleculares antiferromagnéticas significativas en ambos compuestos, lo que resulta en la observación de máximos en χ_M a *ca.* 6.0 y 12.0 K, respectivamente. La mayor deslocalización de espín del ion Re(IV) sobre los ligandos bromuro periféricos, en comparación con los ligandos cloruro, explica la mejora del acoplamiento magnético observado en el segundo compuesto.

Esta publicación en particular la firmo como tercer autor. En este caso mi contribución ha estado directamente relacionada con la caracterización preliminar de los compuestos así como con la medida de sus propiedades magnéticas. Además, he llevado a cabo el tratamiento de los datos experimentales obtenidos en dichas medidas, sobre los cuales he realizado los ajustes teóricos necesarios. Así, este trabajo me ha permitido comenzar a desarrollar mi experiencia como investigador en lo que respecta al tratamiento y ajuste de datos de propiedades magnéticas. Específicamente, para esta publicación se han ajustado las curvas de susceptibilidad molar (χ_M) en función de la temperatura y también el producto $\chi_M T$ en función de la temperatura.

Como continuación del estudio sobre las propiedades magnéticas de sales de los aniones $[ReX_6]^{2-}$ empleando cationes de diferente naturaleza, en el trabajo titulado *"Hexakis(dimethylformamide)iron(II) complex cation in hexahalorhenate(IV)-based salts: synthesis, X-ray structure and magnetic properties"*, han sido preparados y caracterizados dos compuestos conteniendo hierro(II)-renio(IV) de fórmula general

Resumen

[Fe(dmf)$_6$][ReX$_6$] [X = Cl y Br respectivamente; dmf = N, N-dimetilformamida]. Las medidas de difracción de rayos X en polvo sobre muestras de ambos compuestos confirman que se trata de sistemas isoestructurales. La estructura cristalina del compuesto [Fe(dmf)$_6$][ReCl$_6$] se determinó mediante difracción de rayos X de monocristal. Este compuesto cristaliza en el sistema triclínico con grupo espacial $P\bar{1}$. Cada ion Fe(II) se encuentra hexacoordinado por seis oxígenos pertenecientes a seis moléculas de dmf que conforman un entorno de coordinación octaédrico distorsionado. El ion Re(IV) es también hexacoordinado, en este caso, por seis aniones haluro en una geometría octaédrica casi regular. Las propiedades magnéticas de los compuestos fueron estudiadas a través de mediciones de susceptibilidad magnética realizadas sobre muestras microcristalinas. Los datos experimentales obtenidos fueron reproducidos por un modelo de dos centros paramagnéticos aislados [S = 2, Fe(II) y S = 3/2, Re(IV)] observándose grandes valores para los parámetros de desdoblamiento a campo cero (zfs).

En el entendido de completar esta primera etapa de estudio de especies mononucleares de Re(IV), se plantea como perspectiva llevar a cabo la caracterización estructural y magnética de los aniones [ReX$_6$]$^{2-}$ con X = Cl, Br, I, los cuales podrían ser aislados magnéticamente en la estructura cristalina empleando cationes orgánicos voluminosos, tales como tetrabutilamonio o tetrafenilfosfonio.

En la siguiente etapa hemos explorado una nueva estrategia de sustitución de ligando sobre un compuesto mononuclear de Re(IV). La estrategia habitual y más utilizada implica la sustitución directa de iones halógeno sobre las especies mononucleares [ReX$_6$]$^{2-}$ con X = Cl y Br. Sin embargo, este tipo de sustitución no siempre es tan sencilla, y raras veces permite la sustitución de más de uno o dos halogenuros, lo cual lleva a la formación de productos secundarios no deseados y rendimientos generalmente muy bajos. Por otra parte, la estrategia aquí desarrollada se basa en el uso del complejo cis-[ReCl$_4$(MeCN)$_2$] para controlar tanto la cantidad de posiciones de coordinación sustituidas (las dos posiciones ocupadas originalmente por moléculas de acetonitrilo) como la isomería del compuesto obtenido. La publicación titulada "*Ligand substitution in cis-bis(acetonitrile)tetrachlororhenium(IV) complex with N,N-dimethylformamide and N,N-dimethylacetamide*" reporta la preparación, estructuras cristalinas y propiedades magnéticas de dos nuevos complejos mononucleares de Re(IV) de fórmula cis-[ReCl$_4$(dmf)$_2$] y cis-[ReCl$_4$(dma)$_2$] [dma = N, N-dimetilacetamida]. Ambos sistemas de Re(IV) se sintetizaron mediante reacciones de sustitución de ligando del precursor cis-[ReCl$_4$(MeCN)$_2$], al calentar en el disolvente empleado. Los compuestos cristalizan en el sistema cristalino monoclínico con el grupo espacial *C2/c*. Cada ion Re(IV) exhibe un entorno de coordinación octaédrico distorsionado, unido por dos átomos de oxígeno de dos moléculas dmf y dma respectivamente, y cuatro iones cloruro. En la red cristalina, los complejos mononucleares de Re(IV) se colocan generando contactos intermoleculares cortos del tipo Re-Cl···Cl-Re. Por otra parte, se han estudiado las

propiedades magnéticas de los compuestos obtenidos a través de medidas de susceptibilidad magnética a temperatura variable. Estas medidas revelan importantes interacciones antiferromagnéticas entre los iones Re(IV) vecinos. En el compuesto conteniendo dmf, estas interacciones representan un máximo en la curva de susceptibilidad magnética a *ca*. 5.0 K.

Como continuación del trabajo centrado en las especies mononucleares, en la última etapa de nuestra investigación sobre compuestos basados en Re(IV) y sus propiedades magnéticas, hemos enfocado nuestros esfuerzos al diseño y caracterización de especies heteropolinucleares conteniendo Re(IV) y metales de la primera serie de transición. Esto nos ha permitido, no sólo obtener compuestos que podrían ser punto de partida para la obtención de futuros sistemas multifuncionales, sino que además, nos ha dado fundamentalmente la posibilidad de generar un mayor conocimiento sobre el comportamiento y las propiedades magnéticas de las especies basadas en $[ReX_4(ox)]^{2-}$ [X = Cl y Br; ox = anión oxalato]. De estas especies, de las cuales ambas presentan por sí mismas un comportamiento de tipo SIM, el anión $[ReCl_4(ox)]^{2-}$ ha sido el más estudiado, siendo los principales trabajos reportados relacionados a su uso como metaloligando hacia metales 3d. Por su parte, la química del precursor aniónico $[ReBr_4(ox)]^{2-}$ ha sido considerablemente menos explorada.

Es así que en la comunicación titulada "*Field-induced slow relaxation of magnetisation in an anionic heterotetranuclear [Zn^{II}Re^{IV}_3] system*" se utiliza el precursor ampliamente explorado $[ReCl_4(ox)]^{2-}$ hacia el ion Zn(II), el cual es hasta el momento el menos estudiado entre los iones 3d de interés para nuestro campo. Así, en este trabajo se reporta la síntesis y caracterización magneto-estructural del compuesto tetranuclear basado en zinc(II) y renio(IV) de fórmula $(NBu_4)_4[Zn\{ReCl_4(\mu\text{-}ox)\}_3]$. Este compuesto cristaliza en un sistema triclínico con grupo espacial $P\bar{1}$. El empaquetamiento cristalino está constituido por los aniones $[Zn\{ReCl_4(\mu\text{-}ox)\}_3]^{4-}$ y los cationes NBu_4^+ que se mantienen unidos por fuerzas electrostáticas e interacciones débiles. La especie aniónica $[Zn\{ReCl_4(\mu\text{-}ox)\}_3]^{4-}$ presenta una estructura tipo hélice donde el átomo central es el ion Zn(II), unido por puentes oxalato bis-bidentado a tres iones Re(IV) periféricos. Las medidas de susceptibilidad magnética DC a temperatura variable realizadas sobre una muestra microcristalina dan cuenta del alto valor de desdoblamiento a campo cero esperado para los iones Re(IV) ($|D|$ = 46.7 cm^{-1}) así como de posibles interacciones intramoleculares de tipo antiferromagnético. Las medidas de AC a diferentes temperaturas en presencia de un campo externo DC revelan la existencia de una relajación lenta de la magnetización y, por lo tanto, la existencia de un comportamiento de tipo *Single-Molecule Magnet* (SMM). Este es el primer ejemplo de un complejo de Zn(II) unido, a puente oxalato, a un ion metálico 5d que exhibe una relajación lenta de la magnetización. Además, dada la naturaleza diamagnética del ion Zn(II), la obtención de este compuesto nos permitió obtener por primera vez el valor *J* de la interacción magnética entre iones Re(IV) unidos a través de ligandos oxalato. Por

Resumen

lo tanto, este trabajo muestra que la combinación de Re(IV) (ion $5d^3$ con gran anisotropía magnética) y Zn(II) (ion diamagnético $3d^{10}$) proporcionará la síntesis de futuros sistemas y nuevos materiales basados en oxalato que muestren propiedades interesantes y prometedoras.

En el caso particular de este trabajo, el cual firmo como segundo autor, mi contribución personal ha estado centrada en la colaboración en el aspecto práctico del trabajo de síntesis de los compuestos por parte del entonces estudiante del Programa de Máster en Química, Adrián Sanchis Perucho. Asimismo, he desarrollado el aspecto cristalográfico de este trabajo, llevado a cabo la estrategia de medida y la recolección de datos de difracción de rayos X de monocristal, así como el refinamiento de los datos así obtenidos y la resolución estructural.

Finalmente, el último trabajo reportado en esta memoria de Tesis ha involucrado el uso de la especie aniónica $[ReBr_4(ox)]^{2-}$ como metaloligando hacia el ion Cu(II). Este último es uno de los iones de la primera serie de transición que ha sido más explorado en lo que refiere tanto a su química como a las propiedades magnéticas de sus especies basadas en el ligando oxalato y sus derivados. Así, el trabajo titulado *"Synthesis and characterisation of a novel ferrimagnetic chain based on copper(II) and rhenium(IV)"*, publicado en un número especial con motivo del 75° aniversario del Prof. Michel Verdaguer, ha permitido profundizar en el conocimiento de las propiedades de la especie $[ReBr_4(ox)]^{2-}$ frente a un catión ampliamente estudiado como es el Cu(II). De este modo, este artículo reporta la preparación y caracterización de un nuevo polímero de coordinación unidimensional de cobre(II) y renio(IV) de fórmula $\{[ReBr_4(\mu-ox)Cu(pyim)_2]\cdot MeCN\}_n$ [pyim = 2-(2'-piridil)imidazol]. Las medidas de difracción de rayos-X en polvo dan cuenta de la pureza de la muestra del compuesto, mientras que la de difracción de rayos-X de monocristal muestra que este cristaliza en el sistema ortorrómbico con el grupo espacial *Pbca*. La estructura cristalina de este sistema monodimensional está compuesta por cationes $[Cu(pyim)_2]^{2+}$ y aniones $[ReBr_4(ox)]^{2-}$ unidos a través de puentes de grupos bromuro y oxalato, que generan la alternancia Cu(II) y Re(IV) en las cadenas. Las medidas de susceptibilidad magnética de temperatura variable realizadas sobre una muestra microcristalina revelan un acoplamiento antiferromagnético entre los iones Cu(II) y Re(IV); y a temperaturas más bajas, esta interacción conduce a la aparición de comportamiento ferrimagnético. Este compuesto es el primer compuesto ferrimagnético obtenido con el precursor $[ReBr_4(ox)]^{2-}$.

0.

Introduction

Magnetism is a property that was for a long time associated only with metallic and ionic lattices. The origin of the term is probably related with Magnesia, where the phenomenon was discovered by observation of the attraction between iron and lodestone. In addition, there are evidences of the use of compasses in China since very early times. At any rate, magnetism attracted attention because it allows action at distance, which puzzled humankind for millennia, and led to the association of the movement with the existence of a soul in the lodestone.

It was not until 1820 that new perspectives in the understanding of magnetism were opened by the key experiment of Oersted. Thus it was demonstrated that an electric current influences the orientation of a compass needle. Later it would be Ampere suggesting that currents internal to the material should be responsible of the magnetism and that the currents must be molecular in nature, which is microscopic rather than macroscopic. In this sense, Faraday went a step farther in the contribution to the knowledge of the phenomenon. He discovered that almost all the substances are weakly repelled by an applied magnetic field and called these substances diamagnets. Furthermore, he described a less numerous class of compounds that was weakly attracted by a magnetic field and called them as paramagnets. After discovering and naming these two different types of materials, Faraday conceived the concept of a magnetic field, which provided an explanation for the action at a distance that alarmed so much the ancients. Nevertheless, it was Maxwell who provided the mathematical frame that allowed the description of electromagnetism, which meant a giant step toward understanding of magnetism.

Pierre Curie investigated the temperature dependence of the magnetisation, discovering the law that carries his name. All this in the context of his doctoral thesis titled "*Magnetic properties of matter at variable temperatures*". Thus, it was introduced a third type of material, the ferromagnets, with the concomitant report of some examples. This was also the first time that molecular materials were described in the sense of their behaviour in the presence of a magnetic field. These molecules were oxygen and nitric dioxide, described among paramagnets.

Finally, in order to complete the puzzle of the necessary context for the appearing and development of the research in the field to us concerning, it was necessary that the scientific community realised and developed two strongly relevant issues: on one hand, the nature of electron and its relevance as magnetic entity, on the other hand, the consequent development of quantum mechanics, which provided tools for describing magnetic properties and introduced important concepts, such as spin and exchange, which are crucial for our field of research: the Molecular Magnetism.[1,2]

Molecular Magnetism

At the middle of the 20th century, Inorganic Chemists were already studying magnetic properties as a method of characterisation of mononuclear coordination compounds by their geometry and the oxidation state of the metallic centre. In point of fact, it was in the 1970s decade when the synthesis and rationalised design of polynuclear coordination compounds started to be performed. Thus, the magnetic exchange between the metallic ions throughout given ligands became definitely a matter of research. Consequently, the wide amount of results achieved, by using mainly paramagnetic 3d metal ions, led to a better comprehension of the mechanisms that are involved in the magnetic exchange. Most of this knowledge was compiled and published by R. Carlin in his book "*Magnetochemistry*" in 1986.[3]

In this perspective, in the 1980s decade, the achieved knowledge related to the magnetic properties and the structure of the compounds started to be used to design molecular magnetic materials with the aim of developing their potential properties. Hence, a new field of research appeared as a convergence of different branches from chemistry, physics and material sciences, where the chemist as a researcher became relevant in the design and synthesis of the compounds. Quickly, this new field started to be known as Molecular Magnetism. Regarding this new concept, the homonymous book was publishes by O. Kahn in 1993.[4]

In 1986, O. Kahn himself and his co-workers, reported the first molecular-based ferromagnets. The analogous [MnCu(pba)(H_2O)$_3$] and [MnCu(pbaOH)(H_2O)$_3$·$2H_2O$] complexes, where pba = 1,3-propilenebis(oxamate) and pbaOH = 2-hydroxi-1,3-propilenebis(oxamate). These monodimensional complexes are made up by reaction of the mononuclear Cu(II)-containing precursor and Mn(II) ions, leading to a ferrimagnetic arrange alongside the main axis of the chain, which is explained by the occurring alternation of the S = 5/2 and S = 1/2 from Mn(II) and Cu(II) respectively.[5]

In this manner, the structural and magnetic properties of a huge number of magnetically ordered molecular species have been thoroughly investigated for their fundamental interest in chemistry and physics. The properties of these species can potentially provide a gateway for the discovery of new physical phenomena and be used for a diverse array of technological applications.[6] Nevertheless, most of the studies on magnetic properties of polynuclear coordination compounds of different dimensionality have been centred on the first transition raw (3d) and, secondly, on lanthanides (4f). During the last decades it has been increased the study of systems based on second (4d) and third raw (5d) metal ions. Even though, they remind less explored. This fact can be explained having into account different aspects. On one hand, the chemistry of 4d and 5d metal ions is considerably more difficult to deal with, than that of 3d ions. On the other hand, from the magnetic point of view, the magnetic properties are harder to be modelled and interpreted. Furthermore, 4d and 5d metal ions tend to lead to low spin complexes,

which often means that there are no unpaired electrons in the metallic centres, losing all their interest in this discipline. However, when there exist magnetic properties susceptible of being studied, phenomena such as spin-orbit coupling appear, which makes, particularly in 5d metal ions, calculations to be complex and lead the theoretical models to non-satisfactory results. Nonetheless, they still keep the interest of the researchers in the field given the fact that the longer diffusivity and anisotropy of 4d and 5d orbitals may increase the intensity of the magnetic exchange respect from the observed in 3d metal systems.

In this context, the rational design of molecule-based magnetic systems through a bottom-up approach, as general rule, requires the knowledge of the self-assembly guidelines[7] together with the understanding of the exchange interaction[4] and the role that magnetic anisotropy plays on molecular magnetism.[8] The programmed preparation of high-spin molecules constitute an illustrative example of the potential that bottom-up design invest in this area.[9] Thus, very well-known complexes such as $\{Cr[(ox)Ni(Me_6$-$[14]ane$-$N_4)]_3\}(ClO_4)_3$ and $\{Cr[(CN)Ni(tetren)]_6\}(ClO_4)_9 \cdot 2H_2O$ have been obtained by using the $[Cr(ox)_3]^{3-}$ and $Cr(CN)_6]^{3-}$ complexes as metalloligands toward the preformed $[Ni(Me_6$-$[14]ane$-$N_4)]^{2+}$ and $[Ni(tetren)]^{2+}$ species, affording in a single step pathway the desired tetra- and heptanuclear complexes with S = 9/2 and S = 15/2 respectively.[10, 11] The ferromagnetic interaction between the magnetic orbitals of the octahedral Cr(III) (three unpaired electrons in t_{2g} orbitals) and Ni(II) (two unpaired electrons in e_g orbitals) is given for the parallel alignment of the local spins. These polynuclear complexes with large ground spin states and a high anisotropy are at the origin of the development of Single–Molecule Magnets (SMMs).[8b-12]

Single–Molecule Magnets

The phenomenon of single–molecule magnetism was established in the early 1990s. Then, the ability of certain molecular transition-metal complexes to be magnetised, without need of long-range cooperative interaction, was seen for the first time in a coordination complex made of oxo- and acetate-bridged manganese metal ions, with formula $[Mn_{12}O_{12}(O_2C_2H_3)_{16}(H_2O)_4]$;[13] this formula and the corresponding derivatives will be abbreviated from now on generically as $[Mn_{12}]$. The synthesis and crystal structure of this complex, the first one reported as behaving as a SMM, was published in 1980,[14] even though the possibility of formation of dodecanuclear manganese acetate complexes was already suggested as early as in the 1920s decade.[15] Nevertheless, it was only when monocristal X-ray experiments became routine that it was possible to confirm the structure (see Fig. 1a).

Given the tetragonal symmetry that the molecule has, there are three independent manganese ions, namely, two Mn(III) and one Mn(IV), which show an octahedral geometry. The different manganese ions can be easily recognised by the bond lengths and by the elongated Jahn-Teller distorted structure characteristic for Mn(III) ions.
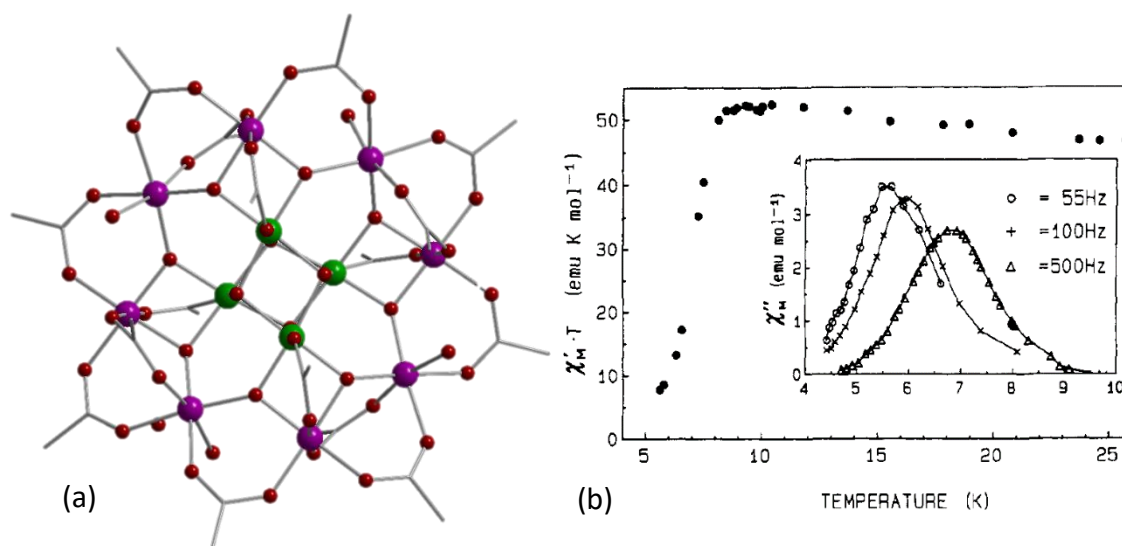
Figure 1. (a) Molecular structure of [Mn$_{12}$]. H atoms are omitted for clarity. Code colour: violet, Mn(III); green, Mn(IV); red O; grey, C atoms. (b) χ_MT vs T plot obtained from a powdered sample of the complex. In the inset is reported the imaginary part (χ''_M) of the ac susceptibility at three frequencies.

Mn(IV) ions are located in the inside of the molecule, coordinated to five oxo ligands and to one oxygen atom of an acetate molecule, whereas there are two different peripheral Mn(III) centres, one of them being bounded to two oxo ligands and to four oxygen atoms of acetate molecules, while the other one is bounded to two oxo ligands and to four oxygen atoms of acetate molecules. All the oxo ligands form μ_3 bridges.

Direct evidence of the possible large spin ground states was obtained by the use of several techniques, such as high field magnetisation, high field EPR, and ac susceptibility measurements. In Figure 1b it is shown the χT versus T plot, obtained from a powdered sample of the complex, and in the inset is reported the imaginary part (χ'') of the ac susceptibility at three frequencies. The simultaneous use of these techniques provided evidence of an S = 10 ground state, and a magnetic behaviour which resembled that of superparamagnets.[13]

As it is revelled in the book *Introduction to Molecular Magnetism*, at that time, Gatteschi's opinion was that the research had achieved the result of characterizing the ground state of this complex, and he suggested Roberta Sessoli to look for some other interesting problem. She said yes, and continued to work on [Mn$_{12}$], obtaining the exciting results that formed the basis for the SMM era.[16] The most exciting was the observation of magnetic hysteresis of molecular origin.[1] In fact, what the new measurements performed by Sessoli showed was a slow relaxation of the magnetisation phenomenon, which led to a magnetic hysteresis, as can be seen in Figure 2. This is often the signature of three-dimensional magnetic order but nothing of that kind occurred in [Mn$_{12}$] compound. The phenomenon was molecular. A few years later, when quantum relaxation was described, this meant a full success.[17]
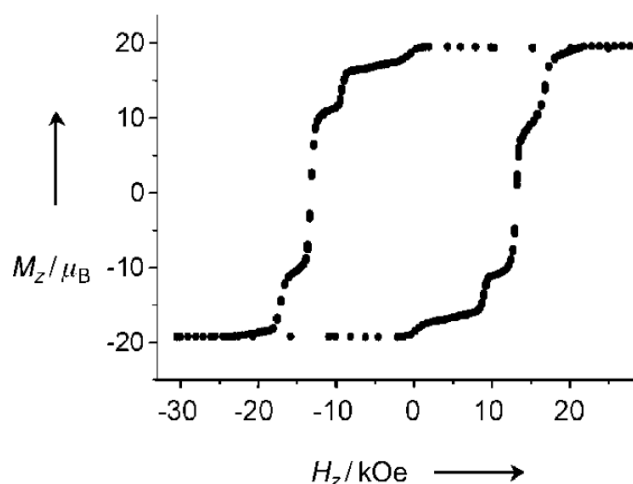
Figure 2. Magnetic hysteresis loop for a single crystal of [Mn$_{12}$] with the field parallel to the tetragonal axis at 2.1 K.

The rising up of the magnetic hysteresis in the molecular system is expected to be seen if the relaxation time of the magnetisation of the sample becomes lower than the time the field is being applied. The observed steps in the case of [Mn$_{12}$] were assigned to the thermally assisted quantum tunnelling of the magnetisation (QTM)[18]. The steps were spouse to correspond to those fields at which pairs of levels become degenerate. Then, they must be related to a minimum in the relaxation times. Thus, it was possible to say that at these fields two mechanisms were operative: the thermally activated and the quantum tunnelling. At the fields corresponding to flat regions of the magnetic hysteresis curve, the degeneracy of the levels was lost and the tunnelling mechanism apparently annulled, giving longer relaxation times.
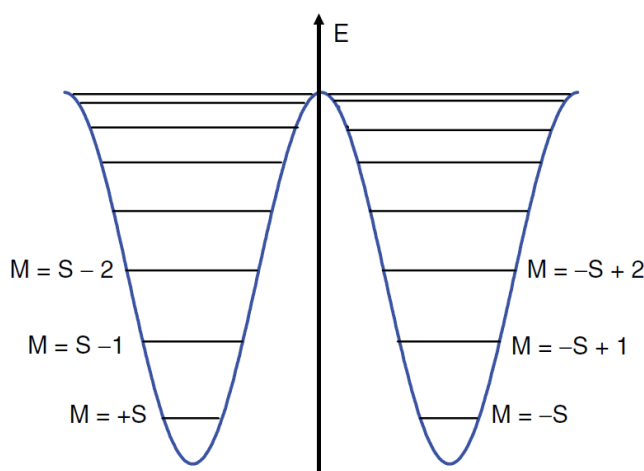
Figure 3. Double-well distribution energies of the spin levels M belonging to a ground manifold S, −S ≤ M ≤ +S. The lowest lying levels are M=±S, the highest one is M=0. Taken from the book *Introduction to Molecular Magnetism*.

Indeed, SMMs are characterised by a magnetic relaxation that is thermally activated. Assuming an approximate model, at low temperature the system could be described by a spin S that is possible to be considered as a "giant" spin as the ground state whose

Zero-Field Splitting (ZFS) levels follow the double-well distribution shown in Figure 3. If a magnetic field is applied parallel to the z axis, the states of one sign go to lower energies, while those of the opposite sign go to higher energies. On switching the field off, the system goes back to equilibrium through the correspondent quantised series of steps. The relaxation follows an Arrhenius low with activation energy U_{eff}, which is normally called the energy barrier of the system. These items are going to be explained thoroughly later in this chapter.
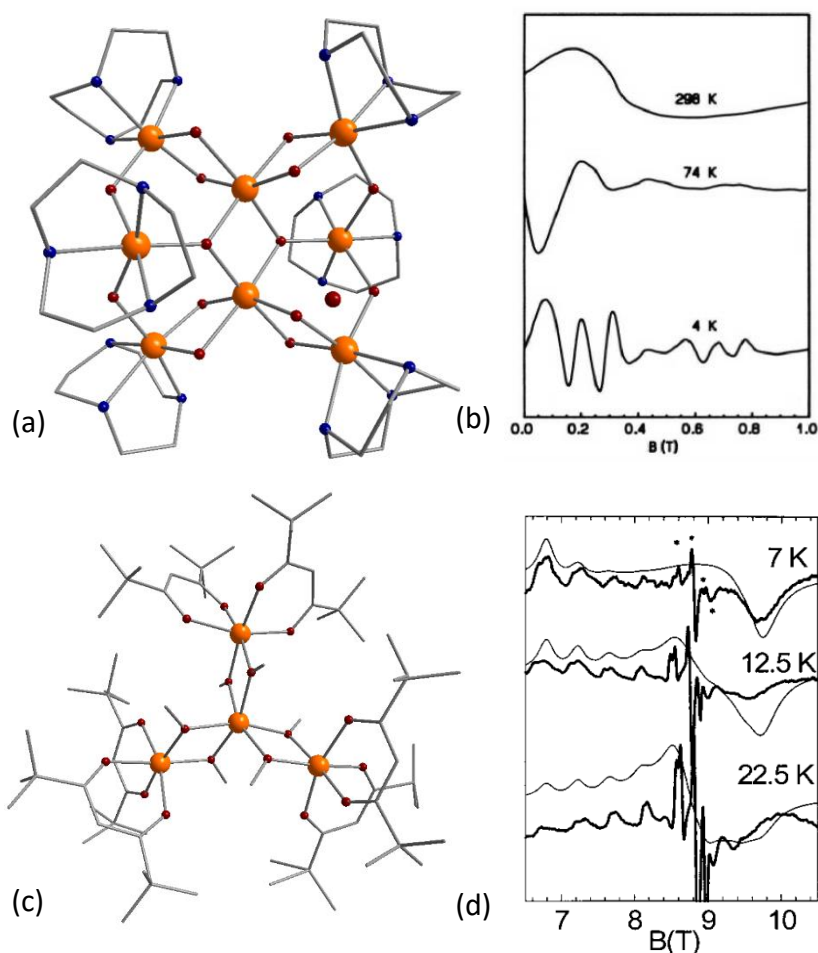
Figure 4. (a) Molecular structure of [Fe$_8$]. Hydrogen atoms are omitted for clarity. Colour code: orange, Fe(III); red O; blue N; grey, C atoms. (b) HF-EPR spectra at three different temperatures of a polycrystalline sample of [Fe$_8$]. (c) molecular structure of [Fe$_4$]. Hydrogen atoms are omitted for clarity. Colour code: orange, Fe; red O; grey, C atoms. (d) HF-EPR spectra at 245 GHz and three different temperatures of a polycrystalline sample of [Fe$_4$] pressed in a pellet (bold) and simulated spectra assuming S = 5. The bands marked (*) are assigned to the excited multiplets and are not reproduced by the simulation.

After the first approaches and the development of new concepts reached by the extensive studies on the [Mn$_{12}$] acetate derivative, several other carboxylate compounds where prepared. Those modifications performed on the [Mn$_{12}$] molecule induced concomitant changes in the crystallographic and redox properties of systems as well as their solubility and stability in solution.[19] Nevertheless, there was non-significant improvement in the magnetic properties of the complex. Besides, the research and the

development of SMM is not confined to the limits of the so called [Mn$_{12}$] family. Quickly, these studies were also performed on other Mn(III) families such as the [Mn$_{10}$],[20] [Mn$_6$][21] or [Mn$_4$],[22] and even before them, on other 3d metal systems like [Fe$_8$],[23] [Fe$_4$],[24] [V$_4$][24], [CrM$_6$][25] and [Ni$_{12}$][26]. In Figure 4, the molecular structure of the cationic [Fe$_8$] and the neutral [Fe$_4$] complexes are shown together with their HF-EPR spectra at different temperatures. An important issue which can be easily deducted from comparing both of the plots is the fact that the Molecular Magnetism has evolved in a rhythmic way with the development of the physical techniques and equipment that requires. This issue limited the field to a very late development, but at the same time impulse it forwards nowadays. Thus, for the [Fe$_8$] system, published at the beginning of the 1990s decade, the obtained HF-EPR spectra is considerably smoother and less defined than the one reported for the [Fe$_4$] system at the end of the decade.

Once the first systems were reported, it was important to find correlations between the observed phenomena and the molecular structure of the complexes. Since at that time it was already established that the total spin S of the molecule and the magnetic anisotropy were the most relevant parameters for SMM behaviour, structural factors such as symmetry and torsion angles, which directly determine the presence or absence of structural anisotropy, must be related. Thus, a deeper research on the [Fe$_4$] and [Fe$_8$] systems lead to the conclusion that torsion angles where the key for switching from a complex which does not behave as SMM to one that actually does.

Further in the design of SMMs, the less explored 4d and 5d metal ions came finally into the discussion and, after approximately a decade of the finding of the first SMM, the first 4d- and 5d-based SMMs were reported.[27] As indicated before, the magnetic anisotropy that the 4d and 5d metal ions can provide to the systems is considerably higher than the one proceeding from 3d ions. This fact is easily explained by the known proportionality of the anisotropy respect the spin-orbit coupling (SOC) factor (λ), which is around one order of magnitude higher for 4d and 5d than for 3d metal ions.

From the Molecular Magnetism point of view, the most explored and studied systems based on 4d and 5d metal ions are those containing Mo(III),[28] Ru(III),[29] Re(IV)[30] and Os(V).[31] Among them, Re(IV) can be pointed out to have been the most studied given its high magnetic anisotropy factor and S value (S = 3/2). Nevertheless, most of the SMMs reported to the date using this metal ion are not homonuclear species, that is, they are not exclusively based on Re(IV), but heteropolynuclear species such as the heterodinuclear anionic complex shown in Figure 5. The structure showed in this picture corresponds to the [Ni{ReCl$_4$(ox)}$_3$]$^{4-}$ anionic species, obtained and reported as a tetrabutylamonium salt, which is the first oxalate-based SMM.[32]

0. Introduction

In the context of that work, the analogous Fe(II)-, Co(II)-, and Cu(II)-containing tetranuclear complexes were also obtained. Nevertheless, only the Ni(II)-based analogous was found to behave as a SMM.
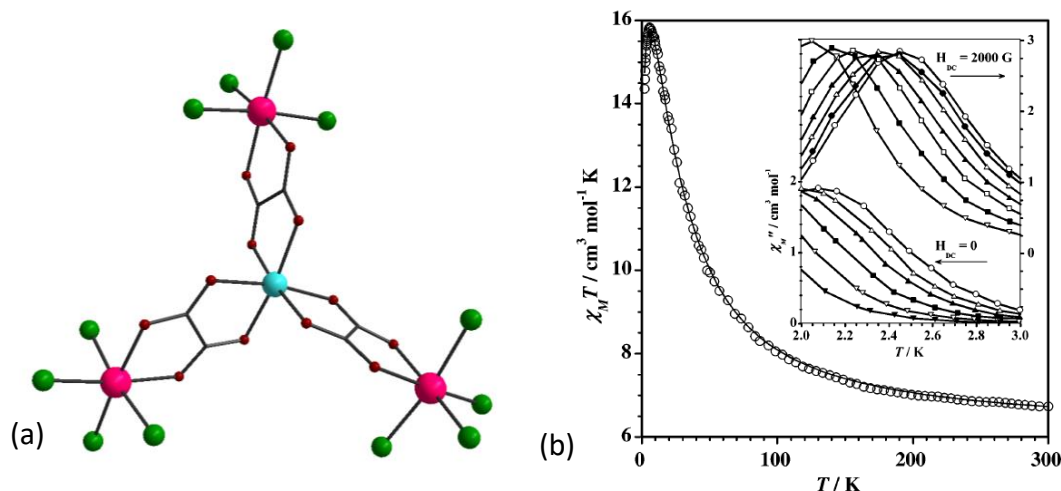

Figure 5. (a) Representation of $[Ni\{ReCl_4(ox)\}_3]^{4-}$ anion. Hydrogen atoms are omitted for clarity. Code colour: sky-blue, Ni; pink, Re(IV); green, Cl; red O; grey, C atoms. (b) $\chi_M T$ vs T plot obtained from a powdered sample of the complex. In the inset is reported the imaginary part (χ''_M) of the ac susceptibility at several frequencies.

Regarding the well-known magneto-structural correlation established for tetranuclear compounds presenting D_{3d} symmetry, such as the previously mentioned [Fe$_4$] family, the dihedral angles between the main planes of the ligands are critical to observe the typical for a SMM behaviour. According to the results of this study, such an angle should be ca. the 42 degrees. Consequently, in the case of Martínez-Lillo's work, only Re$_3$Ni complex fits that requirement (Figure 5).

Looking at the $\chi_M T$ vs T plot, it is possible to deduce the existence of ferromagnetic intramolecular interaction, since the $\chi_M T$ is continuously increasing while the sample is cooled down. The very small decreasing of the values at low temperatures might be assigned to the zero–field splitting effect produced mainly by the Re(IV) ions. Finally, showing the behaviour expected for a SMM, the sample displayed out-of-phase signals, which are susceptible of being observed at higher temperatures when increasing the applied field, but even at $H_{dc} = 0$ signals are observed.

After describing some of the most emblematic examples of SMMs in the still short story of Molecular Magnetism and the singular features of this special type of molecules, there exist another issue that must be pointed out. Despite the agreement in the community on considering the value of S in the ground state and the magnetic anisotropy as the main factors that make the difference for the SMM behaviour rather than the size of the systems, most of these new molecules show slower relaxations effects at low temperature than the [Mn$_{12}$] complexes. Neither the energy barriers nor the relaxation times were actually improved until the mentioned [Mn$_6$] family[33] appeared and the lanthanide-based SMMs were developed.[34] Both of them, in their

times, claimed to present the record energy barrier for a SMM. First it was the [Mn$_6$] oxime-based system, reported by J. Milios et al, which presents an energy barrier U$_{eff}$ equal to 86.4K. Later, it was reported the tetranuclear Dy(III)-based system {[Dy$_4$]} whose U$_{eff}$ was reported to be 177 K. In Figure 6, one example of each of this molecules are shown together with their corresponding hysteresis loops M/M$_s$ vs μ_0H(T).
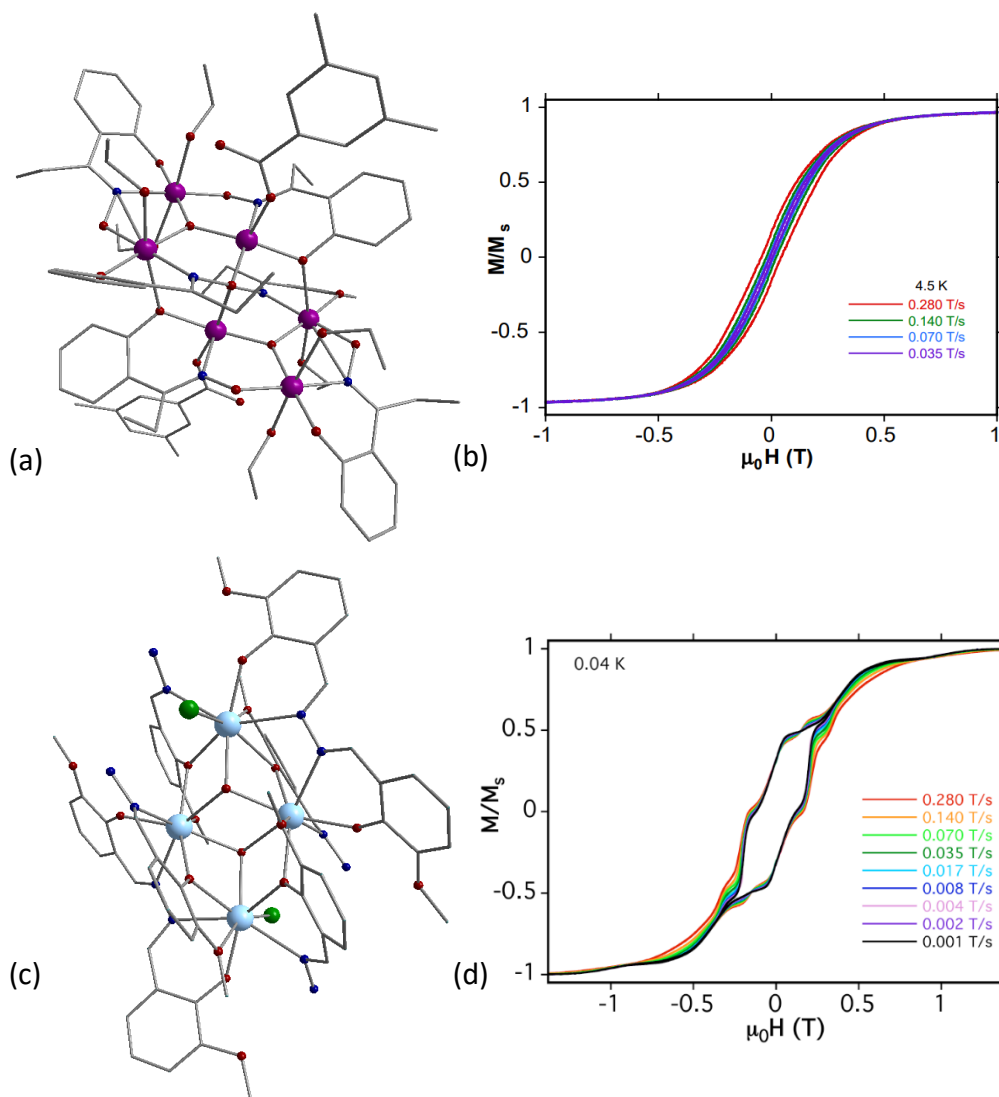
Figure 6. (a) Molecular structure of [Mn$_6$]. H atoms are omitted for clarity. Colour code: violet, Mn(III); red O; blue N; grey, C atoms. (b) Magnetisation (M) vs. applied dc field sweeps at the indicated sweep rates and at 4.5 K. (c) Molecular structure of [Dy$_4$]. (d) Magnetisation (M) vs. applied dc field sweeps at the indicated sweep rates and at 0.04 K.

Single–Ion Magnets

Single–Ion Magnet (SIM) is, in principle, an arbitrary definition adopted for grouping those mononuclear SMMs which are constituted by only one metallic centre confined in an either positive or negative charged molecule, isolated, in the crystal packing, at least, by the corresponding counterions.

Lanthanides, given their high spin and intrinsic magnetic anisotropy values, have constituted the cornerstone for the development of the first families of SIMs and, during last decades, a huge number of this lanthanide-containing complexes have been reported.[35] The first example of mononuclear complex showing SIM behaviour was reported in 2003 by N. Ishikawa et al.[36] This compound, of formula (n-Bu₄N)[TbPc₂] (Pc = phthalocyanine), was found to present an energy barrier equal to 331 K, considerably higher for the one observed until that moment for the most representatives SMMs [Mn₁₂] and [Mn₆]. The χ_M' and χ_M'' vs T plots of the mentioned compound can be seen in the Figure 7, along with the schematic representation of the molecular structure. Surprisingly perhaps, it took almost one decade from the publication of the first SIM to the report of the first 3d-based SIM. Freedman, from the research group of Long, in 2010 reported the first complex based on an element of the first transition raw that was found to behave as a SIM. The molecule consist of an anionic unit of Fe(II) in a trigonal pyramid environment constituted by a tri-pirrolyltetramine tetradentate ligand. In this case the U_{eff} value is similar to that obtained for [Mn₁₂] system; around 60 K.[37] This research led to the development and characterisation of new 3d-based SIMs, containing fundamentally on Mn(III),[38] Fe(II),[39] Co(II)[40] and Ni(II) and, finally, the investigation was also extended to the third transition raw.
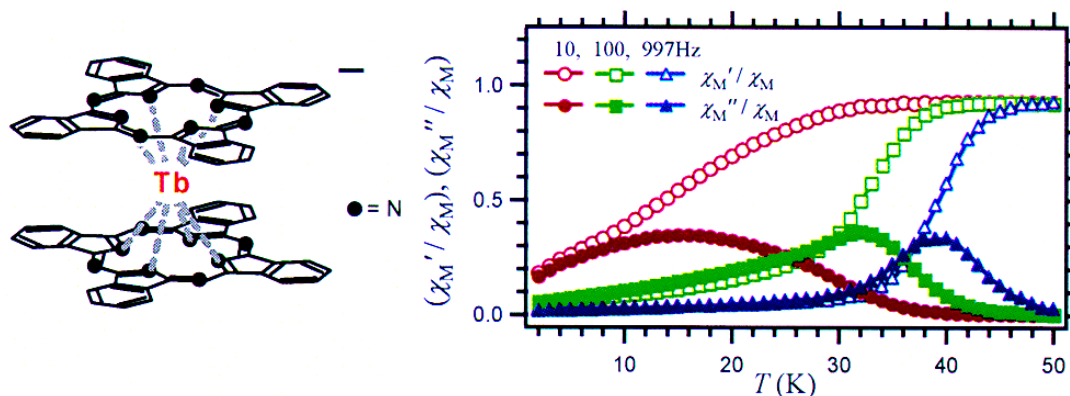

Figure 7. Molecular structure of the (n-Bu₄N)[TbPc₂] complex (left). χ_M' and χ_M'' vs T overlapped plots at three different frequencies obtained from a powdered sample of the complex (right).

At this point, despite there are only a few examples of 5d-based SIMs already reported, Re(IV) becomes once more the star among all the possible 5d metal ions susceptible to be studied from the molecular magnetism point of view. Thus, in 2013, the first two 5d-based SIMs were reported by Martinez-Lillo *et al.* The complexes were the already known (n-Bu₄N)₂[ReX₄(ox)] (X = Br and Cl).[41] They exhibit a fast relaxation of the magnetisation due to QTM effects in the presence of an applied dc magnetic field. The QTM effects was observed to disappear in the presence of an applied dc field and, as a consequence, slow magnetic relaxation takes place. The main question for them was to

understand the mechanism of that relaxation. An energy barrier of about 14.4 K was estimated for the two complexes, derived from the experimental data. However, the energy gap between the ground state and the lowest excited spin level for these molecules was calculated to be *ca.* 160–190 K, which is one order of magnitude greater than the energy barrier. As a consequence, it was postulated that vibrational levels involving molecular distortions may give rise to *D* values closer to those responsible for the energy barrier. Nevertheless, the theoretical studies of these vibrational molecular distortions with low *D* values and a half-life long enough to relax are not developed yet.
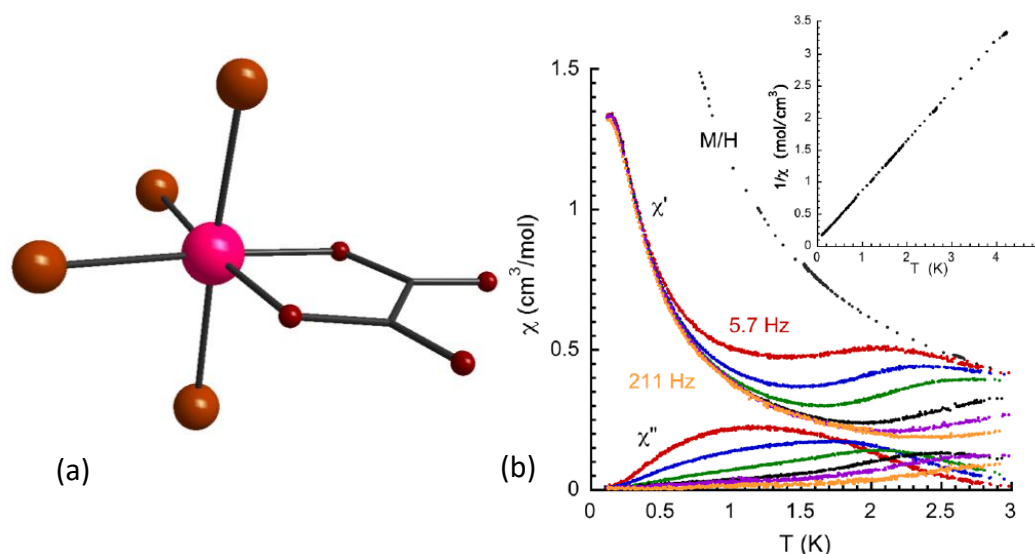
Figure 8. (a) Representation of $[ReBr_4(ox)]^{4-}$ anion. Hydrogen atoms are omitted for clarity. Colour code: pink, Re(IV); soft red, Br; red O; grey, C atoms. (b) Plot of χ_M, χ_M', χ_M'' vs T obtained from a powdered sample of the complex. In the inset is reported the plot o the inverse value of the susceptibility (χ^{-1}) vs T.

One year later, in 2014, Pedersen *et al.* reported the hexafluoride mononuclear complex, $[(Ph)_4P]_2[ReF_6]$ which also behaves as a SIM. [42] Indeed, out-of-phase signals were observed, and also EPR spectroscopy and inelastic neutron scattering (INS) were employed for the fully characterisation of the system.

In this context, admitting that the need to adopt a specific definition for the mononuclear molecular magnets is discussable, it is also necessary to recognise that SIMs as a family of complexes warrants many advantages. First, the presence of only one metallic centre, as the spin carrier in the molecule, guarantee that there is no possibility that an unappropriated orientation of the axis makes the magnitude of the anisotropy value to be neither debilitated nor cancelled. Secondly, there are no chance of intramolecular interactions, which avoid the possibility of a non-magnetic ground state. Finally, from the theoretical and the experimental point of views, SIMs are the simplest model for the study and understanding of the slow relaxation of the magnetisation and quantum tunnelling phenomena.

Basic concepts of Molecular Magnetism and fundamental equations

In the fundamental states of coordination compounds, unpaired electrons are frequently find. Those electrons generate an angular moment and, since they poses a given electric charge, a magnetic moment is also generated. In presence of an external magnetic field, the mentioned magnetic moments tends to align themselves in the direction of the applied field. When such a phenomena come to happen, it is said that the sample is magnetised. The magnetisation, *M*, is a magnitude that measure the value of the total magnetic moment of a sample in the direction of the field. This magnitude is increased with the intensity of the applied field, *H*. Hence, magnetic susceptibility, χ, can be defined as:

$$\chi = \frac{\delta M}{\delta H} \tag{1}$$

Besides, magnetic susceptibility also depends on the amount of sample. Thus it can be either defined in function of a given mass (cm^3g^{-1}) or moles (cm^3mol^{-1}). As chemist, from now on we are adopting the last definition. In the most general of the cases χ must be considered as a second order tensor. However, as far as the sample can be considered magnetically isotropic, χ becomes a scalar magnitude. Moreover, when the applied field is small enough, the molar magnetisation evolves linearly respect from the magnetic field. Thus, χ becomes independent from H and the equation (1) may be expressed as (2).

$$\chi = \frac{M}{H} \tag{2}$$

Nevertheless, the magnetisation is not unlimited. Once all the individual magnetics moments are aligned with the field a maximum value is reached. At this point, when *H* is increased *M* remains constant, it is said that the sample has reached the value of saturating magnetisation.

Magnetic susceptibility is also a temperature dependent parameter. Thermic energy is opposite to the ordering effect of the magnetic field, making that *M*, and consequently χ, slows down when increasing the temperature. From the competition between the applied field and the temperature a certain magnetisation is established in the sample. Thus, the lower the temperature the easier the saturation of the magnetisation is reached.

It can be said that the magnetisation is a spontaneous process in the presence of the external magnetic field because there is a decrease in the energy of the system. The existent relationship that links both magnitudes is expressed by the equation (3)

$$M = -\frac{\delta E}{\delta H} \tag{3}$$

As can be seen in this expression, paramagnetic substances, for which magnetisation is positive, will show a decrease in their energy if the magnetic field increases. This is the reason why, if the field is not homogeneous, these substances will tend to move to regions where the field is larger. The opposite situation is observed when samples are diamagnetic.

According to quantum mechanics, for a molecule with E_n (n = 1, 2, …) energy values, in the presence of a magnetic field H, a microscopic magnetisation μ_n can be defined (4).

$$\mu = -\frac{\delta E_n}{\delta H} \qquad (4)$$

Therefore, in a given molar macroscopic sample magnetisation must be given by the contribution of each level following a Maxwell-Boltzmann distribution (5), where N is Avogadro number, k Boltzmann constant and T the absolute temperature.

$$M = N \frac{\sum_n \left(-\frac{\delta E_n}{\delta H}\right)\exp(-\frac{E_n}{kT})}{\sum_n \exp(-\frac{E_n}{kT})} \qquad (5)$$

As a result, χ may be determined by applying this deduction in (1). Furthermore, considering that H << kT, the deduction might be done by using (2), which is reasonable having in to account that in most of the cases *H* is in fact considerable minor than T.

In the latter case, the magnetic susceptibility can be approximated through what is known as the van Vleck equation, (6) where $E_n^{(0)}$ correspond to the energy of the microstate n under field absence, while $E_n^{(1)}$ and $E_n^{(2)}$ are the first and second order Zeeman coefficient.

$$\chi = N \frac{\sum_n (\frac{E_n^{(1)2}}{kT} - 2E_n^{(2)})\exp(-\frac{E_n^{(0)}}{kT})}{\sum_n \exp(-\frac{E_n^{(0)}}{kT})} \qquad (6)$$

As an example, herein we are solving this equation to the simplest situation. Regarding this, the orbital contribution to the magnetic moment must be L_{ef} = 0. Therefore, there is not possibility of first order spin orbit coupling and the fundamental term is represented by a single level. Another feasible consideration is that the exited terms are high enough in energy to depreciate the possibility of second order spin orbit coupling. Thus, the spin angular moment S is the only contribution to the magnetic moment to be considered. This is what we normally call a spin-only situation. When field is not applied (*H* = 0), the 2S+1 microstates remain degenerated. However, when an external field is applied (H ≠ 0), the 2S+1 functions split in different energy levels. This interaction is known as Zeeman Effect, described by the corresponding Hamiltonian (7).

$$\mathcal{H}_{ZE} = \beta g S \cdot H \qquad (7)$$

In this equation, g represents the gyromagnetic factor (2.0023 for a free electron) and β the Bohr magneton. Then, the corresponding energies of the different 2S+1 microstates can be deduced and are given by the equation (8). In this case M_s value must be comprehended between +S and −S values and the direction of the applied field parallel to the z axis.

$$E_n = M_S\beta g \cdot H \tag{8}$$

Having in account that second order Zeeman coefficient is depreciable in this case, when van Vleck equation is applied (6) the expression (9) is obtained.

$$\chi = (Ng^2\beta^2/3kT)S(S+1) \tag{9}$$

As it can be easily seen, this deduction leads to the so called Curie law, where molar magnetic susceptibility is proportional to a constant C, dependent from the multiplicity of the fundamental term, and inversely proportional to the temperature T ($\chi = C/T$). Thus, when a system behaves following the curie law, the plot of the product χT versus T corresponds to a horizontal line with a χT constant, equal to C.

This general expression, only valid when $H \ll T$, is also not considering second order spin orbit coupling, which is a phenomenon frequently observed in transition metal ions. If we consider a complex with a strict O_h symmetry, the interactions of the functions with those belonging to the excited ones introduces some non-depreciable percentage of angular moment to the ground state. Even more, when the system is less symmetric, the assumed degeneration of the different microstates disappeared and the so call Kramer doublets are formed. This phenomenon is also frequently observed and named by Zero Field Splitting (ZFS). The magnetic properties will then be anisotropic, however, since measurements are generally performed on polycrystalline samples, it is difficult to determine the components of g and χ. This is the reason why only average values are obtained.

Thus far we have considered that the spin carriers does not interact with each other. However, compounds in solid samples can be rarely considered as magnetically isolated. From the point of view of molecular magnetism this problem can be modelled by the approximation of molecular field using the Hamiltonian of interaction (10).

$$\mathcal{H}_{inter} = -zJ\langle S_z\rangle S_z \tag{10}$$

In this expression, z corresponds to the number of neighbouring spin carriers in the crystalline state and J is the interaction parameter between spin carriers, which can take positive or negative values. In the first case it is said that the interaction is ferromagnetic and the spins of neighbouring centres are align in parallel respect to each other. On the other hand, when negatives J happen, the spins tend to engage antiparallel and the interaction is called antiferromagnetic.

Regarding the Zeeman perturbation, in the new situation the final Hamiltonian might be represented by (11). Here *H* is again considered to be applied in the direction of the z axis and g value as an isotropic magnitude.

$$\mathcal{H} = g\beta S_z H\text{-}zJ\text{<}S_z\text{>}S_z \tag{11}$$

Finally, applying this molecular field approximation in van Vleck expression (6), it is observed that susceptibility is given by (12):

$$\chi = \frac{Ng^2\beta^2 S(S+1)}{3kT - zJS(S+1)} = \frac{C}{T-\theta} \tag{12}$$

Namely, the former expression is known as the Curie-Weiss law, where C correspond to the Curie constant and θ to the Weiss constant or Weiss temperature

$$\theta = \frac{zJS(S+1)}{3k} \tag{13}$$

Therefore, a plot of $\chi^{-1} = f(T)$ for a system obeying the Curie-Weiss law is expected to be a straight line of which the slope is C^{-1}. The intercept with the T axis yields both the sign and the value of θ, as shown in Scheme 1b. In the framework of this model positive θ indicates ferromagnetic intermolecular interactions and negative θ indicates antiferromagnetic intermolecular interactions. In the former case ($\theta > 0$) the Curie-Weiss law is clearly limited to the temperature range $T>\theta$. If the magnetic data are represented as a plot of $\chi_M T$ versus T, positive θ leads to an increase in the curve respect from the C value and a negative θ to a decrease of $\chi_M T$ on cooling as shown in Scheme 1b.
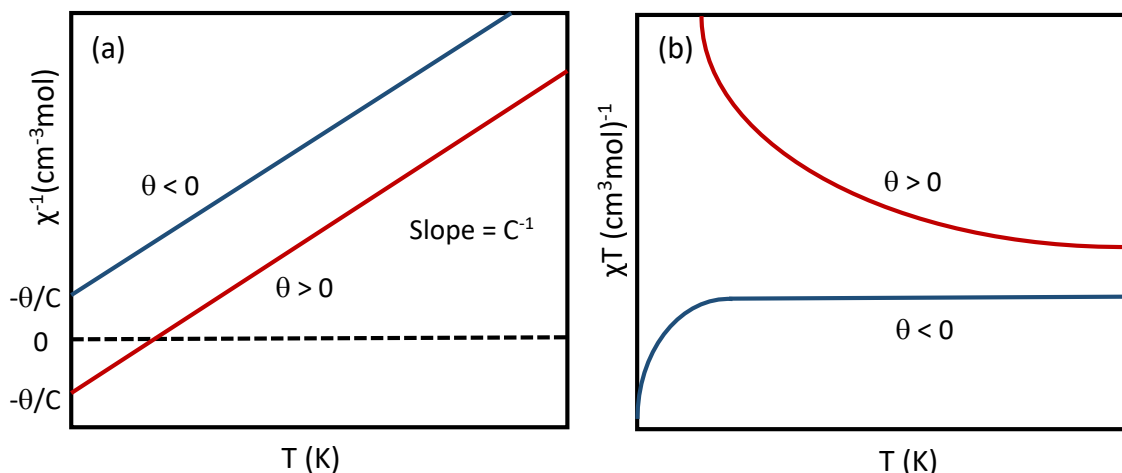
Scheme 1. (a)χ^{-1} vs T plot for an assembly of molecules that obey Curie-Weiss law. (b) Generic scheme of χT vs T plot for an assembly of molecules obeying Curie-Weiss law.

As said before, in a paramagnetic system each spin is orientated independently from the neighbouring ones, however, when reducing the temperature intermolecular interactions become relevant. Therefore, every paramagnetic compound is expected to

present magnetic order at a certain temperature. This temperature is the so called critical temperature T_c and it is a characteristic parameter for each compound in a given conditions. As a general rule it can be said that the stronger the interactions, the higher the value of T_c. The intensity of these interactions is given by their nature. In the case of molecular solids, where the interactions are rather van der Waals-type, T_c value might be considerably small. It becomes higher when interactions are via H-bonds and T_c can reach the room temperature if interactions are given by chemical bonding.

For establishing a magnetic order it is necessary not only to observe an interaction among the existent magnetics moments, but to determine what is called a length of correlation (ξ), which means the distance in which spin carriers interact. This magnitude must tend to infinite at the T_c. ξ is a measure of the quantity of order in the system.

Ferromagnetic systems are characterised by interactions that lead to the parallel ordering of all spins in the same direction. In such a case, a spontaneous magnetisation, M_S, appears at the critical temperature. M_S can be considered the measure of the order of the system below T_c. M_S increases as T decreases when T <T_c. This increase is continuous and tends to saturation magnetisation. On the other way around, when T> T_c Curie-Weiss law is fulfilled and experimentally what is observed is a huge increase of χ and χT values when T_c is reached.

For antiferromagnets, at T_c, ξ tends to infinite but, given that the spins are oriented antiparallel, there is no spontaneous magnetisation. However, if antiferromagnetic systems have certain characteristics, it is possible that the spins are not completely antiparallel but a certain angle remains among the spin carriers as represented in scheme 2. Thus, a small spontaneous magnetisation is generated and a very weak ferromagnetic-type phenomenon takes palce. When it comes to happen, a huge increase in χ versus T and χT versus T plot is observed. This phenomenon is called spin canting. In the same way, there can be the situation in which the spins are parallel oriented but forming a given angle, giving rise to a ferromagnetic canting.
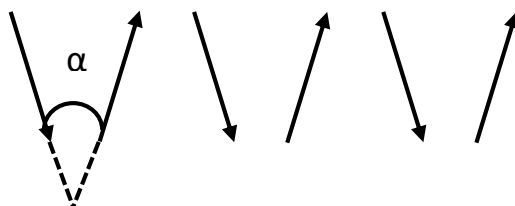
Scheme 2. Representation of magnetic moments arrange in a structure presenting spin canting phenomenon.

Regarding this, the system can be described considering that below T_c the compound presents a magnetic moment and, when a small magnetic field is applied, then an M_w magnetisation appears due to the appearance of the ordered state generated by the spin canting. If the applied field continues to increase, the magnetisation will gradually increase until it reaches a M_S saturation value corresponding to all spins aligned in the

same direction. An estimation of the angle α presented by these spins can be made according to the equation (14).

$$\text{Sen}(\alpha) = M_w/M_S \qquad\qquad (14)$$

Normally, α angle found in thus complexes with a weak ferromagnetism is in de order of the unit of degree. However, there are examples that reach the 10 degrees.[43]

Nowadays there are two mechanisms which may lead to observe a spin canting phenomenon. The first one requires the existence of two non-equivalent sites in the network for spin carriers. Thus, for each of this centres the concomitant symmetry distortion and the spin-orbit coupling lead to a switch of the directions of the respective magnetic anisotropies. Regarding this, the magnetic moments of the metal ions localised in those non-equivalent sites become ordered in different directions. The second mechanism considers the super-exchange interaction between two magnetic centres and the local spin-orbit coupling. Thus, the fundamental and exited states function interact and then there is a splitting. This mechanism is frequently called asymmetric interaction. This interaction introduces a certain canting angle among the spins as a consequence of the stabilisation energy, which is reached when spins are oriented at 90 degrees.

Alternating Current (AC) Susceptibility: a tool for the determination of Relaxation Times.

Previously, we have defined the basic concepts and equation of Molecular Magnetism. Also the most relevant parameter that describe systems that behave as SMMs and related species have been introduced before. Herein, we thoroughly describe the possible methods to calculate the relaxation times τ and the energy barriers U_{eff}.

In general, the basic quantity studied by experimental techniques of macroscopic magnetic measurements is the magnetic moment of the sample, μ. This is a measure of the magnetic field generated by the spin carriers in the sample. Another measure of great interest, for the analysis of the magnetic properties, is the susceptibility χ, magnitude related with the magnetisation *M* by the already described equation (2). Thus, by magnetisation measurements and the use of the mentioned equation, χ value, which from now we are going to call static susceptibility (χ_{est}), is easily determined. These measurements are performed applying a static magnetic field by means of a direct electric current (abbreviated DC) and for this reason they are called DC measurements, such as susceptibility DC, χ_{DC}, magnitude equivalent to the χ_{est}.

Other types of measurements are carried on by applying alternating current (abbreviated AC). This technique measures the change in the magnetic moment, δμ. As a result, information about the slope of the magnetisation curve described by equation

0. Introduction

(1) is obtained. In this new scenario χ is now called χ$_{AC}$. All this constitute the main difference with DC measurements, which actually measure the magnitude of the μ value, as it is shown in the scheme (3).
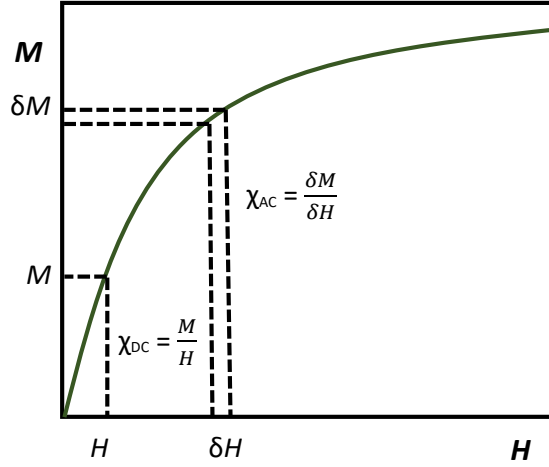
Scheme 3. Representation of a plot of M vs H. Overlapped are shown how are determined the corresponding magnitudes χ$_{DC}$ and χ$_{AC}$.

As it can be easily seen, in those areas of *M* versus *H* curve where the magnetisation is linear with the magnetic field, both susceptibilities are the same, χ$_{DC}$ = χ$_{AC}$, while in saturation the χ$_{AC}$ is cancelled.

A great advantage of AC measurements is that they can be performed both in the presence and in the absence of a static magnetic field, H$_{DC}$, as well as the possibility of changing the frequency of the alternating current. This kind of experiment is considerably relevant to provide information on the relaxation times of the magnetic moment.

During AC experiences, the AC magnetic field (alternating or oscillating magnetic field), H$_{AC}$, varies over the time as indicated by equation (15) or its equivalent equation (16), being ω equal to 2πf (f is the frequency in Hz, t, the time and h, the amplitude of the field, usually in the order of a Gauss, H$_{AC}$ << H$_{DC}$). The resulting magnetisation due to this field is given by equation (17).

$$H_{AC} = h\cos(\omega t) \tag{15}$$

$$H_{AC} = h\exp(i\omega t) \tag{16}$$

$$M_{AC} = \mu\cos(\omega t - \theta) \tag{17}$$

Equation (17) can also be rewritten as equation (18), where χ′ is the real or phase component (also called dispersive susceptibility) and χ″ is the imaginary or out of phase component (also called absorptive susceptibility).

$$M_{AC} = \chi'\cos(\omega t) + \chi''sen(\omega t) \tag{18}$$

$$\chi' = \frac{\mu\cos(\theta)}{h} = \chi_{AC}\cos(\theta) \qquad (19)$$

$$\chi'' = \frac{\mu\text{sen}(\theta)}{h} = \chi_{AC}\text{sen}(\theta) \qquad (20)$$

These equations here presented are related among them by (21) and (22):

$$\chi_{AC} = \sqrt{\chi'^2 + \chi''^2} \qquad (21)$$

$$\theta = \text{arctang}(\chi'/\chi'') \qquad (22)$$

Thus, the complex AC susceptibility is given by the combination of both of this components (23)

$$\chi_{AC} = \chi' + i\dot{\chi}'' \qquad (23)$$

The out-of-phase susceptibility, χ'', is a measure of the dissipative loss that occurs in the magnetic system under study; which means that it is a measure of the energy absorbed by the sample under the applied H_{AC}. If there is any relaxation process in the system, with a time greater than the one of the measurement, the magnetic moment cannot follow the variation of the AC field instantaneously, which leads to a non-zero value of υ – this means a loss of magnetisation phase, (17), respect from H_{AC}, (15) – and therefore a non-zero value of χ'' (the magnetic field and the magnetisation are not in phase).

Scheme 4 attempts to describe the relaxation of the spin in the presence of an external magnetic field, H_{DC}, on which an oscillating field, H_{AC} ($H_{DC} \gg H_{AC}$) is overlapped. Consider N paramagnetic ions occupying the state with $M_S = -1/2$ (moments parallel to H) or $M_S = +1/2$ (moments antiparallel to H). The presence of H_{AC} implies that the magnetic field around the ions changes over time and stimulates the transitions between the two states. Consequently, the paramagnetic N ions will be continuously redistributing between the two energy levels according to the Boltzmann distribution at a given temperature. As a matter of fact, such redistribution requires some time, τ.
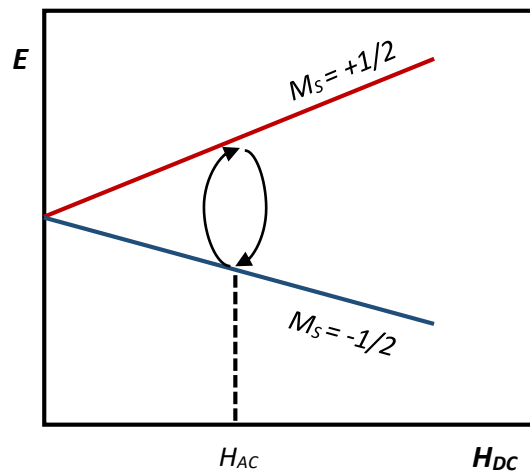
Scheme 4. Relaxation of the spin in the presence of an external magnetic field.

0. Introduction

Three different situation can be described having in account the ratio between both of the magnitudes, the relaxation time of the sample, τ, and the measurement time.

In the first situation, the variation of H_{AC}, requires a shorter time than the sample relaxation ($\omega \ll \tau^{-1}$). In this case, the magnetisation is always in equilibrium throughout the entire measurement time. In other words, the magnetic moments are always parallel to the oscillating field (the sample achieves the minimum energy). Under these conditions, AC susceptibility is called isothermal susceptibility, $\chi_{AC} = \chi_T$. Some authors call it χ_0 because its value corresponds to the susceptibility when the frequency, f, tends to zero ($f \to 0$).

Secondly, when the variation of H_{AC} is much faster than the relaxation time of the sample ($\omega \gg \tau^{-1}$), the previously mentioned equilibrium cannot be achieved, that is, the sample does not reach its minimum energy. The system is effectively isolated from its surroundings (magnetic moments are blocked and cannot be oriented with the H_{AC} field). A measure of susceptibility in these conditions reveals an adiabatic susceptibility, $\chi_{AC} = \chi_S$. Some authors write χ_∞, since it is the value of susceptibility when the frequency tends to infinity ($f \to \infty$). In general, a reduction of redistribution possibilities (of reaching equilibrium) implies a lower capacity of the magnetic system to follow the demands of the external magnetic field and consequently, $\chi_S \ll \chi_T$. Normally χ_S is very small and in some approximations it can be neglected.

Finally, when both, the measurement time and the relaxation time are of the same order, $\omega \approx \tau^{-1}$, and we assume that all the magnetic centres of the sample have the same relaxation time (they have identical transition probabilities), the complex susceptibility AC (for a given H_{DC} and a given T) can be expressed according to equation (24) proposed by Casimir and du Pré (1938).

$$\chi_{AC}(\omega) = \chi_S + \frac{\chi_T - \chi_S}{1 + i\omega\tau} \qquad (24)$$

In fact, this is the case of superparamagnetic compounds with a single relaxation time. For this compounds χ_{AC} is given by (24), as well as χ' and χ'' in this conditions are given by equations (25) and (26) respectively.

$$\chi'(\omega) = \chi_S + \frac{\chi_T - \chi_S}{1 + (\omega\tau)^2} \qquad (25)$$

$$\chi''(\omega) = \frac{(\chi_T - \chi_S)\omega\tau}{1 + (\omega\tau)^2} \qquad (26)$$

From (26) it can be deduced that the representation of χ'', as a function of frequency $\omega = 2\pi f$, presents a maximum when $\omega = \tau^{-1}$, that is when $\omega t = 1$, as shown in Figure 9a. In this figure two graphs of χ'' have been represented for the same value of τ and different values of χ_T and χ_S. It can be seen that the maximum in ordinates is $\frac{\chi_T - \chi_S}{2}$. Thus, for frequencies lower or higher than the maximum, the values of χ'' are cancelled. In Figure

9b a plot of three overlapped χ" have been represented for different relaxation times at a given temperature. There it is possible to observe that the more the decreases of system relaxation time, the higher the frequencies that are required. Thus, a representation of the values of χ", obtained at various frequencies (keeping a constant temperature), gives as a result the value of the relaxation time of the system at that temperature, when determining the maximum frequency value, $\tau(T) = \dfrac{1}{2\pi f_{max}}$. However, the mentioned τ may be determined more precisely by fitting the experimental data of χ" and f to equation (26) and determining the corresponding variables $\Delta\chi = \chi_T - \chi_S$ and τ.
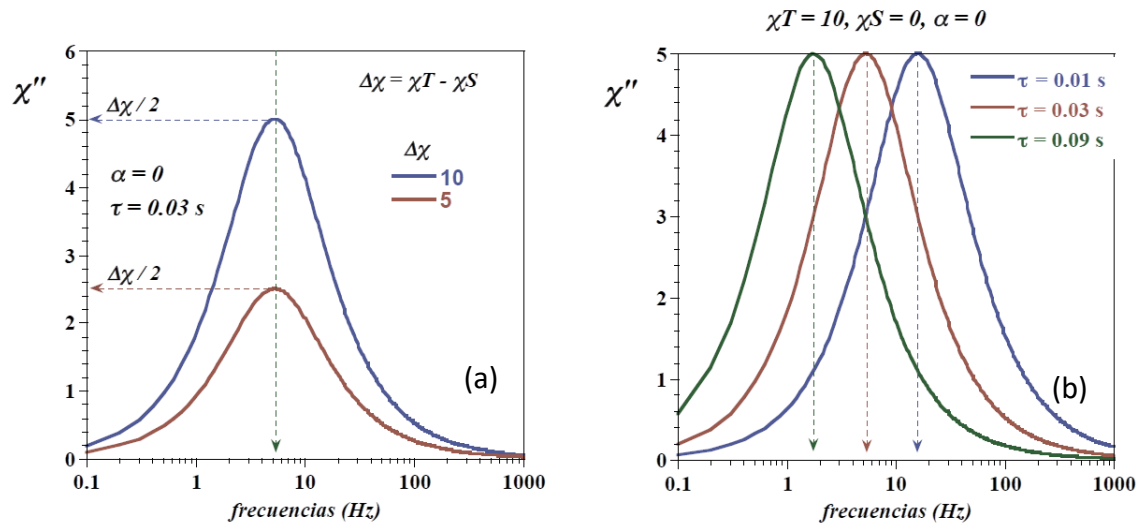
Figure 9. (a) Representation of χ" versus frequency (Hz) and the existence of a maximum at $\omega = \tau^{-1}$. (b) Representation of χ" versus frequency (Hz) at different relaxation times

The relaxation time can also be determined from χ'. In equation (25) it can be seen that when $f \to \infty$, $\chi' \to \chi_S$, while when $f \to 0$, $\chi' \to \chi_T$, as shown in Figure 10a, for various relaxation times. The curve $\chi' = f(\log f)$ presents an inflection point when $\omega = \tau^{-1}$, which corresponds also to the maximum of χ" as shown in Figure 10b. The use of equations (25) and (26) are extremely useful in an exact determination of the value of the relaxation time at a given temperature. Nevertheless, it is usually more convenient to use χ"(26) since there are only two variables to be determined (Δχ and τ) while χ' (25) has three (χ_T, χ_S and τ).

It is interesting to notice that if frequency is kept constant and the temperature varies, the relaxation time of the sample increases as the sample is cooled down. At the same time χ" presents a maximum when the measurement time agrees with the relaxation time, $\omega = \tau^{-1}$, as it was discussed before. In cases where χ_T and χ_S are constant with the temperature, the relaxation time obtained in this way coincides with that determined using equation (26). This provides two types of experiences for the determination of relaxation times: on one hand, keeping the temperature constant and varying the frequency (as indicated above) and, on the other hand, keeping the frequency constant and varying the temperature. The latter is less time consuming (but less accurate),
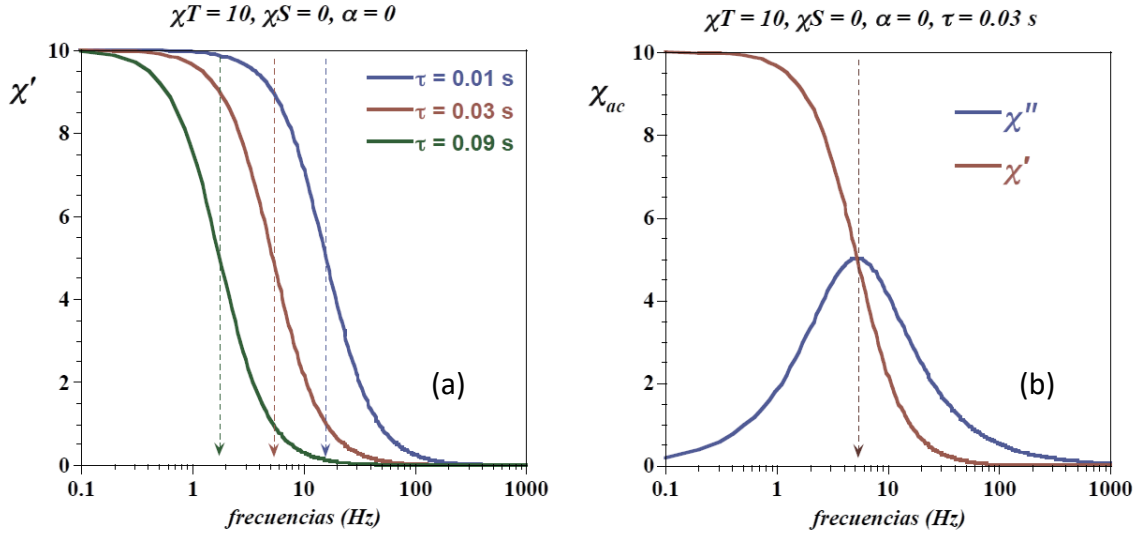
Figure 10. (a) Representation of χ'= f(log f) at different relaxation times. (b) Overlapped representation of χ'= f(log f) and χ" versus f.

therefore, the most commonly used. However, in a proper use, it must be verified that χ_T and χ_S remain constant with the temperature. In general, the temperature zone where the AC signals develop is a region where the DC susceptibility is saturated. Therefore, χ_T ($\approx\chi_{DC}$) varies very little with temperature and χ_S is very small, so the constancy is assumed for both parameters. However, it is not always the case. There are cases when both parameters vary in an unknown way leading to countless mistakes in the relaxation times determination.

Coming to this point, it is necessary to keep in mind that all of the expressed above is based on the existence of a single relaxation time for all the magnetic constituent of the system. This means, a single and identical potential barrier, U, for all of the spin carriers. Under these conditions, relaxation times vary with temperature according to Arrhenius' law, in the form expressed in equations (27) and (28).

$$\tau = \tau_0 \exp\left(\frac{U}{kT}\right) \qquad\qquad (27)$$

If in this equation τ is substituted by $\frac{1}{2\pi f}$ and τ_0 by $\frac{1}{2\pi f_0}$ the analogous Arrhenius expression of energy as a function of the frequency is obtained (28).

$$f = f_0 \exp\left(-\frac{U}{kT}\right) \qquad\qquad (28)$$

From the relaxation times obtained for different temperatures, following any of the two previously described procedures, the energy barrier, U, and the pre-exponential
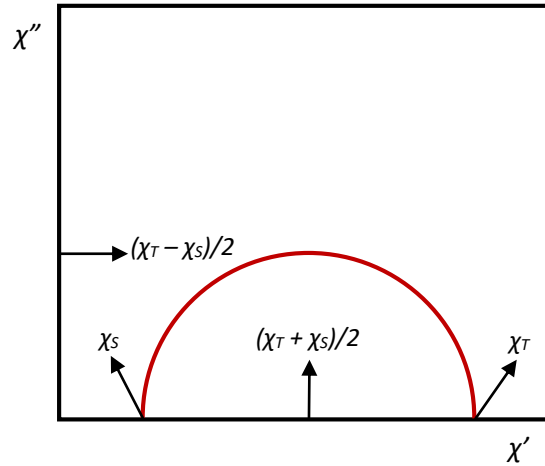
Scheme 5. Argand diagram. Scheme of plot of χ' versus χ". There are also shown the positions of the characteristics points that can be deduced from (31) and (32).

coefficient, τ_0 (or f_0) can be determined, by equation (27) or (28). These two parameters are which are normally used to characterise the slow relaxation of the magnetisation of a compound. In general, the determination is carried on by a graphical representation of the logarithm of τ versus the inverse of the temperature. As can be seen in equations (29) and (30), derived from (27). This representation leads to a line of slope U/k and ordered at the origin $\ln\tau_0$, as indicated in Figure 10 for different values of U and $\tau_0 = 10^{-8}$ seconds.

$$\text{Ln}\tau = \ln\tau_0 + (U/k)\frac{1}{T} \qquad\qquad (29)$$

$$\text{Log}\tau = \log\tau_0 + (0,4343U/k)\frac{1}{T} \qquad\qquad (30)$$

In the Superconducting Quantum Interference Device (SQUID) magnetometers, such as the one available in our Institute, a wide frequency sweep (below 1400Hz) is available and the measurements are usually performed in the range of frequencies between 0.1 and 1000Hz (lower values imply excessive measurement time). Thus, the simulated experimental points in Figure 11 correspond to temperature intervals (the temperature where the maximums of χ"are observed) of 1,9 – 3,8 K (for U = 25 cm^{-1}), 3,8 – 7,5 K (for U = 50 cm^{-1}) and 7,5 - 15 K (for U = 100 cm^{-1}) for this frequency range. As can be seen, high activation energies are required to take the blocking temperature to high temperature. In this sense, and as an example, for AC signals to be observed out of phase within the frequency range we have, an energy U = 2000 cm^{-1} would be required for $\tau_0=10^{-8}$s.

An interesting feature of this systems is that if we represent the values of χ "with respect to the corresponding ones of χ' we get a semicircle. From equations (25) and (26) equation (31) is obtained. This expression corresponds to the typical algebraic equation

of the circle indicated in (32), where (a,b) is the point where it is located the centre of the circle and r the radius of it.

$$\left[\chi' - \left(\frac{\chi_T + \chi_S}{2}\right)\right]^2 + [\chi'']^2 = \left(\frac{\chi_T - \chi_S}{2}\right)^2 \qquad (31)$$

$$(x - a)^2 + (y - b)^2 = r^2 \qquad (32)$$
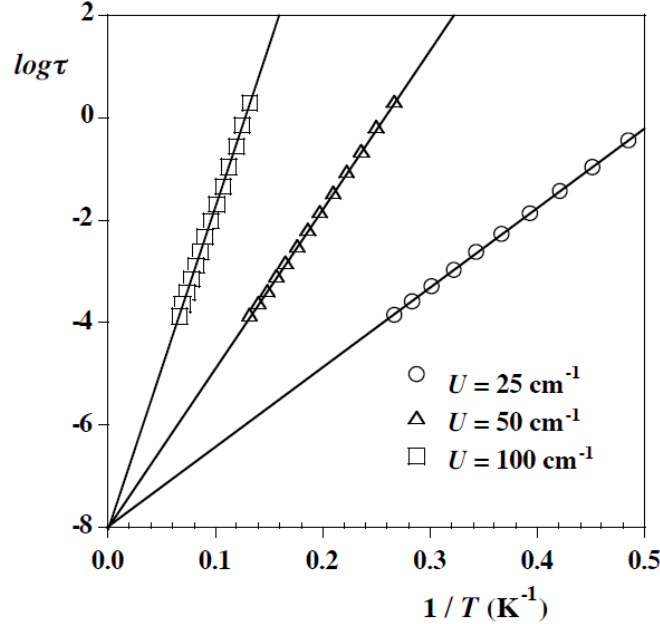
Figure 11. Plot of 1/T versus logτ for different systems with the same τ value and different U.

When comparing term to term equations (31) and (32) it is easy to notice that (31) represents, for positive values of χ' and χ'', a semicircle whose radio, r, is equal to $\frac{\chi_T - \chi_S}{2}$, and its centre at the χ' is located at the position a = $\frac{\chi_T + \chi_S}{2}$ and b = 0, as observed in Scheme 5. The relaxation time can be obtained from the frequency corresponding to the maxima χ'' = $\frac{\chi_T - \chi_S}{2}$. This way of plotting χ'' as a function of χ', normally called Argand diagram, is considerably useful since, when it occurs, to obtain a perfect semicircle is a clear proof of the existence of a single relaxation time, and with this, a unique potential barrier. It is interesting to carry out a few experiences of this type at different temperatures in order to check that a single relaxation time and the values of χ_S and χ_T remain constants with the temperature. If this comes to happen, the Argand diagrams measured at different temperatures should collapse into one. In this conditions, equation (31) is able to be used to fit the experimental data and obtain the values of χ_S and χ_T with precision. In some circumstances it is interesting to represent χ''/ω versus χ'. As shown in equation (33), deduced from (25) and (26), this representation provides a straight line of slope τ (the relaxation time at the temperature of experience) and ordered in the origin τχ_S. Any deviation would indicate the appearance of a new relaxation dynamic. This phenomenon is shown in Figure 12 where a change in relaxation time is observed.
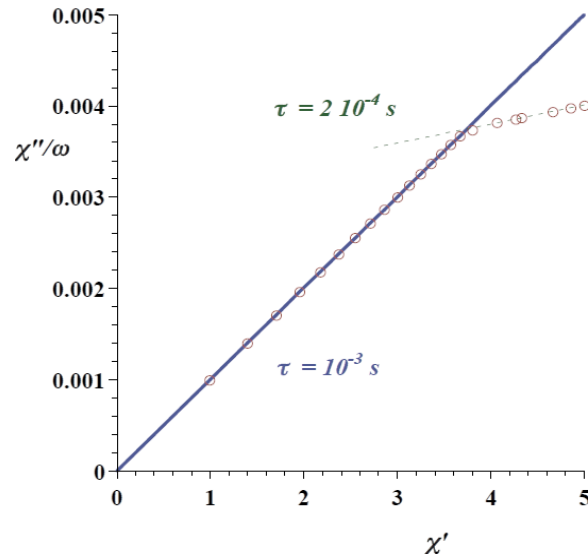
Figure 12. Plot of χ″ versus χ′. Red circles corresponds to the experimental data for a systems presenting two different relaxation times. In a continues blue line it is shown the fitting for the first observed τ and in green dotted line the fitting for the second one.

$$\frac{\chi''(\omega)}{\omega} = \tau\{\chi'(\omega) - \chi_S\} \tag{33}$$

Deviations from the ideal semicircle are rather common to be found. In general, these deviations appear as a consequence of the existence of more than one relaxation time (a certain distribution of relaxation times or potential barriers) in the sample. When this comes to happen, more or less flattened semicircles (circle arcs) are obtained and the values for the pre-exponential coefficient, τ_0, can become excessively small, that is, smaller than 10^{-13}s, losing all physical meaning. The time required for the reorientation of an electronic spin is of the order of 10^{-13}s (a frequency of 1013 reorientations per second). Given that, a shorter time would not make physical sense.

In order to take into account the indicated deviations, K.S. Cole and R.H. Cole (1941) modelled the so called dynamic susceptibility, χ_{CC} (Cole-Cole susceptibility) at a given temperature under the existence of a distribution of supposedly symmetrical relaxation times on a logarithmic time scale. The Cole-Cole formalism introduces a parameter, $0<\alpha<1$, that determines the amplitude of the relaxation times, $G(\ln\tau)$, around an average relaxation time, τ_m, equations expressed in equations (34) and (35).

$$\chi_{CC} = \chi_S + \frac{\chi_T - \chi_S}{1 + (i\omega\tau_m)^{1-\alpha}} \tag{34}$$

$$G(\ln\tau) = \frac{1}{2\pi}\left[\frac{sen(\alpha\tau)}{\cosh(1-\alpha)\ln\left(\frac{\tau}{\tau_m}\right) - \cos(\alpha\tau)}\right] \tag{35}$$

Then, equations (25) and (26) corresponding to χ′ and χ″ respectively, can be expressed as the following (36) and (37) with the introduction of the α parameter.

$$\chi'(\omega) = \chi_S + \frac{(\chi_T-\chi_S)[1+(\omega\tau)^{1-\alpha}sen(\frac{\alpha\pi}{2})]}{1+(\omega\tau)^{2(1-\alpha)}+2(\omega\tau)^{1-\alpha}sen(\frac{\alpha\pi}{2})} \quad (36)$$

$$\chi''(\omega) = \frac{(\chi_T-\chi_S)(\omega\tau)^{1-\alpha}cos(\frac{\alpha\pi}{2})}{1+(\omega\tau)^{2(1-\alpha)}+2(\omega\tau)^{1-\alpha}sen(\frac{\alpha\pi}{2})} \quad (37)$$

From this equations they can be either predicted the maximum in χ'' (38) or determine the α value which rises to the experimental maximum of χ'' (39).

$$\chi''_{max}= \frac{1}{2}(\chi_T - \chi_S)tan\left[\frac{(1-\alpha)\pi}{4}\right] \quad (38)$$

$$\alpha= 1-\frac{1}{4}arctan\left[\frac{2\chi''_{max}}{\chi_T-\chi_S}\right] \quad (39)$$

The last equation is strongly useful for determining the α value.
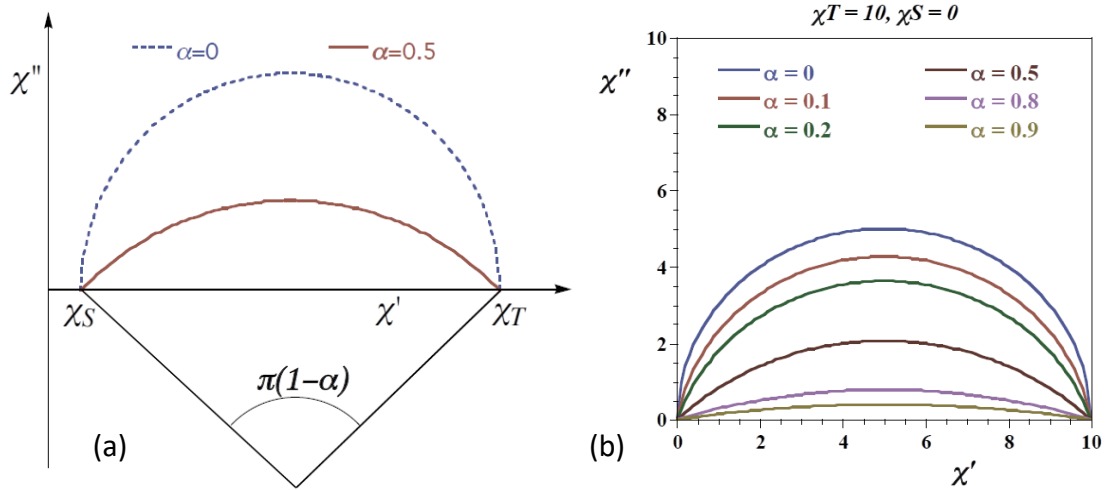
Figure 13. (a) Argand representation for twoα values and visualisation of the angle of the formed arcs for higher α values (b) Plot of χ''= f(χ') for different α values.

From (36) and (37) equation (40) can be deduced. This is the equation for an Argand representation, $\chi'' = f(\chi')$, in the case of the presence of several potential barriers. This equation leads to a semicircle when $\alpha = 0$ (a single relaxation time.) As this parameter increases, the semicircle increases, so that the angle between the axis χ' and the tangents in χ_S and χ_T are $\pm(1- \alpha)\pi/ 2$, respectively. Thus, the formed arc is defined by the angle $(1-\alpha) \pi$, as indicated in Figure 13a. An increase in the value of α indicates a greater distribution of relaxation times. When the number of relaxation times is enormously large the value of α tends to 1.

$$\chi''(\chi) = \frac{\chi_T-\chi_S}{2 \tan(1+\alpha)\pi/2} + \left\{(\chi' - \chi_S)(\chi_T - \chi') + \frac{(\chi_T-\chi_S)^2}{4tan^2(1+\alpha)\pi/2}\right\} \quad (40)$$

Figure 13b shows a series of Argand representations for different values of α. The great flattening of the semicircle for high values of α can be observed. It is interesting to note how the values of χ'' with respect to those of χ' (at the same frequency and temperature) decrease with the increase of α, so that when there is a large distribution of relaxation

times the values of χ″ can reach to be even less than 1% of those of χ′. Figure 14 shows how the curves corresponding to the real and imaginary susceptibility with the value of α are widened.
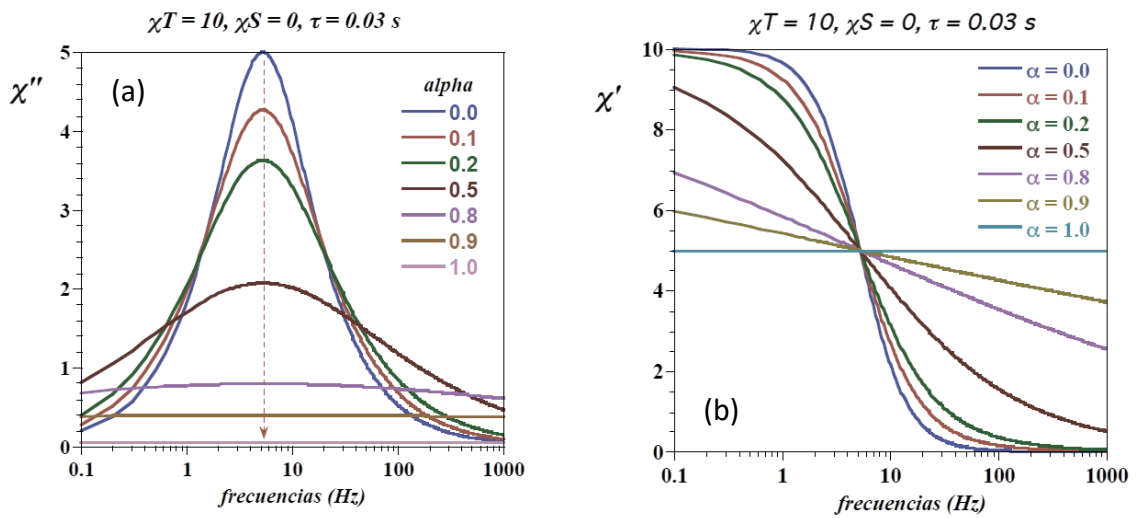
Figure 14. (a) Plot of χ″ versus f for different α values (b) Plot of χ′ versus f for different α values. The two of the plots corresponds to the same samples at the same measurement conditions.

An interesting representation is the distribution of relaxation times, G (lnτ), described by (35). This type of representation shows the relaxation times distribution around the average time, τ_m, at a given temperature. Figure 15a shows this distribution for different α values. It can be seen how the distribution widens with the value of α, that is, with the number of potential barriers. For α = 0 it would be a line while for α = 1 it would collapse with the axis of abscissa (infinite times).
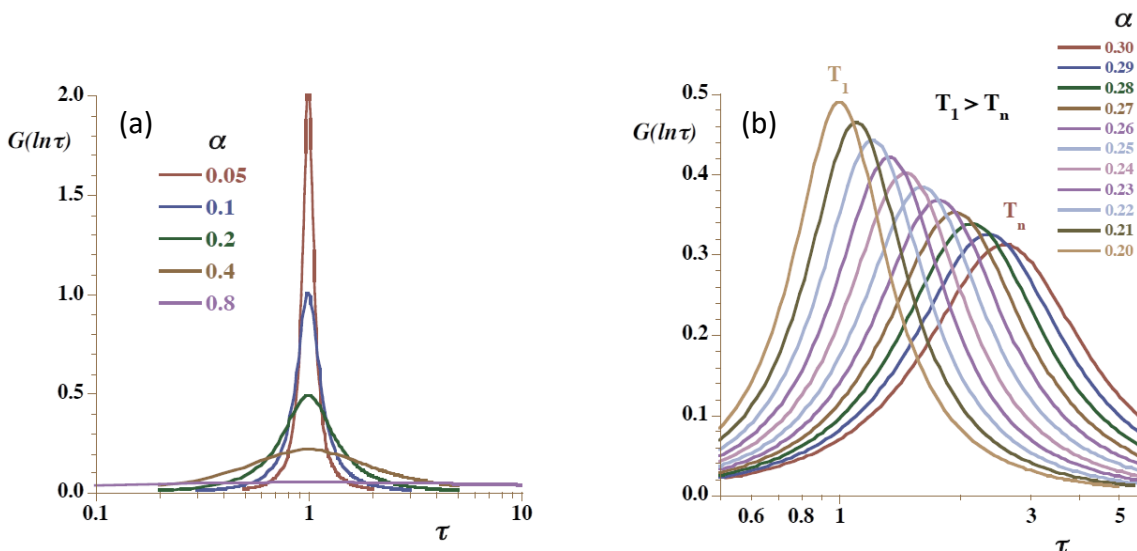
Figure 15. (a) Plot of G (lnτ) versus τ. Distribution of the relaxation times in function of the α values(b) Plot of distribution of the relaxation times for a given α value.

If intermolecular interactions happen, it is possible that as the temperature drops, these interactions begin to dominate, correlating several molecules and increasing the size of the domain molecules, with the consequent increase in relaxation times. In these cases the value of α increases as the temperature decreases. Figure 15b shows a representation of the distribution of times according to (35) for a value of α = 0.1 that increases to 0.2 when the sample is cooled. It can be seen how the dynamic evolves. As the temperature decreases, the average relaxation time increases as the probability curve widens (greater number of times).

General Objectives

The present Thesis work will be centred on the coordination chemistry, structural characterisation and the study of the magnetic properties of systems based on Mn(III) and Re(IV) metal ions. The former being a 3d metal ion while the latter is a 5d metal ion, essentially both have been here selected for the reason that, given their high anisotropy and spin values, they are among the most relevant metal ions from the Molecular Magnetism point of view.

Nowadays the knowledge and understanding of the detailed mechanisms related to 3d-based systems are considerably advanced. Nevertheless, it is not the case of the species containing 4d and 5d metal ions. In the particular case of 5d metal ions, the reported complexes are comparatively less than those based on 3d ions. Therefore, and also as a consequence of the difficulties of dealing with the theoretical aspects related to the electronic structure of the heavier metal ions, there is not a clear understanding and control of the factors that influence the magnetic anisotropy.

Hence, part of this Thesis work will be focused on Mn(III) complexes, with the attempt of improving the properties and functionalise already known systems. A second part of the research will be dedicated to Re(IV)-based systems and to obtain new species, based on this 5d metal ion, in order to contribute to a better understanding of the exchanging phenomena, as well as trying to approach these systems to new possible applications.

Herein we will attempt the functionalisation of already known and thoroughly studied Mn(III)-based systems, such as the [Mn_6] oxime-based family. The [Mn_6]s are a systematically studied family, and there exist well-known ways to modulate their magnetic properties. Thus, as good examples of inside out controlled systems, [Mn_6] are promising candidates to be functionalised an applied in fields such as molecular spintronics and molecular electronics. So that, the fact of reaching such an application establish one of the main aims in our work on [Mn_6] systems.

However, our main goal is not only that. Despite the amount of reported [Mn_6] systems, most of them are anionic species, being significantly less those which are neutral or even cationic species. Consequently, we have considered that it is necessary to develop this less explored type of [Mn_6]s, given that, by including new ligands or anionic counter-ions presenting complementary properties, these systems may be extended to new different applications.

In what Re(IV) concerns, systems containing this metal ion started to be studied from the magnetic point of view since the last years of 1990s decade. There are hundreds of Re(IV)-containing reported structures. However, there is still a huge field to be explored in what concerns the magnetic properties of these species; not only referred to those of a large nuclearity, but also to the mononuclear species.

Given the high magnetic anisotropy that Re(IV) exhibits, it is expected to observe interesting results such as those revelled by the $[Ni\{ReCl_4(ox)\}_3]^{4-}$ and $[ReX_4(ox)]^{2-}$ (X = Cl, Br) anionic complexes, the former being a SMM and the latter SIMs. In this context, cations of different nature, such as biologically active and paramagnetic cations will be used with the aim of introducing some possible multifunctionality and modification on the magnetic properties of these systems. Furthermore, we will also attempt to find new strategies of synthesis of new Re(IV)-based mononuclear species as an isomeric – selective alternative for the classical methods. For such a propose the compound of formula $[ReCl_4(MeCN)_2]$ will be used as a precursor.

Considering all of the above, we expect to do a relevant contribution to the Molecular Magnetism, not only in what the design and development of new systems concerns, but to a deep understanding of the processes involved in the magnetic exchange, as well as the progress of the field in the application of all the already reached knowledge into the new technologies, looking forward to future technological applications.

References

1. C. Benelli, D. Gatteschi, *Introduction to Molecular Magnetism*, **2015**, Wiley-VCH, Weinheim, Germany.

2. J. M. D. Coey, *Magnetism and Magnetic Materials*, **2009**, Cambridge University Press, New York, USA.

3. R.L. Carlin, *Magnetochemistry*, **1986**, Springer Berlin Heidelberg, Berlin, Heidelberg.

4. O. Kahn, *Molecular Magnetism*, **1993**, VCH Publishers, New York, USA.

5. O. Kahn, Y. Pei, M. Verdaguer, J.P. Renard, J. Sletten, *J. Am. Chem. Soc.* **1988**, 110, 782–789.

6. a) R. Sessoli and D. Gatteschi, *Angew. Chem., Int. Ed*., **2003**, 42, 268–297; (b) D. Gatteschi, R. Sessoli and J. Villain, *Molecular Nanomagnets*, **2006,** Oxford University Press, Oxford; (c) G. Aromí and E. K. Brechin, Struct. Bonding, **2006**, 122, 1–67.

7. M. J. Lehn, *Supramolecular Chemistry: Concepts and Perspectives,* **1995**, Wiley-VCH, Weinheim, Germany.

8. (a) A. Cornia, D. Gatteschi, R. Sessoli, *Coord. Chem. Rev*, **2001**, 573, 219–221; (b) D. Gatteschi, R. Sessoli, J. Villain, *Molecular Nanomagnets*, **2006**, Oxford UniversityPress, New York, USA; (c) J. Cirera, E. Ruiz, S. Alvarez, F. Neese, J. Kortus, *Chem.-Eur. J.,* **2009**, 15, 4078–4087; (d) M. Nakano, H. Oshio, *Chem. Soc. Rev.*, **2011**, 40, 3239–3248; (e) J.D. Rinehart, J.R. Long, *Chem. Sci.*, **2011**, 2, 2078–2085.

9. V. Marvaud, J.M. Herrera, T. Barilero, F. Tuyèras, R. Garde, A. Scuiller, C. Decroix, M. Cantuel, C. Desplanches, *Monatsh. Chem*., **2003**, 134, 149–156.

10. Y. Pei, Y. Journaux, O. Kahn, *Inorg. Chem.*, **1989**, 28, 100–103.

11. V. Marvaud, C. Decroix, A. Scuiller, C. Guyard-Duhayon, J. Vaissermann, F. Gonnet, M. Verdaguer, *Chem. Eur. J.,* **2003**, 9, 1678–1683.

12. (a) G. Christou, *Polyhedron*, **2005**, 24, 2065–2075; (b) M. Manini, F. Pineider, C. Danielli, F. Totti, L. Sorace, P. Sainctavit, M.A. Arrio, E. Otero, L. Joly, J.C. Cezar, A. Cornia, R. Sessoli, *Nature*, **2010**, 468, 417–421; (c) D.N. Wooddruff, R.E.P. Winpenny, R.A. Layfield, *Chem. Rev*., **2013**, 113, 5110–5148; (d) K.S. Pedersen, J. Bendix, R. Clérac, *Chem. Commun*., **2014**, 50, 4396–4415; (e) G.E. Kostakis, A.M. Ako, A.K. Powell, *Chem. Soc. Rev*., **2010**, 39, 2238–2271. (f) P. Zhang, Y.-N. Guo, J. Tang, *Coord. Chem. Rev*., **2013**, 257, 1728–1763.

13. A. Caneschi, D. Gatteschi, R. Sessoli, A. L. Barra, L. C. Brunel, M. Guillot, *J. Am. Chem. Soc.*, **1991**, 113, 5873–5875.

14. T. Lis, *Acta Crystallogr. Sect. B*, **1980**, 36, 2042–2044.

15. R. F. Weinland, G. Fischer, *Z. Anorg. Allg. Chem*., **1921**, 120, 161–180.

16. R. Sessoli, D. Gatteschi, A. Caneschi, M. A. Novak, *Nature*, **1993**, 365, 141–143.

17. L. Thomas, F. Lionti, R. Ballou, D. Gatteschi, R. Sessoli, B. Barbara, *Nature*, **1996**, 383, 145–147.

18. (a) D . A. Garanin, E. M. Chudnovsky, *Phys. Rev. B*, **1997**, 56, 11102–11119. (b) A. Fort, A. Rettori, J. Villain, D. Gatteschi, R. Sessoli, *Phys. Rev. Lett.,* **1998**, 80, 612–

616. (c) M. N. Leuenberger, D. Loss, *Europhys. Lett.*, **1999**, 46, 692–698. M. N. Leuenberger, D. Loss, *Phys. Rev. B*, **2000**, 61, 1286–1304.

19. (a) R. Sessoli, H. L. Tsai, A. R. Schake, S. Wang, J. B. Vincent, K. Folting, D. Gatteschi, G. Christou, D. N. Hendrickson, *J. Am. Chem. Soc.*, **1993**, 115, 1804–1816. (b) K. Takeda, K. Awaga, T. Inabe, *Phys. Rev. B*, **1998**, 57, 11062–11065. (c) Z. M. Sun, D. Ruiz, E. Rumberger, C. D. Incarvito, K. Folting, A. L. Rheingold, G. Christou, D. N. Hendrickson, *Inorg. Chem.*, **1998**, 37, 4758–4759. (d) D. Ruiz, Z. Sun, B. Albela, K. Folting, J. Ribas, G. Christou, D. N. Hendrickson, *Angew. Chem.*, **1998**, 110, 315–319. (e) J . An, Z.-D. Chen, J. Bian, J.-T. Chen, S.-X.Wang, S. Gao, G.-X. Xu, *Inorg. Chim. Acta*, **2000**, 299, 28–34. (f) S. M. J. Aubin, Z. M. Sun, H. J. Eppley, E. M. Rumberger, I. A. Guzei, K. Folting, P. K. Gantzel, A. L. Rheingold, G. Christou, D. N. Hendrickson*, Inorg. Chem.*, **2001**, 40, 2127–2146.

20. A. L. Barra, A. Caneschi, D. Gatteschi, D. P. Goldberg, R. Sessoli*, J. Solid State Chem*., **1999**, 145, 484–487.

21. C. J. Milios, C. Raptopoulou, A. Terzis, F. Lloret, R. Vicente, S. Perlepes, A. Escuer, *Angew. Chem*., **2004**, 43, 210–212.

22. (a) S. M. J. Aubin, N. R. Dilley, L. Pardi, J. Krzystek, M.W. Wemple, L. C. Brunel, M. B. Maple, G. Christou, D. N. Hendrickson, *J. Am. Chem. Soc*., **1998**, 120, 4991–4993. (b) E. K. Brechin, J. Yoo, M. Nakano, J. C. Huffman, D. N. Hendrickson, G. Christou, *Chem. Commun.* **1999**, 783–784. (c) A. Yamaguchi, H. Ishimoto, K. Awaga, J. S. Yoo, M. Nakano, D. N. Hendrickson, E. K. Brechin, G. Christou, *Phys. B*, **2000**, 284, 1225–1226. (d) S . Y. Wang, M. S. Wemple, J. Yoo, K. Folting, J. C. Huffman, K. S. Hagen, D. N. Hendrickson, G. Christou*, Inorg. Chem*., **2000**, 39, 1501–1513. (e) J . Yoo, E. K. Brechin, A. Yamaguchi, M. Nakano, J. C. Huffman, A. L. Maniero, L. C. Brunel, K. Awaga, H. Ishimoto, G. Christou, D. N. Hendrickson, *Inorg. Chem*., **2000**, 39, 3615–3623. (f) N . Aliaga, K. Folting, D. N. Hendrickson, G. Christou*, Polyhedron*, **2001**, 20, 1273 – 1277. (g) A. Bhattacharjee, Y. Miyazaki, M. Nakano, J. Yoo, G. Christou, D. N. Hendrickson, M. Sorai, *Polyhedron*, **2001**, 20, 1607–1612.

23. C. Delfs, D. Gatteschi, L. Pardi, R. Sessoli, K. Wieghardt, D. Hanke, *Inorg. Chem.*, **1993**, 32, 3099–3103.

24. A. L. Barra, A. Caneschi, A. Cornia, F. F. De Biani, D. Gatteschi, C. Sangregorio, R. Sessoli, L. Sorace, *J. Am. Chem. Soc,* **1999**, 121, 5302–5310.

25. (a) T. Mallah, C. Auberger, M. Verdaguer, P. Veillet, *J. Chem. Soc. Chem. Commun*., **1995**, 61–69. (b) A. Scuiller, T. Mallah, M. Verdaguer, A. Nivorozkhin, J. L. Tholence, P. Veillet, *New J. Chem*., **1996**, 20, 1–6. (c) A. Scuiller, V. Marvaud, J. Vaissermann, I. Rosenman, M. Verdaguer, *Mol. Cryst. Liq. Cryst. Sci. Technol. Sect. A*, **1999**, 334, 1165–1168. (d) Z. Salman, A. Keren, P. Mendels, A. Scuiller, M. Verdaguer, *Phys. B*, **2000**, 289–290, 106.

26. Y. C. Zhong, M. P. Sarachik, J. Yoo, D. N. Hendrickson, *Phys. Rev. B,* **2000**, 62, R9256–R9259.

27. X. Y. Wang, C. Avendaño, K. R. Dunbar, *Chem. Soc. Rev.*, **2011**, 40, 3213–3238.

28. M. P. Shores, J. J. Sokol, J. R. Long, *J. Am. Chem. Soc.,* **2002**, 124, 2279–2281.

29. H. Y. Shen, D. Z. Liao, Z. H. Jiang, S. P. Yan, *Synth. React. Inorg. Met.-Org. Chem.*, **2002**, 32, 69–80.

30. J. Martínez-Lillo, J. Faus, F. Lloret, M. Julve, *J. Coord. Chem.Rev*, **2015**, 289, 215–238.

31. J. F. Guo, W. F. Yeung, P. H. Lau, X. T. Wang, S. Gao, W. T. Wong, S. S. Y. Chui, C. M. Che, W. Y. Wong, T. C. Lau, *Inorg. Chem.*, **2010**, 49, 1607–1614.

32. J. Martínez-Lillo, D. Armentano, G. D. Munno, W. Wernsdorfer, M. Julve, F. Lloret, J. Faus, *J. Am. Chem. Soc.*, **2006**, 128, 14218–14219.

33. C. J. Milios, A. Vinslava, P. A. Wood, S. Parsons, W. Wernsdorfer, G. Christou, S. P. Perlepes, E. K. Brechin, *J. Am. Chem. Soc.*, **2007**, 129, 8–9.

34. P. H. Lin, T. J. Burchell, L. Ungur, L. F. Chibotaru, W. Wernsdorfer, M. Murugesu, *Angew. Chem. Int. Ed.*, **2009**, 48, 9489–9493.

35. (a) N. Ishikawa, M. Sugita, T. Ishikawa, S. Y. Koshihara, Y. Kaizu, *J. Phys. Chem. B,* **2004**, 108, 11265–11271. (b) N. Lopez, A. V. Prosvirin, H. Zhao, W. Wernsdorfer, K. R. Dunbar, *Chem. Eur. J.,* **2009**,15, 11390–11407. (c) A. Watanabe, A. Yamashita, M. Nakano, T. Yamamura, T. Kajiwara, *Chem. Eur. J.*, **2011**, 17, 7428–7432.

36. N. Ishikawa, M. Sugita, T. Ishikawa, S. Y. Koshihara, Y. Kaizu, *J. Am. Chem. Soc.,* **2003**, 125, 8694–8695.

37. D. E. Freedman, W. H. Harman, T. D. Harris, G. J. Long, C. J. Chang, J. R. Long, *J. Am. Chem. Soc.*, **2010**, 132, 1224–1225.

38. J. Vallejo, A. Pascual-Álvarez, J. Cano, I. Castro, M. Julve, F. Lloret, J. Krzystek, G. De Munno, D. Armentano, W. Wernsdorfer, R. Ruiz-García, E. Pardo, *Angew. Chem. Int. Ed. Engl.*, **2013**, 52, 14075–14079.

39. J. M. Zadrozny, M. Atanasov, A. M. Bryan, C. Y. Lin, B. D. Rekken, P. P. Power, F. Neese, J. R. Long, *Chem. Sci.,* **2013**, 125–138.

40. J. M. Zadrozny, J. R. Long, *J. Am. Chem. Soc.*, **2011**, 133, 2073–2074.

41. (a) R. Chiozzone, A. Cuevas, R. González, C. Kremer, D. Armentano , G. De Munno, J. Faus, *Inorganica Chimica Acta*, **2006**, 359, 2194–2200. (b) J. Martínez-Lillo, T. F. Mastropietro, E. Lhotel, C. Paulsen, J. Cano, G. De Munno, J. Faus, F. Lloret, M. Julve, S. Nellutla, J. Krzystek, *J. Am. Chem. Soc.*, **2013**, 135, 13737–13748.

42. K. S. Pedersen, M. Sigrist, M. A. Sørensen, A. L. Barra, T. Weyhermüller, S. Piligkos, C. A. Thuesen, M. G. Vinum, H. Mutka, H. Weihe, R. Clérac,J Bendix, *Angew. Chem. Int. Ed*, **2014**, 53, 1351–1353.

43. R. Carlin, *Magnetochemistry*. Springer-Verlag. Berlín, **1986**.

A.

[Mn$_6$] Systems

Introduction

The development of molecule-based magnets enabled the specific design and modification of the magnetic properties by established coordination chemistry techniques as well as the combination of magnetic properties with other mechanical, electrical and/or optical properties taking care of the simplicity of preparation.[1]

Phenolic oximes have proven to be particularly relevant in the field of molecular magnetism, especially for the preparation of Mn(III)-based SMMs.[2,3] A diverse range of oxime-derivative ligands have been employed to generate a large family of trimetallic [Mn$_3$] and hexametallic [Mn$_6$] complexes with SMM behaviour. Among the largest families of these complexes are those based on salicylaldoxime (H-saoH$_2$), salicylamidoxime (H$_2$N-saoH$_2$) and their derivatives (scheme 1).[2]
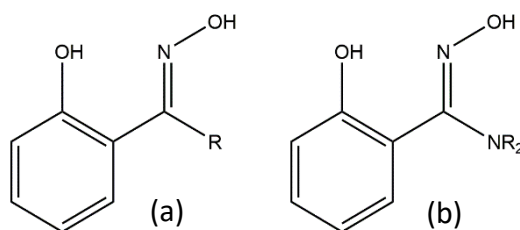
Scheme 1. Structures of (a) salicylaldoxime (R-saoH$_2$) and (b) salicylamidoxime (R$_2$N-saoH$_2$) (R = H, Me, Et).

[Mn$_3$] systems started to be characterised from the crystallographic and magnetic point of view at the same time that the first [Mn$_{12}$] structures were being reported. In the end of 1980s decade and the beginning of 1990s the first crystal structures of the non-oxime based [Mn$_3$] family were published.[4] However, as exposed in Section 0, at that time the magnetic properties studies consisted basically on routine experiments and there were neither hysteresis nor AC susceptibility measurements performed at all. Actually, it was temping to conclude that [Mn$_3$] trinuclear complexes possessing the oxide-centered [Mn$_3$(μ_3-O)] arrange could never show a SMM behaviour. Two arguments were given for assuming this claim. On one hand, the exchange interactions in the [Mn$_3$(μ_3-O)] arranges are antiferromagnetic and thus the molecules possess small or zero ground state S values and, on the other hand, their C$_3$ symmetric structure with local anisotropy axes relatively close to the Mn$_3$ plane leads to small molecular anisotropy.

It was not only until 2005, when T. C. Stamatatos *et al.* communicated their first approaches to the first trinuclear SMMs and the phenomenon of "switching on" the SMM behaviour, that it was shown that the structural distortion imposed on [Mn$_3$(μ_3-O)] complexes by binding of tridentate oximate ligands switches the exchange coupling to ferromagnetic. Thus, they were able to report the initial examples of triangular SMMs (see Figure 1).[5]

Stamatatos shown that relatively small ligand imposed structural distortions can alter the sign of the exchange interactions in [Mn$_3$(μ_3-O)] complexes and switch on the SMM

A. [Mn$_6$] Systems

behaviour. Along last decade, it came to consolidate oximate ligands as appropriate candidates to prepare SMMs.

Regarding this fact, since [Mn$_6$] complexes may be considered as dimeric species of [Mn$_3$], the comprehension of these simpler systems come to constitute a relevant contribution to complete the understanding of the magnetic properties of the former family.
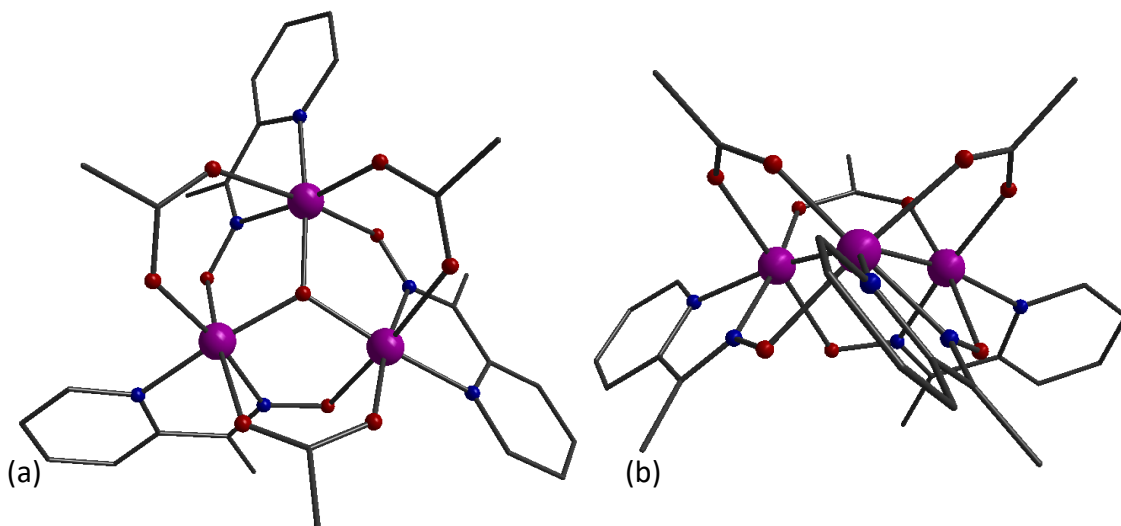
Figure 1. (a) Representation of one example of an oxime-based [Mn$_3$] in the C$_3$ symmetry axis direction. (b) Representation of [Mn$_3$] in the direction of the *a* axis. Hydrogen atoms are omitted for clarity. Code colour: violet, Mn; blue N; red O; grey, C atoms.

However, the known succeed of [Mn$_6$] family (reported at the first time by Milios *et al.*)[2a] was independent from knowledge reached throughout these [Mn$_3$] monomers. Actually, it was in 2004 when Milios *et al.* reported the first example of this [Mn$_6$] SMMs family. Three years later, in 2007, Milios *et al.* reported their study on the magneto-structural correlation on a [Mn$_6$] family,[6] where they went a step farther in the description of the this correlation present into each of the [Mn$_3$(μ_3-O)] arranges of the structure. Although they lacked an exact quantitative mathematical expression, the collected data (12 fully characterised [Mn$_6$] complexes consisting of the same dimeric structure containing two [Mn$_3$(μ_3-O)] units per molecule) clearly demonstrated that for this family of complexes it was possible not only to "control" and "understand" the nature of the spin ground state of a particular complex but also to predict the ground states of any new member of the [Mn$_6$] family. The distortion of the torsion angles (*see Figure 2*) allows to change the spin ground state from S = 4 to S = 12, in a stepwise fashion, passing through the S = 5, 6, 7, 9, and 11 intermediate ground states. There was evidence enough to assume that the steric hindrance introduced by the employed oximate ligands was determining for the reached distortion in the angles. They were able to establish a relation between this phenomenon and the magnetic behaviour of the complexes, and finally, it was postulated that for torsion angles smaller than 27.8° the expected intramolecular coupling was antiferromagnetic, whereas for those torsion angles higher than 34.0° the coupling must be ferromagnetic.[7]
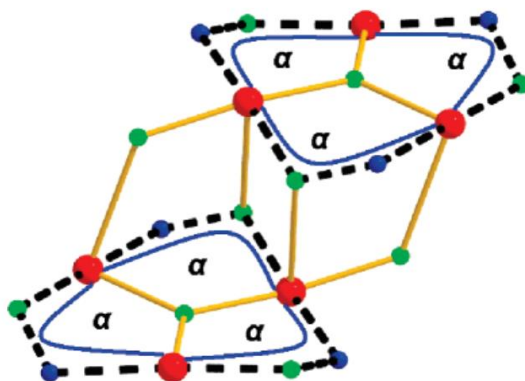
Figure 2. Molecular core of the complexes of the [Mn$_6$] family, highlighting the Mn-N-O-Mn torsion angles (α).

At this point it is necessary to recall the highlight of this huge family of complexes, which was mentioned in the previous section, the [Mn$_6$O$_2$(Et-sao)$_6$(O$_2$CPh(Me)$_2$)$_2$(EtOH)$_6$] complex, whose anisotropy barrier (U$_{eff}$ = 86.4 K) reached the record value for a 3d-based SMM.[2b] This contribution was also reported by Milios *et al* in the very prolific year 2007.

Later, the exchange coupling constants were studied deeper both experimentally, by dc susceptibility, and theoretically, by density functional theory (DFT calculations),[8] and showed that there is a clear dependence among the sign and magnitude of magnetic exchange between the Mn(III) metal ions and the Mn-N-O-Mn torsion angle. In the case of complexes based on H$_2$N-saoH ligand, angles larger than 27.0° lead to ferromagnetic exchange generating high spin SMMs.[7,9]

These Mn-N-O-Mn torsion angles may be easily modified by different strategies already explored, such as oxime functionalisation. Other type of modifications is commonly performed by means of different coordinating solvents. The solvents may coordinate the metal ions and, by steric hindrance, induce distortions in the torsion angles.[9]

Changing the anions may modify the crystal packing of the cationic [Mn$_6$] complexes and, indirectly, alter intramolecular angles. This fact makes the exchanging of the anions of [Mn$_6$]$^{2+}$ salts another useful strategy to be explored. In addition, the use of anions that may bring another physical property or functionality to the material, such as conductivity, luminescence or dynamic relaxation increasing the U$_{eff}$ value of [Mn$_6$] family. For instance, the exchange of ClO$_4^-$ by [ReCl$_6$]$^{2-}$, a paramagnetic anion, clearly modifies the magnetic behaviour of the material.[10]

Besides, nowadays it is of a great interest to develop multifunctional materials. In that sense, SMMs have attracted much attention because of their spin properties and potential applications. The use of auxiliary ligands constitute a good strategy not only to modify the properties but also to attach complementary functionalities into the complexes.

Hence, as a continuation of our investigation on [Mn$_6$] SMMs, we have explored the synthesis of systems with azole-type ligands, in particular benzotriazole and 5-phenyl-tetrazole (see Scheme 2). Benzotriazole and its derivatives constitute a family of versatile heterocyclic compounds with properties that make them very useful in a wide variety of different research fields.[11] Moreover, the good chelating ability of the 5-phenyl-tetrazole together with the presence of its four N atoms allow this ligand to be very suitable for metal coordination and supramolecular assembling.[12] Nevertheless, no crystal structure based on manganese and 5-phenyl-tetrazole has been reported so far.
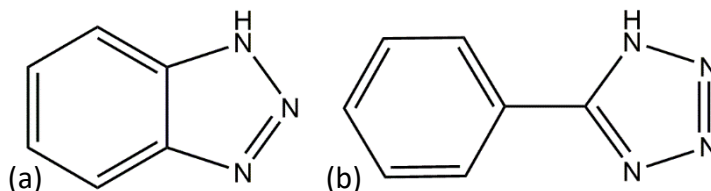
Scheme 2. Structures of (a) benzotriazole (Hbta) and (b) 5-phenyl-tetrazole (Hpta).

On top of all above already mentioned, our work not only attempt to develop new functionalities but to explore the possibility of using the already developed materials in devices at nanoscale level. Since the hysteresis cycle at low temperatures was observed in [Mn$_{12}$], SMMs started to be thought as a possible magnetic storage information material. The fact that magnetic hysteresis in SMMs arises from a purely molecular mechanism rather than from bulk magnetic interaction was firmly established by magnetic dilution experiments.[13] Practical applications of SMMs for both, information storage and "qubits", require the addressing of individual molecules and eventually manipulating individual systems. To deposit the target molecules on a suitable substrate is among the most used techniques to perform such addressing. By using this technique, molecules are deposited individually. The process is performed in scanning tunnelling microscopy (STM), atomic force microscopy (AFM), and magnetic force microscopy (MFM).[14] The former has become particularly interesting for many researchers because of the study of the interplay between charge transport and the magnetic properties of the complexes.

In 2003, Cornia et al. reported a method to deposit derivatized [Mn$_{12}$] complexes on gold films. Then, the authors were able, for the first time, to observe these molecules directly at single-molecule level by STM. It was suggested that, since the complex itself is not capable to adhere to gold surfaces in a stable fashion, it needs to be functionalised. Given that, their work was carried on gold monolayers, the authors suggested that thiol and thioester groups as suitable groups to fix the complexes on the surface, because of the well-known affinity of gold for sulphur.[15] However, treatment of preformed molecules with thiol derivatized ligands afforded intractable solids, presumably as a result of the oxidative instability of free thiols in the presence of Mn(III) centers. In contrast, the use of the corresponding acetyl-protected acid yielded to a fully-substituted derivative compound, which was highly soluble in organic solvents. Hence,

thioester derivatized ligands revelled to be the most suitable functionalizing agents for these Mn(III)-containing molecules.

Subsequently, a great research effort has been devoted to the synthesis of single-molecule systems, with large magnetic anisotropies, and their functionalisation, which is made with functional groups convenient to connect suitable SMMs to junction devices or to perform their grafting on surfaces of Si or Au substrates; in many cases, looking for the improvement of their magnetic properties, the control of the nanoscale organisation or simply to get a reliable description of the electronic structure of the investigated system.[16]

Thioesters-based ligands have proven to be particularly useful to get derivatised and suitable SMMs for this research field. Indeed, [Fe$_4$Ni$_4$] cages have been connected to junction devices,[15d] besides that and apart from [Mn$_{12}$], complexes such as the well-known [Fe$_4$] and [Fe$_3$Cr] systems with star-like structures have been grafted on Au surfaces after being functionalised with thioester groups.[13]

Aliphatic chains are expected to be more isolating than the conjugated ones. Nevertheless, they provide a quite stable system that may be useful to start studying the capability of these type of complexes for connecting junction devices.

In the literature, the aliphatic chains which have been used to functionalize the above-mentioned complexes are normally between 10 and 16 carbon atoms long. This length is strongly important because it determines if molecule will be able to connect electrodes of the device or not. For instance, Cornia *et al.* have used 16-(acetylthio)hexadecanoic acid to functionalize [Mn$_{12}$] complexes.[14] Nevertheless, in the last years, with the development of more powerful technologies, the size of nanodevices have become even smaller and even shorter molecules have been used to connect electrodes. Hence, herein we decided to functionalize our [Mn$_6$] systems with short auxiliary ligands in order to find suitable compounds to connect junction devices. The auxiliary ligands chosen in this work are 3- (acetylthio)propionic acid (3-hatpa) and 6-(acetylthio)hexanoic acid (6-hatha); (see Scheme 3).
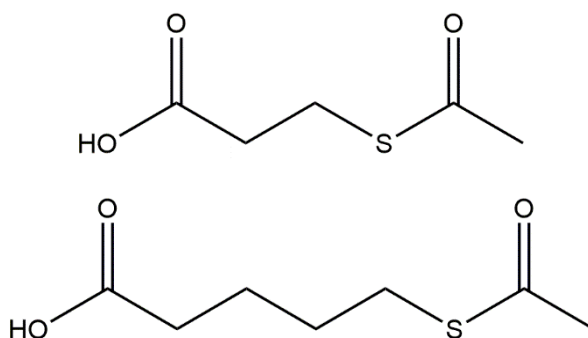
Scheme 3. Molecular structures of thioester-carboxylate ligands; 3-hatpa (top), 6-hatha (bottom).

Objectives

Given the amount of work accumulated and the more than one hundred [Mn$_6$] structures already reported, one could be tempted to think that, all what could be done with these systems is already done. However, as this work aim to demonstrate, there are still relevant aspects to be studied.

First of all, a search on the Cambridge Structural Database (CSD) revealed that, despite the huge amount of reported structures of [Mn$_6$] systems, only six were cationic [Mn$_6$]$^{2+}$ species, all of the other are neutral. The strategy of introducing specific modification to known cationic systems in order to improve their magnetic properties is going to be approached in the present work. Furthermore, modifications will be introduced as a trial to improve the already studied magnetic properties of [Mn$_6$] systems. This strategy will be carried on by changing the coordinating solvents which complete the coordination sphere of the Mn(III) centers in the oxime-based complexes (the typically used ethanol or methanol by, dimethylformamide or pyridine for instance), and employing new anions.

In addition, we will explore the use of new terminal ligands with the attempt of modifying the Mn-N-O-Mn torsion angles and thus the magnetic properties of the [Mn$_6$] complexes. The ligands to use in this section would be able to lead to a good approach to the synthesis and characterisation of new systems based on azole ligands, which belong to a family of versatile heterocyclic compounds with properties that make them very useful in a wide variety of different research fields.

Finally, SMMs have been considered a fundamental link between two novel scientific disciplines, molecular spintronics and molecular electronics. Since neutral [Mn$_6$] complexes constitute the wider group of compounds of the family, which makes them the most characterised and systematised systems, they are the most recommendable species to be used to go a step farther, that is, to the functionalisation. Based on the previous experiences reported in the literature, we consider the possibility of functionalising [Mn$_6$] molecules in order to connect them to junction devices as a good approach to find a direct application of this huge family in devices at nanoscale level. The use of the appropriate ligands may be crucial to achieve the aims of both functionalising and connecting the [Mn$_6$] SMMs.

Regarding the above, this work has the aim of exploring in a didactic way the chemistry and characterisation of a well-known SMMs family, as well as, improving of their magnetic properties.

References

1. J. S. Miller, A. J. Epstein, *Angew. Chem., Int. Ed. Engl.*, **1994**, 33, 385–415; (b) J. S. Miller, A. J. Epstein, *Chem. Br.*, **1994**, 477–479.

2. (a) C. J. Milios, C. P. Raptopoulou, A. Terzis, F. Lloret, R. Vicente, S. P. Perlepes, A. Escuer*, Angew*. *Chem., Int. Ed.*, **2004**, 43, 210–212; (b) C. J. Milios, A. Vinslava, P. A. Wood, S. Parsons, W. Wernsdorfer, G. Christou, S. P. Perlepes, E. K. Brechin, *J. Am. Chem. Soc.*, **2007**, 129, 8–10; (c) C. J. Milios, A. Vinslava, W. Wernsdorfer, A. Prescimone, P. A. Wood, S. Parsons, S. P. Perlepes, G. Christou, E. K. Brechin*, J. Am. Chem. Soc*., **2007**, 129, 6547–6549.

3. G.-Y. An, A.-L. Cui and H.-Z. Kou, *Inorg. Chem. Commun*., **2011**, 14, 1475–1478.

4. (a) J. B. Vincent, H.- R. Chang, K. Folting, J. C. Huffman, G. Christou, D. N. Hendrickson, *J. Am. Chem. Soc.,* **1987**, 109, 5703–5704; (b) J. K. McCusker, H. G. Jang, S. Wang, G. Christou, D. N. Hendrickson, *Inorg. Chem*. **1992**, 31, 1874–1880; (c) J. B. Vincent, H.-L. Tsai, A. G. Blackman, S. Wang, P. D. W. Boyd, K. Folting, J. C. Huffman, E. B. Lobkovsky, D. N. Hendrickson, Christou G., *J. Am. Chem. Soc*., **1993**, 115, 12353–12355.

5. T. C. Stamatatos, D. Foguet-Albiol, S.-C. Lee, C. C. Stoumpos, C. P. Raptopoulou, A. Terzis, W. Wernsdorfer, S. O. Hill, S. P. Perlepes, G. Christou*, J. Am. Chem. Soc.,* **2007**, 129, 9484–9499.

6. C. J. Milios, A. Vinslava, W. Wernsdorfer, S. Moggach, S. Parsons, S. P. Perlepes, G. Christou, E. K. Brechin, *J. Am. Chem. Soc*., **2007**, 129, 2754–2755.

7. A. Tomsa, J Martínez-Lillo, Y. Li, L. Chamoreau, K. Boubekeur, F. Farias, M. Novak, E. Cremades, E. Ruiz, A. Proust, M. Verdaguer, P. Gouzerh, *Chem. Commun*., **2010**, 46, 5106–5108.

8. E. Cremades, J. Cano, E. Ruiz, G. Rajaraman, C. J. Milios, E. K. Brechin, *Inorg. Chem*., **2009**, 48, 8012–8019.

9. J. Martínez-Lillo, A. R. Tomsa, Y. Li, L. M. Chamoreau, E. Cremades, E. Ruiz, A. L.Barra, A. Proust, M. Verdaguer, P. Gouzerh, *Dalton Trans*., **2012**, 41, 13668–13681.

10. J. Martínez-Lillo, J. Cano, W. Wernsdorfer, E. K. Brechin, *Chem. Eur. J.,* **2015**, 21, 8790–8798.

11. (a) F. Giordano, *Acta Crystallogr*, **1980**, *Sect. B 36,* 2458–2459. (b) I. Sotofte, K. Nielsen*, Acta Chem. Scand*, **1981**, *Ser. A 35,* 739–741. (c) J. Emsley, N. M. Reza, H. M. Dawes, M. B. Hursthouse, *Chem.* Commun., **1985**, 1458–1460. (d) X.-G. Meng, J.-L. Qian, *Acta Crystallogr.,* **2006**, *Sect. E 62,* 4178–4179.

12. (a) C. Yélamos, K.R. Gust, A.G. Baboul, M.J. Heeg, H.B. Schlegel, C.H. Winter, *Inorg. Chem*, **2001**, 40, 6451–6462. (b) R. Guilard, I. Perrot, A. Tabard, P. Richard, C. Lecomte, Y.H. Liu, K.M. Kadish, *Inorg. Chem*, **1991**, 30, 27–37. (c) M. Saha, R. Nasani, S.M. Mobin, B. Pathak, S. Mukhopadhyay, *Inorg. Chem. Commun*., **2013**, 34, 62–67. (d) J. Lach, E. Perlt, B. Kirchner, *Z. Anorg. Allg. Chem*., **2013**, 639, 524–532.

13. M. R. Cheesman, V. S. Oganesyan, R. Sessoli, D. Gatteschi, A. J. Thomson, *Chem. Commun*., **1997**, 17, 1677–1678.

14. a) A. Ulman, *Chem. Rev*., **1996**, 96, 1533 – 1554; b) S. A. Levi, P. Guatteri, F. C. J. M. Van Veggel, G. J. Vancso, E. Dalcanale, D. N. Reinhoudt, *Angew. Chem*., **2001**, 113, 1945–1947.

15. A. Cornia, A. C. Fabretti, M. Pacchioni, L. Zobbi, D. Bonacchi, A. Caneschi, D. Gatteschi, R. Biagi, U. Del Pennino, V. De Renzi, L. Gurevich, H. S. J. Van der Zant, *Angew. Chem. Int. Ed.*, **2003**, 42, 1645–1648.

16. (a) D. Li, S. Parkin, R. Clérac, S. M. Holmes, *Inorg. Chem.,* **2006**, 45, 7569–7571. (b) L. Gregoli, C. Danieli, A. L. Barra, P. Neugebauer, G. Pellegrino, G. Poneti, R. Sessoli, A. Cornia, *Chem. Eur. J.*, **2009**, 15, 6456–6467. (c) F. Moro, V. Corradini, M. Evangelisti, V. De Renzi, R. Biagi, U. del Pennino, C. J. Milios, L. F. Jones, E. K. Brechin, *J. Phys. Chem. B*, **2008**, 112, 9729–9735. (d) F. Totti, G. Rajaraman, M. Iannuzzi, R. Sessoli, *J. Phys. Chem. C*, **2013**, 117, 7186–7190. (e) F. Moro, V. Corradini, M. Evangelisti, R. Biagi, V. De Renzi, U. del Pennino, J. C. Cezar, R. Inglis, C. J. Milios, E. K. Brechin, *Nanoscale*, **2010**, 2, 2698–2703. (f) P. Tyagi, D. Li, S. M. Holmes, B. J. Hinds, *J. Am. Chem. Soc.*, **2007**, 129, 4929–4938.

Article 1.

Ferromagnetic Oxime-Based Manganese(III) Single-Molecule Magnets with Dimethylformamide and Pyridine as Terminal Ligands

Ferromagnetic Oxime-Based Manganese(III) Single-Molecule Magnets with Dimethylformamide and Pyridine as Terminal Ligands

Carlos Rojas-Dotti, Nicolás Moliner, Francesc Lloret and José Martínez-Lillo *

Instituto de Ciencia Molecular (ICMol), Universitat de València, C/Catedrático José Beltrán 2, 46980 Paterna, Valencia, Spain; carlos.rojas@uv.es (C.R.-D.); fernando.moliner@uv.es (N.M.); francisco.lloret@uv.es (F.L.)

* Correspondence: f.jose.martinez@uv.es; Tel.: + 34-963-544-460

Abstract: Two new members of the [Mn_6] family of single-molecule magnets (SMMs) of formulae [$Mn_6(\mu_3\text{-}O)_2(H_2N\text{-}sao)_6(dmf)_8$]($ClO_4$)$_2$ (**1**) and [$Mn_6(\mu_3\text{-}O)_2(H_2N\text{-}sao)_6(py)_6(EtOH)_2$][$ReO_4$]$_2 \cdot 4EtOH$ (**2**), (dmf = *N*,*N'*-dimethylformamide, py = pyridine, $H_2N\text{-}saoH_2$ = salicylamidoxime) have been synthesized and characterized structurally and magnetically. Both compounds were straightforwardly prepared from the deprotonation of the $H_2N\text{-}saoH_2$ ligand in the presence of the desired manganese salt and solvent (dmf (**1**) vs. py (**2**)). Compound **1** crystallizes in the triclinic system with space group *P*$\bar{1}$ and **2** crystallizes in the monoclinic system with space group *P*2$_1$/n. In the crystal packing of **1** and **2**, the (ClO_4)$^-$ (**1**) and [ReO_4]$^-$ (**2**) anions sit between the cationic [Mn_6]$^{2+}$ units, which are H-bonded to $-NH_2$ groups from the salicylamidoxime ligands. The study of the magnetic properties of **1** and **2** revealed ferromagnetic coupling between the Mn^{III} metal ions and the occurrence of slow relaxation of the magnetization, which is a typical feature of single-molecule magnet behavior. The cationic nature of these [Mn_6]$^{2+}$ species suggests that they could be used as suitable building blocks for preparing new magnetic materials exhibiting additional functionalities.

Keywords: manganese(III); salicylamidoxime; molecular magnetism; single-molecule magnets

1. Introduction

Single-molecule magnets (SMMs) have attracted a great deal of attention during the last two decades [1], because of their potential applications in quantum information processing [2], low-temperature cooling [3], and molecular spintronics [4,5]. Most of the reported SMMs are based on paramagnetic 3D metal ions, the Mn^{III} ion being one of the more explored in this multidisciplinary research [6].

In this context, the combination of phenolic oximes and Mn^{III} has proven to be particularly successful in the preparation of SMMs [7]. Thus, a large family of hexanuclear [Mn^{III}_6] complexes based on salicylaldoxime and salicylamidoxime ligands (Scheme 1), along with their derivatives, has been investigated [8–20]. All the family members display the SMM phenomenon, with remarkably different magnetic behavior, antiferromagnetic or ferromagnetic, that is strongly affected by the structural distortion of the Mn–N–O–Mn torsion angles. As a result, it established a semi-quantitative magnetostructural correlation that enables the prediction of the magnetic behavior of new [Mn^{III}_6] systems [8–20].

A search on the Cambridge Structural Database (CSD) revealed more than 100 hits of discrete [Mn^{III}_6] molecules based on salicylaldoxime and salicylamidoxime ligands. However, only six of them were cationic [Mn^{III}_6]$^{2+}$ systems, the rest being neutral complexes [17–19]. This singular type of SMMs suggests that they could be used as suitable building blocks for preparing new magnetic materials,

just by replacing the anion by another anionic species exhibiting an additional functionality [17–19]. For that reason, we are motivated to investigate the crystal structure and magnetic properties of cationic [Mn$^{III}_6$]$^{2+}$ SMMs.
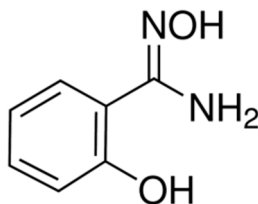
Scheme 1. Structure of the salicylamidoxime ligand (H$_2$N-saoH$_2$).

Herein we report two novel cationic [Mn$_6$]$^{2+}$ complexes with the formulae [Mn$_6$(μ_3-O)$_2$(H$_2$N-sao)$_6$(dmf)$_8$](ClO$_4$)$_2$ (**1**) and [Mn$_6$(μ_3-O)$_2$(H$_2$N-sao)$_6$(py)$_6$(EtOH)$_2$][ReO$_4$]$_2$·4EtOH (**2**) (dmf = *N*,*N'*-dimethylformamide, py = pyridine, H$_2$N-saoH$_2$ = salicylamidoxime), which have been characterized structurally and magnetically. Both **1** and **2** behave as SMMs.

2. Materials and Methods

2.1. Reagents and Instruments

All manipulations were performed under aerobic conditions, using materials as received (reagent grade). Although no problems were encountered in this work, care should be taken when using the potentially explosive perchlorate anion. The salicylamidoxime ligand was prepared following the synthetic method described in the literature [21].

Elemental analyses (C, H, N) were performed with a CE Instruments CHNS 1100 Elemental Analyzer (samples of 25 (**1**) and 20 mg (**2**)) by the Central Service for the Support to Experimental Research (SCSIE) at the University of Valencia. Infrared spectra of **1** and **2** were recorded with a PerkinElmer Spectrum 65 FT-IR spectrometer in the 4000–400 cm^{-1} region. Variable-temperature, solid-state direct current (DC) magnetic susceptibility data down to 2.0 K were collected on a Quantum Design MPMS-XL SQUID magnetometer equipped (Quantum Design, Inc., San Diego, CA, USA) with a 7 T DC magnet. The experimental magnetic data were corrected for the diamagnetic contributions of the constituent atoms (-990.3×10^{-6} (**1**) and -1219.8×10^{-6} emu mol^{-1} (**2**)) and also for the sample holder (-3.58×10^{-6} and -3.45×10^{-6} emu g^{-1} for **1** and **2**, respectively).

2.2. Single-Crystal X-Ray Diffraction

X-ray diffraction data of single crystals of dimensions 0.26 × 0.16 × 0.04 (**1**) and 0.39 × 0.31 × 0.24 mm^3 (**2**) were collected on a Bruker D8 Venture diffractometer with PHOTON II detector and by using monochromatized Mo-K$_\alpha$ radiation (λ = 0.71073 Å). Crystal parameters and refinement results for **1** and **2** are summarized in Table 1.

The structures were solved by standard direct methods and subsequently completed by Fourier recycling by using the SHELXTL software packages. The obtained models were refined with version 2013/4 of SHELXL against F^2 on all data by full-matrix least squares [22]. In both systems, all non-hydrogen atoms were refined anisotropically, and the hydrogen atoms were set in calculated positions and refined isotropically by using the riding model. The highest difference Fourier map peaks were 2.262 (**1**) and 1.282 eÅ^{-3} (**2**), which are located at 0.935 Å of Cl(1) and at 1.029 Å of Re(1), respectively. The graphical manipulations were performed with the DIAMOND program [23].

CCDC numbers for **1** and **2** are 1882221 and 1882222, respectively. These data can be obtained free of charge from the Cambridge Crystallographic Data Center on the web (http://www.ccdc.cam.ac.uk/data_request/cif).

Table 1. Summary of the crystal data and structure refinement for **1** and **2**.

Compound	1	2
CCDC	1882221	1882222
Formula	$C_{66}H_{92}O_{30}N_{20}Cl_2Mn_6$	$C_{84}H_{94}O_{28}N_{18}Mn_6Re_2$
$Mr/g \cdot mol^{-1}$	2046.13	2505.81
Crystal system	triclinic	monoclinic
Space group	$P\bar{1}$	$P2_1/n$
$a/Å$	12.603(8)	13.446(2)
$b/Å$	13.256(8)	23.254(4)
$c/Å$	14.501(9)	16.458(3)
$\alpha/°$	114.71(2)	90
$\beta/°$	98.09(2)	105.06(2)
$\gamma/°$	100.59(2)	90
$V/Å^3$	2098.2(2)	4649.1(1)
Z	1	2
$D_c/g \cdot cm^{-3}$	1.619	1.675
$\mu(MoK_\alpha)/mm^{-1}$	1.032	3.244
$F(000)$	1052	2496
Crystal size	$0.26 \times 0.16 \times 0.04$	$0.39 \times 0.31 \times 0.24$
Goodness-of-fit on F^2	1.079	1.047
R_1 $[I > 2\sigma(I)]$	0.0623	0.0537
wR_2 $[I > 2\sigma(I)]$	0.1731	0.1596
$\Delta\rho_{max,\,min}/e\,Å^{-3}$	2.262, −1.549	1.282, −2.359

2.3. Preparation of the Compounds

2.3.1. Synthesis of $[Mn_6(\mu_3\text{-O})_2(H_2N\text{-sao})_6(dmf)_8](ClO_4)_2$ (**1**)

$Mn(ClO_4)_2 \cdot 6H_2O$ (0.249 g, 0.688 mmol) was dissolved with continuous stirring in dmf (10 mL); then, $H_2N\text{-saoH}_2$ (0.103 g, 0.670 mmol) and NEt_3 (0.5 mL, 3.6 mmol) were added. The resulting dark green mixture was stirred for 1 h, filtered and layered with Et_2O (10 mL). Dark green crystals suitable for X-ray diffraction were obtained in 4 days. Yield: 80%. Elemental analysis calculated (found) for $C_{66}H_{92}O_{30}N_{20}Cl_2Mn_6$ (**1**): C, 39.1 (39.7); H, 5.2 (5.0); N, 13.8 (13.9)%. Selected IR data (in KBr/cm^{-1}): 3332 (m), 2925 (w), 1653 (vs), 1610 (vs), 1533 (m), 1438 (m), 1384 (m), 1317 (m), 1253 (m), 1150 (m), 1121 (s), 1109 (s), 1022 (m), 881 (m), 762 (w), 685 (s), 649 (m), 578 (w).

2.3.2. Synthesis of $[Mn_6(\mu_3\text{-O})_2(H_2N\text{-sao})_6(py)_6(EtOH)_2][ReO_4]_2 \cdot 4EtOH$ (**2**)

$Mn(NO_3)_2 \cdot 4H_2O$ (0.173 g, 0.688 mmol) was dissolved with continuous stirring in EtOH (20 mL), then $H_2N\text{-saoH}_2$ (0.103 g, 0.670 mmol) was added, followed by pyridine (1 mL, 12.4 mmol) and NEt_3 (0.1 mL, 0.72 mmol). Next, $(NH_4)[ReO_4]$ (0.184 g, 0.688 mmol) was added to the dark green solution, which was stirred for 1 h. The final dark brown solution was left to evaporate in a fume hood at room temperature. Crystals of **2** were obtained in 3 days and were suitable for X-ray diffraction. Yield: 70%. Elemental analysis calculated (found) for $C_{84}H_{94}O_{28}N_{18}Mn_6Re_2$ (**2**): C, 40.3 (40.8); H, 3.8 (4.0); N, 10.1 (9.9)%. Selected IR data (in KBr/cm^{-1}): 3426 (vs), 3314 (vs), 1614 (vs), 1564 (m), 1529 (s), 1483 (w), 1442 (s), 1384 (w), 1311 (w), 1251 (w), 1147 (vw), 1022 (m), 910 (s), 881 (m), 755 (w), 683 (m), 642 (w), 580 (vw).

3. Results and Discussion

3.1. Synthetic Procedure

By reacting $Mn(ClO_4)_2 \cdot 6H_2O$ (**1**) and $Mn(NO_3)_2 \cdot 4H_2O$ (**2**) with the salicylamidoxime ligand (Scheme 1) in the presence of the coordinating solvent dmf (**1**) and py (**2**), along with NEt_3 (**1** and **2**) and $[ReO_4]^-$ (**2**), we obtained dark green crystals of hexametallic Mn^{III} complexes of the well-known family of $[Mn_6]$ systems. Both $(ClO_4)^-$ and $[ReO_4]^-$ anions were chosen because of their diamagnetic character, and also for giving a suitable solubility to the final compounds. The crystallization techniques

employed for **1** and **2** were slow diffusion by layering with Et_2O (10 mL) and slow evaporation at room temperature of the resulting solutions, respectively. Both compounds were obtained in satisfactory yields.

It is worth noting that both **1** and **2** are cationic oxime-based $[Mn_6]^{2+}$ complexes, and only six systems of this type exist in literature, all of them being obtained with the salicylamidoxime ligand [17–19]. This fact is in contrast to the results obtained from analogous reactions employing similar phenolic oximes, such as salicylaldoxime and its alkyl derivatives, where the isolated complex of the reported works is always a neutral $[Mn_6]$ or $[Mn_3]$ system.

3.2. Description of the Crystal Structures

The crystal structure and exact chemical composition of **1** and **2** were established by single-crystal X-ray diffraction. While **1** crystallizes in the triclinic crystal system with space group $P\bar{1}$, **2** crystallizes in the monoclinic crystal system with space group $P2_1/n$ (Table 1). The structures of **1** and **2** are made up of $[Mn_6]^{2+}$ cations (**1** and **2**) and $(ClO_4)^-$ (**1**) and $[ReO_4]^-$ (**2**) anions. There are solvent molecules of crystallization in only **2**, these are EtOH molecules.

Each cationic $[Mn_6]^{2+}$ unit contains two symmetry equivalent $\{Mn_3(\mu_3\text{-}O)\}$ triangular moieties, which are linked by two phenolate and two oximate O-atoms and related by an inversion center (Figure 1). Each edge of the triangle is spanned by the –N–O– group of the salicylamidoxime ligand, with the central oxo ion displaced 0.102 (**1**) and 0.184 Å (**2**) above the plane of the $[Mn_3]$ triangle, towards the dmf (**1**) and py (**2**) terminal ligands.

(**a**)   (**b**)
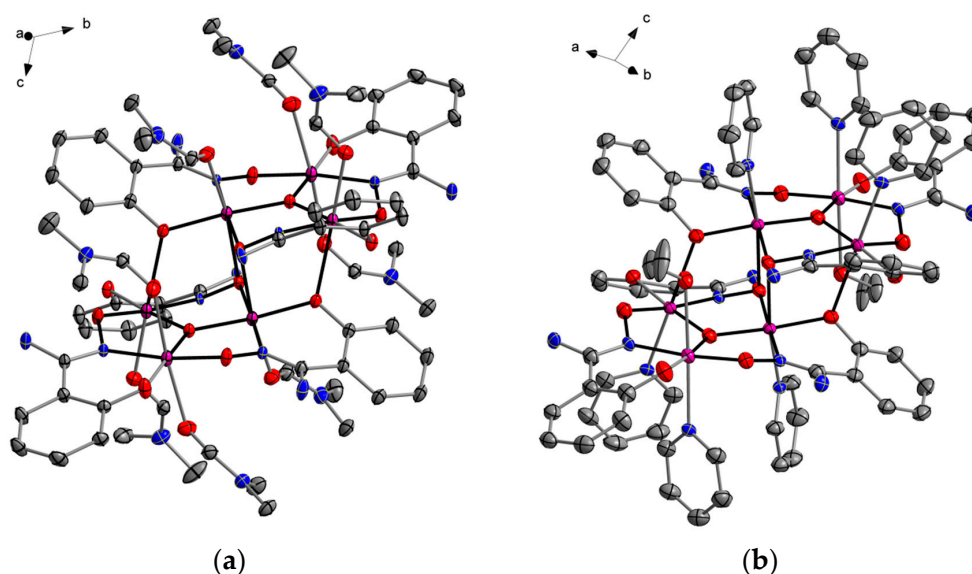
Figure 1. (**a**) Molecular structure of the $[Mn_6(\mu_3\text{-}O)_2(H_2N\text{-}sao)_6(dmf)_8]^{2+}$ cation of **1**. H atoms and $(ClO_4)^-$ anion have been omitted for clarity. Thermal ellipsoids are depicted at 50% probability level. (**b**) Molecular structure of the $[Mn_6(\mu_3\text{-}O)_2(H_2N\text{-}sao)_6(py)_6(EtOH)_2]^{2+}$ cation of **2**. H atoms, $[ReO_4]^-$ anions and EtOH solvent molecules have been omitted for clarity. Thermal ellipsoids are depicted at 50% probability level. Color code: Pink, Mn; red, O; blue, N; grey, C.

The six Mn^{III} ions in the core of **1** and **2** exhibit coordination environments rather similar to those of previously reported salicylamidoxime-based $[Mn_6]^{2+}$ complexes [17–19], with distorted octahedral geometries and Jahn-Teller axes approximately perpendicular to the $[Mn_3]$ planes. The remaining coordination site on the third Mn ion [Mn(2a)] ((a) = 1 − x, 1 − y, 1 − z for **1** and (a) = 1 − x, 1 − y, −z for **2**) is occupied by a dmf (in **1**) or EtOH (in **2**) molecule. The Mn–N–O–Mn torsion angles of the $[Mn^{III}_3(\mu_3\text{-}O)\text{-}(H_2N\text{-}sao)_3]$ triangular units are 46.5°, 36.3° and 30.3° for **1** and 41.4°, 38.1°, 28.9° for **2** (Table 2).

Table 2. Selected magneto-structural parameters for compounds **1** and **2**.

Compound	Crystal System	Space Group	$\alpha/°$ (Mn–N–O–Mn)	J_1/cm^{-1}	J_2/cm^{-1}	g	τ_o/s^{-1}	$E^{\#}/K$
1	triclinic	$P\bar{1}$	46.5, 36.3, 30.3	+0.90	+0.84	1.99	1.6×10^{-11}	66
2	monoclinic	$P2_1/n$	41.4, 38.1, 28.9	+1.88	+0.72	1.98	8.4×10^{-9}	41

In the crystal packing of **1** and **2**, the $(ClO_4)^-$ (**1**) and $[ReO_4]^-$ (**2**) anions sit between the cationic $[Mn_6]^{2+}$ units, which are H-bonded to $-NH_2$ groups from salicylamidoxime ligands. In **2** the $O\cdots N$ distances are shorter than in **1**, linking the anions and cations into chains $[N(4)\cdots O(14b)$ distance of 2.895(1) Å; (b) = $\frac{1}{2} - x$, $\frac{1}{2} + y$, $\frac{1}{2} - z$], as shown in Figure 2. In **1**, the cationic $[Mn_6]^{2+}$ units are somewhat less separated from each other, the shortest intermolecular $Mn\cdots Mn$ distance being 9.831(1) Å $[Mn(1)\cdots Mn(2c)$, (c) = $1 - x$, $1 - y$, $2 - z$] (Figure 3), whereas the shortest intermolecular $Mn\cdots Mn$ distance in **2** is 10.467(1) Å $[Mn(1)\cdots Mn(2b)$, (b) = $\frac{1}{2} - x$, $\frac{1}{2} + y$, $\frac{1}{2} - z$] (Figure 4).
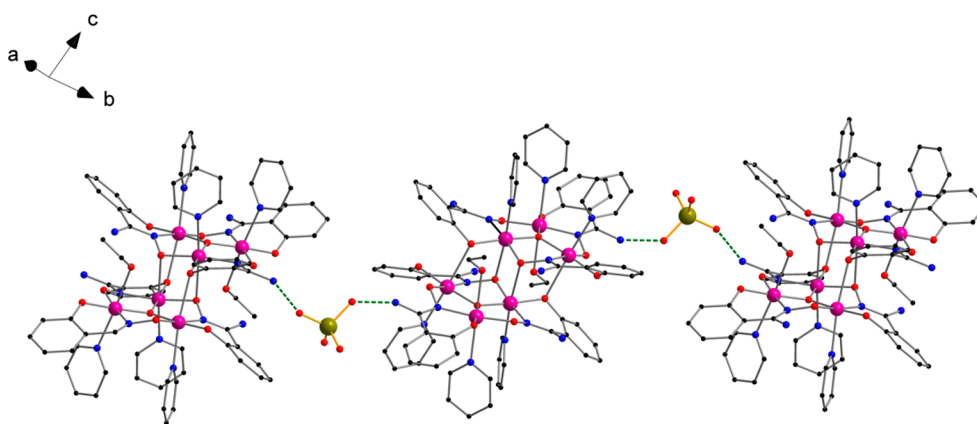
Figure 2. Perspective view of the one-dimensional arrangement of $[Mn_6(\mu_3\text{-}O)_2(H_2N\text{-}sao)_6(py)_6(EtOH)_2]^{2+}$ cations and $[ReO_4]^-$ anions in the crystal of compound **2** through H-bonding interactions (dashed lines). H atoms and solvent molecules have been omitted for clarity. Color code: Pink, Mn; red, O; blue, N; black, C; green, Re.
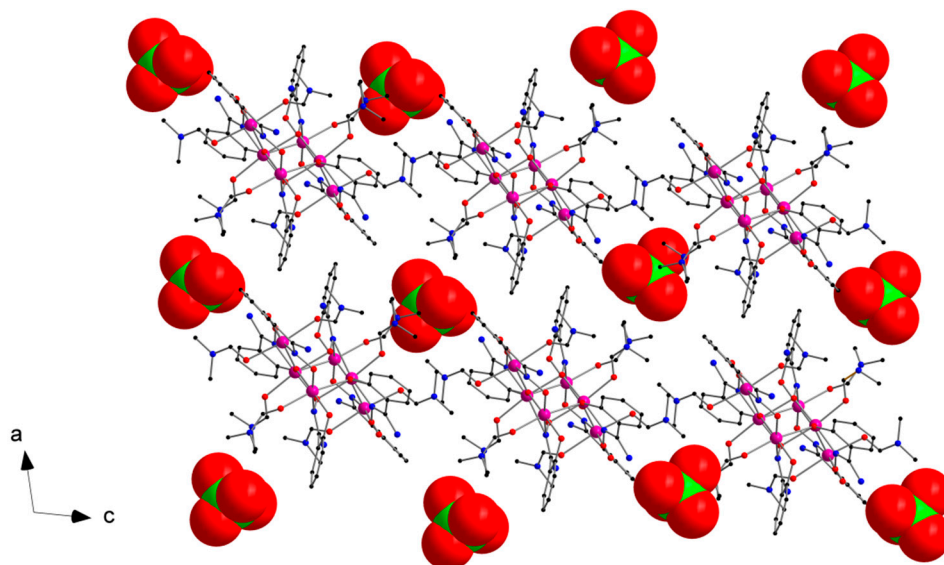
Figure 3. View along the crystallographic *b* axis of a fragment of the packing of **1** showing the arrangement of the $[Mn_6]^{2+}$ cations and $(ClO_4)^-$ anions (space-filling model). H atoms have been omitted for clarity. Colour code: Pink, Mn; red, O; blue, N; black, C; green, Cl.
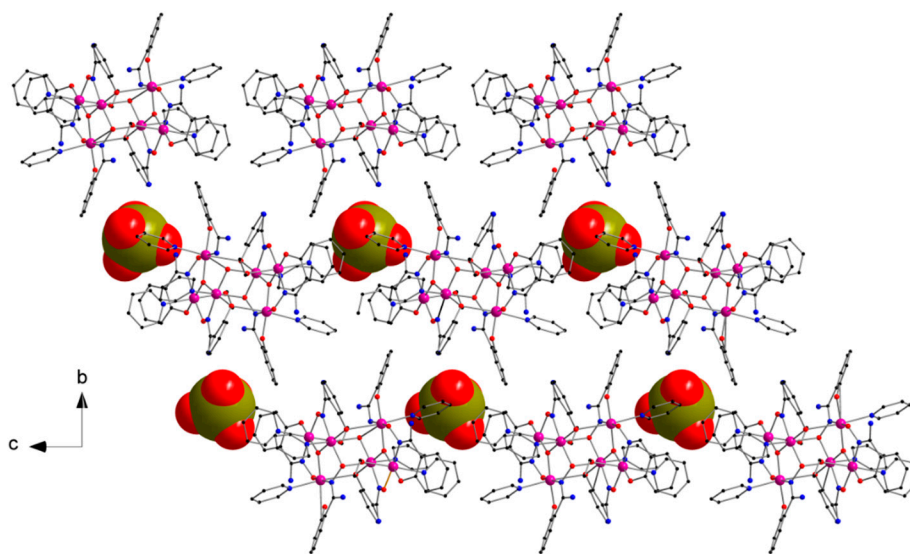
Figure 4. View along the crystallographic *a* axis of a fragment of the packing of **2** showing the arrangement of the $[Mn_6]^{2+}$ cations and $[ReO_4]^-$ anions (space-filling model). H atoms have been omitted for clarity. Color code: Pink, Mn; red, O; blue, N; black, C; green, Re.

In both compounds, additional weak C···C interactions of different types are also observed. In **1**, there exist $\pi \cdots \pi$ off-center parallel stacking interactions of approximately 3.38 Å between aromatic rings of salicylamidoxime ligands of adjacent $[Mn_6]^{2+}$ complexes, and also weak C–H···C(O) interactions between dmf molecules of neighboring $[Mn_6]^{2+}$ cations (ca. 3.45 Å). In **2**, $\pi \cdots \pi$ edge-to-face stacking interactions of ca. 3.49 Å connect aromatic rings of coordinated py molecules and salicylamidoxime ligands of adjacent $[Mn_6]^{2+}$ units. All these additional interactions help in stabilizing the supramolecular arrangement in **1** and **2**.

3.3. Magnetic Properties

DC magnetic susceptibility measurements were performed on microcrystalline samples of **1** and **2** in the 2.0–300 K temperature range and under an external magnetic field of 0.1 T. The magnetic properties of **1** and **2** in the form of $\chi_M T$ vs. *T* plot (χ_M being the molar magnetic susceptibility), are shown in Figure 5. The $\chi_M T$ values observed at 300 K are approximately 20.2 and 20.7 cm$^3 \cdot$mol^{-1} K for **1** and **2**, respectively. Although these values are somewhat higher than that expected for six magnetically isolated Mn^{III} ions ($\chi_M T \approx 18.0$ cm$^3 \cdot$mol^{-1} K with $g = 1.99$), they have been previously observed in ferromagnetically coupled $[Mn_6]$ systems [8–20]. Upon cooling, the $\chi_M T$ values rise gradually with decreasing temperature for both compounds, reaching maxima of 38.9 cm^{3}mol^{-1}K at 8.0 K for **1** and 35.8 cm$^3 \cdot$mol^{-1} K at 17.0 K for **2**. In both compounds, $\chi_M T$ values decrease at lower temperatures giving final values of 23.0 (**1**) and 13.0 cm$^3 \cdot$mol^{-1} K (**2**) at 2.0 K, which are observed due to the presence of intermolecular interactions and/or zero-field splitting (ZFS) effects.

The experimental data of the $\chi_M T$ vs. *T* plots of **1** and **2** were treated by using the 2*J* model described by the Hamiltonian of Equation (1), where J_1 and J_2 are the exchange coupling constants for the intramolecular Mn–Mn interactions associated with exchange pathways involving the Mn–N–O–Mn torsion angles of the $[Mn_6]$ core, and *g* is the Landé factor for the Mn^{III} ions. The theoretical parameters thus obtained are summarized in Table 2.

$$\hat{H} = -2J_1 \, (\hat{S}_1 \, \hat{S}_3 + \hat{S}_1 \hat{S}_{3\prime} + \, \hat{S}_1 \hat{S}_{1\prime} + \, \hat{S}_{1\prime} \hat{S}_3 \, + \, \hat{S}_{1\prime} \hat{S}_{3\prime})$$
$$-2J_2 \, (\hat{S}_1 \, \hat{S}_2 + \hat{S}_2 \, \hat{S}_3 \, + \hat{S}_{1\prime} \hat{S}_{2\prime} + \, \hat{S}_2 \hat{S}_{3\prime}) + \mu_B g H \hat{S} \tag{1}$$

These features reveal an intramolecular ferromagnetic coupling between the Mn^{III} metal ions in both **1** and **2**. In previous studies dealing with DFT calculations on salicylamidoxime-based $[Mn_6]$ complexes [16], a critical angle (ca. 27.0°) that is directly correlated to the Mn–N–O–Mn exchange pathway between neighboring Mn^{III} ions was found. Mn–N–O–Mn torsion angles upper than this critical angle switch the magnetic exchange from antiferromagnetic ($J < 0$) to ferromagnetic ($J > 0$). Given that **1** and **2** show Mn–N–O–Mn torsion angles higher than 27.0°, it would be expected to obtain a ferromagnetic coupling as the predominant magnetic interaction for both compounds, as observed experimentally (Figure 5 and Table 2).

(a)   (b)
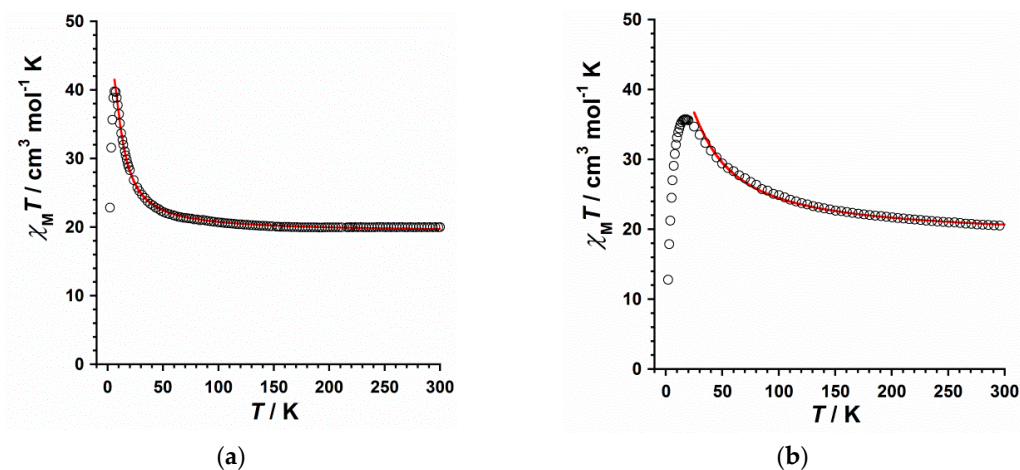
Figure 5. Thermal variation of the $\chi_M T$ product for compounds **1** (**a**) and **2** (**b**). The solid red line represents the best-fit of the experimental data.

The complexes that form the large family of oxime-based $[Mn^{III}_6]$ SMMs display ground state spin values that vary from 4 to 12. In general, a spin value of S = 4 is found in antiferromagnetic $[Mn^{III}_6]$ systems, whereas ferromagnetic $[Mn^{III}_6]$ complexes show a spin value of S = 12. A ground state spin value of S = 12 was obtained for **1** and **2** from the magnetic susceptibility data, hence supporting the ferromagnetic nature for both compounds. Thus, the isotropic simulation of the magnetic susceptibility of **1** and **2** generated the plots of the energy versus total spin shown in Figure 6. The first excited state found in **1** is S = 11 placed at 2.25 cm^{-1}, and the first excited state in **2** is also S = 11, which is located at 1.85 cm^{-1} (Figure 6).

(a)   (b)
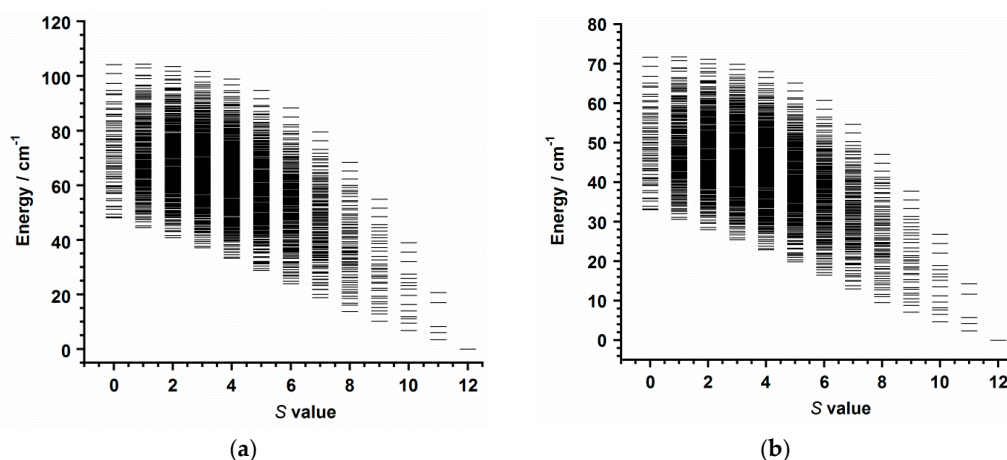
Figure 6. Plot of energy versus total spin state, extracted from the isotropic simulation of the susceptibility data for **1** (**a**) and **2** (**b**).

Additionally, variable temperature-variable field DC magnetization data were measured for **1** and **2** in the 2–7 K temperature and 0.5–7.0 T field ranges. The experimental data are given as reduced magnetization ($M/N\mu_B$ *versus* $\mu_o H/T$) in Figure 7, which were fitted to a Zeeman plus axial zero-field splitting Hamiltonian ($\hat{H} = D(\hat{S}_z^2 - S(S + 1)/3) + \mu_B g H \hat{S}$, where D is the axial anisotropy of the cationic $[Mn_6]^{2+}$ complex, μ_B is the Bohr magneton, $\hat{S}_z$ is the easy-axis spin operator, and H is the applied field) assuming only the ground state is populated. The best fits afforded the parameters S = 12, g = 1.99 and $D = -0.48$ cm^{-1} for **1** and S = 12, g = 1.98 and $D = -0.39$ cm^{-1} for **2**, which are in line with those values reported for similar cationic $[Mn_6]^{2+}$ complexes [17–19].
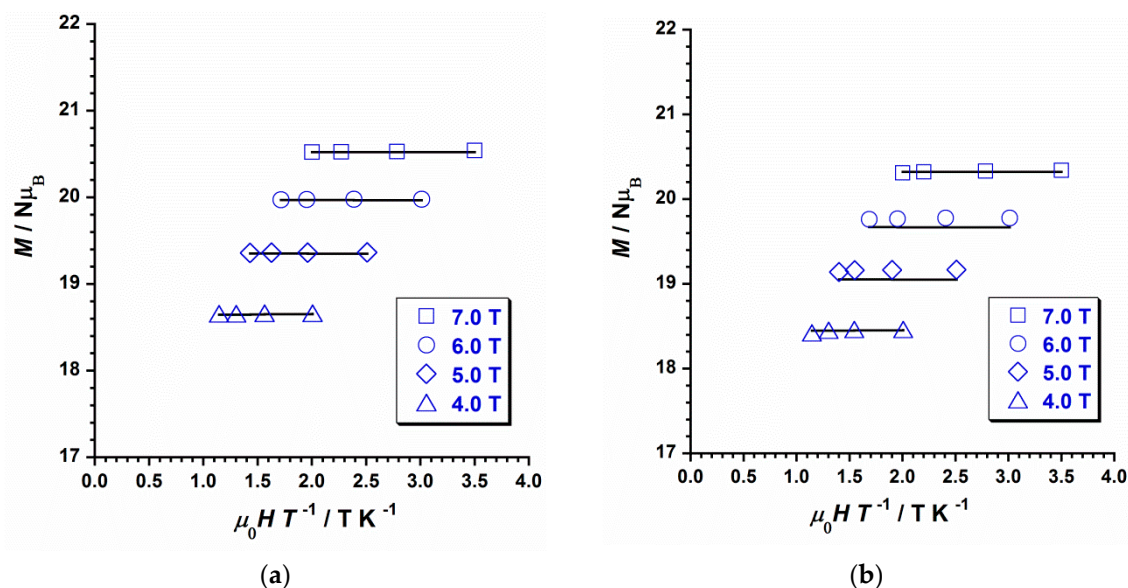
Figure 7. Plot of the reduced magnetization ($M/N\mu_B$ *versus* $\mu_o H/T$) for **1** (**a**) and **2** (**b**) at 4, 5, 6 and 7 T fields and temperatures 2–5 K. The solid lines represent the best fit of the experimental data.

AC susceptibility measurements were performed on samples of **1** and **2** in the temperature range 2–10 K, in zero applied DC field, and a 3.9 G AC field oscillating in the 5–1000 Hz range of frequencies. Out-of-phase AC signals (χ''_M) for **1** and **2** are shown in Figure 8. The respective χ''_M versus T plots exhibited frequency dependence of the χ''_M maxima for **1** and **2**. This feature is consistent with SMM behavior. In addition, it was observed that the χ''_M maxima increased with the decreasing frequency for both compounds. These data were fitted to the Arrhenius equation ($\tau = \tau_o \exp(E^\#/k_B T)$, where τ_o is the pre-exponential factor, τ is the relaxation time, $E^\#$ is the barrier to relaxation of the magnetization, and k_B is the Boltzmann constant) and plotted in the respective insets of Figure 8. The values obtained for the τ_o and $E^\#$ parameters are listed in Table 2. The $E^\#$ values for **1** [66.0 K (45.9 cm^{-1})] and **2** [41.0 K (28.5 cm^{-1})] fall into the range for previously reported salicylamidoxime-based $[Mn^{III}_6]$ complexes (24.0 K (16.7 cm^{-1}) < $E^\#$ < 86.0 K (59.8 cm^{-1})). Nevertheless, it is worth pointing out that the $E^\#$ value calculated for **1** is the higher obtained so far for a cationic oxime-based $[Mn^{III}_6]^{2+}$ single-molecule magnet.

This last result is interesting since this type of cationic SMMs can be used as precursors of new multifunctional magnetic materials because the $(ClO_4)^-$ (**1**) and $[ReO_4]^-$ (**2**) anions can be changed through the incorporation of anionic species that bring another physical property or functionality to the final material, for instance, conductivity or luminescence.
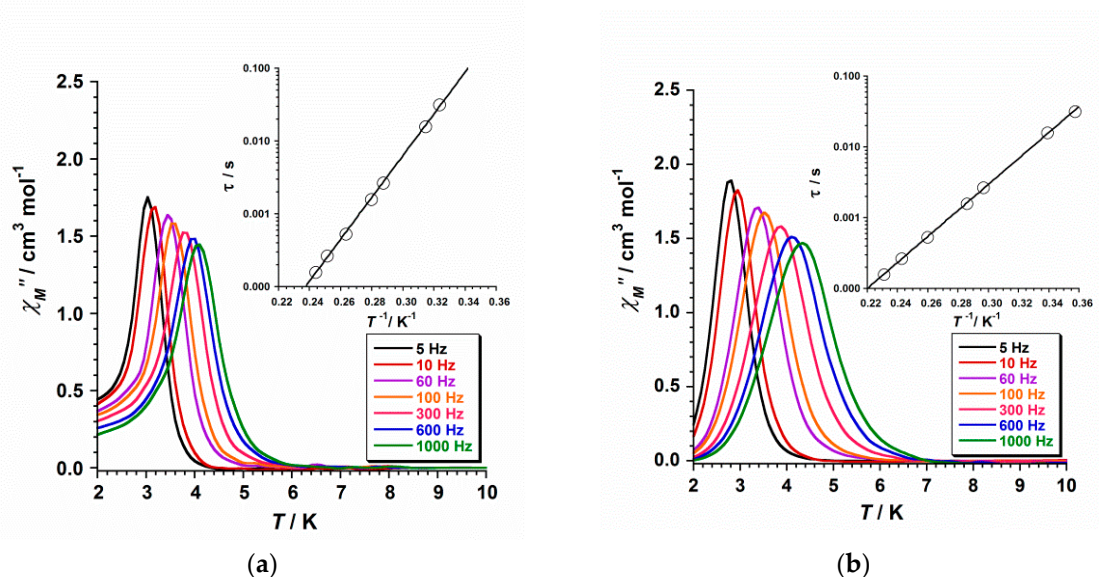
Figure 8. Out-of-phase AC susceptibility (χ''_M) versus *T* plots for compounds **1** (**a**) and **2** (**b**). The insets show the Arrhenius best-fit plot (see text).

4. Conclusions

In summary, two new members of the family of oxime-based [Mn$_6$] complexes have been synthesized and magnetostructurally characterized. Both compounds display a magnetic behavior consistent with the single-molecule magnet (SMM) phenomenon. The barrier value to the relaxation of the magnetization ($E^{\#}$) for compound **1** is the highest reported so far for cationic oxime-based [Mn$_6$]$^{2+}$ systems. Finally, due to their cationic character, these singular SMMs could be used as suitable building blocks for preparing new magnetic materials, just by replacing the anion by another anionic species exhibiting an additional functionality, namely, conductivity or luminescence. This work is in progress.

Author Contributions: J.M.-L. and F.L. obtained funding for the project. C.R.-D. performed the synthesis and the X-ray data collection. N.M. designed and carried out the SQUID measurements. J.M.-L. analyzed the data associated with all the experiments and wrote the manuscript, which all authors discussed and commented on.

Conflicts of Interest: The authors declare no conflict of interest.

References

1. Sessoli, R.; Gatteschi, D. Quantum Tunneling of Magnetization and Related Phenomena in Molecular Materials. *Angew. Chem. Int. Ed.* **2003**, *42*, 268–297. [CrossRef]
2. Timco, G.A.; McInnes, E.J.L.; Winpenny, R.E.P. Physical studies of heterometallic rings: An ideal system for studying magnetically-coupled systems. *Chem. Soc. Rev.* **2013**, *42*, 1796–1806. [CrossRef] [PubMed]
3. Evangelisti, M.; Brechin, E.K. Recipes for enhanced molecular cooling. *Dalton Trans.* **2010**, *39*, 4672–4676. [CrossRef] [PubMed]
4. Bogani, L.; Wernsdorfer, W. Molecular spintronics using single-molecule magnets. *Nat. Mater.* **2008**, *7*, 179–186. [CrossRef] [PubMed]
5. Tyagi, P.; Li, D.; Holmes, S.M.; Hinds, B.J. Molecular Electrodes at the Exposed Edge of Metal/Insulator/Metal Trilayer Structures. *J. Am. Chem. Soc.* **2007**, *129*, 4929–4938. [CrossRef]
6. Ferrando-Soria, J.; Vallejo, J.; Castellano, M.; Martínez-Lillo, J.; Pardo, E.; Cano, J.; Castro, I.; Lloret, F.; Ruiz-García, R.; Julve, M. Molecular magnetism, quo vadis? A historical perspective from a coordination chemist viewpoint. *Coord. Chem. Rev.* **2017**, *339*, 17–103. [CrossRef]

7.   Milios, C.J.; Raptopoulou, C.P.; Terzis, A.; Lloret, F.; Vicente, R.; Perlepes, S.P.; Escuer, A. Hexanuclear manganese(III) single-molecule magnets. *Angew. Chem. Int. Ed.* **2004**, *43*, 210–212. [CrossRef]

8.   Milios, C.J.; Vinslava, A.; Wood, P.A.; Parsons, S.; Wernsdorfer, W.; Christou, G.; Perlepes, S.P.; Brechin, E.K. A Single-Molecule Magnet with a "Twist". *J. Am. Chem. Soc.* **2007**, *129*, 8–9. [CrossRef]

9.   Milios, C.J.; Vinslava, A.; Wernsdorfer, W.; Moggach, S.; Parsons, S.; Perlepes, S.P.; Christou, G.; Brechin, E.K. A Record Anisotropy Barrier for a Single-Molecule Magnet. *J. Am. Chem. Soc.* **2007**, *129*, 2754–2755. [CrossRef]

10.   Milios, C.J.; Piligkos, S.; Brechin, E.K. Ground state spin-switching via targeted structural distortion: Twisted single-molecule magnets from derivatised salicylaldoximes. *Dalton Trans.* **2008**, *14*, 1809–1817. [CrossRef]

11.   Inglis, R.; Milios, C.J.; Jones, L.F.; Piligkos, S.; Brechin, E.K. Twisted molecular magnets. *Chem. Commun.* **2012**, *48*, 181–190. [CrossRef] [PubMed]

12.   Kalofolias, D.A.; Flamourakis, A.G.; Siczek, M.; Lis, T.; Milios, C.J. A bulky oxime for the synthesis of Mn(III) clusters. *J. Coord. Chem.* **2015**, *68*, 1–20. [CrossRef]

13.   Tomsa, A.-R.; Martínez-Lillo, J.; Li, Y.; Chamoreau, L.-M.; Boubekeur, K.; Farias, F.; Novak, M.A.; Cremades, E.; Ruiz, E.; Proust, A.; et al. A new family of oxime-based hexanuclear manganese(III) single molecule magnets with high anisotropy energy barriers. *Chem. Commun.* **2010**, *46*, 5106–5108. [CrossRef] [PubMed]

14.   An, G.-Y.; Cui, A.-L.; Kou, H.-Z. Assembly of oximate-bridged Mn$_6$ cluster to a one-dimensional chain. *Inorg. Chem. Commun.* **2011**, *14*, 1475–1478. [CrossRef]

15.   Martínez-Lillo, J.; Chamoreau, L.-M.; Proust, A.; Verdaguer, M.; Gouzerh, P. Hexanuclear manganese(III) single-molecule magnets from derivatized salicylamidoximes. *C. R. Chim.* **2012**, *15*, 889–894. [CrossRef]

16.   Martínez-Lillo, J.; Tomsa, A.-R.; Li, Y.; Chamoreau, L.-M.; Cremades, E.; Ruiz, E.; Barra, A.-L.; Proust, A.; Verdaguer, M.; Gouzerh, P. Synthesis, crystal structure and magnetism of new salicylamidoxime-based hexanuclear manganese(III) single-molecule magnets. *Dalton Trans.* **2012**, *41*, 13668–13681. [CrossRef] [PubMed]

17.   Martínez-Lillo, J.; Dolan, N.; Brechin, E.K. A cationic and ferromagnetic hexametallic Mn(III) single-molecule magnet based on the salicylamidoxime ligand. *Dalton Trans.* **2013**, *42*, 12824–12827. [CrossRef]

18.   Martínez-Lillo, J.; Dolan, N.; Brechin, E.K. A family of cationic oxime-based hexametallic manganese(III) single-molecule magnets. *Dalton Trans.* **2014**, *43*, 4408–4414. [CrossRef]

19.   Martínez-Lillo, J.; Cano, J.; Wernsdorfer, W.; Brechin, E.K. The Effect of Crystal Packing and Re[IV] Ions on the Magnetisation Relaxation of [Mn$_6$]-Based Molecular Magnets. *Chem. Eur. J.* **2015**, *21*, 8790–8798. [CrossRef]

20.   Rojas-Dotti, C.; Martínez-Lillo, J. Thioester-functionalised and oxime-based hexametallic manganese(III) single-molecule magnets. *RSC Adv.* **2017**, *7*, 48841–48847. [CrossRef]

21.   Eloy, F.; Lenaers, R. The Chemistry of Amidoximes and Related Compounds. *Chem. Rev.* **1962**, *62*, 155–183. [CrossRef]

22.   *SHELXTL-2013/4, Bruker Analytical X-ray Instruments*; Bruker: Madison, WI, USA, 2013.

23.   *DIAMOND 4.5.0, Crystal Impact GbR*; Crystal Impact: Bonn, Germany, 2018.

Article 2.

Hexanuclear manganese(III) single-molecule magnets based on oxime and azole-type ligands
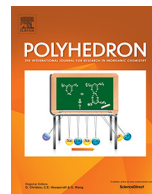
Hexanuclear manganese(III) single-molecule magnets based on oxime and azole-type ligands

Carlos Rojas-Dotti, Nicolás Moliner, Francesc Lloret, José Martínez-Lillo *

Instituto de Ciencia Molecular (ICMol)/Departament de Química Inorgànica, Universitat de València, c/ Catedrático José Beltrán 2, 46980 Paterna, Valencia, Spain

ABSTRACT

Two novel hexanuclear manganese(III) complexes belonging to the Mn_6 family of single-molecule magnets (SMMs), of formulae $[Mn_6(\mu_3\text{-}O)_2(H_2N\text{-}sao)_6(bta)_2(EtOH)_6]\cdot2EtOH\cdot4H_2O$ (**1**) and $[Mn_6(\mu_3\text{-}O)_2(H_2N\text{-}sao)_6(pta)_2(EtOH)_6]\cdot4EtOH$ (**2**) $[H_2N\text{-}saoH_2 = $ salicylamidoxime, bta = 1,2,3-benzotriazolate anion, pta = 5-phenyl-tetrazolate anion], have been synthesized and characterized structurally and magnetically. Both compounds crystallize in the triclinic system with space group $P\bar{1}$ (**1** and **2**). In their crystal packing, adjacent Mn_6 complexes are connected through non-coordinating solvent molecules, which are H-bonded to N atoms of azole rings and $-NH_2$ groups of salicylamidoxime ligand. The study of the magnetic properties of **1** and **2** through magnetic susceptibility measurements reveals as predominant interaction an antiferromagnetic coupling between the Mn^{III} metal ions in both compounds. A ground state spin value of $S = 4$ for **1** and **2** was confirmed through variable temperature-variable field dc magnetization data, and the occurrence of slow relaxation of the magnetization in both **1** and **2** indicates single-molecule magnet behavior.

© 2019 Elsevier Ltd. All rights reserved.

1. Introduction

In the multidisciplinary field of Molecular Magnetism, the structural and magnetic properties of single-molecule magnets (SMMs) have been thoroughly investigated for their fundamentally interesting chemistry and physics, which can potentially provide a gateway for the discovery of new physical phenomena in a diverse array of technological applications [1].

Mn^{III} has been one of the metal ions more explored in this multidisciplinary research. In this context, the combination of Mn^{III} and phenolic oximes, such as salicylaldoxime and salicylamidoxime, has proven to be particularly successful in the preparation of SMMs [2–16]. Thus, a large family of hexanuclear Mn^{III} complexes has been studied. All the family members display the SMM phenomenon, with remarkably different magnetic behavior, antiferromagnetic or ferromagnetic, which is strongly affected by the structural distortion of the Mn—N—O—Mn torsion angles. As a result, it was established a semi-quantitative magneto-structural correlation that enables the prediction of the magnetic behavior of new Mn_6^{III} systems [2–16].

As far as we know, from this family of discrete Mn_6^{III} molecules based on salicylaldoxime and salicylamidoxime, only one has been prepared with a nitrogen-based azole-type ligand, the cationic $[Mn_6]^{2+}$ complex of formula $[Mn_6(\mu_3\text{-}O)_2(H_2N\text{-}sao)_6(Him)_6(EtOH)_2]$ $(ClO_4)_2\cdot6EtOH$ $[H_2N\text{-}saoH_2 = $ salicylamidoxime and Him = imidazole] [13].

As a continuation of our investigation on Mn^{III} single-molecule magnets, we have explored the synthesis of Mn_6 systems with these azole-type ligands. In particular, we have focused on the benzotriazole and 5-phenyl-tetrazole ligands (Scheme 1). Benzotriazole and its derivatives constitute a family of versatile heterocyclic compounds with properties that make them very useful in a wide variety of different research fields [17–21]. Aside from that, the good chelating ability of the 5-phenyl-tetrazole together with the presence of its four N atoms allow this ligand to be very suitable for metal coordination and supramolecular assembling [22–41], as shown in previous works dealing with the first-row metal ions Ti^{IV} [22,23], Fe^{III} [24], $Co^{II,III}$ [25–27], Ni^{II} [28–32], $Cu^{I,II}$ [33–37] and Zn^{II} [38–41]. Nevertheless, no crystal structure based on manganese and 5-phenyl-tetrazole has been reported so far.

Herein we report the synthesis, crystal structures and magnetic properties of two hexanuclear Mn^{III} compounds of general formula $[Mn_6(\mu_3\text{-}O)_2(H_2N\text{-}sao)_6(bta)_2(EtOH)_6]\cdot2EtOH\cdot4H_2O$ (**1**) and $[Mn_6(\mu_3\text{-}O)_2(H_2N\text{-}sao)_6(pta)_2(EtOH)_6]\cdot4EtOH$ (**2**) $[H_2N\text{-}saoH_2 = $ salicylamidoxime, bta = 1,2,3-benzotriazolate anion, pta = 5-phenyl-tetrazolate anion], which are based on oxime and azole-type ligands (Scheme 2).
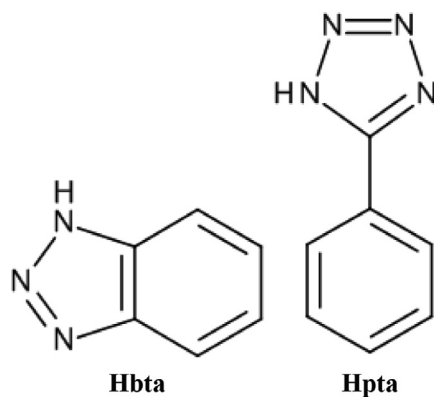
Scheme 1. Structure of the 1,2,3-benzotriazole (Hbta) and 5-phenyl-tetrazole (Hpta) ligands.

2. Experimental

2.1. Materials

All starting chemicals and solvents were purchased from commercial sources and used without further purification. The salicylamidoxime ligand was prepared following the synthetic method described in the literature [42].

2.2. Synthesis

2.2.1. $[Mn_6(\mu_3\text{-}O)_2(H_2N\text{-}sao)_6(bta)_2(EtOH)_6]\cdot 2EtOH\cdot 4H_2O$ (1)

$MnCl_2\cdot 4H_2O$ (0.594 g, 3.0 mmol) was added dropwise and with constant stirring to a solution of $H_2N\text{-}saoH_2$ (0.456 g, 3.0 mmol) and benzotriazole (Hbta) ligand (0.357 g, 3.0 mmol) in EtOH (40 mL), then NEt_3 (2.0 mL, 3.58 mmol) was added. After stirring for 1 h, a dark green solution was generated and let to evaporate at room temperature. Dark green crystals of **1** were obtained in 4–5 days and were suitable for X-ray diffraction. Yield: 47%. Elemental *Anal. Calc.* (found) for $C_{70}H_{100}N_{18}O_{26}Mn_6$ (**1**): C, 43.4 (42.9); H, 5.2 (4.8); N, 13.0 (12.7). Selected IR data (in KBr/cm^{-1}): 3314 (m), 1609 (vs), 1563 (m), 1440 (m), 1384 (m), 1311 (m), 1251 (m), 1148 (w), 1120 (s), 1022 (m), 880 (m), 759 (w), 683 (s), 642 (m), 580 (w).

2.2.2. $[Mn_6(\mu_3\text{-}O)_2(H_2N\text{-}sao)_6(pta)_2(EtOH)_6]\cdot 4EtOH$ (2)

Compound **2** was prepared as for **1** but by using 5-phenyl-1H-tetrazole (Hpta) (0.439 mg, 3.0 mmol) instead of the benzotriazole ligand. In 3–4 days, dark green crystals of **2** were obtained, which were suitable for single-crystal X-ray diffraction studies. Yield: *ca.* 67%. Elemental *Anal. Calc.* (found) for $C_{76}H_{106}N_{20}O_{24}Mn_6$ (**2**): C, 45.3 (45.8); H, 5.3 (5.8); N, 13.9 (13.5). Selected IR data (KBr pellets/cm^{-1}): 3326 (m), 1610 (vs), 1565 (m), 1443 (m), 1384 (m), 1311 (w), 1250 (w), 1147 (vw), 1022 (m), 910 (s), 881 (m), 758 (w), 683 (m), 640 (w), 580 (vw).

2.3. Physical measurements

Elemental analysis (C, H, N) were performed on a CE Instruments EA 1110 CHNS analyser. Infrared spectra were recorded on a Thermo-Nicolet 6700 FT-IR spectrophotometer in the 4000–400 cm^{-1} region. Dc magnetic susceptibility measurements of **1** and **2** were carried out with a Quantum Design SQUID magnetometer in the temperature range 2.0–300 K and under an applied dc fields of 0.025 and 0.1 T. Ac magnetic susceptibility measurements were performed in the temperature range 2–8 K, at zero applied dc field, and $3.9 \cdot 10^{-4}$ T ac field oscillating at frequencies of 10–1000 Hz. Diamagnetic corrections of the constituent atoms were estimated from Pascal's constants [43].

2.4. Crystallographic data collection and structure determination

X-ray diffraction data of single crystals of dimensions $0.22 \times 0.04 \times 0.02$ (**1**) and $0.13 \times 0.09 \times 0.04$ (**2**) were collected on a Bruker D8 Venture diffractometer, with PHOTON II detector, by using Cu K$_\alpha$ ($\lambda = 1.54184$ Å) and Mo K$_\alpha$ ($\lambda = 0.71073$ Å) radiation for **1** and **2**, respectively. Crystal parameters and refinement results for **1** and **2** are summarized in Table 1. The structures were solved by standard direct methods and subsequently completed by Fourier recycling by using the SHELXTL software packages. The obtained models were refined with version 2013/4 of SHELXL against F^2 on all data by full-matrix least squares [44]. In both samples, all non-hydrogen atoms were refined anisotropically. All the
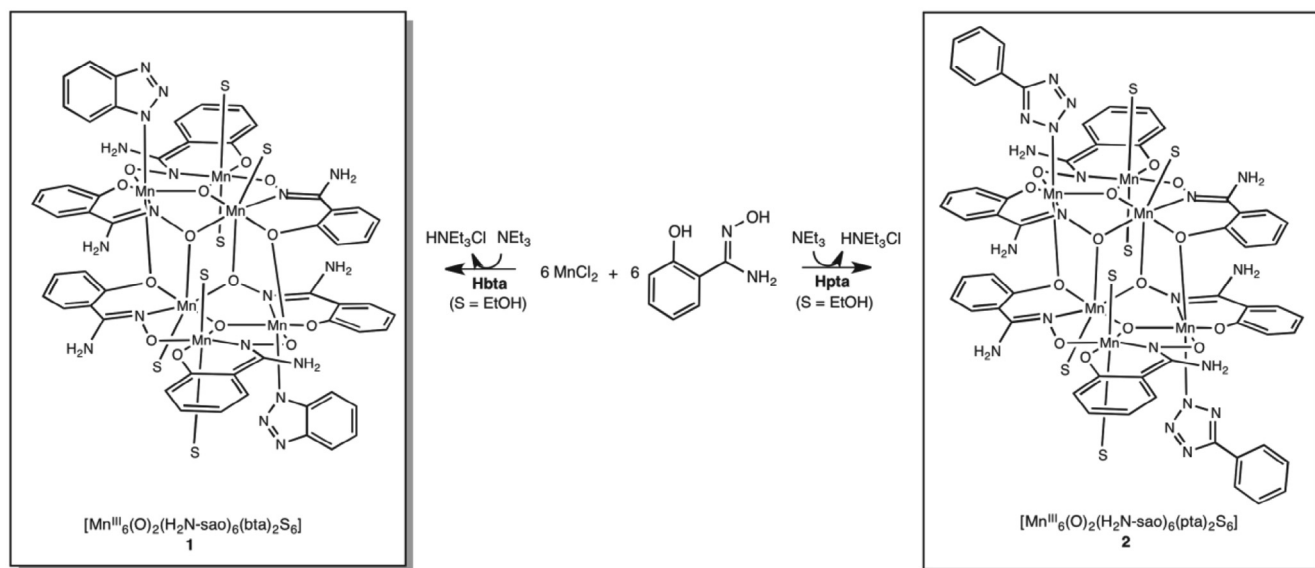
Scheme 2. Synthesis of **1** and **2** with 1,2,3-benzotriazole (Hbta) and 5-phenyl-tetrazole (Hpta) ligands, respectively.

Table 1
Crystal data and structure refinement for compounds **1** and **2**.

Compound	**1**	**2**
Formula	$C_{70}H_{92}N_{18}O_{26}Mn_6$	$C_{76}H_{106}N_{20}O_{24}Mn_6$
Formula weight	1931.25	2012.43
Crystal system	triclinic	triclinic
Space group	$P\bar{1}$	$P\bar{1}$
a (Å)	12.116(1)	12.361(1)
b (Å)	13.313(1)	13.087(1)
c (Å)	15.006(1)	15.909(1)
α (°)	98.18(1)	70.58(1)
β (°)	113.58(1)	89.16(1)
γ (°)	93.41(1)	65.33(1)
V (Å^3)	2177.6(3)	2182.3(1)
Z	1	1
D_c (g cm^{-3})	1.473	1.531
μ (mm^{-1})	7.576	0.927
$F(0\,0\,0)$	996	1043
Goodness-of-fit (GoF) on F^2	1.013	1.133
R_1 [$I > 2\sigma(I)$][a]	0.0671	0.0430
wR_2 [$I > 2\sigma(I)$][b,c]	0.1755	0.1070
Largest difference peak and hole (e Å^{-3})	1.223 and −0.619	1.162 and −0.527

[a] $R_1 = \sum||F_o| - |F_c||/\sum|F_o|$.
[b] $wR_2 = \{\sum[w(F_o{}^2 - F_c{}^2)^2]/[(w(F_o{}^2)^2)]\}^{1/2}$.
[c] $w = 1/[\sigma^2(F_o{}^2) + (aP)^2 + bP]$ with $P = [F_o{}^2 + 2F_c{}^2]/3$.

hydrogen atoms of the EtOH molecules (**1** and **2**) were set in calculated positions and refined isotropically by using the riding model. Hydrogen atoms on the water molecules (**1**) were neither found nor calculated. Graphical manipulations were performed using

Table 2
Selected hydrogen-bonding interactions in compound **1**.[a]

D–H···A	D–H/Å	H···A/Å	D···A/Å	(DHA)/°
O(11)–(11A)···N(9)	0.820	2.02(1)	2.834(1)	175.8
N(2)–H(2A)···O(1w)	0.860	2.25(1)	3.093(1)	168.7
N(2)–H(2B)···O(11a)	0.860	2.18(1)	2.941(1)	147.4
O(9)–H(9A)···O(2c)	0.820	2.23(1)	3.042(1)	170.8
N(6)–H(6A)···O(9c)	0.860	2.10(1)	2.947(1)	170.1
N(4)–H(4B)···O(6d)	0.860	2.17(1)	2.976(1)	156.6

[a] Symmetry codes: (a) = −x + 2, −y, −z + 4; (c) = −x + 1, −y, −z + 4; (d) = −x + 1, −y + 1, −z + 4.

Table 3
Selected hydrogen-bonding interactions in compound **2**.[a]

D–H···A	D–H/Å	H···A/Å	D···A/Å	(DHA)/°
O(15)–H(15A)···N(13)	0.820	2.28(1)	2.842(1)	127.6
O(16)–H(16A)···N(13)	0.820	2.18(1)	2.957(4)	158.9
O(17)–H(17A)···O(8)	0.820	2.15(1)	2.950(1)	164.9
O(18)–H(18B)···O(8)	0.820	2.09(1)	2.912(1)	176.2
O(19)–H(19D)···N(17)	0.820	2.37(1)	2.965(1)	129.8
O(20)–H(20A)···O(2)	0.820	2.19(1)	3.000(1)	168.3
N(4)–H(4A)···O(23a)	0.860	2.12(1)	2.965(1)	167.0
N(4)–H(4B)···N(20a)	0.860	2.19(1)	2.950(1)	146.8
O(21)–H(21A)···O(3c)	0.820	2.50(1)	3.026(1)	123.2
O(21)–H(21A)···O(4c)	0.820	2.20(1)	3.007(1)	167.1
O(22)–H(22A)···O(10)	0.820	2.13(1)	2.945(1)	172.8
O(23)–H(23A)···O(5d)	0.820	2.61(1)	3.062(1)	116.0
O(23)–H(23A)···O(6d)	0.820	2.20(1)	3.021(1)	175.2
N(10)–H(10B)···N(16d)	0.820	2.26(1)	3.027(1)	148.7
N(12)–H(12B)···O(21e)	0.860	2.47(1)	3.038(1)	124.5
O(24)–H(24A)···O(11)	0.820	2.22(1)	3.006(1)	162.1
N(6)–H(6A)···O(20)	0.860	2.04(1)	2.888(1)	168.0
N(6)–H(6B)···O(22)	0.860	2.41(1)	3.001(1)	126.2
N(10)–H(10A)···O(24)	0.860	2.16(1)	2.996(1)	163.7
N(12)–H(12A)···O(17)	0.860	2.06(1)	2.914(1)	174.2

[a] Symmetry codes: (a) = x, y, z − 1; (c) = x + 1, y − 1, z + 1; (d) = x, y, z + 1; (e) = x − 1, y + 1, z − 1.

DIAMOND [45] and CRYSTALMAKER [46]. CCDC 1910059 (**1**) and 1910060 (**2**).

3. Results and discussion

3.1. Crystal structures of compounds **1** and **2**

Both compounds (**1** and **2**) crystallize in the triclinic system with the centrosymmetric space group $P\bar{1}$ (Table 1). The crystal structure of **1** and **2** is made up of neutral Mn$_6$ complexes along with H$_2$O (**1**) and EtOH (**1** and **2**) solvent molecules of crystallization, which are held together mainly by means of H-bonding interactions (Tables 2 and 3). Perspective drawings showing the Mn$_6$ complexes in **1** and **2** are given in Fig. 1 and Fig. 2, respectively.

The core of these Mn$_6$ complexes is formed by two {Mn$_3$(μ_3-O)} triangular moieties, which are connected each other by means of two phenolate and two oximate O-atoms (Fig. 1 and Fig. 2). Each edge of the triangle is bridged through the –N—O– groups of the salicylamidoxime ligands, with the central oxo ion placed in the plane of the Mn$_3$ triangle in both compounds. The six Mn^{III} ions in the core of **1** and **2** exhibit coordination environments rather similar to those of previously reported salicylamidoxime-based Mn$_6$ complexes [8–16], with distorted octahedral geometries and Jahn-Teller axes approximately perpendicular to the Mn$_3$ planes. The Mn—N—O—Mn torsion angles of the [Mn$_3$(μ_3-O)(H$_2$N-sao)$_3$] triangular units are 43.9, 25.8 and 25.2° for 1, and 38.5, 30.3 and 17.4° for **2**.

In **1**, the coordinating benzotriazolate ligand is linked to both Mn(3) and its symmetry equivalent. In **2**, the 5-phenyl-tetrazolate anion is coordinate to Mn(3) and its two rings, azolate and pyridyl rings, are non coplanar. Indeed, the dihedral angle through the inter-ring carbon–carbon bond is approximately 41.0°. Both azole-type ligands coordinate the Mn ions in a monodentate fashion, and their average values of the C—C and C—N bond lengths are in agreement with those of previously reported systems containing these anionic ligands [22–41].

In the crystal packing of **1**, adjacent Mn$_6$ complexes are connected through lattice EtOH molecules, which are H-bonded to N atoms of azole rings and –NH$_2$ groups from benzotriazole and salicylamidoxime ligands, respectively (Fig. 3). These intermolecular interactions led to the formation of a one-dimensional motif of Mn$_6$ complexes that grow along the crystallographic a axis through
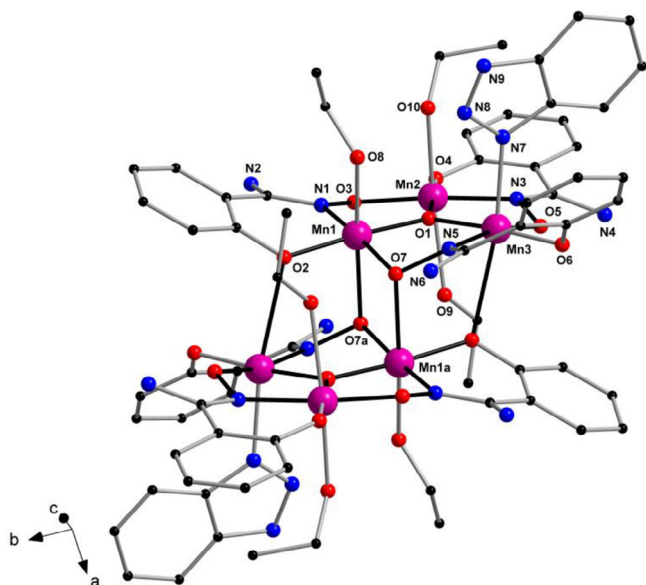
Fig. 1. Perspective drawing of the molecular structure of the $[Mn_6(\mu_3\text{-}O)_2(H_2N\text{-}sao)_6(bta)_2(EtOH)_6]$ complex of **1**. H atoms and solvent molecules have been omitted for clarity. Color code: pink, Mn; red, O; blue, N; black, C. (Colour online.)
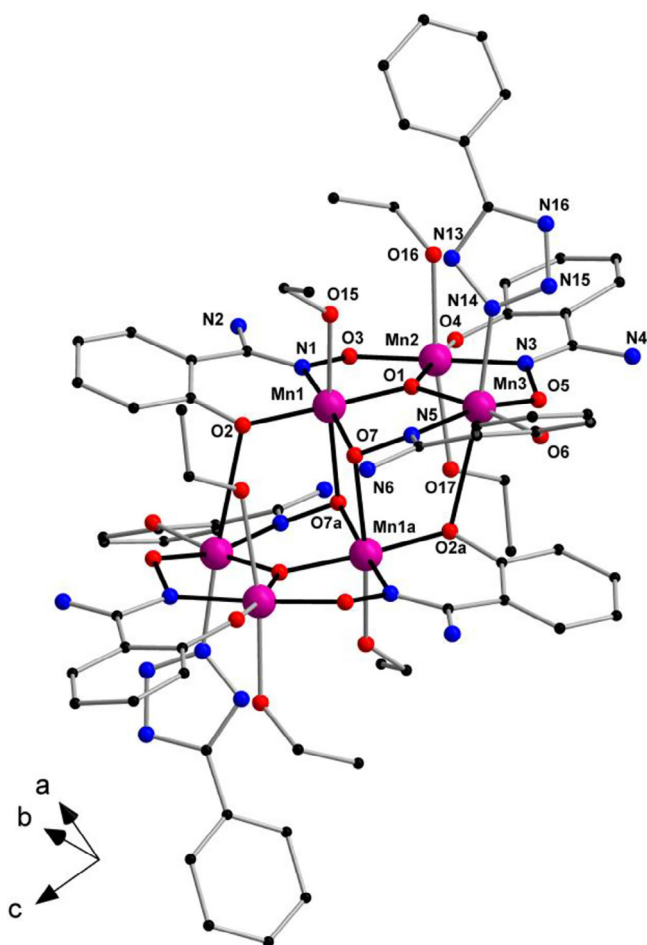

Fig. 2. Perspective drawing of the molecular structure of the $[Mn_6(\mu_3\text{-}O)_2(H_2N\text{-}sao)_6(pta)_2(EtOH)_6]$ complex of **2**. H atoms and EtOH solvent molecules have been omitted for clarity. Color code: pink, Mn; red, O; blue, N; black, C. (Colour online.)

the $N(9)\cdots O(11)\cdots N(2a)$ [(a) = $-x + 2$, $-y$, $-z + 4$] pathway, with $N\cdots O$ distances showed in Table 2. Additional hydrogen-bonding

interactions involving H_2O molecules connect the resulting Mn_6 chains, which generate a layered structure that grows along the *ac* plane by means of the $N(2)\cdots O(1wb)\cdots O(1w)\cdots N(2b)$ [(b) = $-x + 1$, $-y$, $-z + 3$] pathway (Fig. 4).

In the crystal packing of **2**, Mn_6 complexes are directly linked through H-bonding interactions and arranged in rows that grow along the *c*-axis direction (Fig. 5). These intermolecular interactions are promoted by the azole ring of one Mn_6 complex and one $-NH_2$ group of the neighboring Mn_6 molecule [$N(4)\cdots N(20a)$ = 2.95 Å and $N(16)\cdots N(10a)$ = 3.05 Å; (a) = x, y, $z - 1$] (Table 3). These rows are extended to layers on the crystallographic *ac* plane through offset face-to-face $\pi\cdots\pi$ interactions involving the pyridyl ring of the 5-phenyl-tetrazolate ligand [intercentroid distance of *ca.* 3.7 Å; (b) = $x + 1$, y, $z - 1$] (Fig. 6). In both compounds, additional weak $C\cdots C$ interactions are also observed, which help to stabilize the supramolecular arrangement in both **1** and **2**.

3.2. Magnetic properties

Direct current magnetic susceptibility measurements were carried out on microcrystalline samples of **1** and **2** in the 2.0–300 K temperature range, under external magnetic fields of 0.1 T (at $T > 25$ K) and 0.025 T (at $T < 25$ K). The $\chi_M T$ vs. T plots of **1** and **2** are shown in Figs. 7 and 8, respectively. At room temperature, the $\chi_M T$ values are approximately 17.4 and 17.7 cm³ mol⁻¹ K for **1** and **2**, respectively. These values are as expected for six magnetically isolated Mn^{III} ions ($\chi_M T \approx 18.0$ cm³ mol⁻¹ K with $S = 2$ and $g = 1.99$) and are in agreement with those previously reported for antiferromagnetically coupled Mn_6 systems [2–16]. Upon cooling, the $\chi_M T$ value in compound **1** approximately follows the Curie law to *ca.* 100 K, before $\chi_M T$ decreases to reach a final value of *ca.* 4.9 cm³ mol⁻¹ K at 2.0 K (Fig. 7). In **2**, the $\chi_M T$ value decreases, at first slowly, and then more abruptly with decreasing temperature reaching a small plateau at 10.0 K, then it decreases further to reach a final value of *ca.* 5.4 cm³ mol⁻¹ K at 2.0 K (Fig. 8). The decrease of the $\chi_M T$ values observed for **1** and **2** at low temperature are likely due to the presence of intermolecular interactions and (at lower temperatures) zero-field splitting (ZFS) effects, which have been previously reported for similar Mn_6 complexes [2–16].

The experimental data of the $\chi_M T$ vs. T plots of **1** and **2** were treated by using the $2J$ model described by the Hamiltonian of Eq. (1), where J_1 and J_2 are the exchange coupling constants for the intramolecular Mn–Mn interactions associated to exchange pathways involving the Mn—N—O—Mn torsion angles of the Mn_6 core (which is highlighted in black in Figs. 1 and 2), J_1 being associated with the higher torsion angles and J_2 with the lower ones (see point 3.1 Crystal structures of **1** and **2**). A term of Zeeman effect is included at the end of the Hamiltonian, g being the Landé factor for the Mn^{III} ions. The best-fit theoretical parameters are: $g = 1.99$, $J_1 = +0.14$ cm⁻¹, $J_2 = -0.86$ cm⁻¹ for **1**, and $g = 1.99$, $J_1 = +0.33$ cm⁻¹, $J_2 = -3.75$ cm⁻¹ for **2**. Despite a $3J$ model did not improve the fit, the curves calculated through the $2J$ model reproduce the experimental data well in the temperature ranges 2.0–300 and 5.0–300 K for **1** and **2**, respectively.

$$\hat{H} = -2J_1\left(\hat{S}_1\hat{S}_3 + \hat{S}_1\hat{S}_{3'} + \hat{S}_1\hat{S}_{1'} + \hat{S}_{1'}\hat{S}_3 + \hat{S}_{1'}\hat{S}_{3'}\right) \\ -2J_2\left(\hat{S}_1\hat{S}_2 + \hat{S}_2\hat{S}_3 + \hat{S}_{1'}\hat{S}_{2'} + \hat{S}_{2'}\hat{S}_{3'}\right) + \mu_B g H \hat{S} \tag{1}$$

The values obtained for J_1 and J_2 result to be consistent with the torsion angles found in the crystal structures of **1** and **2**, and agree with those previously reported for similar Mn_6 systems [8–16]. In both compounds, the antiferromagnetic contribution (J_2 value) is clearly the predominant magnetic interaction between the Mn^{III} metal ions, which is observed in their experimental curves (Figs. 7 and 8). DFT studies were performed in a previous work dealing
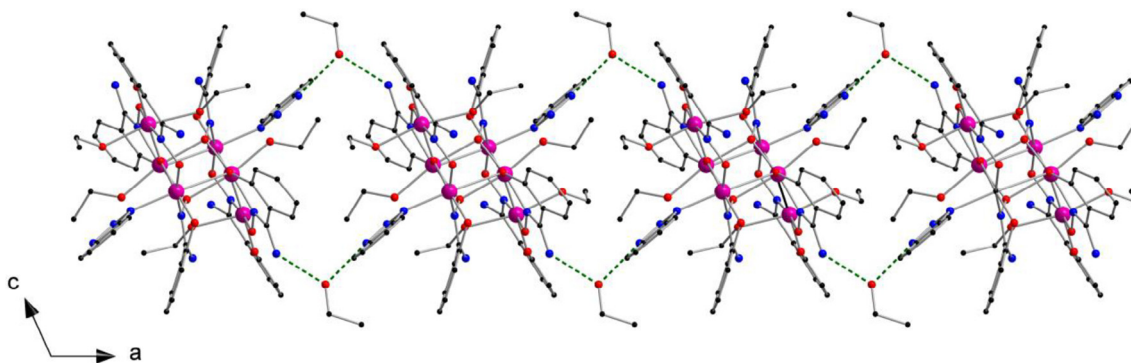
Fig. 3. View along the crystallographic *b* axis of one-dimensional motif of [$Mn_6(\mu_3\text{-}O)_2(H_2N\text{-}sao)_6(bta)_2(EtOH)_6$] complexes linked through EtOH molecules in **1**. H-bonding interactions are showed as dashed lines. Color code: pink, Mn; red, O; blue, N; black, C. (Colour online.)
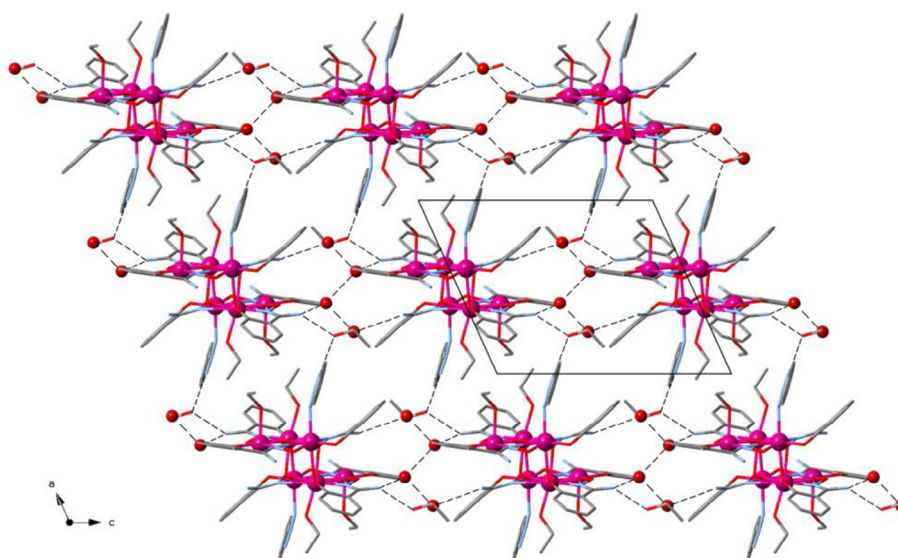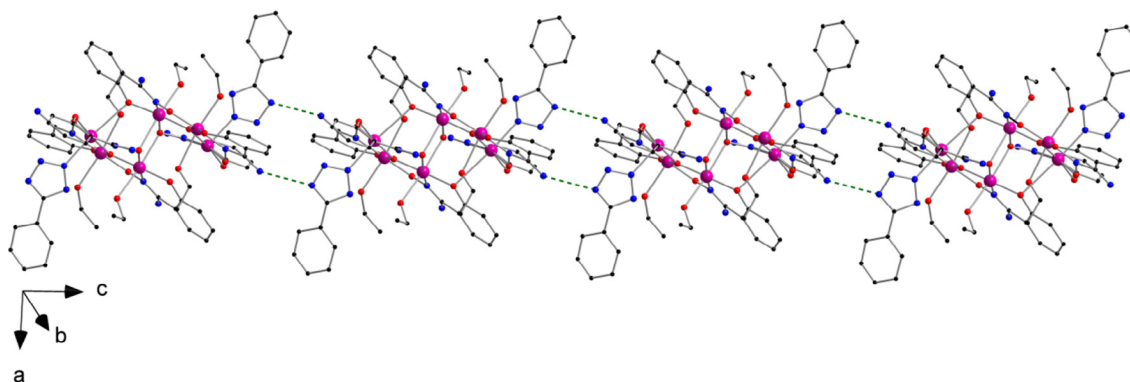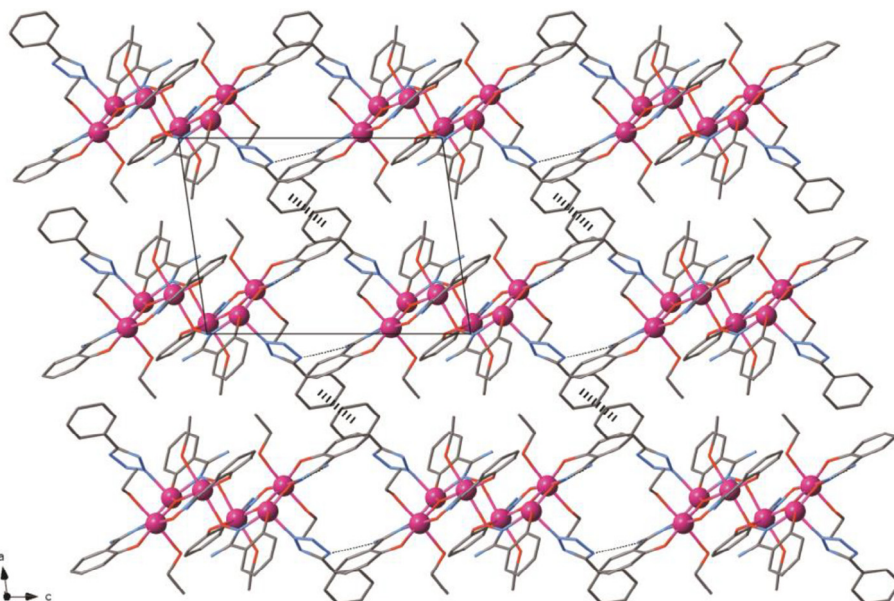

Fig. 4. View along the crystallographic *ac* plane of the two-dimensional arrangement of [$Mn_6(\mu_3\text{-}O)_2(H_2N\text{-}sao)_6(bta)_2(EtOH)_6$] complexes linked through H_2O molecules in **1**. H-bonding interactions are showed as dashed lines. Color code: pink, Mn; red, O; blue, N; black, C. (Colour online.)

Fig. 5. View of the one-dimensional motif generated through N—H⋯N interactions (dashed lines) between adjacent [$Mn_6(\mu_3\text{-}O)_2(H_2N\text{-}sao)_6(pta)_2(EtOH)_6$] complexes in **2**. Color code: pink, Mn; red, O; blue, N; black, C. (Colour online.)

with salicylamidoxime-based Mn_6 complexes [11]. It was found a critical angle of approximately 27.0°, which is directly correlated to the Mn—N—O—Mn exchange pathway between couples of Mn^{III} ions in the Mn_6 complex. Mn—N—O—Mn torsion angles upper than this critical angle switch the magnetic exchange from antiferromagnetic ($J < 0$) to ferromagnetic ($J > 0$) and vice versa. Given that

1 and **2** exhibit some Mn—N—O—Mn torsion angles lower than 27.0°, it would be expected to obtain an antiferromagnetic coupling as the predominant magnetic interaction for both compounds, as observed experimentally.

Most of the systems that form the family of oxime-based Mn_6 complexes exhibit ground state spin values that vary from 4 to

Fig. 6. View along the crystallographic *ac* plane of the two-dimensional arrangement of [Mn$_6$(μ_3-O)$_2$(H$_2$N-sao)$_6$(pta)$_2$(EtOH)$_6$] complexes linked through $\pi\cdots\pi$ interactions (dashed lines) in **2**. Color code: pink, Mn; red, O; blue, N; black, C. (Colour online.)
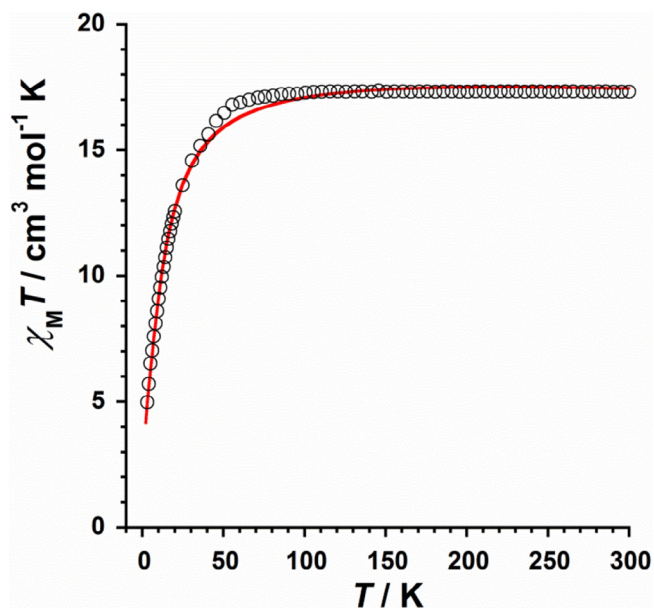
Fig. 7. Thermal variation of the $\chi_M T$ (o) product for **1**: (——) best-fit curve (see text).
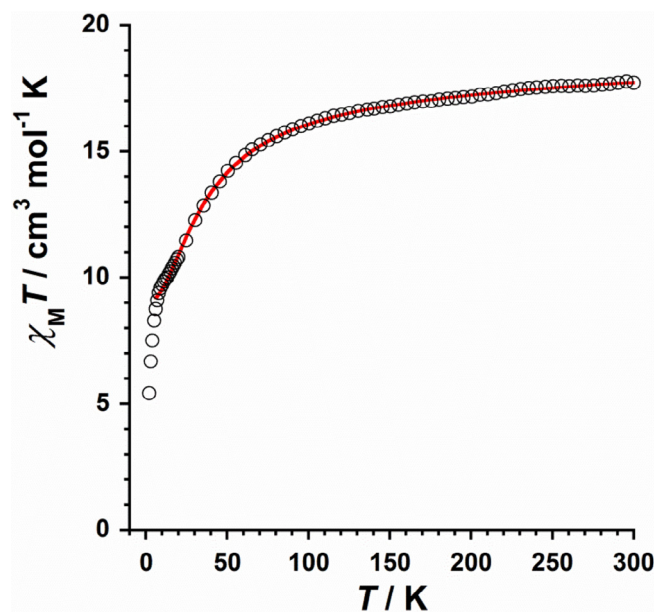
Fig. 8. Thermal variation of the $\chi_M T$ (o) product for **2**: (——) best-fit curve (see text).

12. In general, antiferromagnetic Mn$_6$ systems show a spin value of $S = 4$, whereas ferromagnetic Mn$_6$ complexes display a $S = 12$ spin value. The experimental $\chi_M T$ vs. T curve of both **1** and **2** is consistent with a predominant antiferromagnetic interaction and, therefore, a ground state spin value of $S = 4$ would be expected for both compounds. Indeed, it is what we observed from the isotropic simulation of the magnetic susceptibility of **1** and **2**, that generated the plots of the energy vs. total spin shown in Figs. 9 and 10, respectively. For both systems, the ground state spin value is $S = 4$ and the first excited state is a $S = 3$, which is placed at 2.65 and 7.04 cm^{-1} in **1** and **2**, respectively.

To substantiate these results, variable temperature-variable field dc magnetization data were measured for **1** and **2** in the 2–7 K temperature and 0.5–5.0 T field ranges. The experimental data

are given as reduced magnetization ($M/N\mu_B$ vs. $\mu_o H/T$) in Fig. 11 and Fig. 12, which were fitted to a Zeeman plus axial zero-field splitting Hamiltonian [$\hat{H} = D(\hat{S}_z^2 - S(S + 1)/3) + \mu_B g H \hat{S}$, where D is the axial anisotropy of these systems, μ_B is the Bohr magneton, $\hat{S}_z$ is the easy-axis spin operator and H is the applied field] assuming only the ground state is populated. The best fits afforded the parameters: $S = 4$, $g = 1.99$ and $D = -0.78$ cm^{-1} for **1** and $S = 4$, $g = 1.99$ and $D = -0.94$ cm^{-1} for **2**, which are in agreement with those values reported for similar Mn$_6$ complexes based on salicylamidoxime ligand [8–16].

Ac susceptibility measurements were performed on samples of **1** and **2** in the temperature range 2–8 K, in zero applied dc field, and a 3.9 G ac field oscillating in the 10–1000 Hz range of frequencies. Out-of-phase ac signals (χ''_M) for **1** and **2** are shown in Fig. 13
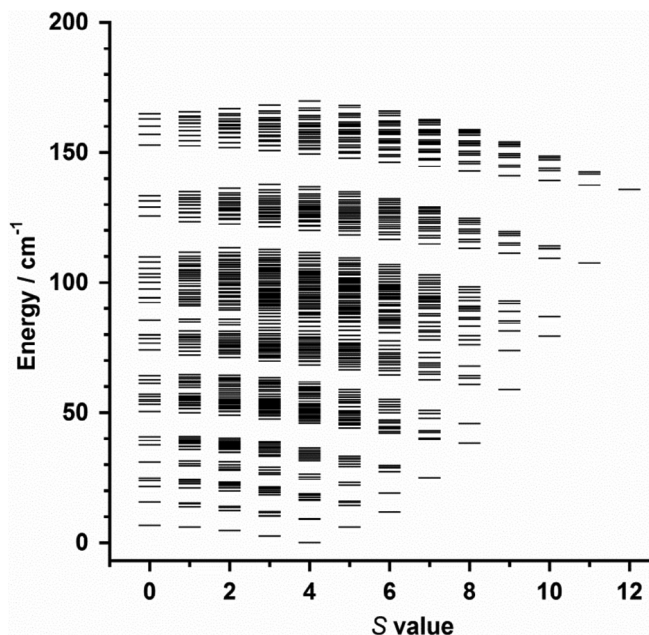
Fig. 9. Plot of energy vs. total spin state extracted from the isotropic simulation of the magnetic susceptibility data for **1**.

Fig. 10. Plot of energy vs. total spin state extracted from the isotropic simulation of the magnetic susceptibility data for **2**.

Fig. 11. Plot of the reduced magnetization ($M/N\mu_B$ vs. $\mu_o H/T$) at the indicated dc fields and temperatures 2–7 K for **1**. The solid lines represent the best fit of the experimental data.
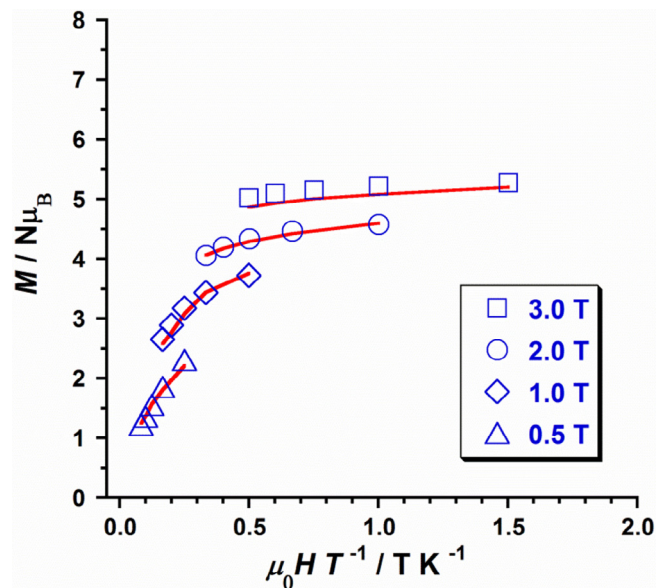
Fig. 12. Plot of the reduced magnetization ($M/N\mu_B$ vs. $\mu_o H/T$) at the indicated dc fields and temperatures 2–7 K for **2**. The solid lines represent the best fit of the experimental data.

and Fig. 14, respectively. The respective χ''_M vs. T plots exhibit frequency dependence of the χ''_M maxima for **1** and **2**. This feature is consistent with SMM behavior. In addition, it is observed that the χ''_M maxima increase with decreasing frequency for both compounds. Given that these data are in the thermally activated region and do not draw any curved line, they were fitted to the Arrhenius equation [$\tau = \tau_o \exp(E^{\#}/k_B T)$, where τ_o is the pre-exponential factor, τ is the relaxation time, $E^{\#}$ is the barrier to relaxation of the magnetization and k_B is the Boltzmann constant] and plotted in the respective insets of Figs. 13 and 14. The values obtained for the τ_o parameter are $1.05 \cdot 10^{-9}$ (**1**) and $2.16 \cdot 10^{-10}$ s^{-1} (**2**), whereas

the $E^{\#}$ values are 36.9 K (25.7 cm^{-1}) for **1** and 45.1 K (31.4 cm^{-1}) for **2**. These $E^{\#}$ values fall into the range for previously reported hexanuclear salicylamidoxime-based Mn$_6$ SMMs [24.0 K (16.7 cm^{-1}) < $E^{\#}$ < 86.0 K (59.8 cm^{-1})] [8–16].

4. Conclusions

In summary, two new members of the family of oxime-based Mn$_6$ complexes, with formula [Mn$_6$(μ_3-O)$_2$(H$_2$N-sao)$_6$(bta)$_2$ (EtOH)$_6$]·2EtOH·4H$_2$O (**1**) and [Mn$_6$(μ_3-O)$_2$(H$_2$N-sao)$_6$(pta)$_2$
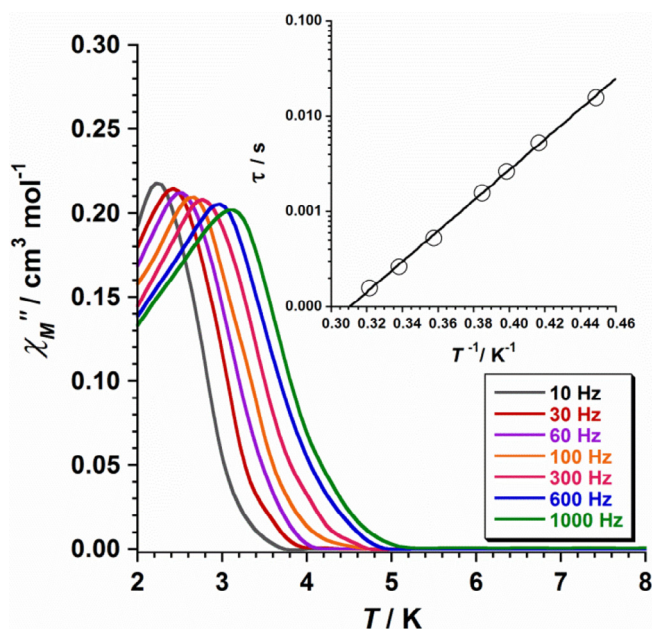
Fig. 13. Out-of-phase AC susceptibility (χ''_M) vs. T plot for compound **1**. The inset shows the Arrhenius best-fit plot (see text).
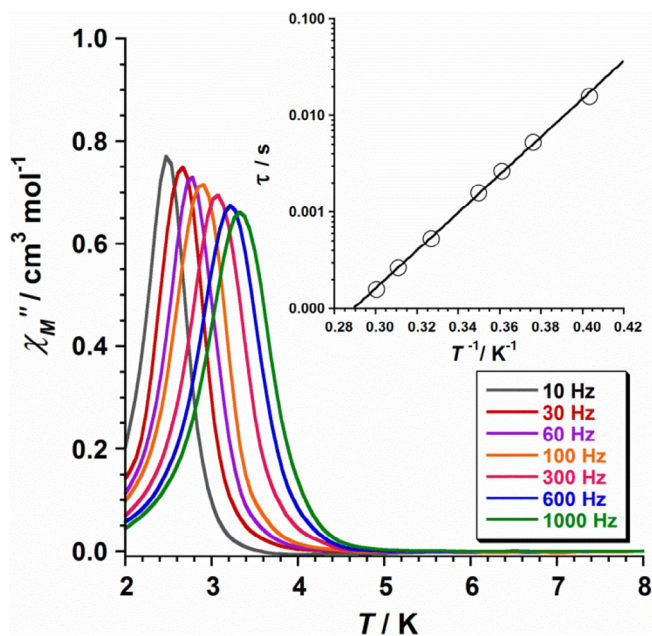
Fig. 14. Out-of-phase AC susceptibility (χ''_M) vs. T plot for compound **2**. The inset show the Arrhenius best-fit plot (see text).

$(EtOH)_6$]·4EtOH (**2**) [H_2N-saoH$_2$ = salicylamidoxime, bta = 1,2,3-benzotriazolate anion, pta = 5-phenyl-tetrazolate anion] have been synthesized with azole-type ligands and magnetostructurally characterized. Our results revealed that **1** and **2** display a ground state spin value $S = 4$, that is consistent with the values of their Mn—N—O—Mn torsion angles. Both compounds exhibit out-of-phase AC signals typical of single-molecule magnet (SMM) phenomenon. Remarkably, the crystal structure of compound **2** is the first reported example of Mn complex containing 5-phenyl-tetrazole.

Appendix A. Supplementary data

CCDC 1910059–1910060 contain the supplementary crystallographic data for **1** and **2**. These data can be obtained free of charge via http://www.ccdc.cam.ac.uk/conts/retrieving.html, or from the Cambridge Crystallographic Data Centre, 12 Union Road, Cambridge CB2 1EZ, UK; fax: (+44) 1223-336-033; or e-mail: deposit@ccdc.cam.ac.uk.

References

[1] J. Ferrando-Soria, J. Vallejo, M. Castellano, J. Martínez-Lillo, E. Pardo, J. Cano, I. Castro, F. Lloret, R. Ruiz-García, M. Julve, Coord. Chem. Rev. 339 (2017) 17.
[2] C.J. Milios, C.P. Raptopoulou, A. Terzis, F. Lloret, R. Vicente, S.P. Perlepes, A. Escuer, Angew. Chem., Int. Ed. 43 (2004) 210.
[3] C.J. Milios, A. Vinslava, P.A. Wood, S. Parsons, W. Wernsdorfer, G. Christou, S.P. Perlepes, E.K. Brechin, J. Am. Chem. Soc. 129 (2007) 8.
[4] C.J. Milios, A. Vinslava, W. Wernsdorfer, S. Moggach, S. Parsons, S.P. Perlepes, G. Christou, E.K. Brechin, J. Am. Chem. Soc. 129 (2007) 2754.
[5] C.J. Milios, S. Piligkos, E.K. Brechin, Dalton Trans. (2008) 1809.
[6] R. Inglis, C.J. Milios, L.F. Jones, S. Piligkos, E.K. Brechin, Chem. Commun. 48 (2012) 181.
[7] D.A. Kalofolias, A.G. Flamourakis, M. Siczek, T. Lis, C.J. Milios, J. Coord. Chem. 68 (2015) 1.
[8] A.-R. Tomsa, J. Martínez-Lillo, Y. Li, L.-M. Chamoreau, K. Boubekeur, F. Farias, M.A. Novak, E. Cremades, E. Ruiz, A. Proust, M. Verdaguer, P. Gouzerh, Chem. Commun. 46 (2010) 5106.
[9] G.-Y. An, A.-L. Cui, H.-Z. Kou, Inorg. Chem. Commun. 14 (2011) 1475.
[10] J. Martínez-Lillo, L.-M. Chamoreau, A. Proust, M. Verdaguer, P. Gouzerh, C. R. Chim. 15 (2012) 889.
[11] J. Martínez-Lillo, A.-R. Tomsa, Y. Li, L.-M. Chamoreau, E. Cremades, E. Ruiz, A.-L. Barra, A. Proust, M. Verdaguer, P. Gouzerh, Dalton Trans. 41 (2012) 13668.
[12] J. Martínez-Lillo, N. Dolan, E.K. Brechin, Dalton Trans. 42 (2013) 12824.
[13] J. Martínez-Lillo, N. Dolan, E.K. Brechin, Dalton Trans. 43 (2014) 4408.
[14] J. Martínez-Lillo, J. Cano, W. Wernsdorfer, E.K. Brechin, Chem. Eur. J. 21 (2015) 8790.
[15] C. Rojas-Dotti, J. Martínez-Lillo, RSC Adv. 7 (2017) 48841.
[16] C. Rojas-Dotti, N. Moliner, F. Lloret, J. Martínez-Lillo, Crystals 9 (2019) 23.
[17] F. Giordano, Acta Crystallogr., Sect. B 36 (1980) 2458.
[18] I. Sotofte, K. Nielsen, Acta Chem. Scand., Ser. A 35 (1981) 739.
[19] J. Emsley, N.M. Reza, H.M. Dawes, M.B. Hursthouse, Chem. Commun. (1985) 1458.
[20] X.-G. Meng, J.-L. Qian, Acta Crystallogr., Sect. E 62 (2006) o4178.
[21] J. Martínez-Lillo, J. Kong, M. Julve, E.K. Brechin, Cryst. Growth Des. 14 (2014) 5985.
[22] C. Yélamos, K.R. Gust, A.G. Baboul, M.J. Heeg, H.B. Schlegel, C.H. Winter, Inorg. Chem. 40 (2001) 6451.
[23] M.S. Hill, P.B. Hitchcock, Polyhedron 23 (2004) 801.
[24] R. Guilard, I. Perrot, A. Tabard, P. Richard, C. Lecomte, Y.H. Liu, K.M. Kadish, Inorg. Chem. 30 (1991) 27.
[25] O.M. El-Kadri, M.J. Heeg, C.H. Winter, J. Organomet. Chem. 696 (2011) 1975.
[26] M. Saha, R. Nasani, S.M. Mobin, B. Pathak, S. Mukhopadhyay, Inorg. Chem. Commun. 34 (2013) 62.
[27] M. Saha, R. Nasani, M. Das, S.M. Mobin, B. Pathak, S. Mukhopadhyay, Inorg. Chem. Front. 1 (2014) 599.
[28] J. Lach, E. Perlt, B. Kirchner, Z. Anorg. Allg. Chem. 639 (2013) 524.
[29] R. Nasani, M. Saha, S.M. Mobin, S. Mukhopadhyay, Polyhedron 55 (2013) 24.
[30] M. Saha, R. Nasani, M. Das, A. Mahata, B. Pathak, S.M. Mobin, L.M. Carrella, E. Rentschler, S. Mukhopadhyay, Dalton Trans. 43 (2014) 8083.
[31] N. Malviya, P. Mandal, M. Das, R. Ganguly, S. Mukhopadhyay, J. Coord. Chem. 70 (2017) 261.
[32] M. Saha, N. Malviya, M. Das, I. Choudhuri, S.M. Mobin, B. Pathak, S. Mukhopadhyay, Polyhedron 121 (2017) 155.
[33] Z.-H. Shao, J. Luo, R.-F. Cai, X.-G. Zhou, L.-H. Weng, Z.-X. Chen, Acta Crystallogr., Sect. E. 60 (2004) m225.
[34] X. He, C.-Z. Lu, C.-D. Wu, L.-J. Chen, Eur. J. Inorg. Chem. (2006) 2491.
[35] W.-C. Song, J.-R. Li, C. Sañudo, J. Liu, X.-H. Bu, Aust. J. Chem. 62 (2009) 941.
[36] A.P. Mosalkova, S.V. Voitekhovich, A.S. Lyakhov, L.S. Ivashkevich, P.N. Gaponik, O.A. Ivashkevich, Z. Anorg. Allg. Chem. 638 (2012) 103.

[37] M. Saha, K.M. Vyas, L.M.D.R.S. Martins, N.M.R. Martins, A.J.L. Pombeiro, S.M. Mobin, D. Bhattacherjee, Polyhedron 132 (2017) 53.

[38] Q. Ye, Y.-H. Li, Y.-M. Song, X.-F. Huang, R.-G. Xiong, Z. Xue, Inorg. Chem. 44 (2005) 3618.

[39] W.-C. Song, J.-R. Li, P.-C. Song, Y. Tao, Q. Yu, X.-L. Tong, X.-H. Bu, Inorg. Chem. 48 (2009) 3792.

[40] D.-S. Liu, Y. Sui, W.-T. Chen, P. Feng, Cryst. Growth Des. 15 (2015) 4020.

[41] M.-Y. Li, H.-X. Zhang, F. Wang, J. Zhang, Inorg. Chem. Front. 5 (2018) 675.

[42] F. Eloy, R. Lenaers, Chem. Rev. 62 (1962) 155.

[43] G.A. Bain, J.F. Berry, J. Chem. Educ. 85 (2008) 532.

[44] SHELXTL-2013/4, Bruker Analytical X-ray Instruments, Madison, WI, 2013.

[45] DIAMOND 4.5.0, Crystal Impact GbR, CRYSTAL IMPACT, 2018.

[46] D.C. Palmer, CrystalMaker Software Ltd, Begbroke, Oxfordshire, England, 2014.

Article 3.

Thioester-functionalised and oxime-based hexametallic manganese(III) single-molecule magnets

Check for updates

Thioester-functionalised and oxime-based hexametallic manganese(III) single-molecule magnets†

Carlos Rojas-Dotti and José Martínez-Lillo (ID)*

Two novel hexametallic Mn^{III} complexes of formulae [Mn$_6$(μ_3-O)$_2$(H$_2$N-sao)$_6$(3-atpa)$_2$(EtOH)$_6$]·2EtOH·2H$_2$O (**1**) and [Mn$_6$(μ_3-O)$_2$(H$_2$N-sao)$_6$(6-atha)$_2$(EtOH)$_6$]·6EtOH (**2**) [H$_2$N-saoH$_2$ = salicylamidoxime, 3-hatpa = 3-(acetylthio)propionic acid, 6-hatha = 6-(acetylthio)hexanoic acid] have been synthesised by using thioester-carboxylate ligands and magnetostructurally characterised. **1** crystallises in the triclinic system with space group $P\bar{1}$ and **2** crystallises in the monoclinic system with space group $P2_1/c$. The study of the dc and ac magnetic susceptibility reveals single-molecule magnet behaviour for both compounds with spin-ground states $S = 12$ and $S = 4$ for **1** and **2**, respectively. Hence, **1** and **2** are new members of the oxime-based family of [Mn$_6$] single-molecule magnets, containing the thioester group functionalisation, which could be used to connect devices in molecular spintronics studies.

Introduction

Single-Molecule Magnets (SMMs) have attracted much interest because of their spin properties and potential applications, and have also been considered a fundamental link between two novel scientific disciplines, molecular spintronics and molecular electronics.[1–4] In recent years, great research effort has been devoted to the synthesis of single-molecule systems, with large magnetic anisotropies, and their functionalization, which is made with functional groups convenient to connect suitable SMMs to junction devices or to perform their grafting on surfaces of Si or Au substrates;[5–10] in many cases, looking for the improvement of their magnetic properties,[7,8] the control of the nanoscale organization[10] or simply to get a reliable description of the electronic structure of the investigated system.[11]

Thioesters-based ligands have proven to be particularly useful to get derivatised and suitable SMMs for this research field (Scheme 1). Indeed, [Fe$_4^{III}$Ni$_4^{II}$] cages have been connected to junction devices,[9] besides that, complexes such as the well-known [Mn$_8^{III}$Mn$_4^{IV}$] system and the [Fe$_4^{III}$] and [Fe$_3^{III}$Cr^{III}] complexes with star-like structures have been grafted on Au surfaces after being thioester-functionalised.[10]

Oxime-based hexanuclear Mn^{III} SMMs have intensively been studied in the field of molecular magnetism.[12–16] In these

systems, the magnetic exchange between Mn^{III} ions depends basically on the Mn–N–O–Mn torsion angles, they possess generally spin ground states varying from 4 to 12, and the anisotropy energy barriers vary from 24 to 86 K.[12–16] Some of these [Mn$_6^{III}$] SMMs have also been grafted on Au surfaces and studied, as thiophene-carboxylate [Mn$_6^{III}$] derivatives.[7,8] Nevertheless, no thioester-functionalised [Mn$_6^{III}$] compound has been reported up to date.

Herein we report the synthesis and magnetostructural characterisation of two novel hexanuclear Mn^{III} compounds of formulae [Mn$_6$(μ_3-O)$_2$(H$_2$N-sao)$_6$(3-atpa)$_2$(EtOH)$_6$]·2EtOH·2H$_2$O (**1**) and [Mn$_6$(μ_3-O)$_2$(H$_2$N-sao)$_6$(6-atha)$_2$(EtOH)$_6$]·6EtOH (**2**) [H$_2$N-saoH$_2$ = salicylamidoxime, 3-hatpa = 3-(acetylthio)propionic acid, 6-hatha = 6-(acetylthio)hexanoic acid]. **1** and **2** are the first reported structures of thioester-functionalised [Mn$_6^{III}$] SMMs.

Instituto de Ciencia Molecular (ICMol), Departament de Química Inorgànica, Universitat de València, c/ Catedrático José Beltrán 2, Paterna, 46980, Valencia, Spain. E-mail: f.jose.martinez@uv.es

Scheme 1 Molecular structures of: (A) 3-(acetylthio)propionic acid and (B) 6-(acetylthio)hexanoic acid.

Results and discussion

Synthetic procedure

By reacting $MnCl_2 \cdot 4H_2O$ with the salicylamidoxime ligand in the presence of the desired S-acetyl-carboxylic acid and NEt_3 we obtain a dark green microcrystalline solid of hexametallic Mn^{III} complexes in satisfactory yields. Good-sized crystals were obtained from concentrated solutions of the microcrystalline solid in ethanol by layering them with acetone (1) and ethanol (2) (see Experimental section). Hence, this is a straightforward synthetic procedure to add the S-acetyl function [CH$_3$–C(O)–S–] to the well-known family of [Mn$_6$] complexes (Fig. 1, 2, S1 and S2†).

Description of the crystal structures of 1 and 2

Compound 1 crystallises in the triclinic system with space group $P\bar{1}$, and compound 2 crystallises in the monoclinic system with space group $P2_1/c$ (Table 1). Their structures are made up of neutral hexanuclear [Mn$_6$] complexes together with water (1) and ethanol (1 and 2) molecules of crystallisation, which are self-assembled through hydrogen-bonding interactions (see Fig. 3 and S3†).

Each hexanuclear [Mn$_6$(μ_3-O)$_2$(H$_2$N-sao)$_6$(L)$_2$(EtOH)$_6$] [L = 3-acetylthiopropionate (3-atpa) in 1 and 6-acetylthiohexanoate (6-atha) in 2] complex contains two symmetry equivalent {Mn$_3$(μ_3-O)} triangular moieties, which are linked by two phenolate and two oximate oxygen atoms that are related by an inversion centre. Their hexanuclear cores are rather similar to previously reported salicylamidoxime-based [Mn$_6$] complexes.[13–16] The six Mn^{III} ions exhibit distorted octahedral geometries with the Jahn–Teller axes approximately perpendicular to the {Mn$_3$(μ_3-O)} planes, with the central O^{2-} ion displaced 0.04 Å and 0.03 Å above the plane of the [Mn$_3$] triangle for 1 and 2, respectively. The monodentate carboxylate ligand is coordinate on the Mn(1) atom in 1, on the Mn(3) atom in 2 and

on their symmetry equivalents. The remaining coordination sites are occupied by EtOH molecules. The Mn–N–O–Mn torsion angles of the [Mn$_3$(μ_3-O)(H$_2$N-sao)$_3$] triangular units are 42.6, 30.1 and 27.5 for 1 and 38.9, 36.5 and 26.0 for 2.

In the crystal packing of 1 and 2, the neutral [Mn$_6$] complexes are mainly connected by hydrogen bonding interactions. In 1, the acetylthio groups are H-bonded through the carbonyl to the –NH$_2$ groups on the salicylamidoxime ligands of adjacent [Mn$_6$] units (O⋯N distance, ∼3.01 Å) (see Fig. 3).

Each [Mn$_6$] is involved in four of these interactions, linking them into chains that grow along the c axis (Fig. 3). In 2, EtOH molecules sit between neighbouring [Mn$_6$] complexes and are

Fig. 2 Perspective view of the molecular structure of the [Mn$_6$(μ_3-O)$_2$(H$_2$N-sao)$_6$(6-atha)$_2$(EtOH)$_6$] complex of 2. H atoms and solvent molecules of crystallisation have been omitted for clarity [colour code: pink, Mn; yellow, S; red, O; blue, N; black, C].
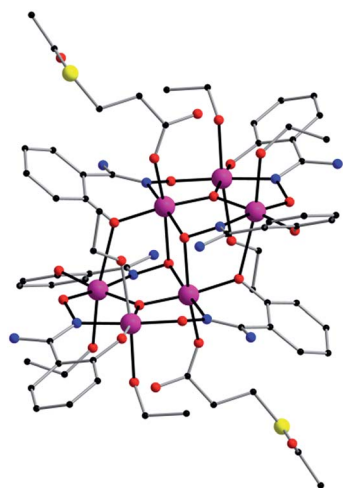
Fig. 1 Perspective view of the molecular structure of the [Mn$_6$(μ_3-O)$_2$(H$_2$N-sao)$_6$(3-atpa)$_2$(EtOH)$_6$] complex of 1. H atoms and solvent molecules of crystallisation have been omitted for clarity [colour code: pink, Mn; yellow, S; red, O; blue, N; black, C].

Table 1 Summary of the crystal data for compounds 1 and 2

Compound	1	2
Formula	C$_{68}$H$_{102}$O$_{30}$N$_{12}$S$_2$Mn$_6$	C$_{82}$H$_{134}$O$_{32}$N$_{12}$S$_2$Mn$_6$
M_r	1961.34	2193.77
Crystal system	Triclinic	Monoclinic
Space group	$P\bar{1}$	$P2_1/c$
a/Å	12.614(1)	15.993(1)
b/Å	13.146(1)	13.559(1)
c/Å	14.873(1)	23.506(1)
α/°	70.67(1)	90
β/°	76.15(1)	97.23(1)
γ/°	66.10(1)	90
V/Å^3	2111.8(3)	5056.6(2)
Z	1	2
D_c/g cm^{-3}	1.539	1.441
μ(Mo-K$_\alpha$)/mm^{-1}	8.283	0.850
$F(000)$	1012	2296
Goodness-of-fit on F^2	1.008	1.009
R_1 [$I > 2\sigma(I)$]	0.0733	0.0751
wR_1 [$I > 2\sigma(I)$]	0.1887	0.1739

104

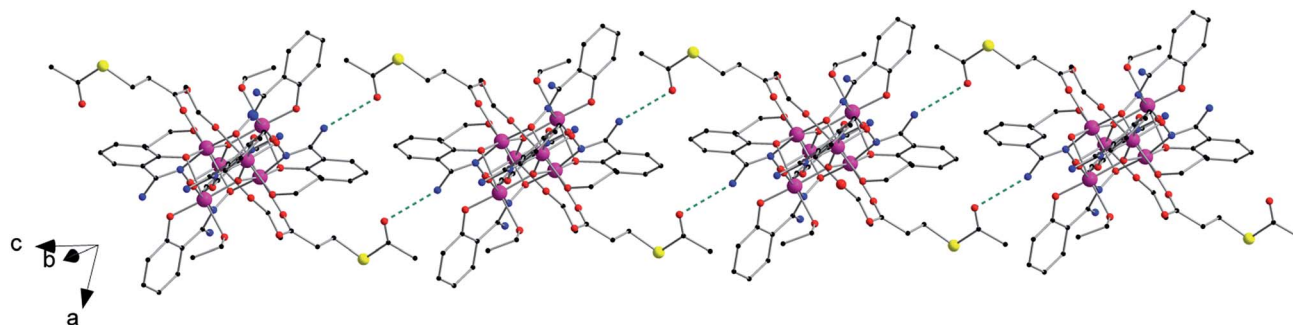**Fig. 3** View of the one-dimensional motif generated by hydrogen bonds (N⋯O distance, ~3.01 Å) between the −NH₂ and CH₃−C(O)−S− groups of adjacent [Mn₆] units in the crystal of **1** (dashed green lines) [colour code: pink, Mn; yellow, S; red, O; blue, N; black, C].

simultaneously H-bonded to –NH$_2$ (O⋯N distance, ~2.85 Å) and carboxylate (O⋯O distance, ~2.72 Å) groups generating chains that grow along the c axis (Fig. S3†). Intermolecular S⋯S contacts are observed neither in **1** nor in **2**, the shortest S⋯S distances being *ca.* 5.31 Å (**1**) and *ca.* 7.99 (**2**) Å. Additional weak C⋯C interactions are also observed, in **1**, between aromatic rings of salicylamidoxime ligands of neighbouring [Mn$_6$] complexes (*ca.* 3.33 Å) and, in **2**, between aromatic rings of salicylamidoxime ligands and thioester groups of adjacent [Mn$_6$] units (*ca.* 3.67 Å), which stabilize the supramolecular arrangement in **1** and **2**.

Magnetic properties of 1 and 2

Dc magnetic susceptibility measurements were performed on microcrystalline samples of **1** and **2** in the 2.0–300 K temperature range, under an external magnetic field of 0.1 T. The magnetic properties of **1** and **2** in the form of $\chi_M T$ *vs.* T plot (χ_M being the molar magnetic susceptibility) are shown in Fig. 4. At room temperature the $\chi_M T$ values are 20.0 (**1**) and 18.0 cm^3 mol^{-1} K (**2**). Upon cooling, these values approximately follows the Curie law to *ca.* 100 K for both compounds. Then, for complex **1**, $\chi_M T$ rises gradually with decreasing temperature, reaching a maximum value of 28.0 cm^3 mol^{-1} K at 8.0 K. This feature reveals an intramolecular ferromagnetic coupling between the Mn^{III} ions. $\chi_M T$ is then decreasing at lower temperatures. The value of $\chi_M T$ in **2** decreases with decreasing temperature reaching a final value of *ca.* 6.5 cm^3 mol^{-1} K at 2.0 K, indicating antiferromagnetic interaction as the resulting magnetic exchange (Fig. 4). The decrease of the $\chi_M T$ for both compounds at lower temperatures is likely due to the presence of intermolecular interactions and/or zero-field splitting (zfs) effects.

These experimental data were treated by using the 2J model described by the Hamiltonian of eqn (1) and Fig. S4,† affording the parameters: $J_1 = +0.45$ cm^{-1}, $J_2 = +0.11$ cm^{-1} and $g = 1.99$ for **1** and $J_1 = +0.86$ cm^{-1}, $J_2 = -1.14$ cm^{-1} and $g = 1.99$ for **2**. This data treatment has satisfactorily been performed in previous works.[12]

$$\hat{H} = -2J_1(\hat{S}_1\hat{S}_3 + \hat{S}_1\hat{S}_3 + \hat{S}_1\hat{S}_{1'} + \hat{S}_{1'}\hat{S}_3 + \hat{S}_{1'}\hat{S}_{3'})$$
$$- 2J_2(\hat{S}_1\hat{S}_2 + \hat{S}_2\hat{S}_3 + \hat{S}_{1'}\hat{S}_{2'} + \hat{S}_{2'}\hat{S}_{3'}) + \mu_B g H \hat{S} \qquad (1)$$
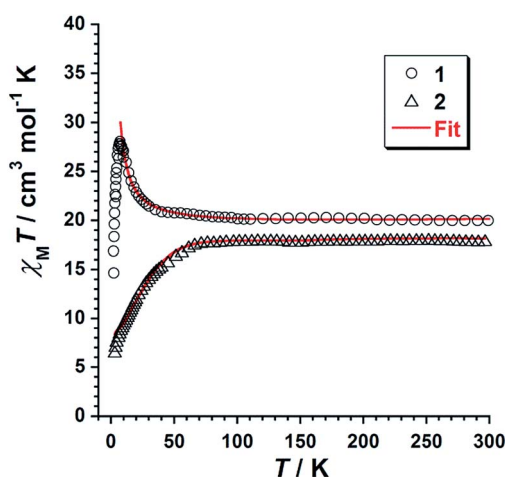
Fig. 4 Plot of $\chi_M T$ *vs.* T obtained from compounds **1** and **2**. The solid red line represents the fit of the experimental data obtained for **1** and **2** using the 2J model of Hamiltonian (1).

The obtained J_1, J_2 and g values result to be consistent with the torsion angles found in the crystal structures of **1** and **2**, and agree with those previously reported for similar [Mn$_6$] systems.[12–16]

In a previous work dealing with DFT studies on salicylamidoxime-based [Mn$_6$] complexes,[13c] it was established that the critical angle where the exchange pathway between neighbouring Mn^{III} ions switches from antiferromagnetic ($J < 0$) to ferromagnetic ($J > 0$) is *ca.* 27.0°, which is somewhat lower than that of the related salicylaldoxime-based [Mn$_6$] complexes.[13c]

Our results nicely reflect that fact, given that compound **1**, with the lowest torsion angle being 27.5°, gave positive J_1 and J_2 values indicating a ferromagnetic exchange, whereas in compound **2**, with 26.0° as the lowest torsion angle, the sign and magnitude of the obtained J_2 value indicate that the main magnetic exchange is antiferromagnetic. Given that the value of J_1 (exchange between Mn^{III} ions of different [Mn$_3$] triangles of the [Mn$_6$] unit) is positive in both compounds, what is making the difference to get a $S = 4$ or $S = 12$ total spin is the value of J_2 (exchange constant within each trinuclear [Mn$_3$] subunit).

105

Variable temperature-variable field dc magnetisation data were measured for **1** and **2** in the 2–7 K temperature and 0.5–7.0 T field ranges. The experimental data are given as reduced magnetisation in Fig. 5 and 6. These data do not reach the saturation values, maybe because excited states with lowest spins are also populated. Anyway, they were well fitted to a Zeeman plus axial zero-field splitting Hamiltonian [$\hat{H} = D(\hat{S}_z^2 - S(S + 1)/3) + \mu_B g H \hat{S}$, where D is the axial anisotropy of the [Mn$_6$] cluster, μ_B is the Bohr magneton, $\hat{S}_z$ is the easy-axis spin operator and H is the applied field] assuming only the ground state is populated.[12] The best fits afforded the parameters $S = 12$, $g = 1.98$ and $D = -0.44$ cm^{-1} for **1** and $S = 4$, $g = 2.00$ and $D = -0.98$ cm^{-1} for **2**, which are in line with other members of the [Mn$_6$] family.[12–16] Besides the results obtained by fitting the experimental data of the reduced magnetisation, ground state spin values of $S = 12$ (**1**) and $S = 4$ (**2**) were also obtained

from dc susceptibility measurements. Indeed, plots of the energy *versus* total spin, extracted from the isotropic simulation of the magnetic susceptibility, are shown in Fig. 7 and 8 for **1** and **2**, respectively. The first excited state found in **1** is a $S = 11$ located at 1.75 cm^{-1}, and the first excited state in **2** is a $S = 3$ located at 0.85 cm^{-1} (Fig. 7 and 8).

Ac susceptibility measurements were performed on samples of **1** and **2** in the temperature range 2–8 K, in zero applied dc field and a 3.9 G ac field oscillating in the 5–1000 Hz range of frequencies. Out-of-phase ac signals (χ''_M) for **1** and **2** are shown in Fig. 9 (**1**) and Fig. 10 (**2**), which exhibit frequency dependence of the χ''_M maxima. This feature is consistent with SMM behaviour. In **2**, it is observed that the χ''_M maxima decrease with decreasing frequency, which is a peculiarity typical of strong intermolecular interactions in single-molecule and chain magnets (SMMs and SCMs).[17,18]

We fitted these data to the Arrhenius equation [$\tau = \tau_o \exp(U_{eff}/k_B T)$, where τ_o is the pre-exponential factor, τ is the relaxation time, U_{eff} is the barrier to relaxation of the magnetisation and k_B is the Boltzmann constant]. The inset of the Fig. 9
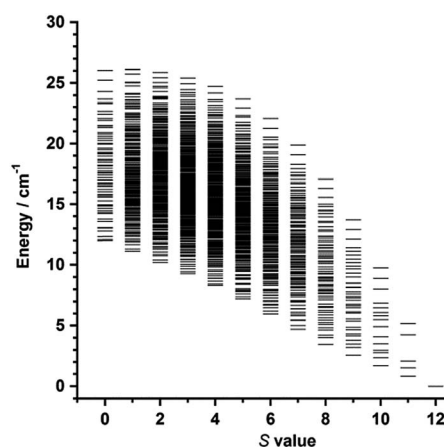
Fig. 5 Plot of the reduced magnetisation ($M/N\mu_B$ *vs.* $\mu_0 H/T$) for **1** in 4, 5, 6 and 7 T fields and temperatures 2−5 K. The solid lines represent the best fit of the experimental data.

Fig. 7 Plot of energy *versus* total spin state, extracted from the isotropic simulation of the susceptibility data, for **1**.

Fig. 6 Plot of the reduced magnetisation ($M/N\mu_B$ *vs.* $\mu_0 H/T$) for **2** in 0.5, 1, 2 and 3 T fields and temperatures 2−5 K. The solid lines represent the best fit of the experimental data.
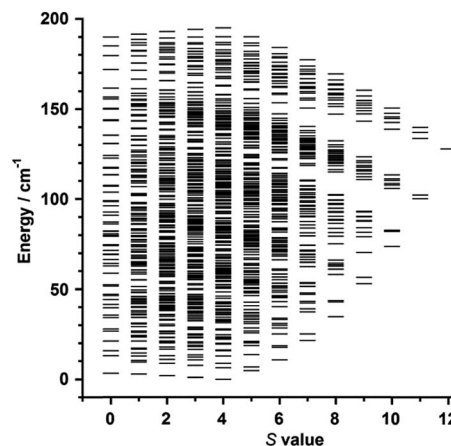
Fig. 8 Plot of energy *versus* total spin state, extracted from the isotropic simulation of the susceptibility data, for **2**.
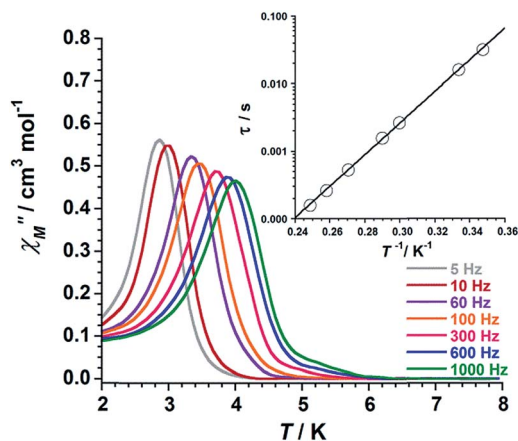
Fig. 9 Out-of-phase ac susceptibility (χ''_M) versus T plot for **1**. The inset shows the Arrhenius best-fit plot (see text).
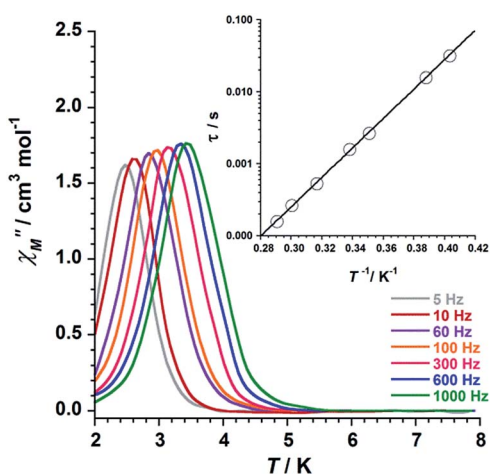
Fig. 10 Out-of-phase ac susceptibility (χ''_M) versus T plot for **2**. The inset shows the Arrhenius best-fit plot (see text).

(**1**) and Fig. 10 (**2**) shows these Arrhenius plots. The obtained values for τ_o and U_{eff} are 2.6×10^{-10} s and 54.0 K for **1** and 1.9×10^{-10} s and 47.0 K for **2**, respectively. These U_{eff} values for **1** and **2** fall into the range (24.0 K < U_{eff} < 86.0 K) for previously reported salicylamidoxime-based [Mn$_6$] complexes.[13–16]

Conclusions

In summary, the crystal structures and magnetic behaviour of two novel [Mn$_6$] single-molecule magnets (SMMs) of formula [Mn$_6(\mu_3$-O)$_2$(H$_2$N-sao)$_6$(3-atpa)$_2$(EtOH)$_6$]·2EtOH·2H$_2$O (**1**) and [Mn$_6(\mu_3$-O)$_2$(H$_2$N-sao)$_6$(6-atha)$_2$(EtOH)$_6$]·6EtOH (**2**) [H$_2$N-saoH$_2$ = salicylamidoxime, 3-hatpa = 3-(acetylthio)propionic acid, 6-hatha = 6-(acetylthio)hexanoic acid] have been reported. **1** and **2** are the first examples of thioester-functionalised complexes in the coordination chemistry of oxime-based [Mn$_6$] SMMs, these structures also being the first reported complexes containing the 3-(acetylthio)propionate (3-atpa) and 6-(acetylthio)hexanoate (6-atha) ligands. Such features, together with their

relative stability, make **1** and **2** suitable SMMs to be studied on devices in the field of molecular spintronics. Indeed, we believe that our compounds could be adequate systems to be connected to junction devices. This investigation is underway.

Experimental

Materials and physical measurements

All manipulations were performed under aerobic conditions, using chemicals as received from Sigma-Aldrich. Elemental analyses (C, H, and N) were performed by the Central Service for the Support to Experimental Research (SCSIE) at the University of Valencia. Infrared spectra of **1** and **2** were recorded as KBr pellets using a PerkinElmer Spectrum 65 FT-IR spectrometer in the 4000–400 cm^{-1} region. Dc and ac magnetic susceptibility measurements on microcrystalline samples of **1** and **2** were carried out on a Quantum Design MPMS-XL SQUID magnetometer. The dc studies were performed in the temperature range of 2–300 K in an applied magnetic field of 0.1 T. The ac susceptibility measurements were performed in zero applied dc field and a 3.9 G ac oscillating field with temperature and frequency ranges of 2–8 K and 5–1000 Hz, respectively. Diamagnetic corrections were applied to the observed paramagnetic susceptibilities using Pascal's constants.[19,20]

Preparation of the complexes

1. MnCl$_2$·4H$_2$O (0.594 g, 3.0 mmol) was added dropwise and with constant stirring to a solution formed by H$_2$N-saoH$_2$ (0.456 g, 3.0 mmol) and 3-acetylthiopropionic acid (1.0 g, 6.8 mmol) in EtOH (100 mL), then NEt$_3$ (2.0 mL, 3.58 mmol) was added. After stirring for 1 h a dark green solution was generated and left to evaporate at room temperature. A dark green microcrystalline solid was formed in 1 day, separated by filtration and washed with EtOH and ether. Yield: 84%. Suitable crystals for X-ray diffraction studies were formed by layering a concentrated acetone solution of the microcrystalline solid with EtOH. Anal. calcd (found) for C$_{68}$H$_{102}$O$_{30}$N$_{12}$S$_2$Mn$_6$ (**1**): C, 41.6 (41.5); H, 5.2 (4.9); N, 8.6 (9.0)%. Selected IR peaks (in KBr, cm^{-1}): 3332m, 1605vs, 1575m, 1530s, 1481m, 1439m, 1420m, 1315s, 1253s, 1146m, 1023s, 881s, 757m, 684vs, 649m, 579w, 474w.

2. Complex **2** was prepared as **1** but by using 6-acetylthiohexanonic acid (1.0 mL, 6.0 mmol) instead of 3-acetylthiopropionic acid. Yield: 77%. A concentrated ethanolic solution of **2** was layered with the same solvent to give suitable crystals by slow diffusion. Anal. calcd (found) for C$_{82}$H$_{134}$O$_{32}$N$_{12}$S$_2$Mn$_6$ (**2**): C, 44.9 (45.1); H, 6.2 (5.9); N, 7.7 (8.1)%. Selected IR peaks (in KBr/cm^{-1}): 3326m, 2928m, 1604vs, 1574m, 1527s, 1482m, 1440m, 1418m, 1317s, 1254s, 1146m, 1023s, 883s, 750m, 686vs, 648m, 579w, 553w, 474w.

X-ray data collection and structure refinement

X-ray diffraction data on single crystals of **1** and **2** were collected on a Rigaku Oxford Diffraction SuperNova diffractometer with graphite-monochromated and Cu-K$_\alpha$ radiation (λ = 1.54184 Å) for **1** and Mo-K$_\alpha$ radiation (λ = 0.71073 Å) for **2**. Crystal

parameters and refinement results are summarized in Table 1. The structures of **1** and **2** were solved by direct methods and subsequently completed by Fourier recycling using the SHELXTL[21-23] software packages. The final full-matrix least-squares refinements on F^2, minimising the function

$$\sum w(|F_o| - |F_c|)^2,$$

reached convergence with the values of the discrepancy indices given in Table 1. Disorder of free solvent molecules was detected in both compounds (**1** and **2**). The graphical manipulations were performed with the DIAMOND program.[24] CCDC 1568972 (**1**) and 1568973 (**2**).†

Conflicts of interest

There are no conflicts to declare.

Acknowledgements

Notes and references

1 L. Bogani and W. Wernsdorfer, *Nat. Mater.*, 2008, **7**, 179–186.

2 T. Komeda, H. Isshiki, J. Liu, Y.-F. Zhang, N. Lorente, K. Katoh, B. K. Breedlove and M. Yamashita, *Nat. Commun.*, 2011, **2**, 217.

3 J. M. Clemente-Juan, E. Coronado and A. Gaita-Ariño, *Chem. Soc. Rev.*, 2012, **41**, 7464–7478.

4 J. Ferrando-Soria, J. Vallejo, M. Castellano, J. Martínez-Lillo, E. Pardo, J. Cano, I. Castro, F. Lloret, R. Ruiz-García and M. Julve, *Coord. Chem. Rev.*, 2017, **339**, 17–103.

5 D. Li, S. Parkin, R. Clérac and S. M. Holmes, *Inorg. Chem.*, 2006, **45**, 7569–7571.

6 L. Gregoli, C. Danieli, A.-L. Barra, P. Neugebauer, G. Pellegrino, G. Poneti, R. Sessoli and A. Cornia, *Chem.–Eur. J.*, 2009, **15**, 6456–6467.

7 (*a*) F. Moro, V. Corradini, M. Evangelisti, V. De Renzi, R. Biagi, U. del Pennino, C. J. Milios, L. F. Jones and E. K. Brechin, *J. Phys. Chem. B*, 2008, **112**, 9729–9735; (*b*) F. Totti, G. Rajaraman, M. Iannuzzi and R. Sessoli, *J. Phys. Chem. C*, 2013, **117**, 7186–7190.

8 F. Moro, V. Corradini, M. Evangelisti, R. Biagi, V. De Renzi, U. del Pennino, J. C. Cezar, R. Inglis, C. J. Milios and E. K. Brechin, *Nanoscale*, 2010, **2**, 2698–2703.

9 P. Tyagi, D. Li, S. M. Holmes and B. J. Hinds, *J. Am. Chem. Soc.*, 2007, **129**, 4929–4938.

10 (*a*) A. Cornia, A. C. Fabretti, M. Pacchioni, L. Zobbi, D. Bonacchi, A. Caneschi, D. Gatteschi, R. Biagi, U. Del Pennino, V. De Renzi, L. Gurevich and H. S. J. Van der Zant, *Angew. Chem., Int. Ed.*, 2003, **42**, 1645–1648; (*b*) M. Mannini, F. Pineider, Ph. Sainctavit, C. Danieli, E. Otero, C. Sciancalepore, A. M. Talarico, M.-A. Arrio, A. Cornia, D. Gatteschi and R. Sessoli, *Nat. Mater.*, 2009, **8**, 194–197; (*c*) M. Mannini, F. Pineider, C. Danieli, F. Totti, L. Sorace, Ph. Sainctavit, M.-A. Arrio, E. Otero, L. Joly, J. C. Cezar, A. Cornia and R. Sessoli, *Nature*, 2010, **468**, 417–421; (*d*) E. Tancini, M. Mannini, Ph. Sainctavit, E. Otero, R. Sessoli and A. Cornia, *Chem.–Eur. J.*, 2013, **19**, 16902–16905.

11 S. Wagner, F. Kisslinger, S. Ballmann, F. Schramm, R. Chandrasekar, T. Bodenstein, O. Fuhr, D. Secker, K. Fink, M. Ruben and H. B. Weber, *Nat. Nanotechnol.*, 2013, **8**, 575–579.

12 (*a*) C. J. Milios, C. P. Raptopoulou, A. Terzis, F. Lloret, R. Vicente, S. P. Perlepes and A. Escuer, *Angew. Chem., Int. Ed.*, 2004, **43**, 210–212; (*b*) C. J. Milios, A. Vinslava, P. A. Wood, S. Parsons, W. Wernsdorfer, G. Christou, S. P. Perlepes and E. K. Brechin, *J. Am. Chem. Soc.*, 2007, **129**, 8–9; (*c*) C. J. Milios, A. Vinslava, W. Wernsdorfer, S. Moggach, S. Parsons, S. P. Perlepes, G. Christou and E. K. Brechin, *J. Am. Chem. Soc.*, 2007, **129**, 2754–2755; (*d*) C. J. Milios, A. Vinslava, W. Wernsdorfer, A. Prescimone, P. A. Wood, S. Parsons, S. P. Perlepes, G. Christou and E. K. Brechin, *J. Am. Chem. Soc.*, 2007, **129**, 6547–6561; (*e*) C. J. Milios, R. Inglis, R. Bagai, W. Wernsdorfer, A. Collins, S. Moggach, S. Parsons, S. P. Perlepes, G. Christou and E. K. Brechin, *Chem. Commun.*, 2007, 3476–3478; (*f*) C. J. Milios, R. Inglis, A. Vinslava, R. Bagai, W. Wernsdorfer, S. Parsons, S. P. Perlepes, G. Christou and E. K. Brechin, *J. Am. Chem. Soc.*, 2007, **129**, 12505–12511; (*g*) C. J. Milios, S. Piligkos and E. K Brechin, *Dalton Trans.*, 2008, 1809–1817; (*h*) R. Inglis, C. J. Milios, L. F. Jones, S. Piligkos and E. K. Brechin, *Chem. Commun.*, 2012, **48**, 181–190.

13 (*a*) A.-R. Tomsa, J. Martínez-Lillo, Y. Li, L.-M. Chamoreau, K. Boubekeur, F. Farias, M. A. Novak, E. Cremades, E. Ruiz, A. Proust, M. Verdaguer and P. Gouzerh, *Chem. Commun.*, 2010, **46**, 5106–5108; (*b*) G.-Y. An, A.-L. Cui and H.-Z. Kou, *Inorg. Chem. Commun.*, 2011, **14**, 1475–1478; (*c*) J. Martínez-Lillo, A.-R. Tomsa, Y. Li, L.-M. Chamoreau, E. Cremades, E. Ruiz, A.-L. Barra, A. Proust, M. Verdaguer and P. Gouzerh, *Dalton Trans.*, 2012, **41**, 13668–13681; (*d*) J. Martínez-Lillo, L.-M. Chamoreau, A. Proust, M. Verdaguer and P. Gouzerh, *C. R. Chim.*, 2012, **15**, 889–894.

14 J. Martínez-Lillo, N. Dolan and E. K. Brechin, *Dalton Trans.*, 2013, **42**, 12824–12827.

15 J. Martínez-Lillo, N. Dolan and E. K. Brechin, *Dalton Trans.*, 2014, **43**, 4408–4414.

16 J. Martínez-Lillo, J. Cano, W. Wernsdorfer and E. K. Brechin, *Chem.–Eur. J.*, 2015, **21**, 8790–8798.

17 L. M. Toma, R. Lescouëzec, J. Pasán, C. Ruiz-Pérez, J. Vaissermann, J. Cano, R. Carrasco, W. Wernsdorfer, F. Lloret and M. Julve, *J. Am. Chem. Soc.*, 2006, **128**, 4842–4853.

18 L. M. Toma, C. Ruiz-Pérez, J. Pasán, W. Wernsdorfer, F. Lloret and M. Julve, *J. Am. Chem. Soc.*, 2012, **134**, 15265–15268.

19 A. Earnshaw, *Introduction to Magnetochemistry*, Academic Press, London, Kahn, 1968.

20 G. A. Bain and J. F. Berry, *J. Chem. Educ.*, 2008, **85**, 532–536.

21 G. M. Sheldrick, *Acta Crystallogr., Sect. A: Found. Crystallogr.*, 2008, **64**, 112.

22 G. M. Sheldrick, *Acta Crystallogr., Sect. C: Struct. Chem.*, 2015, **71**, 3–8.

23 *SHELXTL, Bruker Analytical X-ray Instruments*, Madison, WI, 1998.

24 DIAMOND. 3.2d, Crystal Impact GbR, CRYSTAL IMPACT; K. Bra.

Supporting Information

Thioester-functionalised and oxime-based hexametallic manganese(III) single-molecule magnets

Carlos Rojas-Dotti and José Martínez-Lillo

Electronic Supplementary Information (ESI)

Thioester-functionalised and oxime-based hexametallic manganese(III) single-molecule magnets

Carlos Rojas-Dotti[a] and José Martínez-Lillo*[a]

[a] *Instituto de Ciencia Molecular (ICMol)/Departament de Química Inorgànica, Universitat de València, c/ Catedrático José Beltrán 2, 46980, Paterna, Valencia, Spain. f.jose.martinez@uv.es*
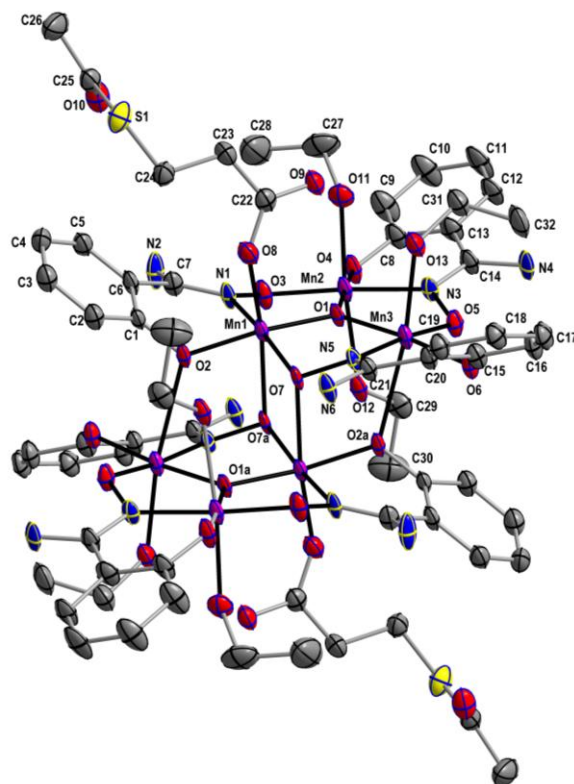
Figure S1. Perspective drawing of the [Mn$_6$] complex showing the atom numbering in **1**. Thermal ellipsoids are drawn at the 50% probability level. H atoms and solvent molecules of crystallisation have been omitted for clarity.

1
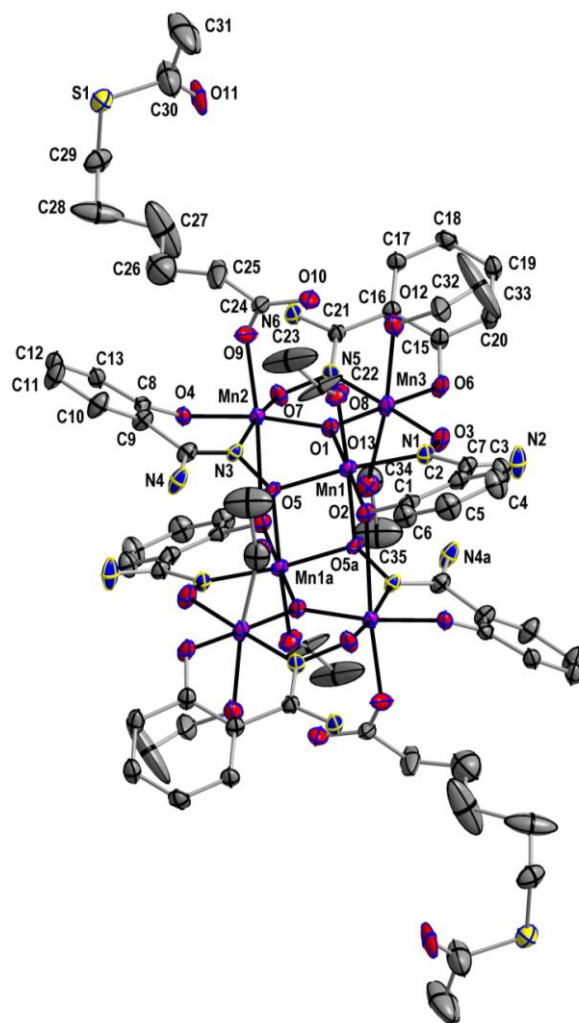
Figure S2. Perspective drawing of the [Mn$_6$] complex showing the atom numbering in **2**. Thermal ellipsoids are drawn at the 50% probability level. H atoms and solvent molecules of crystallisation have been omitted for clarity.

2
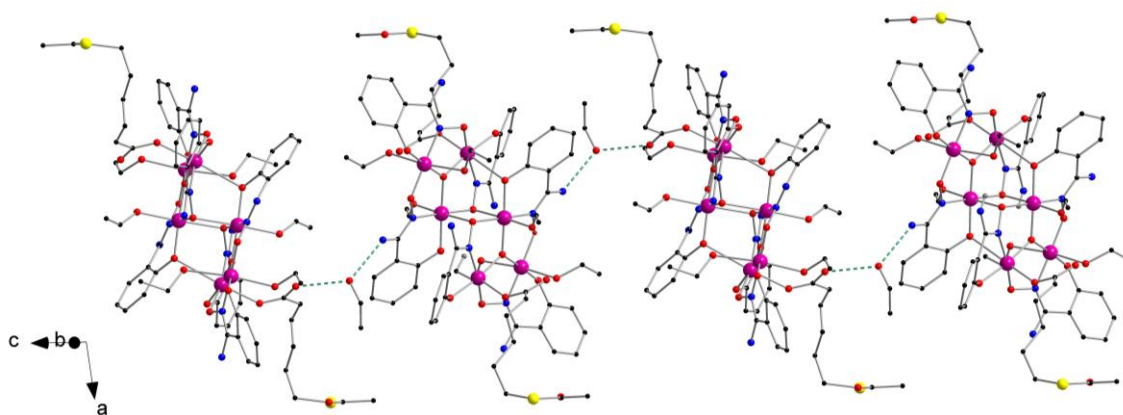
Figure S3. View of the one-dimensional motif generated by EtOH molecules sit between neighbouring [Mn$_6$] complexes and simultaneously H-bonded to the amino and carboxylate groups of adjacent [Mn$_6$] units in the crystal of **2** (dashed green lines) [Colour code: pink, Mn; yellow, S; red, O; blue, N; black, C].

3
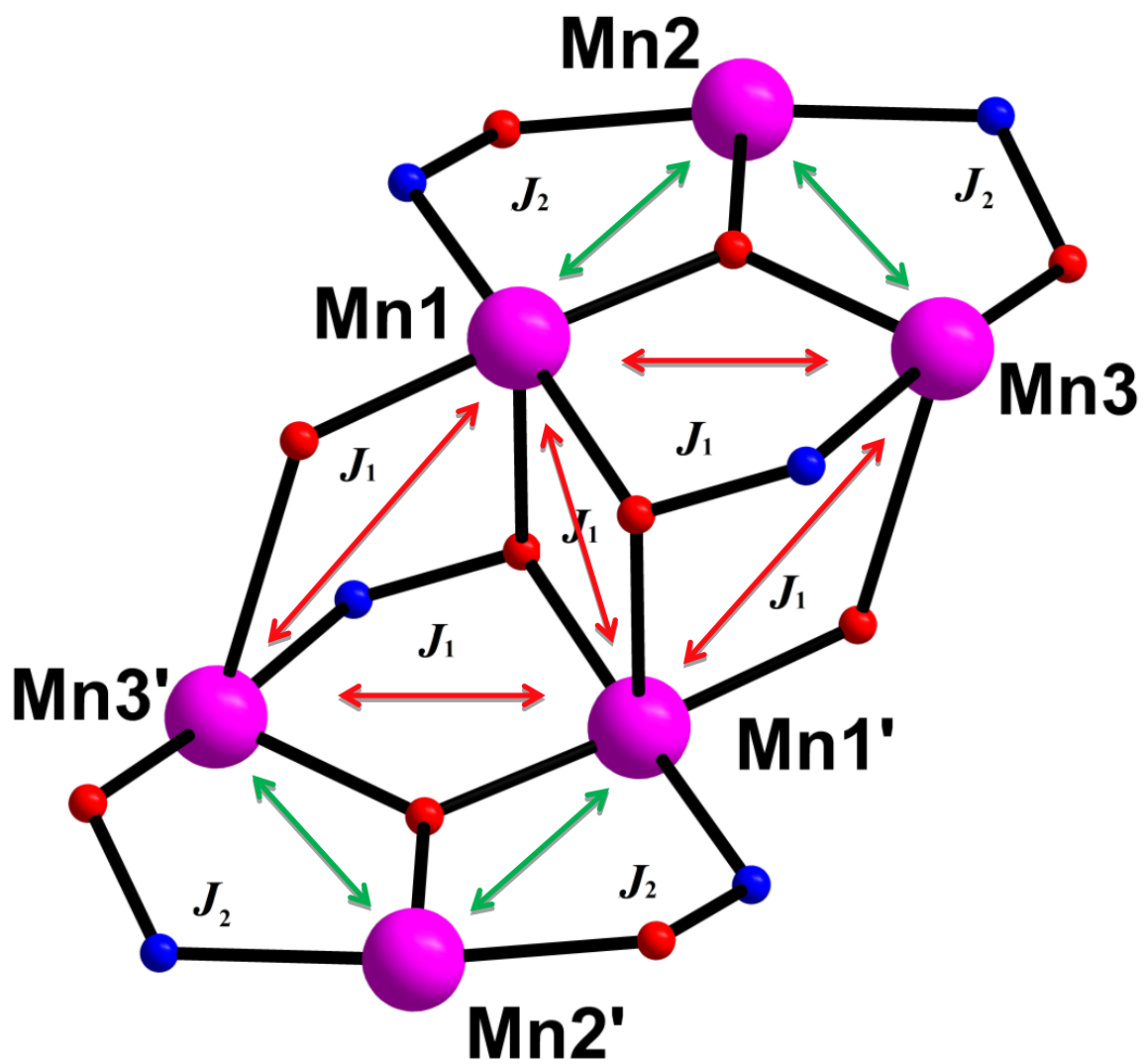
Figure S4. The 2-*J* coupling exchange model used to fit the experimental magnetic data of **1** and **2**.

B.

Re(IV)-based Systems

Introduction

Among the ions of the d-block elements of the second and third raw, Re(IV) is one of the most relevant and studied metal ions from the Molecular Magnetism point of view. Re(IV) is a $5d^3$ ion whose complexes generally display an octahedral geometry (O_h). In the O_h symmetry configuration, the ground term is $^4A_{2g}$ and the first exited state corresponds to a $^4T_{2g}$ term. However, an axial distortion is frequently found (tetragonal distortion) in the octahedral configuration of these complexes. In those cases, the actual symmetry is a D_{4h} and the ground state splits in an orbital singlet $^4B_2$ and a doublet ^4E. Even more, because of the combined effect of the mentioned distortion and the spin-orbit coupling, the ground term splits into the so called Kramer doublets $|\pm3/2\rangle$ and $|\pm1/2\rangle$ (see Scheme 1). This phenomenon is going to be demonstrated later in this section. Finally, given the high value of the spin-orbit coupling constant, $\lambda \approx 1000$ cm^{-1} for the free ion, Re(IV) presents a highly, local magnetic anisotropy with high Zero Field Splitting (ZFS) values.

As a consequence of these intrinsic features, Re(IV) comes to be an appropriated ion to look for remarkable magnetic properties, in both isolated mononuclear species and heteropolynuclear complexes. Furthermore, since the local anisotropy is originated by a second order spin-orbit coupling effect, the magnetic properties of the Re(IV) complexes may be modelled and fitted with relative ease, different from Co(II), for instance, where the high anisotropy is originated by a first order spin-orbit coupling. On top of that, the magnetic orbitals of the Re(IV) ion are considerably diffused, which means that a huge spin delocalisation is spread on the ligands, leading to a possible increase of the intensity of the magnetic interaction respect from analogous complexes of ions belonging to the first and second raws.[1]
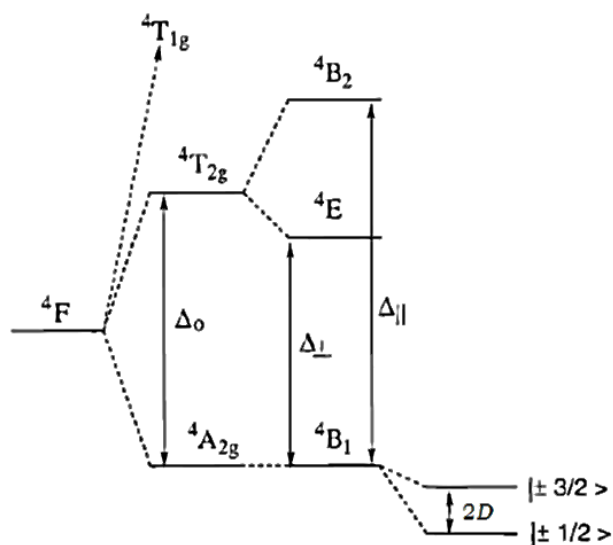
Scheme 1. Splitting of the ^4F ground term by cubic and axial ligand fields, and second-order spin–orbit coupling.

From both structural and synthetic points of view, the hexahalorhenate(IV) complexes $[ReX_6]^{2-}$ (X = F, Cl, Br and I) are the simplest systems to be studied. The chlorine and

bromide derivatives compounds are the most common and easy to be prepared. They are conveniently prepared by the reduction of perrhenic acid through $(OH)H_2PO$ in concentrated HX.[2] For instance, the preparative route for the $[ReCl_6]^{2-}$ salts, starting from the commercially perrhenic acid is illustrated by the reaction (1), the yield being in the range 85–90%.

$$4HReO_4 + 8(Cat)Cl + 3(HO)H_2PO + 16HCl \Leftrightarrow 4(Cat)_2[ReCl_6] + 3(HO)_3PO + 10H_2O \qquad (1)$$
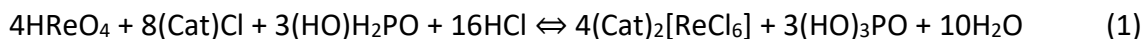
Herein, Cat corresponds to univalent countercations (alkaline cations as well as ammonium). The use of perrhenic acid as source of rhenium allows the isolation of the hexachloro- or hexabromorhenate(IV) anions with the cation coming from the starting halide salt.

Different is the case of the hexaiodorhenate(IV) salts, where the preparation is carried out by direct reduction of the perrhenic acid with concentrated HI.[3] This synthetic strategy allowed the isolation of the $[ReI_6]^{2-}$ species with univalent cations as black crystals. Other ionic salts with bulkier organic cations have been isolated by means of metathetic reactions in organic solvents. For instance, $(AsPh_4)_2[ReI_6]$ separates as a brown microcrystalline solid by reaction of stoichiometric amounts of $AsPh_4Cl$ and $K_2[ReI_6]$.[3c] Unluckily, the hexaiodorhenate(IV) derivatives are not very stable, violet vapour of iodine can be seen in these salts kept in close containers on standing after a couple of months at room temperature. Such a instability is the explanation of why only two structures, $K_2[ReI_6]$ and $(NH_4)_2[ReI_6]$, have been reported so far.[3c]

Finally, the investigation of the hexafluororhenate(IV) analogue has taken longer, due to the difficulties found in its preparation and purification. Actually, $(Cat)_2[ReF_6]$ salts (M = alkaline cation, NH_4^+) are obtained in a very different way respect from the other $[ReX_6]^{2-}$ derivatives, by dissolving $(Cat)_2[ReX_6]$ (X = Cl, Br and I) in melted $CatHF_2$.[4] Recently, Pedersen *et al*. found that the use of the melted NH_4HF_2 as fluoride source in the process affords the water soluble salt $(NH_4)_2[ReF_6]$ which, by metathesis, lead to the isolation of $(PPh_4)_2[ReF_6] \cdot 2H_2O$. Given these synthetic difficulties, a few crystal structures for the $[ReF_6]^{2-}$ anion are known. In what to our field concerns, only two are of interest: $(PPh_4)_2[ReF_6] \cdot 2H_2O$[5] and $K_2[ReF_6]$.[6]

In the mentioned publication, Pedersen *et al.* reported the first full magnetic study performed on a $[ReF_6]^{2-}$ salt of a bulky cation. By using dc and ac magnetic susceptibility measurements, INS and EPR spectroscopies, the magnetic properties of the isolated $[ReF_6]^{2-}$ unit in $(PPh_4)_2[ReF_6] \cdot 2H_2O$ was fully studied and a slow relaxation of the magnetisation was observed below ca. 4 K.[5] Besides, they reported a one-dimensional coordination polymer $[ReF_5(\mu\text{-}F)Zn(viz)_4]$(viz=1-vinylimidazole) and proved that the slow dynamic is preserved, demonstrating the irrelevance of low symmetry for such magnetisation dynamics in systems with easy-plane-type anisotropy.[5]

By contrast, even when they are known since several years, there is no report of a full magnetic study on the other hexahalogen derivatives bulky cation salts. Up to now, the

fact that the hexafluororhenate(IV) was reported as showing slow relaxation of the magnetisation, and thus, behaving as a SIM, took us to explore the magnetic behaviour of the rest of the analogous hexahalogen complexes of the series.

The magnetic properties of the mononuclear $[ReX_6]^{2-}$ complexes as salts with diamagnetic cations have been subject of study during the last 60 years.[3c,6-8] All of that research has exposed the occurrence of significant through space antiferromagnetic interactions between the paramagnetic Re(IV) ions. The magnitude of the interaction depends on the nature of the halogen ligand and the halogen···halogen distance between the anionic complexes in the crystal lattice. These magnetic interactions are in general transmitted through space *via* Re-X···X-Re contacts, the halogen–halogen separation being strongly dependent of the size on the countercations. For instance, magnetic susceptibility and neutron diffraction measurements on K_2ReCl_6 and K_2ReBr_6 revealed the occurrence of antiferromagnetic ordering below 12 and 14 K, respectively.[9,10]

After their development in the end of the 1950s, and with the development of the field involving the design and study of novel heteropolynuclear complexes, hexahalogen-derivatives of Re(IV) have been mostly used as precursors to synthetize new mononuclear complexes which can be used as metalloligands toward other metal ions, mainly 3d metal ions.

Replacement of two halogen ions from the $[ReX_6]^{2-}$ molecule by (potential) bridging ligands, such as oxalate (ox^{2-}),[11] cyanide (CN$^-$),[12] 2,2'-bipyrimidine (bpym)[13] or malonate (mal^{2-}),[14] has increased the coordination potential of this metalloligand towards both 3d and 4f metal ions,[15] making them exceptional building blocks for the synthesis of molecule-based magnetic materials Figure 1. These substitution reactions are
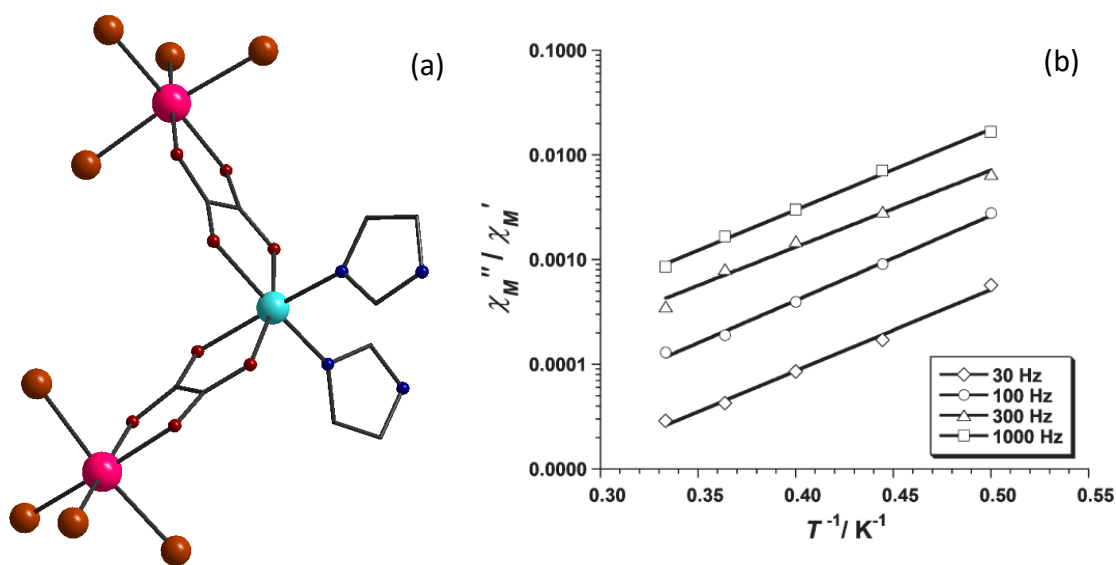
Figure 1. (a) Molecular structure of the {[ReBr$_4$(ox)]$_2$Ni(Him)$_2$} SMM. Hydrogen atoms are omitted for clarity. Colour code: pink, Re; pale blue, Ni; brown, Br; red O; blue, N; grey, C. (b) χ''_M/χ'_M vs 1/T plot at four different frequencies (1-1000 Hz range). The solid lines are the best-fit curves.

commonly performed in non-aqueous solvents, with the anionic complexes being isolated as a salt of a bulky organic cation. In this way, the preparation and study of the complexes $[ReX_4(ox)]^{2-}$ (X = Cl and Br) and $[ReCl_4(CN)_2]^{2-}$ provided the first examples of Re(IV)-based single-ion,[16] single-molecule[17] and single-chain[18] magnets (SIMs, SMMs and SCMs); Figure 1.

Besides, the $[ReX_6]^{2-}$ anions have not only been used for ligand substitution, but also as metalloligands towards diamagnetic or paramagnetic transition metal ions. Nevertheless, the number of reported crystal structures containing the $[ReX_6]^{2-}$ anion acting as a ligand is limited to two structures.[19] Firstly, the polymeric $\{Ag_2ReCl_6\}_n$ compound present interesting results. In its crystal structure, the $[ReX_6]^{2-}$ unit adopts the hexakis-monodentate coordination mode towards diamagnetic Ag(I) cations, leading to a corrugated layered structure which behaves as a three-dimensional antiferromagnet.[20] The other example of the remarkable results reported in the use of the $[ReX_6]^{2-}$ as metalloligand is the polymeric compound of formula $\{Cu(pyim)(Him)_2ReCl_6\}_n \cdot MeCN$, which exhibits a metamagnetic behavior (Figure 2).[21]

Regarding the indicated above, one of the great advantages of Re(IV)-based systems is that the high anisotropy is given by a second order SOC, which makes easier to model and fit the experimental magnetic data.

Herein it is deducted a magnetic model for a d^3 ion [as Re(IV)] in octahedral (O_h) and distorted octahedral symmetries (D_{4h}).
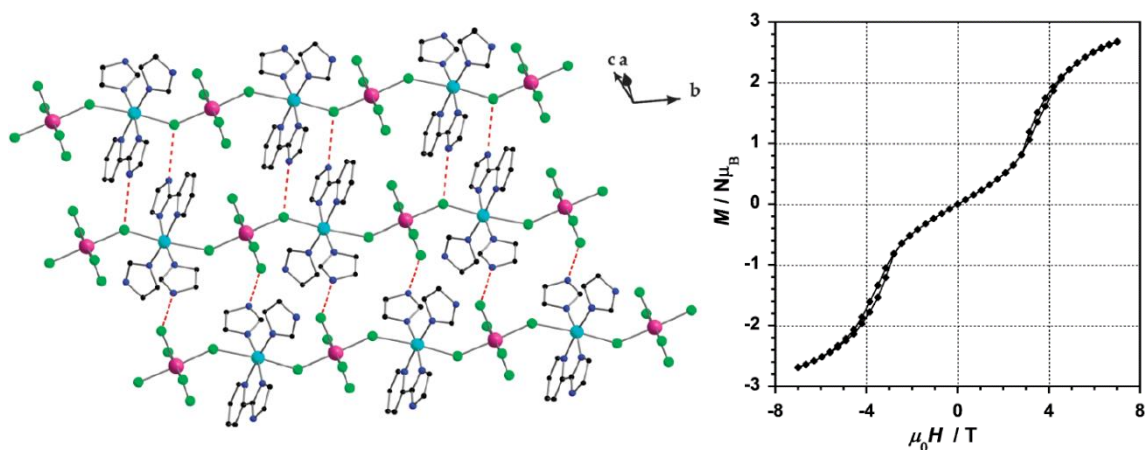
Figure 2. (a) View of a fragment of the crystal packing of the metamagnetic chain $\{Cu(pyim)(Him)_2ReCl_6\}_n \cdot MeCN$ highlighting the supramolecular two-dimensional network of adjacent chains linked through H-bonding interactions (dashed red lines). H atoms and MeCN solvent molecules have been omitted for clarity. Colour code: pink, Re; pale blue, Cu; green, Cl; dark blue, N; black, C. (b) Variable-field magnetisation data at T = 2.0 K.

Magnetic model for a d³ ion in an octahedral (O_h) symmetry system

Any transition metal ion, absolutely isolated in the space, presents five degenerated d orbitals. Having into account the ligand field theory (LFT), such a degeneration is broken because of the interaction with the ligands. Consequently, the nature of the splitting depends on the symmetry of the environment in which the ion is placed.

A d^3 free ion, as Re(IV), has three unpaired electrons which must be distributed in the d orbitals. Thus, the total spin S of the ion is S = 3/2 and the orbital component L, calculated as (L = $2m_\ell$ +1), where m_ℓ corresponds to those of the state of maximum orbital component (see Scheme 2), must be L = 3. Therefore, the fundamental term, defined as $^{2S(S+1)}L$, for a d^3 free ion must be ^4F.
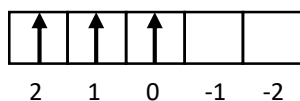
Scheme 2. Filling of the degenerated d orbitals for a d^3 ion in the maximum orbital component configuration.

Once the free ion is subjected to a ligands field with a regular octahedral symmetry (O_h), the d orbitals split in the way showed in Scheme 3.
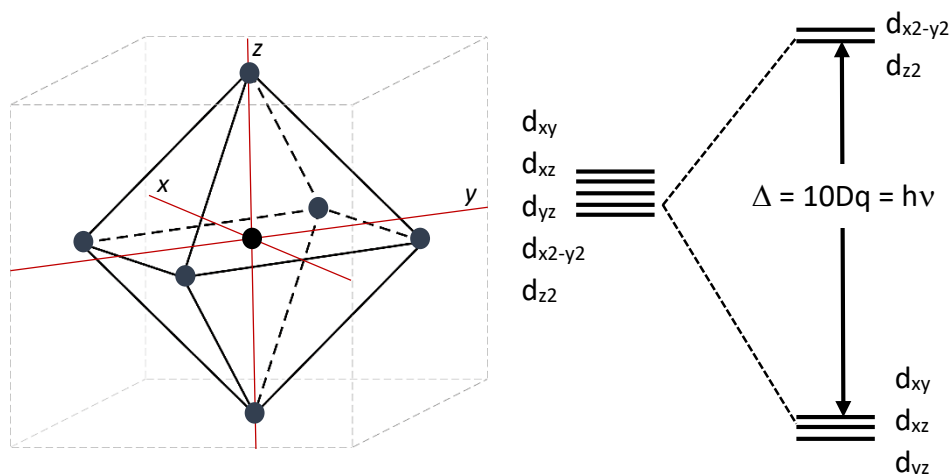
Scheme 3. Octahedral geometry and d orbitals splitting in an O_h symmetry.

In this new context, the splitting of the d orbitals leads to three possible energy configurations (Scheme 4).

Ground State   First Exited State   Second Exited State
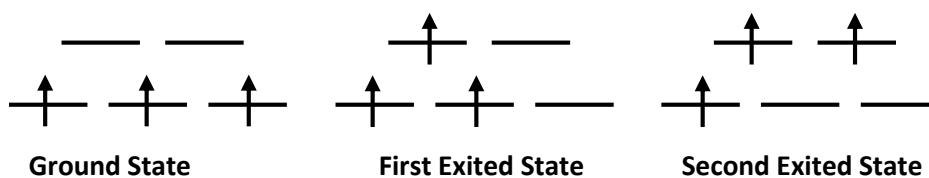
Scheme 4. Energy configurations for a d^3 metal ion in an O_h symmetry.

Thus, the fundamental ^4F term, in an O_h symmetry, splits as shown in Scheme 5.

The energy of 10 Dq, between the lowest energy levels, is in the order of thousands of cm^{-1} (8000-15000 cm^{-1}), whereas the thermal energy expressed as the product kT is *ca.*

200 cm^{-1}. Therefore, the $^4T_{2g}$ term is not expected to be thermally populated at all, which means that we expect to work and focus on the ground state $^4A_{2g}$.

In order to go farther in the modelling of the system, we can keep applying the perturbations theory. Actually, we have already applied the first perturbation to the system, the effect of the ligands field. A posterior step is to consider the spin-orbit coupling (SOC), but before that some formal remarks are needed.
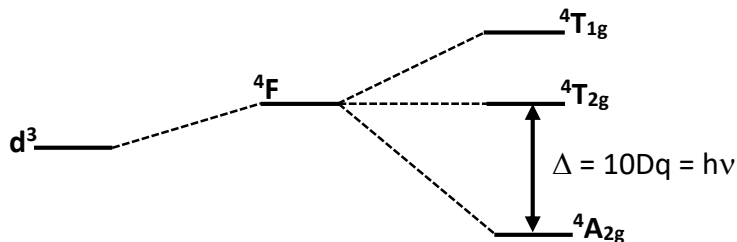
Scheme 5. Splitting of a ^4F term in an O$_h$ symmetry.

The ground term ^4F has 28 associated wave functions [(2L+1)(2S+1)], which are related to the quantic numbers L = 2 and S = 3/2. The effects of the operators of SOC and magnetic moment may be evaluated by means of the numbers L, M_L, S and M_S. Thus, the wave function can be expressed in terms of the corresponding quantic numbers, which means, |L, M_L, S, M_S >.

However, our calculations are going to be limited to the ground state $^4A_{2g}$, which means that L as well as S are going to be constant parameters and the wave function can be abbreviated as |M_L, M_s >.

Accordingly, the wave function corresponding to the $^4A_{2g}$ term are the following:

$$\Psi_1 = \tfrac{1}{\sqrt{2}}\{|2, 3/2 > - | - 2, 3/2 >\} \qquad (41)$$

$$\Psi_2 = \tfrac{1}{\sqrt{2}}\{|2, 1/2 > - | - 2, 1/2 >\} \qquad (42)$$

$$\Psi_3 = \tfrac{1}{\sqrt{2}}\{|2, -1/2 > - | - 2, -1/2 >\} \qquad (43)$$

$$\Psi_4 = \tfrac{1}{\sqrt{2}}\{|2, -3/2 > - | - 2, -3/2 >\} \qquad (44)$$

The wave function belonging to the first exited state will be needed later in the farther calculations. They are not displayed here only in order to make a simpler exposition, but some of them will be called later on when they are needed.

Once we have these functions, the energy of the SOC effect is calculated by solving the determinant of the 4 x 4 matrix. Each of the elements of the matrix is given by the terms $\langle \Psi_i | Hsoc | \Psi_j \rangle$, where the SOC Hamiltonian is:

$$H_{soc} = \lambda \hat{L}\hat{S} = \lambda \widehat{L_z}\widehat{S_z} + \tfrac{\lambda}{2}\left[\widehat{L^+}\widehat{S^-} + \widehat{L^-}\widehat{S^+}\right] \qquad (45)$$

In this equation λ corresponds to the SOC-constant. Thus, the matrix must be written as follows:

	$\lvert \Psi_1 \rangle$	$\lvert \Psi_2 \rangle$	$\lvert \Psi_3 \rangle$	$\lvert \Psi_4 \rangle$
$\langle \Psi_1 \rvert$	$H_{11} - \varepsilon$	H_{21}	H_{31}	H_{41}
$\langle \Psi_2 \rvert$	H_{12}	$H_{22} - \varepsilon$	H_{32}	H_{42}
$\langle \Psi_3 \rvert$	H_{13}	H_{23}	$H_{33} - \varepsilon$	H_{43}
$\langle \Psi_4 \rvert$	H_{14}	H_{24}	H_{34}	$H_{44} - \varepsilon$

As expressed before, the only term that matters to our aims is the magnetic term $^4A_{2g}$, since it is going to be the only populated term in the working temperatures (2 – 300 K). Furthermore, the wave functions $\lvert \Psi \rangle$ are orthogonal and also linear combinations adapted to the symmetry of the system they belong to.

At the moment of applying H_{soc} to the functions, there exist another issue to have into account. The operators $\widehat{L_z}$ and $\widehat{S_z}$ are proper operators of the wave functions Ψ, M_L and M_s being the proper values, respectively. Thus, for instance, $\widehat{L_z}\lvert \Psi_1 \rangle$ = $M_L \lvert \Psi_1 \rangle$. Nevertheless, the operators $\widehat{L^+}, \widehat{S^-}, \widehat{L^-}, \widehat{S^+}$ are not proper to the functions. As a result, they operate in the following manner:

$$\widehat{L^+}\lvert L, M_L, S, M_L \rangle = [L(L+1) - M_L(M_L + 1)]^{1/2}\lvert L, \boldsymbol{M_L + 1}, S, M_S \rangle \ (46)$$

$$\widehat{L^-}\lvert L, M_L, S, M_L \rangle = [L(L+1) - M_L(M_L - 1)]^{1/2}\lvert L, \boldsymbol{M_L - 1}, S, M_S \rangle \ (47)$$

$$\widehat{S^+}\lvert L, M_L, S, M_L \rangle = [S(S+1) - M_S(M_S + 1)]^{1/2}\lvert L, M_L, S, \boldsymbol{M_S + 1} \rangle \ (48)$$

$$\widehat{S^-}\lvert L, M_L, S, M_L \rangle = [S(S+1) - M_S(M_S - 1)]^{1/2}\lvert L, M_L, S, \boldsymbol{M_S - 1} \rangle \ (49)$$

Formerly, when the only operators of the Hamiltonian that do not change the original function are applied, one can see that they never give back the original function multiplied by a scalar, but also change the sign of it, as it can be seen in the following example:

$$\lambda \hat{L}\hat{S}\lvert \Psi_1 \rangle = \lambda \frac{1}{2}\left\{3\lvert 2,\frac{3}{2} > +3\rvert - 2, 3/2 > \right\} = 3\lambda\lvert \Psi_{13} \rangle$$

where Ψ_{13} is a new wave function different from Ψ_1. As a result, when afterwards $\langle \Psi_1 \rvert$ is applied to this result in the form $\langle \Psi_1 \lvert 3\lambda \rvert \Psi_{13} \rangle$, the result is 0 given that the functions are orthogonal. In fact, this phenomenon comes to prove that in a d^3 metal ion placed in an octahedral environment there is no first order SOC.

Nonetheless, Ψ_{13} is actually a function belonging to the first exited state $^4T_{2g}$, which means that there may exist a little percentage of mixing of these function by second order SOC. Indeed, when all the operations are completed the second order SOC is confirmed. Only one energy value $\varepsilon = -\dfrac{15\lambda^2}{10Dq}$ is obtained and, that means that after the mixing with the functions of the other term, the ground state keeps degenerated. There is no ZFS, which is expectable for a regular octahedron.

Finally, new functions have been obtained as a consequence of the coupling. These functions can be constructed as:

$$\Phi_i = \Psi_i + \sum_j C_{ij} \Psi_j \tag{50}$$

$$C_{ij} = \frac{\langle \Psi_i | \widehat{H} | \Psi_j \rangle}{\varepsilon_i - \varepsilon_j} \tag{51}$$

Hence, the new functions are given by:

$$\Phi_1 = \Psi_1 - \frac{3\lambda}{10Dq} \Psi_{13} + \frac{\sqrt{6}\lambda}{10Dq} \Psi_{10} \tag{52}$$

$$\Phi_2 = \Psi_2 - \frac{\lambda}{10Dq} \Psi_{14} + \frac{\sqrt{8}\lambda}{10Dq} \Psi_{11} - \frac{\sqrt{6}\lambda}{10Dq} \Psi_5 \tag{53}$$

$$\Phi_3 = \Psi_3 - \frac{\lambda}{10Dq} \Psi_{15} + \frac{\sqrt{6}\lambda}{10Dq} \Psi_{12} - \frac{\sqrt{6}\lambda}{10Dq} \Psi_6 \tag{54}$$

$$\Phi_4 = \Psi_4 - \frac{3\lambda}{10Dq} \Psi_{16} + \frac{\sqrt{6}\lambda}{10Dq} \Psi_7 \tag{55}$$

Besides Ψ_{13}, the wave functions presented here as $\Psi_5, \Psi_6, \Psi_7, \Psi_{10}, \Psi_{11}, \Psi_{12}, \Psi_{14}, \Psi_{15}, \Psi_{16}$, are also functions that belong to the $^4T_{2g}$ exited term. These functions appear in the calculations when the non-proper operators are applied as a consequence of being linear combinations, which belong to the same group, the ^4F term.

At this point, the system is defined and, so far no external perturbation is applied, these functions describe a d^3 ion in an O_h symmetry. However, we do want to apply another perturbation. We will subject the system to a magnetic field in order to study its magnetic properties. Then, going forward with the perturbations theory, the so called Zeeman Hamiltonian, $\widehat{H_z}$, must be applied:

$$H_Z = \beta H \big[\widehat{L_Z} + 2\widehat{S_Z} \big] \tag{56}$$

Herein, β is the Bohr magneton and H the experimental field applied. In this case, since the system is isotropic, to apply the magnetic Hamiltonian in only one direction is enough.

When the Zeeman Hamiltonian is applied to the new wave functions the obtained results are:

$$\langle \Phi_1 | H_Z | \Phi_1 \rangle = 3\beta H (1 - \frac{4\lambda}{\Delta})$$

$$\langle \Phi_2 | H_Z | \Phi_2 \rangle = \beta H (1 - \frac{4\lambda}{\Delta})$$

$$\langle \Phi_3 | H_Z | \Phi_3 \rangle = -\beta H \left(1 - \frac{4\lambda}{\Delta} \right)$$

$$\langle \Phi_4 | \widehat{H_z} | \Phi_4 \rangle = -3\beta H (1 - \frac{4\lambda}{\Delta})$$

These results clearly mean that, in the presence of a magnetic field, the ground state $^4A_{2g}$ splits in four different energy levels as shown in Scheme 6.

$$3\beta H\left(1-\frac{4\lambda}{\Delta}\right) = \frac{3}{2}g\beta H$$

$$\beta H\left(1-\frac{4\lambda}{\Delta}\right) = \frac{1}{2}g\beta H$$

$$^4A_{2g}$$

$$-\beta H\left(1-\frac{4\lambda}{\Delta}\right) = -\frac{1}{2}g\beta H$$

$$-3\beta H\left(1-\frac{4\lambda}{\Delta}\right) = -\frac{3}{2}g\beta H$$
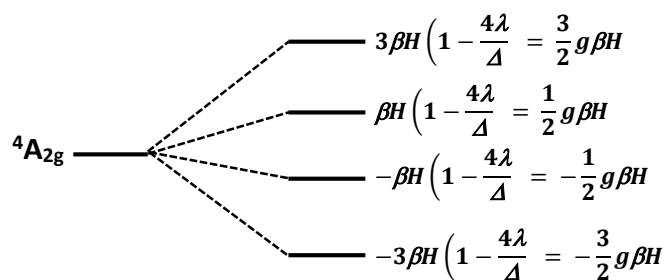
Scheme 6. Splitting of a $^4A_{2g}$ term under an applied magnetic field H.

If now we define $g = 2\left(1-\frac{4\lambda}{\Delta}\right)$ what we obtain is that the energy of the levels depends only on the constants of the system and the applied field, and they are defined by the possible spin states of the metal ion S = ±1/2 and S=±3/2 (see Scheme 6).

Magnetic model for a d^3 ion in a distorted octahedral (D$_{4h}$) symmetry system

Up to here deductions have taken place in an ideal octahedral system. However, most of the reported structures do not display such a regular geometry, but present some distortions. Therefore, the previously obtained model shows very restricted applications, what makes necessary to approach this model to more real systems.

When the system is distorted and the regular symmetry avoided, then both, a structural and the consequent magnetic anisotropies appear. Thus, magnetic susceptibility will not be equal for all the directions of the space. In our specific case, Re(IV) complexes are generally axially distorted, which means that the symmetry of the system is transformed from O$_h$ to D$_{4h}$.

These changes lead to the splitting of the terms, as represented in Scheme 7.
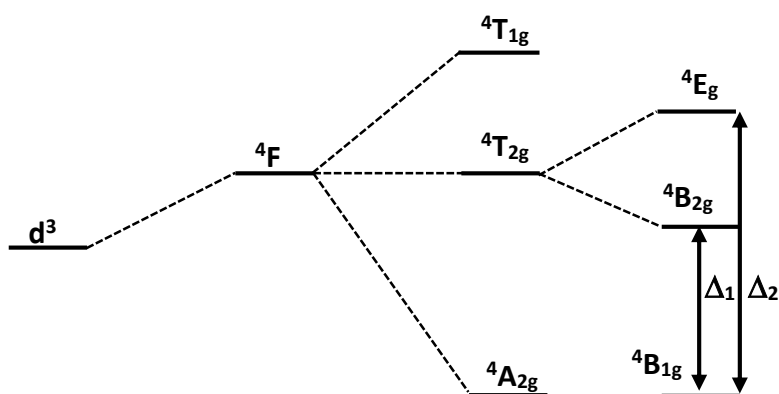
Scheme 7. Splitting of a ^4F term in a D$_{4h}$ symmetry.

The wave functions in this new environment are conserved and redistributed in the new terms. However, those belonging to the $^4A_{2g}$ term are the same that now are under the label of $^4B_{1g}$.

Now, when the H_{soc} is applied to the functions $\Psi_1, \Psi_2, \Psi_3, \Psi_4$ the first order coupling is still zero, but there exist a ZFS as a consequence of the second-order SOC. The ZFS value is found to correspond to $D = 8\lambda^2 \left[\frac{1}{\Delta_2} - \frac{1}{\Delta_1}\right]$. From this result it can be deducted that if $\Delta_1 = \Delta_2$ there is no splitting. Furthermore, the higher the λ value, the longer the splitting (see Scheme 8).

The magnetic anisotropy actually found is the reason why, in a distorted system, a field applied in the z direction does not produce the same effect than one applied in the x or y directions.
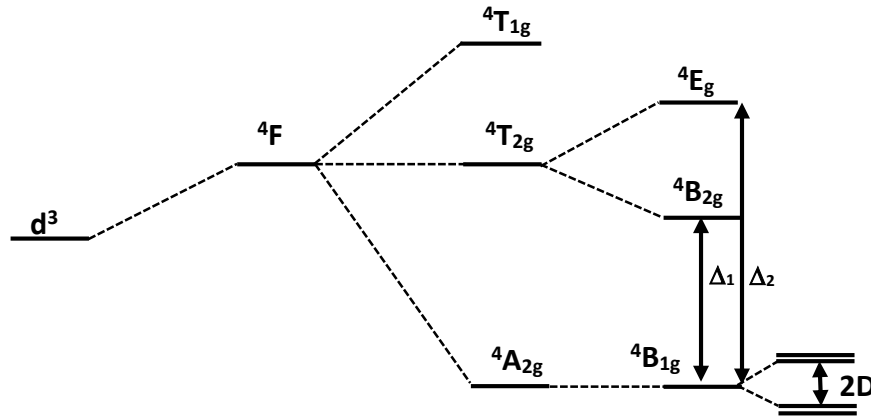
Scheme 8. Splitting of a ^4F term in a D$_{4h}$ symmetry after applying SOC.

Additionally, the new wave functions obtained after applying the SOC are the following:

$$\Phi_1 = \Psi_1 - \frac{3\lambda}{\Delta_1}\Psi_{13} + \frac{\sqrt{6}\lambda}{\Delta_2}\Psi_{10} \tag{57}$$

$$\Phi_2 = \Psi_2 - \frac{\lambda}{\Delta_1}\Psi_{14} + \frac{\sqrt{8}\lambda}{\Delta_2}\Psi_{11} - \frac{\sqrt{6}\lambda}{\Delta_2}\Psi_5 \tag{58}$$

$$\Phi_3 = \Psi_3 - \frac{\lambda}{\Delta_1}\Psi_{15} + \frac{\sqrt{6}\lambda}{\Delta_2}\Psi_{12} - \frac{\sqrt{6}\lambda}{\Delta_2}\Psi_6 \tag{59}$$

$$\Phi_4 = \Psi_4 - \frac{3\lambda}{\Delta_1}\Psi_{16} + \frac{\sqrt{6}\lambda}{\Delta_2}\Psi_7 \tag{60}$$

Once the new functions are described, the Zeeman Hamiltonian can be applied in order to study the magnetic properties. However, the new system is anisotropic. As a consequence, $\chi_y = \chi_x \neq \chi_z$, what means that there are two different expressions of the Hamiltonian to be applied, the one expressed in equation (56), which corresponds to the field applied parallel to the z direction, and that of the perpendicular components:

$$H_{Z\perp} = \beta H \left[\widehat{L_x} + 2\widehat{S_x} + \widehat{L_y} + 2\widehat{S_y}\right] \tag{61}$$

The two components must be solved separately. Nevertheless, the normal procedure is to measure the magnetic susceptibility of a powdered sample. Accordingly, the measurements display to us the average value of all of the components. That is why, after determining each component of χ by using Van Vleck equation, the final average χ value must be calculated.

When the Hamiltonian H_Z, which from now on must be called $H_{Z\parallel}$, is applied to the functions, the results are the following:

$$\langle \Phi_1 | H_Z | \Phi_1 \rangle = 3\beta H_z \left(1 - \frac{4\lambda}{\Delta_1}\right)$$

$$\langle \Phi_2 | H_Z | \Phi_2 \rangle = \beta H_z \left(1 - \frac{4\lambda}{\Delta_1}\right)$$

$$\langle \Phi_3 | H_Z | \Phi_3 \rangle = -\beta H_z \left(1 - \frac{4\lambda}{\Delta_1}\right)$$

$$\langle \Phi_4 | \widehat{H_z} | \Phi_4 \rangle = -3\beta H_z \left(1 - \frac{4\lambda}{\Delta_1}\right)$$

With these results, the parallel determinant can be described:

	$|\Phi_1\rangle$	$|\Phi_2\rangle$	$|\Phi_3\rangle$	$|\Phi_4\rangle$
$\langle \Phi_1 |$	$3\beta H_z \left(1 - \frac{4\lambda}{\Delta_1} - \varepsilon + D\right)$	0	0	0
$\langle \Phi_2 |$	0	$\beta H_z \left(1 - \frac{4\lambda}{\Delta_1} - \varepsilon + D\right)$	H_{32}	0
$\langle \Phi_3 |$	0	0	$-\beta H_z \left(1 - \frac{4\lambda}{\Delta_1} - \varepsilon + D\right)$	0
$\langle \Phi_4 |$	0	0	0	$-3\beta H_z \left(1 - \frac{4\lambda}{\Delta_1} - \varepsilon + D\right)$

Then, the first order Zeeman energies in the z direction are given by:

$$\varepsilon_1' = 3\beta H_z \left(1 - \frac{4\lambda}{\Delta_1}\right) + D$$

$$\varepsilon_2' = \beta H_z \left(1 - \frac{4\lambda}{\Delta_1}\right)$$

$$\varepsilon_3' = -\beta H_z \left(1 - \frac{4\lambda}{\Delta_1}\right)$$

$$\varepsilon_4' = -3\beta H_z \left(1 - \frac{4\lambda}{\Delta_1}\right) + D$$

Once the first order Zeeman energies are calculated, and having into account that there is no second order energies, the values can be introduced in Van Vleck equation (62).

$$\chi = N \frac{\sum_{i=1}^{n} \left(\frac{\varepsilon_i'^2}{kT} - 2\varepsilon_i''\right) exp\left(\frac{-\varepsilon_i^0}{kT}\right)}{\sum_{i=1}^{n} exp\left(\frac{-\varepsilon_i^0}{kT}\right)} \qquad (62)$$

Thus, the $\chi_\parallel$ and $g_\parallel$ values are found to be:

$$\chi_\parallel = \frac{N\beta^2 g_\parallel^2}{4kT} \left[\frac{1 + 9exp\left(\frac{-D}{kT}\right)}{1 + exp\left(\frac{-D}{kT}\right)}\right]$$

$$g_\parallel = \left(1 + \frac{4\lambda}{\Delta_1}\right)$$

At this point, the parallel component of the magnetic susceptibility is determined. The next step would be to apply the Hamiltonian H_Z to the functions and follow the same procedure already exemplified above.

An interesting phenomenon that happens when the perpendicular energies are calculated is that the determinant is not diagonal, which leads us to the observation of second-order contributions in the energy.

The final expression obtained for the perpendicular component of χ is given by the following expression:

$$\chi_\perp = \frac{N\beta^2 g_\perp^2}{2kT}\left[\frac{\left(2-\frac{3kT}{D}\right)exp\left(\frac{-D}{kT}\right)+\frac{3kT}{D}}{1+exp\left(\frac{-D}{kT}\right)}\right] + \frac{8N\beta^2}{\Delta_2}$$

where $\frac{8N\beta^2}{\Delta_2}$ account for the so called temperature independent paramagnetism (TIP), and $g_\perp = 2\left(1+\frac{4\lambda}{\Delta_2}\right)$.

Finally, the magnetic susceptibility of a powdered sample can be calculated by:

$$\chi = \frac{\chi_\parallel + 2\chi_\perp}{3} \tag{63}$$

Objectives

During the last 20 years rhenium(IV) has proven to be one of the most promising metal ions to be studied in the research field of Molecular Magnetism. Regarding the high spin and anisotropy values that are characteristics for this 5d metal ion, great results are expected for its complexes. Indeed, many of the Re(IV)-containing complexes reported in the literature present remarkable properties, such as, SIM, SMM, SCM behaviours, apart from singular magnetic phenomena as can be spin-canting, metamagnetism and ferrimagnetism. Many of these interesting results are still being investigated and improved.

This second part of the present Thesis work is dedicated to the study of Re(IV)-based complexes. We will focus mainly on two types of systems. On one hand the systems based on $[ReX_6]^{2-}$ anions, with X = Cl and Br, and, on the other hand, those employing the $[ReX_4(ox)]^{2-}$ anions, X = Cl and Br, as metalloligands toward 3d metal ions. Furthermore, we will explore a new route of isomeric selective synthesis by using the $[ReCl_4(MeCN)_2]$ precursor.

First of all, we will research the synthesis and magnetic properties of a wide spectrum of salts based on the $[ReX_6]^{2-}$ anions and cations of different nature, which can open the possibility to add new functionalities to the final material. First of all, by using protonated biological molecules as counter-cations, we will attempt to obtain interesting magnetic properties in systems with biological interest. Even more, we will try to find new structures, which may also be later studied to perform proton transportation.

As a second step, we will look for paramagnetic salts of these Re(IV)-based anions where the cation must also be a paramagnetic complex. Thus, the effect of a paramagnetic counter-ion and the possible magnetic exchange between the metallic centres will be studied. On that propose mononuclear complexes containing solvated Fe(II) ions will be employed.

As a middle step, before continuing with the $[ReX_4(ox)]^{2-}$ based systems, we will explore new synthetic strategies for ligands substitution on Re(IV) complexes. In previous works, the hexahalogen complexes have been the prevalent choice for this propose. However, there exist other possibilities to be explored. For this reason, we will investigate the ligand substitution in the $[ReCl_4(CH_3CN)_2]$ complex by using different solvents. This research may open a new way of synthetic strategy for the ligands substitution on Re(IV) complexes.

Finally, with the aim of obtaining new interesting materials based on the $[ReX_4(ox)]^{2-}$ anions, we will explore the synthesis of heteropolynuclear complexes using these metalloligands toward 3d metal ions. On one hand, we will use the widely explored $[ReCl_4(ox)]^{2-}$ complex as metalloligand toward less explored 3d metal ion, for instance the Zn(II). The synthesis and characterisation of systems analogous to the already

reported involving other 3d metal ions would contribute to the knowledge and understanding of their magnetic properties. On the other hand, the less explored of the precursors, the anionic $[ReBr_4(ox)]^{2-}$, will be used toward one of the most explored of the 3d metal ions with these type of metaloligands: Cu(II). In both of the cases, we will attempt to obtain low-dimensionality complexes that could display interesting magnetic properties.

On the subject of all the above, this work has the aim of exploring the chemistry and magnetic properties of well-known Re(IV) systems, not only as an attempt of improving the knowledge and understanding of the compounds, but also to look for withering the possible functionalities, multifunctionalities and future applications in nanotechnology and nanoscience.

References

1. R. Chiozzone, R. González, C. Kremer, G. De Munno, J. Cano, F. Lloret, M. Julve, J. Faus, *Inorg. Chem*. **1999**, 38, 4745–4752.

2. J. Kleinberg (Ed.), *Inorganic Synthesis*, vol. 7, **1963**, McGraw-Hill, New York, p. 189-190.

3. (a) H.V.A. Briscoe, P.L. Robinson, A. J. Rudge, *J. Chem. Soc*., **1931**, 3218–3219. (b) M. C. Chakravorty, T. Gangopadhyay, in: A. P. Ginsberg (Ed.), *Inorganic Synthesis* vol 27, **1990**, Wiley, New York, p. 294. (c) R. González, R. Chiozzone, C. Kremer, G. De Munno, F. Nicolò, F. Lloret, M. Julve, J. Faus, *Inorg. Chem*., **2003**, 42, 2512–2518.

4. (a) R. D. Peacock, *J. Chem. Soc*., **1956**, 1291–1292; (b) E. Weise, *Z. Anorg, Allg. Chem*., **1956**, 283, 377–389.

5. K. S. Pedersen, M. Sigrist, M. A. Sørensen, A. L- Barra, T. Weyhermüller, S. Piligkos, C. Aa. Thuesen, M. G. Vinum, H. Mutka, H. Weihe, R. Clérac, J. Bendix, *Angew. Chem. Int. Ed.,* **2014**, 53, 1351–1353.

6. G. R. Clark, D. L. Russell, *Acta Crystallogr*., **1978**, B34, 94–102.

7. C. M. Nelson, G. E. Boyd, W. T. Smith, *J. Am. Chem. Soc*., **1954**, 76, 348–352.

8. J. Malecka, L. Jäger, Ch. Wagner, J. Mrozinski, *Polish. J. Chem*., **1998**, 72, 1879–1884.

9. R. González, R. Chiozzone, C. Kremer, F. Guerra, G. De Munno, F. Lloret, M. Julve, J. Faus, *Inorg. Chem*., **2004**, 43, 3013–3019.

10. R. H. Busey, E. Sonder, *J. Phys. Chem*., **1962**, 36, 93–97.

11. V. Minkiewicz, G. Shirane, B. Frazer, R. Wheeler, P. Dorain, *J. Phys. Chem. Solids*, **1968**, 29, 881–884.

12. (a) J. Martínez-Lillo, D. Armentano, G. De Munno, W. Wernsdorfer, M. Julve, F. Lloret, J. Faus, *J. Am. Chem. Soc*., **2006**, 128, 14218 – 141219; (b) J. Martínez-Lillo, T. F. Mastropietro, G. De Munno, F. Lloret, M. Julve, J. Faus, *Inorg. Chem*., **2011**, 50, 5731 – 5739.

13. (a) D. E. Freedman, D. M. Jenkins, A. T. Iavarone, J. R. Long, *J. Am. Chem. Soc*., **2008**, 130, 2884–2885. (b) J. M. Zadrozny, D. E. Freedman, D. M. Jenkins, T. D. Harris, A. T. Iavarone, C. Mathonière, R. Clérac, J. R. Long, *Inorg. Chem*., **2010**, 49, 8886–8896. (c) T. D. Harris, M. V. Bennett, R. Clérac, J. R. Long, *J. Am. Chem. Soc*., **2010**, 132, 3980–3988.

14. (a) R. Chiozzone, R. González, C. Kremer, M. F. Cerdá, D. Armentano, G. De Munno, J. Martínez-Lillo, J. Faus, *Dalton Trans*., **2007**, 653–660. (b) J. Martínez-Lillo, D. Armentano, G. De Munno, J. Cano, F. Lloret, M. Julve, J. Faus, *Inorg. Chem*., **2011**, 50, 12405–12407.

15. (a) A. Cuevas, R. Chiozzone, C. Kremer, L. Suescun, A. Mombrú, D. Armentano, G. De Munno, F. Lloret, J. Cano, J. Faus, *Inorg. Chem*., **2004**, 43, 7823–7831. (b) A. Cuevas, C. Kremer, L. Suescun, S. Russi, A. W. Mombrú, F. Lloret, M. Julve, J. Faus, *Dalton Trans*., **2007**, 5305–5315.

16. J. Martínez-Lillo, L. Cañadillas-Delgado, J. Cano, F. Lloret, M. Julve, J. Faus, *Chem. Commun*., **2012**, 48, 9242–9244.

17. (a) R. Chiozzone, A. Cuevas, R. González, C. Kremer, D. Armentano , G. De Munno, J. Faus, *Inorg. Chim. Acta*, **2006**, 359, 2194–2200. (b) J. Martínez-Lillo, T. F. Mastropietro, E. Lhotel, C. Paulsen, J. Cano, G. De Munno, J. Faus, F. Lloret, M. Julve, S. Nellutla, J. Krzystek, *J. Am. Chem. Soc.*, **2013**, 135, 13737–13748.

18. (a) J. Martínez-Lillo, D. Armentano, G. De Munno, W. Wernsdorfer, M. Julve, F. Lloret, J. Faus, *J. Am. Chem. Soc.*, **2006**, 128, 14218 – 14219; (b) J. Martínez-Lillo, T. F. Mastropietro, G. De Munno, F. Lloret, M. Julve, J. Faus, *Inorg. Chem*., **2011**, 50, 5731–5739.

19. (a) D. E. Freedman, D. M. Jenkins, A. T. Iavarone, J. R. Long, *J. Am. Chem. Soc*., **2008**, 130, 2884–2885.

20. J. Martínez-Lillo, D. Armentano, G. De Munno, F. Lloret, M. Julve, J. Faus, *Cryst. Growth Des*, **2006**, 6, 2204–2206.

21. J. Martínez-Lillo, J. Kong, W. P. Barros, J. Faus, M. Julve, E. K. Brechin, *Chem. Commun*., **2014**, 50, 5840–5842.

Article 4.

Enhancement of Intermolecular Magnetic Exchange through Halogen···Halogen Interactions in Bisadeninium Rhenium(IV) Salts

Francisco Lloret Pastor, Doctor en Química, Catedrático de la Universidad de Valencia, Francisco José Martínez Lillo, Doctor en Química, miembros ellos del Instituto de Ciencia Molecular (ICMol) y del Departamento de Química Inorgánica de la Facultad de Química de la Universidad de Valencia,

CERTIFICAN:

Que Don. Carlos Alberto Rojas Dotti ha tenido una participación relevante en el trabajo en coautoría que presenta en esta Memoria, titulado *"Enhancement of Intermolecular Magnetic Exchange through Halogen···Halogen Interactions in Bisadeninium Rhenium(IV) Salts"*, y publicado en la revista *Crystal Growth and Design*. Específicamente, Rojas ha llevado a cabo la caracterización preliminar y las medidas de las propiedades magnéticas de los compuestos reportados. Asimismo, ha llevado a cabo la interpretación y ajuste de los datos experimentales obtenidos. Para poder llevar a cabo el estudio, el doctorando se ha familiarizado durante su formación con el uso de técnicas de caracterización como el análisis elemental por microscopia electrónica de rayos X (EDAX), la espectroscopia infrarroja y el estudio de las propiedades magnéticas mediante magnetometría SQUID.

Rojas firma esta publicación científica como tercer autor puesto que, en este caso, el lugar de los primeros firmantes se ha reservado para los responsables de la síntesis original de los compuestos aquí reportados.

Por último, hemos de dejar constancia de que los resultados reportados en esta publicación no han sido utilizados implícita ni explícitamente por ninguno de los coautores para la realización de una Tesis Doctoral.

Y para que así conste, firmamos el presente certificado en Paterna a 7 de noviembre de 2019.

Prof. Francisco Lloret Pastor
Director

Dr. Francisco José Martínez Lillo
Director y Tutor

Enhancement of Intermolecular Magnetic Exchange through Halogen···Halogen Interactions in Bisadeninium Rhenium(IV) Salts

Donatella Armentano,[†] Miguel A. Barquero,[‡] Carlos Rojas-Dotti,[‡] Nicolas Moliner,[‡] Giovanni De Munno,[†] Euan K. Brechin,*[,§] and José Martínez-Lillo*[,‡]

[†]Dipartimento di Chimica e Tecnologie Chimiche (CTC), Università della Calabria, via P. Bucci 14/c, 87036, Rende, Cosenza, Italy
[‡]Instituto de Ciencia Molecular (ICMol), Universitat de València, c/Catedrático José Beltrán 2, 46980, Paterna, Valencia, Spain
[§]EaStCHEM School of Chemistry, The University of Edinburgh, David Brewster Road, EH9 3FJ, Edinburgh, U.K.

S *Supporting Information*

ABSTRACT: Two novel Re^{IV} salts of general formula $[H_2ade]_2[Re^{IV}X_6]X_2\cdot 4H_2O$ [H_2ade^{2+} = 9H-adenine-1,7-diium; X = Cl(**1**) and Br(**2**)] have been synthesized and magnetostructurally characterized. **1** and **2** are isostructural salts that crystallize in the orthorhombic system with space group *Fdd*2. Both compounds are made up of discrete mononuclear $[Re^{IV}X_6]^{2-}$ and X^- anions and doubly protonated adenine cations. The six-coordinate rhenium(IV) ion is bonded to six halide ligands [X = Cl (**1**) and Br (**2**)] in an octahedral geometry. Short intermolecular $Re^{IV}-X\cdots X-Re^{IV}$ interactions, as well as $Re^{IV}-X\cdots H-N(H_2ade)$ and $Re^{IV}-X\cdots H-O_w$ hydrogen bonds, are present in the crystal lattice of **1** and **2**. Magnetic susceptibility measurements on polycrystalline samples of **1** and **2** in the temperature range 2.0−300 K show the occurrence of significant intermolecular antiferromagnetic interactions in both compounds, resulting in the observation of maxima in χ_M at ca. 6.0 (**1**) and 12.0 K (**2**). The larger spin delocalization from the Re^{IV} ion onto the peripheral bromide ligands when compared to the chloride ligands accounts for the enhancement of the magnetic exchange observed in **2**.
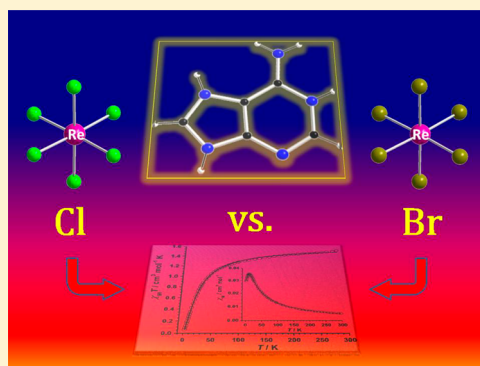
A denine is one of the five main natural nucleobases that are precursors and part of the self-assembled structures of nucleic acids (DNA and RNA). As with other nucleobases, adenine has been studied for decades due to its capacity to establish diverse noncovalent interactions and its potential metal ion binding ability in complex, natural, and artificial nanostructures.[1−11] It is well-known that the combination of hydrogen bonds and π−π stacking interactions among nucleobases provides the conformation and function of macromolecular biological systems.[1−3] Protonated and deprotonated nucleobases play a key role in many biochemical processes and can also generate supramolecular compounds of interest in crystal engineering, molecular recognition, liquid crystals, molecule-based magnetism, and materials science.[12−19]

The nucleobase adenine presents up to four endocyclic (N1, N3, N7, and N9) and one exocyclic (N6) protonatable N atoms (in basicity order: N9 > N1 > N7 > N3 > N6) which can afford a wide range of neutral tautomers and protonated forms (Chart 1). Both organic and inorganic salts based on mono- and diprotonated adenine [adeninium (B) or bisadeninium (C), respectively] are found in the literature. While paramagnetic compounds exist with adeninium, all bisadeninium-based salts reported to date are diamagnetic in nature.[20−26]

Anionic halorhenate(IV) salts are very appealing because of their unique magnetic properties, which include both slow relaxation and quantum tunneling of the magnetization and long-

Chart 1. Molecular Structures of 9H-Adenine (A) and its Mono- and Diprotonated, 9H-Adenine-1-ium (B) and 9H-Adenine-1,7-diium (C) Derivatives
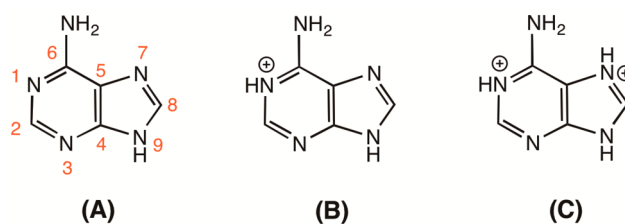
range magnetic order originating from single-ion or cooperative magnetic behaviors, respectively.[27−46] In particular, the simple hexahalorhenate(IV) salts $[Re^{IV}X_6]^{2-}$ (X = F, Cl, Br, and I) of paramagnetic and diamagnetic cations generally show significant short-range intermolecular ferro- or antiferromagnetic interactions, which are mainly transmitted through relatively short intermolecular Re−X···X−Re contacts, occasionally leading to collective magnetic phenomena such as ferromagnetism and spin canting (weak ferromagnetism).[47−59]

5342

Supporting Information

Enhancement of Intermolecular Magnetic Exchange through Halogen···Halogen Interactions in Bisadeninium Rhenium(IV) Salts

Donatella Armentano, Miguel A. Barquero, Carlos Rojas-Dotti, Nicolas Moliner, Giovanni De Munno, Euan K. Brechin, José Martínez-Lillo

Supporting Information

Enhancement of Intermolecular Magnetic Exchange through Halogen···Halogen interactions in Bisadeninium Rhenium(IV) Salts

Donatella Armentano,[a] Miguel A. Barquero,[b] Carlos Rojas-Dotti,[b] Nicolas Moliner,[b] Giovanni De Munno,[a] Euan K. Brechin*[c] and José Martínez-Lillo*[b]

[a]Dipartimento di Chimica e Tecnologie Chimiche (CTC), Università della Calabria, via P. Bucci 14/c, 87036, Rende, Cosenza, Italy

[b]Instituto de Ciencia Molecular (ICMol), Universitat de València, c/ Catedrático José Beltrán 2, 46980, Paterna, Valencia, Spain

[c]EaStCHEM School of Chemistry, The University of Edinburgh, David Brewster Road, EH9 3FJ, Edinburgh, UK

E-mail: ebrechin@ed.ac.uk and lillo@uv.es

1

a)
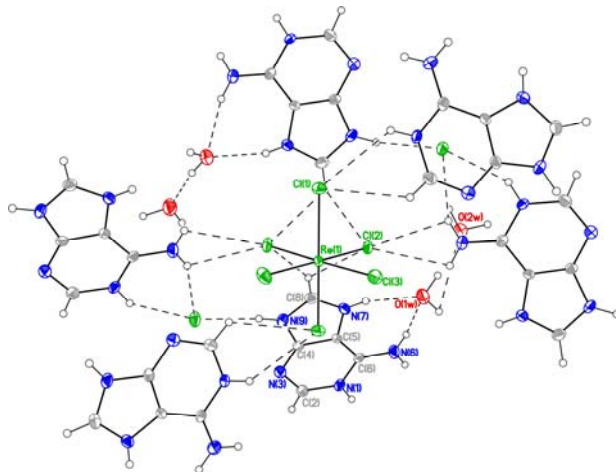
b)
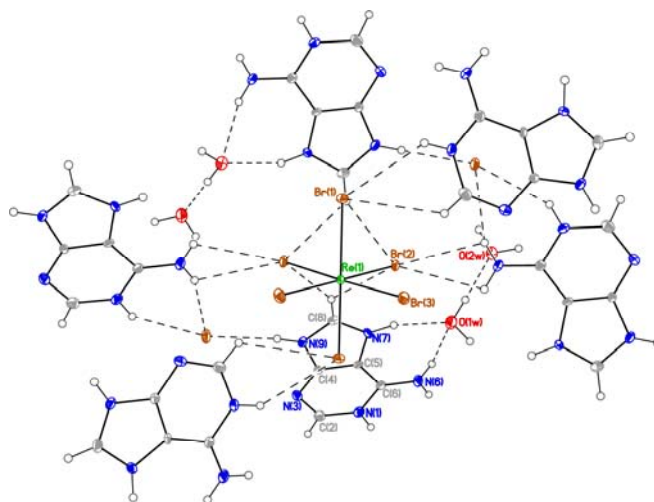
Figure S1. ORTEP drawing of $[ReCl_6]^{2-}$ (a) and $[ReBr_6]^{2-}$ (b) anions and their intermolecular interactions with $[H_2ade]^{2+}$ cations and X^- [X = Cl (**1**) and Br (**2**)] anions connected by means of C-H···X and H-bonds type interactions. short Cl···Cl contacts (dashed lines) in **1**. Ellipsoids are depicted at the 50% probability level.
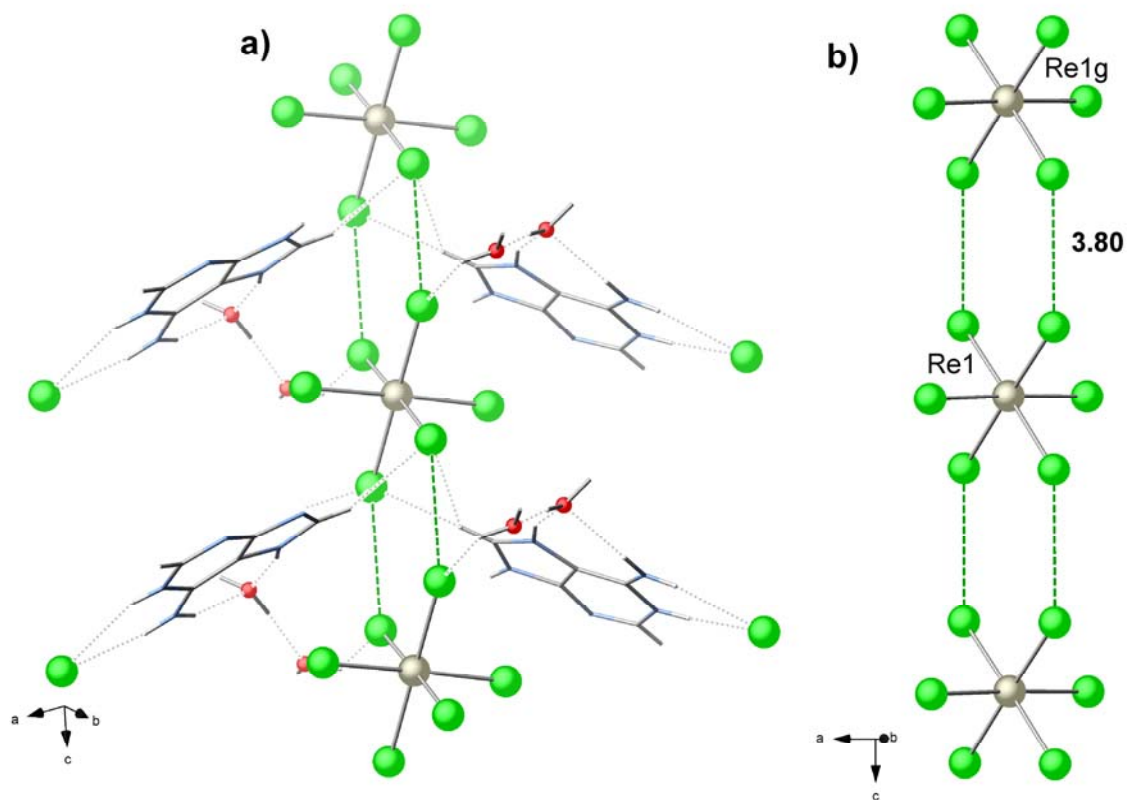
Figure S2. (a) View of a fragment of the supramolecular motif generated by hydrogen bonds involving $[H_2ade]^{2+}$ cations, Cl^- and $[ReCl_6]^{2-}$ anions and lattice water molecules in the crystal packing of **1**. (b) Perspective view of the branched chain connecting $[ReCl_6]^{2-}$ anions through $Cl \cdots Cl$ type interactions (dashed green lines) and growing in the *c*-axis direction.

3
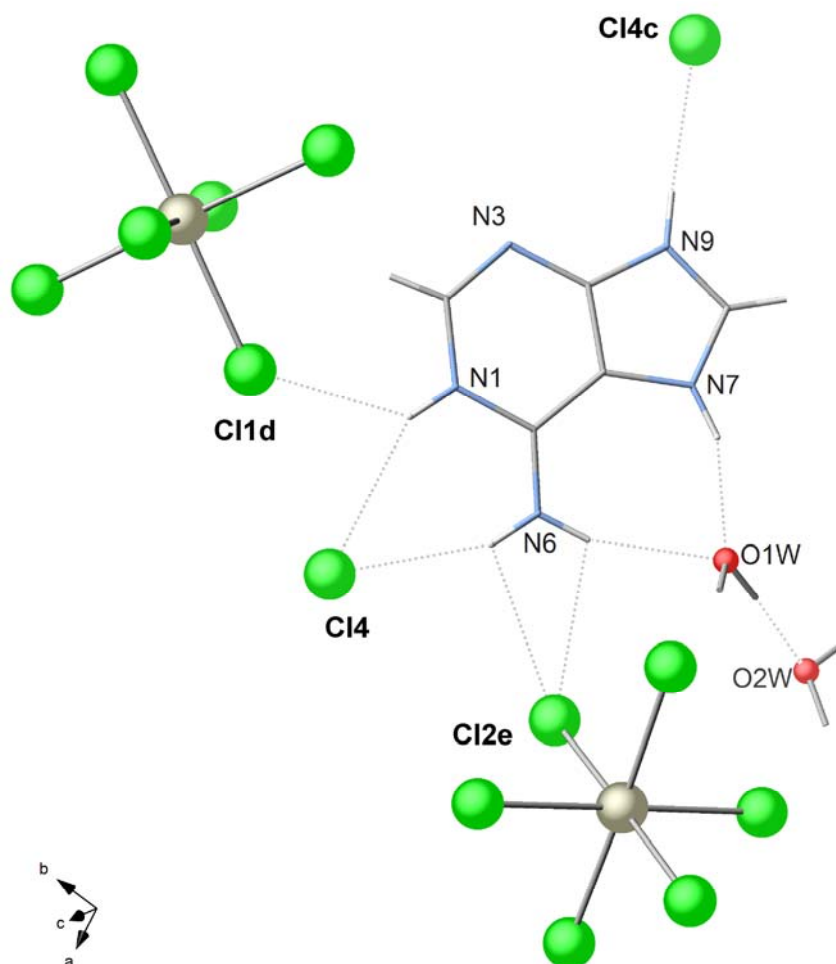
Figure S3. Perspective view of a fragment of crystal packing showing detailed N-H···Cl and N-H···O$_{waters}$ hydrogen bonds interactions (dashed lines), which involve the diprotonated [H$_2$ade]$^{2+}$ cation in **1**.

4
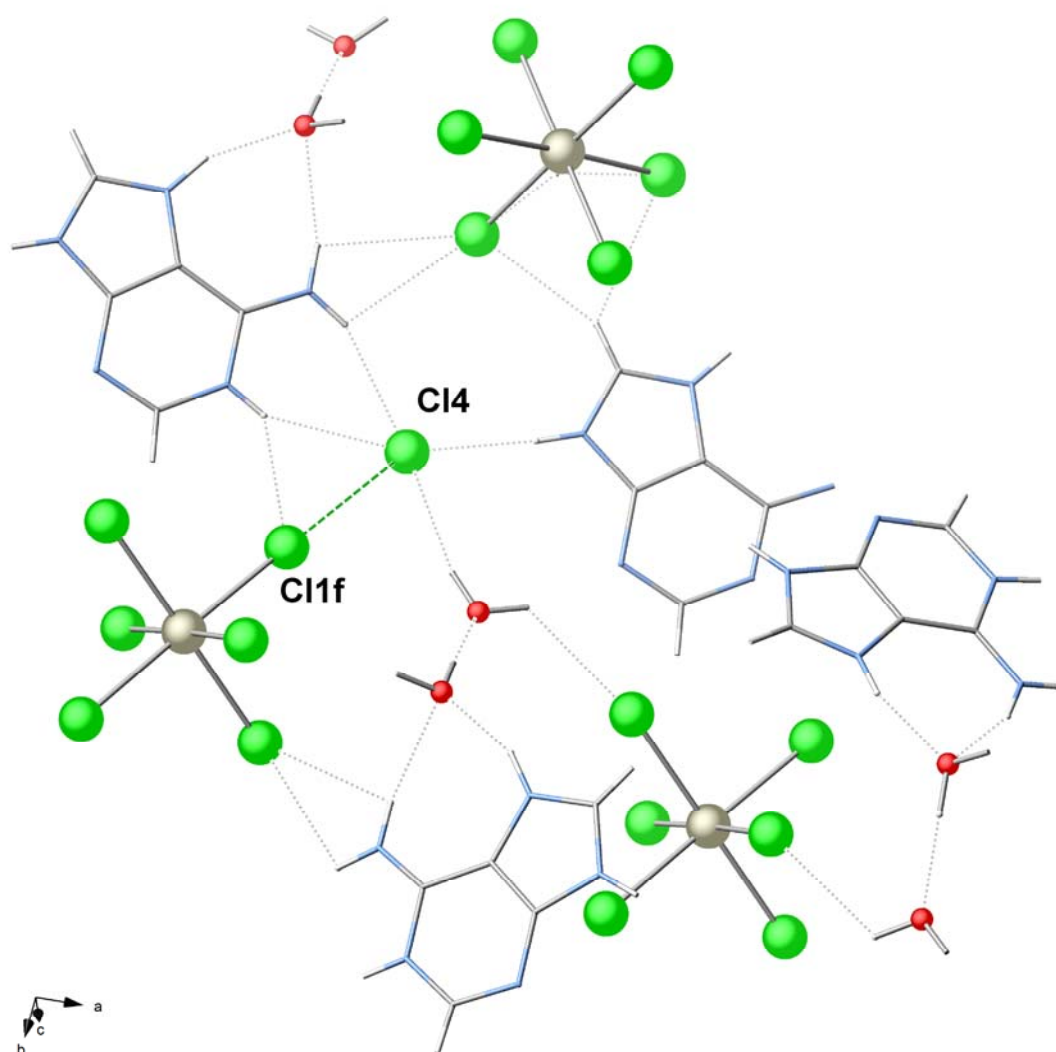
Figure S4. Details of the Cl···[ReCl$_6$]$^{2-}$ interaction (dashed brown lines) and surroundings built through H-bonds (dashed gray lines) involving the Cl$^-$ anion in the crystal packing of **1**.
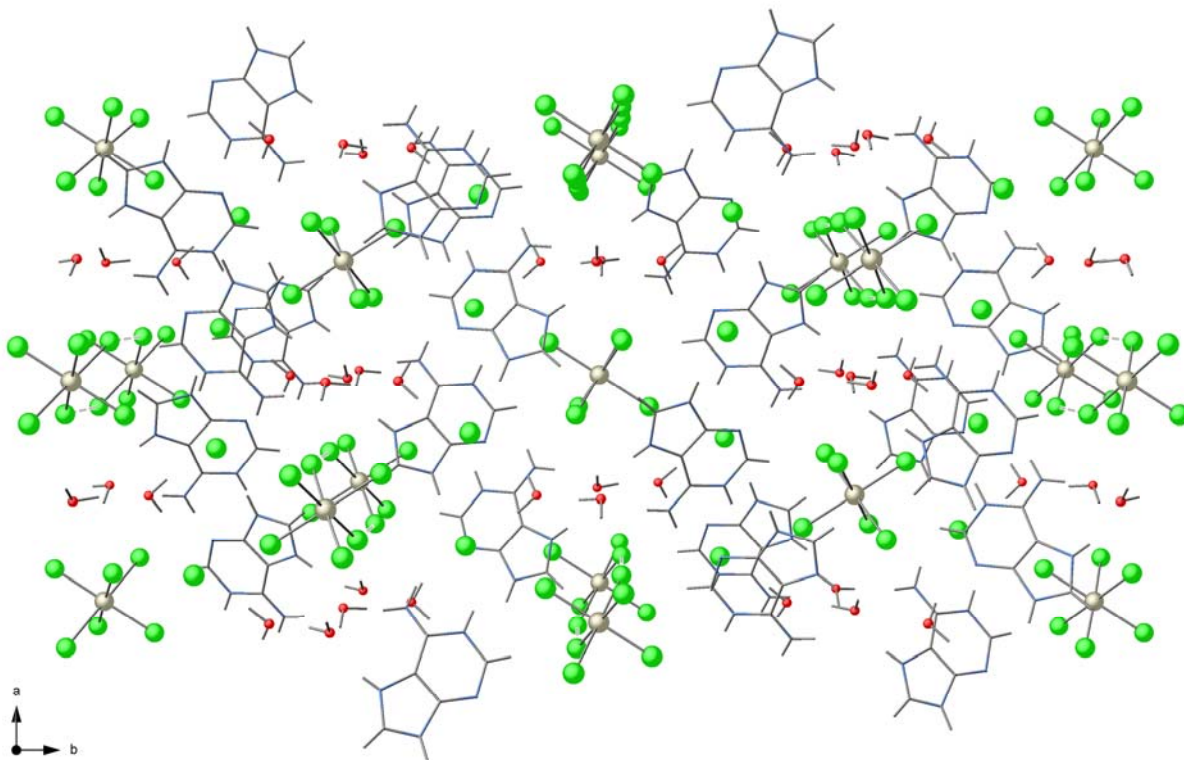
Figure S5. Perspective view along the crystallographic *c* axis of the overall supramolecular assembly of cations, anions and water molecules of **1**, showing the regularly intercalating [H$_2$ade]$^{2+}$ cations and the eclipsed one-dimensional arrangement of [ReCl$_6$]$^{2-}$ anions along the *c*-axis direction through double Re^{IV}−Cl···Cl−Re^{IV} contacts.

6

Article 5.

Hexakis(dimethylformamide)iron(II) complex cation in hexahalorhenate(IV)-based salts: synthesis, X-ray structure and magnetic properties

Taylor & Francis
Taylor & Francis Group

Check for updates
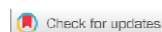
Hexakis(dimethylformamide)iron(II) complex cation in hexahalorhenate(IV)-based salts: synthesis, X-ray structure and magnetic properties

Carlos Rojas-Dotti[a,b], Nicolás Moliner[a], Ricardo González[b] and José Martínez-Lillo[a] (iD)

[a]departament de Química inorgànica/institut de Ciencia molecular (iCmol), universitat de València, Valencia, spain; [b]Cátedra de Química inorgánica, facultad de Química, departamento estrella Campos, universidad de la república, montevideo, uruguay

ABSTRACT

Two iron(II)-rhenium(IV) compounds of general formula $[Fe^{II}(dmf)_6]$ $[Re^{IV}X_6]$ [X = Cl (**1**) and Br (**2**); dmf = N,N-dimethylformamide] have been prepared and characterized. X-ray powder diffraction measurements on samples of **1** and **2** support the same structure for both systems. The crystal structure of **1** was determined by single-crystal X-ray diffraction. **1** crystallizes in the triclinic system with space group $P\bar{1}$. Each iron(II) is six-coordinate and bonded to six oxygens from six dmf molecules building a distorted octahedral environment. Rhenium(IV) is six-coordinate by six halide anions in an almost regular octahedral geometry. The magnetic properties were investigated from variable-temperature magnetic susceptibility measurements performed on microcrystalline samples of **1** and **2**, whose experimental data were reproduced by a model of two isolated paramagnetic centers [S = 2 (Fe^{II}) and S = 3/2 (Re^{IV})] with large values of zero-field splitting (zfs) parameter.
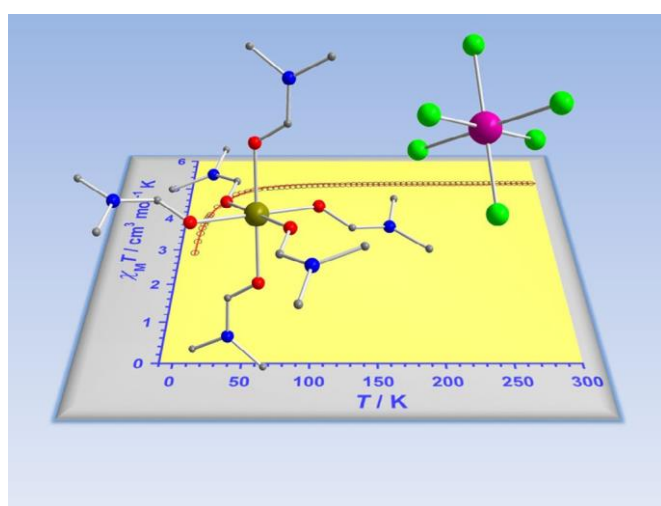
Supporting Information

Hexakis(dimethylformamide)iron(II) complex cation in hexahalorhenate(IV)-based salts: synthesis, X-ray structure and magnetic properties

Carlos Rojas-Dotti, Nicolás Moliner, Ricardo González and José Martínez-Lillo

Supplementary Material

Hexakis(dimethylformamide)iron(II) complex cation in hexahalorhenate(IV)-based salts: synthesis, X-ray structure and magnetic properties

Carlos Rojas-Dotti,[a,b] Nicolás Moliner,[a] Ricardo González,[*b] José Martínez-Lillo[*a]

[a]Instituto de Ciencia Molecular (ICMol)/Departament de Química Inorgànica, Universitat de València, c/ Catedrático José Beltrán 2, 46980 Paterna, Valencia, Spain. [b]Cátedra de Química Inorgánica, Departamento Estrella Campos, Facultad de Química, Universidad de la República, Avda. General Flores 2124, CC 1157 Montevideo, Uruguay.

E-mail: rgonzale@fq.edu.uy; f.jose.martinez@uv.es
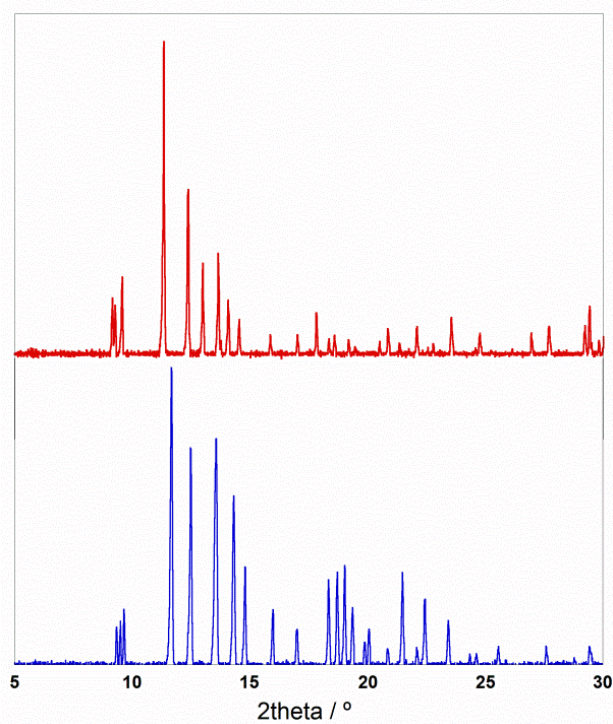
Figure S1. PXRD plots for samples of compounds **1** (blue) and **2** (red).

Article 6.

Ligand substitution in cis-bis(acetonitrile) tetrachloro rhenium(IV) complex with **N,N**-dimethylformamide and **N,N**-dimethylacetamide
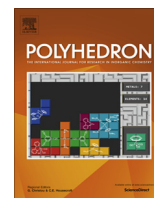
Ligand substitution in *cis*-bis(acetonitrile)tetrachlororhenium(IV) complex with *N,N*-dimethylformamide and *N,N*-dimethylacetamide

Carlos Rojas-Dotti [a,b], Nicolás Moliner [a], Ricardo González [b,*], José Martínez-Lillo [a,*]

[a] *Instituto de Ciencia Molecular (ICMol)/Departament de Química Inorgànica, Universitat de València, c/Catedrático José Beltrán 2, 46980 Paterna, Valencia, Spain*
[b] *Cátedra de Química Inorgánica, Departamento Estrella Campos, Facultad de Química, Universidad de la República, Avda. General Flores 2124, CC 1157 Montevideo, Uruguay*

A B S T R A C T

The preparation, crystal structures, and magnetic properties of two novel mononuclear Re^{IV} complexes of formula *cis*-[Re^{IV}Cl$_4$(dmf)$_2$] (**1**) and *cis*-[Re^{IV}Cl$_4$(dma)$_2$] (**2**) (dmf = *N,N*-dimethylformamide and dma = *N,N*-dimethylacetamide) have been studied. Both Re^{IV} systems were synthesized through ligand substitution reactions from the *cis*-[Re^{IV}Cl$_4$(MeCN)$_2$] precursor, upon heating in the employed solvent. **1** and **2** crystallize in the monoclinic crystal system with space group *C2/c*. Each Re^{IV} ion exhibits a distorted octahedral environment, being bonded by two oxygen atoms from two dmf (**1**) and dma (**2**) molecules and four chloride ions. In the crystal lattice of **1** and **2**, the mononuclear Re^{IV} complexes are placed generating short intermolecular Re^{IV}-Cl⋯Cl-Re^{IV} contacts. The magnetic properties of **1** and **2** were investigated through variable-temperature magnetic susceptibility measurements, which reveal significant antiferromagnetic exchange interactions between neighboring Re^{IV} ions. In **1**, these interactions account for a maximum in the magnetic susceptibility curve at *ca.* 5.0 K.

© 2018 Elsevier Ltd. All rights reserved.

1. Introduction

The synthesis and development of new magnetic systems based on the paramagnetic Re^{IV} metal ion has intensively been investigated in the field of molecular magnetism, because of the broad variety of interesting magnetic phenomena that these systems can display [1–7]. Re^{IV} is a 5d^3 ion with a ground electronic state ^{4}A$_{2g}$ containing three unpaired electrons (t$_{2g}^3$ configuration), and a large value of the spin–orbit coupling constant ($\lambda \sim 1000$ cm^{-1} for the free ion) that accounts for the high magnetic anisotropy that Re^{IV} compounds generally exhibit [6]. Many of these compounds have been prepared from mononuclear Re^{IV} complexes containing potential bridging ligands [8–30], which in turn originate from ligand substitution processes of the well-known hexahalorhenate(IV) salts, [ReX$_6$]$^{2-}$ (X = F, Cl, Br and I) [31–44].

Although to a much lesser extent than hexahalorhenate(IV) salts, *cis*-[Re^{IV}Cl$_4$(MeCN)$_2$] complex has also been used as a starting material to obtain Re^{IV} systems that can exhibit interesting magnetic behaviors [45]. The synthetic procedure of this Re^{IV}-based precursor is known since 1968 [46]. However, the study of its magnetic properties was recently reported, which revealed a magnetic ordering through spin canting at 6.5 K [47]. Hence, it seems that [Re^{IV}Cl$_4$(MeCN)$_2$] complex could be a good candidate to prepare

mononuclear Re^{IV} systems that can exhibit interesting magnetic behaviors, just by replacing the MeCN molecules by another commercial solvent.

In this work, we present our first results concerning this investigation, namely, the synthesis and magnetostructural characterization of two novel Re^{IV} complexes of general formula *cis*-[Re^{IV}Cl$_4$L$_2$], with L = *N,N*-dimethylformamide (dmf, **1**) and *N,N*-dimethylacetamide (dma, **2**). Remarkably, **2** is the first example of crystal structure containing *N,N*-dimethylacetamide molecules coordinate to a paramagnetic 5d metal ion.

2. Experimental

2.1. Materials

All manipulations were performed under aerobic conditions, using chemicals as received. *cis*-[ReCl$_4$(MeCN)$_2$] precursor was prepared following a literature procedure [46]. *N,N*-dimethylformamide and *N,N*-dimethylacetamide solvents were dried and kept with molecular sieves (type 4 Å) before use.

2.2. Synthesis

2.2.1. *cis*-[ReCl$_4$(dmf)$_2$] (**1**)

A solution of [ReCl$_4$(MeCN)$_2$] (41.0 mg, 0.10 mmol) in 3 mL *N,N*-dimethylformamide was heated at 100 °C with continuous stirring

* Corresponding authors.
E-mail addresses: rgonzale@fq.edu.uy (R. González), f.jose.martinez@uv.es (J. Martínez-Lillo).

for 3 h. Once cooled, the resulting green solution was layered with ^{i}PrOH and let to diffuse at room temperature. After complete diffusion, X-ray quality pale green crystals of **1** were formed. Yield: *ca.* 70%. Found: C, 15.0; H, 3.1; N, 5.9. Calc. for $C_6H_{14}N_2O_2Cl_4Re$ (**1**): C, 15.2; H, 3.0; N, 5.9%. X-ray microanalysis gave a Re/Cl molar ratio of 1:4. IR (KBr pellets, v/cm^{-1}): 2964 (w), 1638 (vs), 1482 (w), 1432 (s), 1345 (s), 1242 (m), 1126 (m), 1056 (w), 863 (w), 708 (s), 430 (m).

2.2.2. cis-[ReCl$_4$(dma)$_2$] (2)

Compound **2** was prepared as for **1** but using *N,N*-dimethylacetamide instead of *N,N*-dimethylformamide. Yield: *ca.* 50%. Found: C, 19.0; H, 4.0; N, 5.6. Calc. for $C_8H_{18}N_2O_2Cl_4Re$ (**2**): C, 19.1; H, 3.6; N, 5.6%. X-ray microanalysis gave a Re/Cl molar ratio of 1:4. IR (KBr pellets, v/cm^{-1}): 2945 (m), 1605 (vs), 1477 (m), 1422 (m), 1392 (s), 1365 (w), 1241 (m), 1026 (m), 965 (m), 756 (s), 624 (m), 588 (w), 490 (w), 438 (w).

2.3. Physical measurements

Elemental analysis (C, H, N) were performed on a CE Instruments EA 1110 CHNS analyser. Infrared spectra were recorded on a Thermo-Nicolet 6700 FT-IR spectrophotometer in the 4000–400 cm^{-1} region. Re/Cl molar ratio was analyzed for both compounds by means of a Philips XL-30 scanning electron microscope (SEM) equipped with a system of X-ray microanalysis from the Central Service for the Support to Experimental Research (SCSIE) at the University of Valencia. Magnetic susceptibility measurements of **1** and **2** were carried out with a Quantum Design SQUID magnetometer in the temperature range 2.0–300 K and under an applied magnetic field of 0.1 T, in the Institute of Molecular Science (ICMol) at the University of Valencia. Diamagnetic corrections of the constituent atoms were estimated from Pascal's constants [48,49].

2.4. Crystallographic data collection and structure determination

X-ray diffraction data of single crystals of dimensions $0.20 \times 0.13 \times 0.11$ (**1**) and $0.48 \times 0.34 \times 0.17$ mm^3 (**2**) were collected on a Bruker-Nonius X8APEXII CCD area detector diffractometer using graphite-monochromated Mo-K$_\alpha$ radiation ($\lambda = 0.71073$ Å). Crystal parameters and refinement results for **1** and **2** are summarized in Table 1. The structures of **1** and **2** were solved by Patterson methods and subsequently completed by Fourier recycling using SHELXTL [50–52]. The final full-matrix least squares refinements based on F^2, minimizing the function $\Sigma w(|F_o| - |F_c|)^2$, reached convergence with the values of the discrepancy indices given in Table 1. The graphical manipulations were performed with DIAMOND [53].

3. Results and discussion

3.1. Synthesis of the complexes

The synthesis of both [Re^{IV}Cl$_4$L$_2$] complexes (**1** and **2**) is quite similar, L being *N,N*-dimethylformamide (dmf, **1**) and *N,N*-dimethylacetamide (dma, **2**). Both Re^{IV} systems were synthesized through ligand substitution reactions from the [Re^{IV}Cl$_4$(MeCN)$_2$] precursor, upon heating at 100 °C for 3 h in the employed solvent. A two-step process is expected to take place and it is represented in Eqs. (1) and (2), which refers to compound **1**.
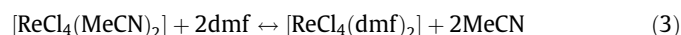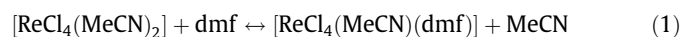
$$[ReCl_4(MeCN)_2] + dmf \leftrightarrow [ReCl_4(MeCN)(dmf)] + MeCN \qquad (1)$$

$$[ReCl_4(MeCN)(dmf)] + dmf \leftrightarrow [ReCl_4(dmf)_2] + MeCN \qquad (2)$$

$$[ReCl_4(MeCN)_2] + 2dmf \leftrightarrow [ReCl_4(dmf)_2] + 2MeCN \qquad (3)$$

Table 1
Crystal data and structure refinement for [ReCl$_4$(dmf)$_2$] (**1**) and [ReCl$_4$(dma)$_2$] (**2**).

Compound	1	2
Formula	$C_6H_{14}N_2O_2Cl_4Re$	$C_8H_{18}N_2O_2Cl_4Re$
$Mr.$ (g mol^{-1})	474.20	502.24
Crystal system	monoclinic	monoclinic
Space group	C2/c	C2/c
a (Å)	16.010(1)	7.680(1)
b (Å)	8.345(1)	13.642(1)
c (Å)	12.488(1)	14.643(1)
α (°)	90.00	90.00
β (°)	125.77	99.89
γ (°)	90.00	90.00
V (Å^3)	1353.7(1)	1511.3(1)
Z	4	4
D_c (g cm^{-3})	2.327	2.207
μ (Mo-K$_\alpha$) (mm^{-1})	9.750	8.739
$F(000)$	892	956
Goodness-of-fit (GOF) on F^2	1.045	1.107
R_1/wR_2 [$I > 2\sigma(I)$]	0.0164/0.0359	0.0241/0.0573
Largest difference in peak and hole (e Å^{-3})	0.974 and −0.971	0.708 and −1.657

According to Eqs. (1) and (2), an outgoing MeCN group would be substituted by a dmf molecule to generate the intermediate [ReCl$_4$(MeCN)(dmf)] species, which could not be isolated. This [ReCl$_4$(MeCN)(dmf)] complex would react with a second dmf molecule, as an entering ligand, to release another MeCN molecule and form [ReCl$_4$(dmf)$_2$] (**1**). The same process would occur for [ReCl$_4$(dma)$_2$] (**2**). Eq. (3) summarizes Eqs. (1) and (2).

It is interesting to note that in either case the Re^{IV} ion retains the four Cl ligands, which were not substituted even if the reaction time was increased to ca. 45 h, obtaining the same compounds **1** and **2**. It has been previously reported that the inertia to ligand substitution of mononuclear Re^{IV} complexes increases with the substitution degree [54]. The reluctance of hexahalorhenate(IV) anions, [ReX$_6$]$^{2-}$ (X = F, Cl, Br, I), to undergo a full substitution of the ligands in their coordination sphere has been observed in previous studies performed on oxalate-based Re^{IV} complexes [55]. Indeed, in a previous work dealing with the substitution reaction of the [ReCl$_6$]$^{2-}$ precursor in dmf, only the monosubstituted species, [ReCl$_5$(dmf)]$^-$, was isolated and characterized [56]. So that, the reported synthesis constitutes a straightforward preparative method to increase the substitution degree of solvent molecules in mononuclear Re^{IV} complexes.

3.2. Crystal structure of cis-[ReCl$_4$(dmf)$_2$] (1) and cis-[ReCl$_4$(dma)$_2$] (2)

Compounds **1** and **2** crystallize in the monoclinic crystal system with space group C2/c (Table 1). Their structures are made up of neutral [Re^{IV}Cl$_4$L$_2$] complexes, where L = *N,N*-dimethylformamide (dmf, **1**) and *N,N*-dimethylacetamide (dma, **2**), which are held together mainly by van der Waals interactions. Two chloride ions [Cl(1) and Cl(2)] and a L molecule are present in the asymmetric unit of **1** and **2**, the rhenium(IV) cation being located on a special position.

Each rhenium(IV) ion exhibits a distorted octahedral environment, being bonded by two oxygen atoms from two dmf (**1**) or two dma (**2**) molecules and four chloride ions (Figs. 1 and 2). No significant differences are seen in the Re-Cl and Re-O bond lengths of **1** and **2**, which vary in the ranges 2.319(1)–2.344(1) and 2.058 (2)–2.066(1) Å, respectively (Table 2). In **1**, the O-Re-O angle is 86.55(8)°, whereas it is 91.74(13)° in **2**. The best equatorial plane around rhenium(IV) ion is defined by O(1)-O(1a)-Cl(2)-Cl(2a) set of atoms in **1** and **2**, each rhenium(IV) ion lying in the plane in both compounds. The C–C, C–O, and C–N bond lengths of the dmf and dma ligands exhibit expected values for these molecules [56–59].
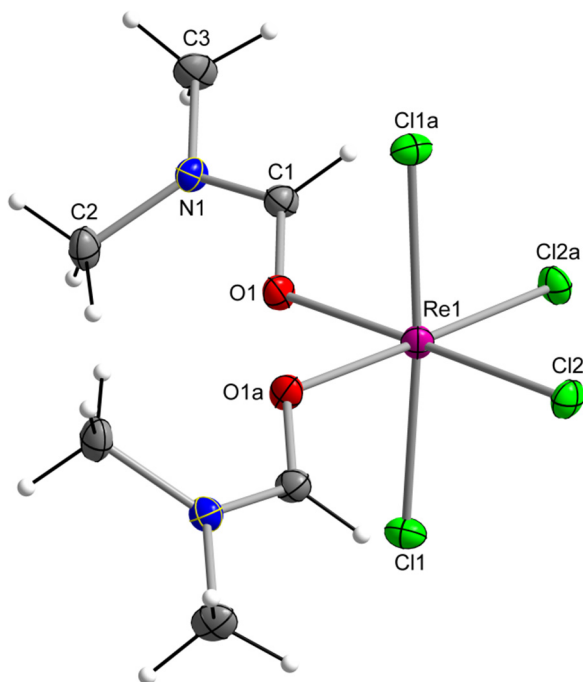
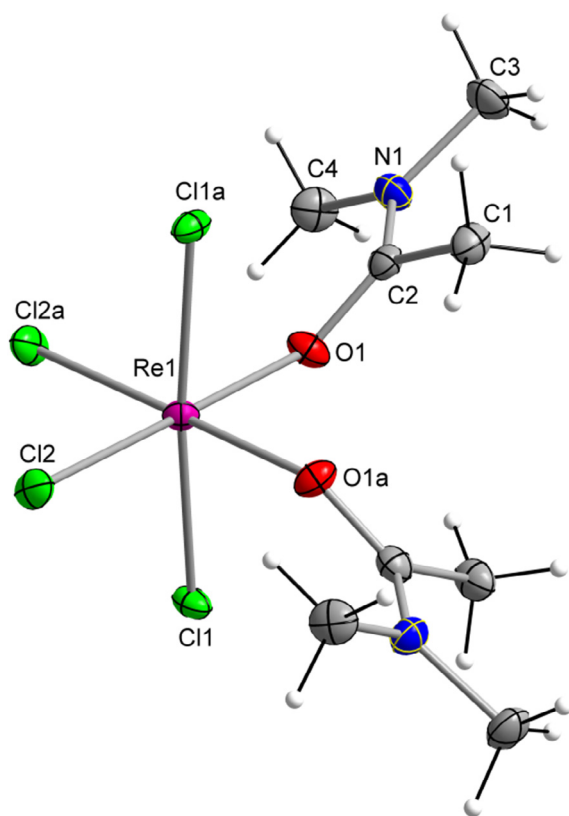Fig. 1. Molecular structure of [ReCl4(dmf)2] complex showing the atom numbering in 1. Thermal ellipsoids are drawn at 50% probability level.

Fig. 2. Molecular structure of [ReCl4(dma)2] complex showing the atom numbering in 2. Thermal ellipsoids are drawn at 50% probability level.

Remarkably, 2 is the first example of crystal structure containing dma molecules coordinate to a paramagnetic 5d metal ion. Indeed, a survey of the literature and Cambridge Structural Database (CSD) reveals that only 15 crystal structures of mononuclear Re^{IV} com-

Table 2
Selected bond lengths (Å) and angles (°) for 1 and **2**.

	1	**2**
Re(1)-O(1)	2.066(1)	2.058(2)
Re(1)-O(1a)	2.066(1)	2.058(2)
Re(1)-Cl(1)	2.334(1)	2.344(1)
Re(1)-Cl(1a)	2.334(1)	2.344(1)
Re(1)-Cl(2)	2.319(1)	2.322(1)
Re(1)-Cl(2a)	2.319(1)	2.322(1)
N(1)-C(3)	1.466(3)	1.473(4)
N(1a)-C(3a)	1.466(3)	1.473(4)
O(1)-Re(1)-Cl(1)	88.06(4)	88.08(7)
O(1)-Re(1)-Cl(2)	176.98(4)	179.50(7)
Cl(1)-Re(1)-Cl(2)	92.48(2)	92.11(3)
O(1)-Re(1)-O(1a)	86.55(8)	91.74(13)
O(1)-Re(1)-Cl(1a)	88.35(4)	87.96(7)
O(1)-Re(1)-Cl(2a)	90.50(4)	88.73(7)
Cl(1)-Re(1)-Cl(1a)	175.08(2)	174.31(4)
Cl(2)-Re(1)-Cl(1a)	90.93(2)	91.88(3)
Cl(2)-Re(1)-Cl(2a)	92.46(2)	90.80(5)
O(1a)-Re(1)-Cl(1)	88.35(4)	87.96(7)
O(1a)-Re(1)-Cl(2)	90.50(4)	88.73(7)
Cl(2a)-Re(1)-Cl(1)	90.93(2)	91.88(3)
O(1a)-Re(1)-Cl(1a)	88.06(4)	88.08(7)
O(1a)-Re(1)-Cl(2a)	176.98(4)	179.50(7)

Symmetry transformation used to generate equivalent atoms:
(a) = −x, y, −z + 1/2.

plexes containing an octahedral cis-[ReCl4O2] geometry have been up to date reported, the O atoms coming from catecholato [60], malonato and oxalato anions [8,11,61], dimethoxyethane and tetrahydrofuran solvents [62,63], crown ethers (18-crown-6) [64] and triphenylarsine oxides [65]. By comparing all these crystal structures, we observe that there are no significant differences in the Re-Cl bond lengths. The Re-O bond lengths vary in the range 2.000(7)–2.142(1) Å, and the Re-O values of 1 and 2 fall into this range. The complex obtained with 18-crown-6 ligand exhibit the longest Re-O bond length, whereas the shortest value is observed in the complex prepared with triphenylarsine oxide. Concerning the value of the O-Re-O angle, which varies from about 77.2 to 91.7° in this family, compound 2 shows the higher value and the complex obtained with 18-crown-6 ligand exhibits the lower value.

In the crystal packing of 1 and 2 there exist different spatial arrangements of [$Re^{IV}Cl_4L_2$] complexes. In 1, neutral [$Re^{IV}Cl_4(dmf)_2$] units are arranged forming a one-dimentional motif that is generated through double Re-Cl···Cl-Re contacts (Fig. 3), the shortest Cl···Cl distance being 3.595(1) Å [Cl(2)···Cl(1b), (b) = −x, −y + 1, −z + 1]. Additional Re-Cl···Cl-Re interactions of 3.879(1) Å [Cl(1)···Cl(1c), (c) = −x − 1/2, −y + 1/2, −z + 1], that connect neighboring chains of [$Re^{IV}Cl_4(dmf)_2$] units, lead to a layered structure (Fig. 4). In 2, the shortest Cl···Cl contact of 3.757(1) Å [Cl(1)···Cl(1b), (b) = −x + 1/2, −y + 3/2, −z + 1] links [$Re^{IV}Cl_4(dma)_2$] complexes generating chains that grow through single Re-Cl···Cl-Re interactions (Fig. 5). A two-dimensional assembly is achieved by means of weak Cl···H-C type contacts [Cl(1)···C(4c) distance of ca. 3.4 Å, (c) = −x + 1, y, −z + 1/2] between adjacent [$Re^{IV}Cl_4(dma)_2$] units (see Fig. 6).

3.3. Magnetic properties

Dc magnetic susceptibility measurements were carried out on microcrystalline samples of 1 and 2 in the 2.0–300 K temperature range. The magnetic properties of 1 and 2 in the form of both $\chi_M T$ and χ_M vs. T plots (χ_M being the molar magnetic susceptibility) are shown in Figs. 7 and 8, respectively. At room temperature, the $\chi_M T$ value for both compounds is 1.56 cm³ mol⁻¹ K, which is expected for a magnetically isolated mononuclear Re^{IV} ($S_{Re} = 3/2$, g = 1.8)
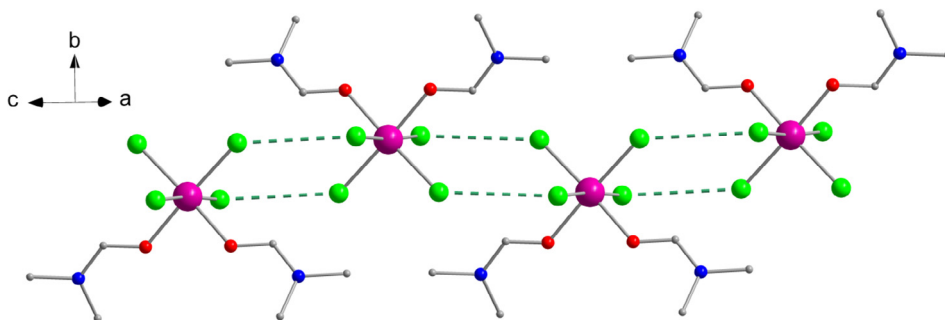
Fig. 3. View along the crystallographic [101] direction of one-dimensional arrangement of [ReCl$_4$(dmf)$_2$] complexes generated through double Cl···Cl interactions (dashed green line) in **1**. H atoms have been omitted for clarity. Color code: pink, Re; green, Cl; red, O; blue, N; gray, C. (Colour online.)
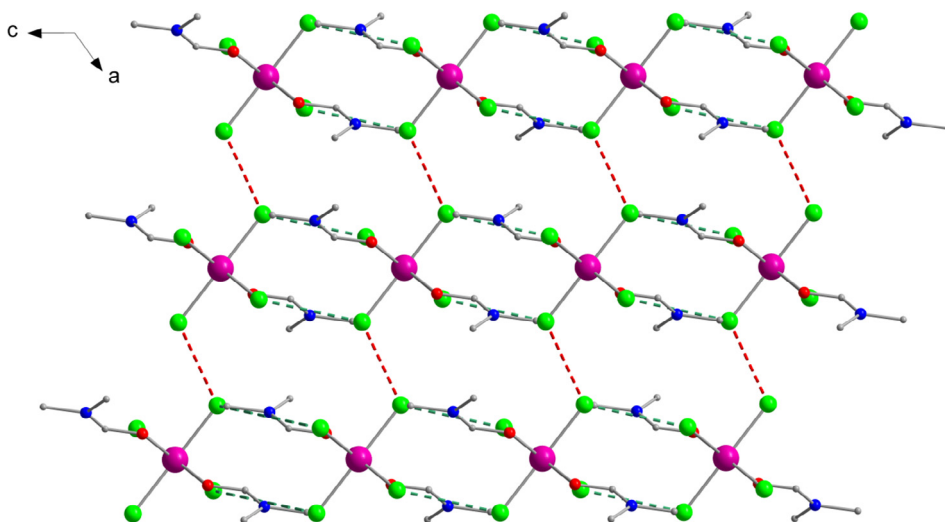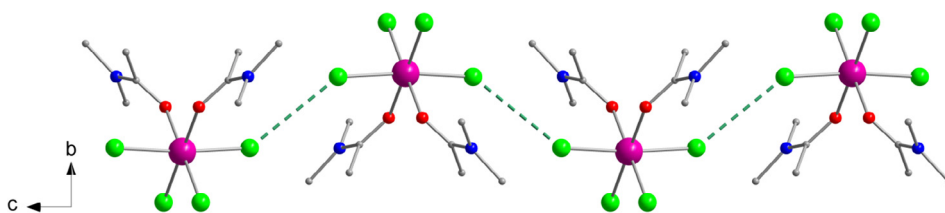

Fig. 4. Perspective view of two-dimensional assembly of [ReCl$_4$(dmf)$_2$] complexes connected through intermolecular Cl···Cl interactions generated from symmetries (b) = −x, −y + 1, −z + 1 (dashed green line) and (c) = −x − 1/2, −y + 1/2, −z + 1 (dashed red line) in **1**. H atoms have been omitted for clarity. Color code: pink, Re; green, Cl; red, O; blue, N; gray, C. (Colour online.)

Fig. 5. View along the crystallographic *a* axis of the one-dimensional motif of [ReCl$_4$(dma)$_2$] complexes mediated through single Cl···Cl interactions (dashed green line) in **2**. H atoms have been omitted for clarity. Color code: pink, Re; green, Cl; red, O; blue, N; gray, C. (Colour online.)

complex [6]. Upon cooling, $\chi_M T$ values slowly decrease with decreasing the temperature reaching final values of 0.15 (**1**) and 0.69 (**2**) cm^3 mol^{-1} K at 2.0 K (Figs. 7 and 8). The decrease of $\chi_M T$ values observed for **1** and **2**, at the lower temperature range, is likely due to the presence of intermolecular interactions and zero-field splitting (zfs) effects [6]. While a maximum of magnetic susceptibility is observed at *ca.* 5.0 K in the χ_M *vs.* *T* plot for **1** (inset, Fig. 7), which is characteristic of an antiferromagnetically coupled system, this does not occur in **2** (inset, Fig. 8).

An analysis of the crystal packing of both compounds reveals that short intermolecular Cl···Cl contacts (covering the range 3.60–3.88 Å) take place between neighboring [Re^{IV}Cl$_4$L$_2$] units in both **1** and **2**. Hence, to analyze the magnetic behavior of **1** and

2, we have treated the experimental data through Hamiltonian of Eq. (4) and its derived theoretical expression for the magnetic susceptibility, Eq. (5) [66]. In addition, a θ parameter was included to account for the observed intermolecular interactions.

$$\hat{H} = D[(\hat{S}_Z)^2 - S(S+1)/3] + g_{//}\,\beta\,H_Z\,\hat{S}_Z + g_\perp\beta(H_X\hat{S}_X + H_Y\hat{S}_Y) \quad (4)$$

$$\chi_M = \frac{\chi_{//} + 2\chi_\perp}{3} \quad (5)$$

where

$$\chi_{//} = \frac{N\beta^2 g_{//}^2}{4k\,(T-\theta)}\frac{1 + 9\exp\,(-2D/kT)}{1 + \exp\,(-2D/kT)}$$
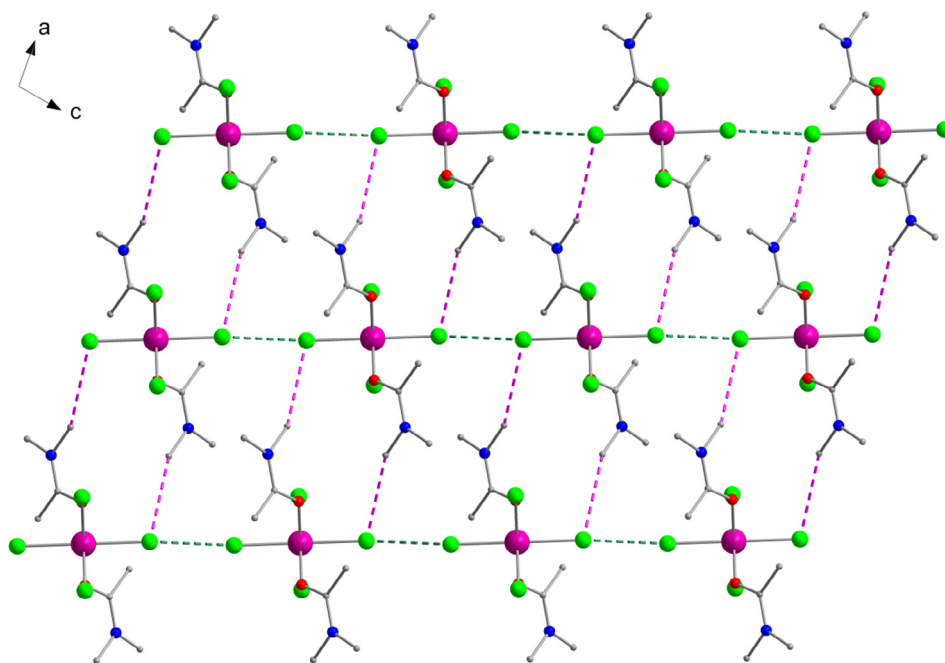
Fig. 6. Perspective view of two-dimensional assembly of [ReCl₄(dma)₂] complexes connected through intermolecular Cl···Cl (dashed green line) and C–H···Cl type interactions (dashed pink line) in **2**. H atoms have been omitted for clarity. Color code: pink, Re; green, Cl; red, O; blue, N; gray, C. (Colour online.)
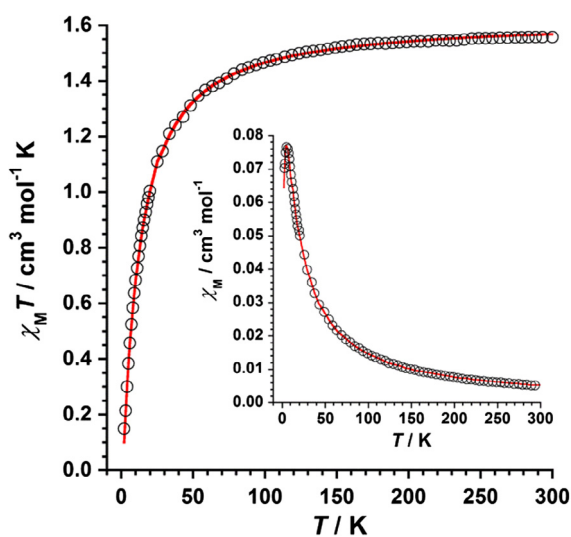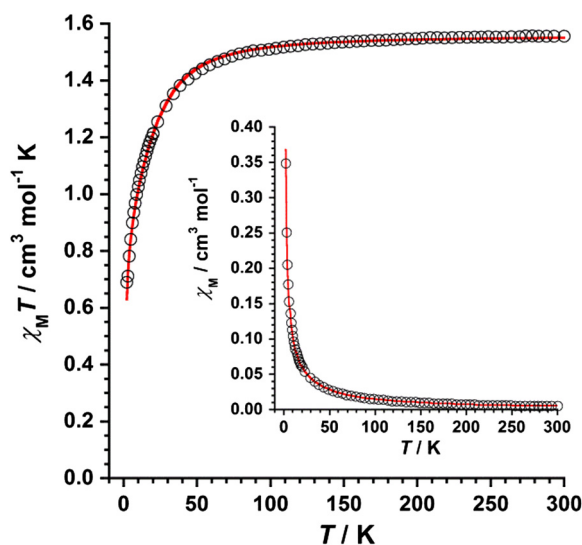

Fig. 7. Thermal variation of the $\chi_M T$ product for **1**. The solid red line represents the best-fit of the experimental data. The inset shows the temperature dependence of the magnetic susceptibility. (Colour online.)

Fig. 8. Thermal variation of the $\chi_M T$ product for **2**. The solid red line represents the best-fit of the experimental data. The inset shows the temperature dependence of the magnetic susceptibility. (Colour online.)

$$\chi_\perp = \frac{N\beta^2 g_\perp^2}{k\,(T-\theta)} \frac{1 + (3kT/4D)\,[1 - \exp(-2D/kT)]}{1 + \exp(-2D/kT)}$$

In Eq. (4), D is the zfs parameter of Re^{IV} ion ($2D$ being the energy gap between the two $M_S = \pm 3/2$ and $M_S = \pm 1/2$ Kramers doublets), whereas last two terms account for the Zeeman effect. In order to avoid overparameterization, we have assumed that $g = g_{//} = g_\perp$ for Re^{IV} ion. Best least-squares fits of the experimental magnetic data in the 2–300 K temperature range afforded: $g = 1.87$, $|D| = 21.1$ cm^{-1}, and $\theta = -9.3$ K with $R = 6.6 \times 10^{-5}$ for **1**, and $g = 1.82$, $|D| = 24.5$ cm^{-1}, and $\theta = -1.1$ K with $R = 4.2 \times 10^{-5}$ for **2** {R being the agreement factor defined as $\Sigma i[(\chi_M T)_{obs}(i) - (\chi_M T)_{calc}(i)]^2 / \Sigma i [(\chi_M T)_{obs}(i)]^2$}. The theoretical curves are shown as red solid lines in Figs. 7 and 8, which match the experimental data very well in the explored temperature range. The g values found for **1** and **2** are in agreement with those previously reported for other mononuclear Re^{IV} complexes exhibiting a similar octahedral environment [6,8,11,12,61]. Concerning the D values obtained for **1** and **2**, they are quite close when compared between them, but are somewhat lower than that computed for the [Re^{IV}Cl₄(MeCN)₂] precursor ($|D| = 30.0$ cm^{-1}) [47]. The negative θ values obtained from the fitting process imply the occurrence of an antiferromagnetic exchange which would be transmitted through short Re-Cl···Cl-Re pathways in both compounds. The θ value is clearly larger in compound **1** [-9.3 (**1**) *vs.* -1.1 K (**2**)], where the shortest Re-Cl···Cl-Re separation occurs (ca. 3.6 Å), with a 1D motif that is spread out to a layered structure by means of additional Re-Cl···Cl-Re contacts (see Figs. 3 and 4). By comparing both compounds, it turns out that the extra methyl group present on the dma molecule in **2**, in comparison with the dmf ligand in **1**, produces enough steric hindrance to get a different spatial

arrangement and somewhat more separated [Re^{IV}Cl$_4$L$_2$] units in the crystal lattice (see Figs. 5 and 6). These features would explain the fact that only in **1** a maximum in the χ_M *vs.* *T* curve is observed.

4. Conclusions

In summary, two novel mononuclear Re^{IV} complexes of general formula *cis*-[Re^{IV}Cl$_4$L$_2$], with L = *N,N*-dimethylformamide (dmf, **1**) and *N,N*-dimethylacetamide (dma, **2**), have been synthesized and magnetostructurally characterized. **1** and **2** have been prepared from the well-known *cis*-[Re^{IV}Cl$_4$(MeCN)$_2$] precursor, by means of ligand substitution reactions upon heating in the employed solvent. Both compounds crystallize in the same space group (*C*2/c), but they pack in a different way. In their crystal packing there exist different spatial arrangements of [Re^{IV}Cl$_4$L$_2$] complexes with short intermolecular Re-Cl···Cl-Re interactions, which transmit an antiferromagnetic exchange between neighboring Re^{IV} ions in **1** and **2**. In the case of **1**, such interactions account for a maximum observed in the magnetic susceptibility curve. Remarkably, **2** is the first example of crystal structure containing *N,N*-dimethylacetamide molecules coordinate to a paramagnetic 5d metal ion.

Acknowledgements

Appendix A. Supplementary data

CCDC 1586971 and 1586972 contain the supplementary crystallographic data for **1** and **2**, respectively. These data can be obtained free of charge via http://www.ccdc.cam.ac.uk/conts/retrieving.html, or from the Cambridge Crystallographic Data Centre, 12 Union Road, Cambridge CB2 1EZ, UK; fax: (+44) 1223-336-033; or e-mail: deposit@ccdc.cam.ac.uk.

References

[1] C.M. Nelson, G.E. Boyd, W.T.J. Smith, J. Am. Chem. Soc. 76 (1954) 348.
[2] B.N. Figgis, J. Lewis, F.E. Mabbs, J. Chem. Soc. (1961) 3138.
[3] R. Busey, E. Sonder, J. Chem. Phys. 36 (1962) 93.
[4] R.H. Busey, H.H. Dearman, R.B. Bevan Jr., J. Phys. Chem. 66 (1962) 82.
[5] V. Minkiewicz, G. Shirane, B. Frazer, R. Wheeler, P. Dorain, J. Phys. Chem. Solids 29 (1968) 881.
[6] J. Martínez-Lillo, J. Faus, F. Lloret, M. Julve, Coord. Chem. Rev. 289–290 (2015) 215.
[7] J. Ferrando-Soria, J. Vallejo, M. Castellano, J. Martínez-Lillo, E. Pardo, J. Cano, I. Castro, F. Lloret, R. Ruiz-García, M. Julve, Coord. Chem. Rev. 339 (2017) 17.
[8] R. Chiozzone, R. González, C. Kremer, G. De Munno, J. Cano, F. Lloret, M. Julve, J. Faus, Inorg. Chem. 38 (1999) 4745.
[9] R. Chiozzone, R. González, C. Kremer, G. De Munno, D. Armentano, J. Cano, F. Lloret, M. Julve, J. Faus, Inorg. Chem. 40 (2001) 4242.
[10] R. Chiozzone, R. González, C. Kremer, G. De Munno, D. Armentano, F. Lloret, M. Julve, J. Faus, Inorg. Chem. 42 (2003) 1064.
[11] A. Cuevas, R. Chiozzone, C. Kremer, L. Suescun, A. Mombrú, D. Armentano, G. De Munno, F. Lloret, J. Cano, J. Faus, Inorg. Chem. 43 (2004) 7823.
[12] J. Martínez-Lillo, D. Armentano, G. De Munno, W. Wernsdorfer, M. Julve, F. Lloret, J. Faus, J. Am. Chem. Soc. 128 (2006) 14218.
[13] A. Cuevas, C. Kremer, L. Suescun, S. Russi, A.W. Mombrú, F. Lloret, M. Julve, J. Faus, Dalton Trans. (2007) 5305.
[14] J. Martínez-Lillo, D. Armentano, N. Marino, L. Arizaga, R. Chiozzone, R. González, C. Kremer, J. Cano, J. Faus, Dalton Trans. (2008) 4585.
[15] A. Bieńko, J. Kłak, J. Mroziński, R. Kruszyński, D.C. Bieńko, R. Boča, Polyhedron 27 (2008) 2464.
[16] J. Martínez-Lillo, D. Armentano, G. De Munno, F. Lloret, M. Julve, J. Faus, Dalton Trans. 40 (2008).
[17] J. Martínez-Lillo, D. Armentano, G. De Munno, W. Wernsdorfer, J.M. Clemente-Juan, J. Krzystek, F. Lloret, M. Julve, J. Faus, Inorg. Chem. 48 (2009) 3027.
[18] A. Cuevas, C. Kremer, L. Suescun, A.W. Mombrú, F. Lloret, M. Julve, J. Faus, Dalton Trans. 39 (2010) 11403.
[19] J. Martínez-Lillo, D. Armentano, G. De Munno, F. Lloret, M. Julve, J. Faus, Dalton Trans. 40 (2011) 4818.
[20] J. Martínez-Lillo, L. Cañadillas-Delgado, J. Cano, F. Lloret, M. Julve, J. Faus, Chem. Commun. 48 (2012) 9242.
[21] I. Bhowmick, E.A. Hilard, P. Dechambenoit, C. Coulon, T.D. Harris, R. Clérac, Chem. Commun. 48 (2012) 9717.
[22] X. Feng, J. Liu, T.D. Harris, S. Hill, J.R. Long, J. Am. Chem. Soc. 134 (2012) 7521.
[23] J. Martínez-Lillo, T.F. Mastropietro, E. Lhotel, C. Paulsen, J. Cano, G. De Munno, J. Faus, F. Lloret, M. Julve, S. Nellutla, J. Krzystek, J. Am. Chem. Soc. 135 (2013) 13737.
[24] A. Bieńko, R. Kruszyński, D. Bieńko, Polyhedron 75 (2014) 1.
[25] J. Martínez-Lillo, D. Armentano, F.R. Fortea-Pérez, S.-E. Stiriba, G. De Munno, F. Lloret, M. Julve, J. Faus, Inorg. Chem. 54 (2015) 4594.
[26] C. Pejo, G.P. Guedes, M.A. Novak, N.L. Speziali, R. Chiozzone, M. Julve, F. Lloret, M.G.F. Vaz, R. González, Chem. Eur. J. 21 (2015) 8696.
[27] L. Arizaga, R. González, D. Armentano, G. De Munno, M.A. Novak, F. Lloret, M. Julve, C. Kremer, R. Chiozzone, Eur. J. Inorg. Chem. (2016) 1835.
[28] I. Gryca, J. Palion-Gazda, B. Machura, M. Penkala, F. Lloret, M. Julve, Eur. J. Inorg. Chem. (2016) 5418.
[29] D. Armentano, J. Martínez-Lillo, Cryst. Growth Des. 16 (2016) 1812.
[30] A.H. Pedersen, M. Julve, J. Martínez-Lillo, J. Cano, E.K. Brechin, Dalton Trans. 46 (2017) 11890.
[31] R. González, R. Chiozzone, C. Kremer, G. De Munno, F. Nicolò, F. Lloret, M. Julve, J. Faus, Inorg. Chem. 42 (2003) 2512.
[32] R. González, R. Chiozzone, C. Kremer, F. Guerra, G. De Munno, F. Lloret, M. Julve, J. Faus, Inorg. Chem. 43 (2004) 3013.
[33] J. Martínez-Lillo, D. Armentano, G. De Munno, F. Lloret, M. Julve, J. Faus, Cryst. Growth Des. 6 (2006) 2204.
[34] J. Martínez-Lillo, D. Armentano, G. De Munno, N. Marino, F. Lloret, M. Julve, J. Faus, CrystEngComm 10 (2008) 1284.
[35] K.I. Suzuki, T. Kodama, K. Kikuchi, W. Fujita, Chem. Lett. 39 (2010) 1096.
[36] D. Armentano, J. Martínez-Lillo, Inorg. Chim. Acta 380 (2012) 118.
[37] J. Martínez-Lillo, J. Kong, M. Julve, E.K. Brechin, Cryst. Growth Des. 14 (2014) 5985.
[38] F. Pop, M. Allain, P. Auban-Senzier, J. Martínez-Lillo, F. Lloret, M. Julve, E. Canadell, N. Avarvari, Eur. J. Inorg. Chem. (2014) 3855.
[39] K.S. Pedersen, M. Sigrist, M.A. Sørensen, A.-L. Barra, T. Weyhermüller, S. Piligkos, C.Aa. Thuesen, M.G. Vinum, H. Mutka, H. Weihe, R. Clérac, J. Bendix, Angew. Chem., Int. Ed. 53 (2014) 1351.
[40] J. Martínez-Lillo, J. Kong, W.P. Barros, J. Faus, M. Julve, E.K. Brechin, Chem. Commun. 50 (2014) 5840.
[41] J. Martínez-Lillo, A.H. Pedersen, J. Faus, M. Julve, E.K. Brechin, Cryst. Growth Des. 15 (2015) 2598.
[42] J. Martínez-Lillo, J. Cano, W. Wernsdorfer, E.K. Brechin, Chem. Eur. J. 21 (2015) 8790.
[43] J. Martínez-Lillo, M. Julve, E.K. Brechin, Polyhedron 35 (2015) 98.
[44] D. Armentano, M.A. Barquero, C. Rojas-Dotti, N. Moliner, G. De Munno, E.K. Brechin, J. Martínez-Lillo, Cryst. Growth Des. 17 (2017) 5342.
[45] P.A. Reynolds, B.N. Figgis, D. Martin y Marero, J. Chem. Soc., Dalton Trans. (1999) 945.
[46] G. Rouschias, W. Wilkinson, J. Chem. Soc. A (1968) 489.
[47] Ch.H. Woodall, G.A. Craig, A. Prescimone, M. Mišek, J. Cano, J. Faus, M.R. Probert, S. Parsons, S. Moggach, J. Martínez-Lillo, M. Murrie, K.V. Kamenev, E.K. Brechin, Nat. Commun. 7 (2016) 13870.
[48] A. Earnshaw, Introduction to Magnetochemistry, Academic Press, London, Kahn, 1968.
[49] G.A. Bain, J.F. Berry, J. Chem. Educ. 85 (2008) 532.
[50] M. Nardelli, J. Appl. Crystallogr. 28 (1995) 659.
[51] G.M. Sheldrick, Acta Crystallogr., Sect. A 64 (2008) 112.
[52] SHELXTL NT – Version 5.1 Copyright©, Bruker Analytical X-ray Systems Inc., Madison, Wisconsin, USA, 1998.
[53] DIAMOND 3.2d: Crystal Impact GbR, CRYSTAL IMPACT, K. Brandeburg & H. Putz GBR, Bonn, Germany, 2000.
[54] J. Martínez-Lillo, D. Armentano, G. De Munno, F. Lloret, M. Julve, J. Faus, Inorg. Chim. Acta 359 (2006) 4343.
[55] R. Chiozzone, A. Cuevas, R. González, C. Kremer, D. Armentano, G. De Munno, J. Faus, Inorg. Chim. Acta 359 (2006) 2194.
[56] J. Martínez-Lillo, D. Armentano, G. De Munno, F. Lloret, M. Julve, J. Faus, Inorg. Chim. Acta 359 (2006) 3291.
[57] J. Martínez-Lillo, D. Armentano, T.F. Mastropietro, M. Julve, J. Faus, G. De Munno, Cryst. Growth Des. 11 (2011) 1733.
[58] R.M. Roat, S. Yolles, A.L. Rheingold, Inorg. Chem. 25 (1986) 3102.
[59] S.D. Drouin, G.P.A. Yap, D.E. Fogg, Inorg. Chem. 39 (2000) 5412.
[60] A. Cuevas, L. Geis, V. Pintos, R. Chiozzone, J. Sanchíz, M. Hummert, H. Schumann, C. Kremer, J. Mol. Struct. 921 (2009) 80.
[61] A.H. Pedersen, M. Julve, E.K. Brechin, J. Martínez-Lillo, CrystEngComm 19 (2017) 503.
[62] D.W. von Gudenberg, I. Sens, U. Muller, B. Neumuller, K. Dehnicke, Z. Anorg. Allg. Chem. 613 (1992) 49.
[63] L.M. Engelhardt, B.N. Figgis, A.N. Sobolev, P.A. Reynolds, Aust. J. Chem. 49 (1996) 489.
[64] D.W. von Gudenberg, G. Frenzen, W. Massa, K. Dehnicke, Z. Anorg. Allg. Chem. 621 (1995) 621.
[65] B. Machura, J.O. Dziegielewski, S. Michalik, T.J. Bartczak, R. Kruszynski, J. Kusz, Polyhedron 21 (2002) 2617.
[66] O. Kahn, Molecular Magnetism, VCH, New York, 1993.

Article 7.

Field-induced slow relaxation of magnetisation in an anionic heterotetranuclear $[\text{Zn}^{\text{II}}Re_3^{IV}]$ system

Francisco Lloret Pastor, Doctor en Química, Catedrático de la Universidad de Valencia, Francisco José Martínez Lillo, Doctor en Química, miembros ellos del Instituto de Ciencia Molecular (ICMol) y del Departamento de Química Inorgánica de la Facultad de Química de la Universidad de Valencia,

CERTIFICAN:

Que Don. Carlos Alberto Rojas Dotti ha tenido una participación relevante en el trabajo en coautoría que presenta en esta Memoria, titulado "*Field-induced slow relaxation of magnetisation in an anionic heterotetranuclear [$Zn^{II}Re^{IV}_3$] system*", y publicado en la revista *Dalton Transactions*. La contribución del estudiante a este trabajo ha sido fundamentalmente de carácter cristalográfico, ha llevado a cabo el desarrollo de la estrategia de medida y la recolección de datos de difracción de rayos X de monocristal, así como el refinamiento de los datos cristalográficos y la resolución estructural. Asimismo, ha colaborado en la supervisión de los aspectos prácticos de la síntesis y caracterización preliminar del sistema reportado.

Rojas firma esta publicación científica como segundo autor puesto que, en este caso, el lugar de primer firmante ha sido reservado para el responsable de la síntesis original del compuesto aquí publicado.

Por último, hemos de dejar constancia de que los resultados reportados en esta publicación no han sido utilizados implícita ni explícitamente por ninguno de los coautores para la realización de una Tesis Doctoral.

Y para que así conste, firmamos el presente certificado en Paterna a 7 de noviembre de 2019.

Prof. Francisco Lloret Pastor
Director

Dr. Francisco José Martínez Lillo
Director y Tutor

Dalton Transactions

An international journal of inorganic chemistry

rsc.li/dalton
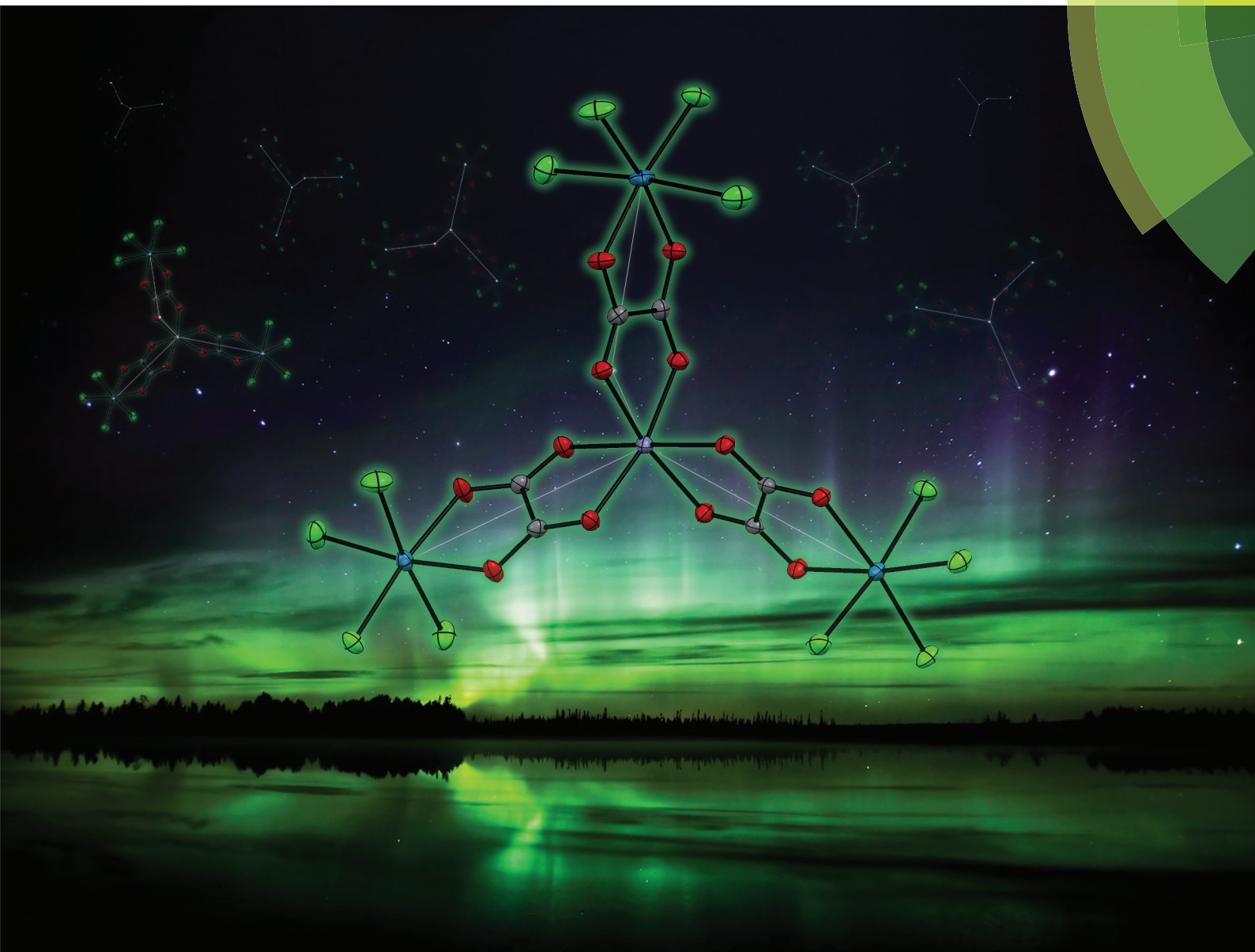
ROYAL SOCIETY OF CHEMISTRY | Celebrating IYPT 2019

COMMUNICATION
José Martínez-Lillo et al.
Field-induced slow relaxation of magnetisation in an anionic
heterotetranuclear [Zn^{II}Re$^{IV}_3$] system

187

COMMUNICATION

Check for updates

Field-induced slow relaxation of magnetisation in an anionic heterotetranuclear [Zn^II Re_3^IV] system†

Adrián Sanchis-Perucho, [ID] Carlos Rojas-Dotti, Nicolás Moliner [ID] and José Martínez-Lillo [ID] *

The compound $(NBu_4)_4[Zn^{II}\{Re^{IV}Cl_4(\mu\text{-}ox)\}_3]$ (1) $[NBu_4^+$ = tetra-*n*-butylammonium cation and ox^{2-} = oxalate dianion] is the first example of an oxalato-bridged Zn^{II} system coordinated to a 5d metal ion that exhibits slow relaxation of magnetisation.

Oxalate-based Zn^{II} compounds have undergone considerable development in diverse research fields during recent years.[1–5] Promising oxalate-based Zn^{II} systems that display catalysis,[6] luminescence[7,8] and proton conduction[9–12] processes have been investigated with the goal of establishing current and future technological applications in materials science.[1–12]

Given the diamagnetic nature of Zn^{II} ($3d^{10}$ ion), the incorporation of a paramagnetic 5d metal ion to this type of system would offer added value and interesting effects, in terms of magnetic properties, to the final material.[13]

Thus, we have used the highly anisotropic Re^{IV} ($5d^3$ ion) in the form of the $[ReCl_4(ox)]^{2-}$ $[ox^{2-}$ = oxalate dianion] metallo-ligand towards Zn^{II} as a rational approach to obtain multifunctional materials based on the Zn^{II} and Re^{IV} metal ions.[14] Indeed, the number of reported crystal structures of oxalato-bridged Zn^{II} compounds containing a 5d metal ion is limited to just one, the heterodinuclear complex $[ReCl_4(\mu\text{-}ox)Zn(bdmpzm)_2]\cdot2MeCN$ [bdmpzm = bis(3,5-dimethyl-1*H*-pyrazol-1-yl)methane], which shows a behaviour typical of a magnetically isolated Re^{IV} complex that does not exhibit slow relaxation of magnetisation, its magnetic behaviour being governed only by the large zero-field splitting (ZFS) of this paramagnetic 5d metal ion.[15]

As far as we know, there exist in the literature only half a dozen oxalate-based 0D systems exhibiting slow relaxation of magnetisation, which behave as either single-ion magnets (SIMs) or single-molecule magnets (SMMs),[16–21] most of them

Instituto de Ciencia Molecular (ICMol)/Departament de Química Inorgànica, Universitat de València, c/Catedrático José Beltrán 2, 46980 Paterna, Valencia, Spain. E-mail: f.jose.martinez@uves

†Electronic supplementary information (ESI) available. CCDC 1866320. For ESI and crystallographic data in CIF or other electronic format see DOI: 10.1039/c8dt03728k

being obtained with the Re^{IV} metal ion.[16,17,19,21] Furthermore, the majority of the reported systems that exhibit field-induced slow relaxation of magnetisation are based on 3d or 4f metal ions. In comparison, compounds of this type based on 5d metal ions have been scarcely explored and studied.[22]

Herein we report an unusual Zn^{II}–Re^{IV} compound of the formula $(NBu_4)_4[Zn^{II}\{Re^{IV}Cl_4(\mu\text{-}ox)\}_3]$ (1) $[NBu_4^+$ = tetra-*n*-butylammonium cation and ox^{2-} = oxalate dianion] which has been characterised structurally and magnetically (Fig. 1). 1 is the first example of an oxalato-bridged Zn^{II} system coordinated to a 5d metal ion that exhibits slow relaxation of magnetisation.

The reaction of $(NBu_4)_2[ReCl_4(ox)]$ and $Zn(ClO_4)_2\cdot6H_2O$ in an isopropanol–MeCN mixture at room temperature results in the formation of pale green crystals of 1 (see the ESI†). Compound 1 is stable under air for a period of several months and does not oxidise under ambient conditions. The phase
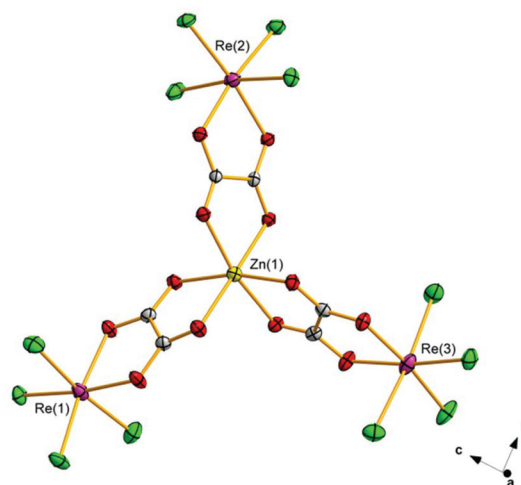

Fig. 1 Molecular structure of the anionic heterotetranuclear $[Zn\{ReCl_4(\mu\text{-}ox)\}_3]^{4-}$ complex in 1. NBu_4^+ cations have been omitted for clarity. Thermal ellipsoids are depicted at the 50% probability level. Colour code: pink, Re; yellow, Zn; green, Cl; red, O; grey, C.

The article has been deleted for the publisher copyright policy

DOI: 10.1039/c8dt03728k

Pag. 189 – 193.

Supporting Information

Field-induced slow relaxation of magnetisation in an anionic heterotetranuclear $[\text{Zn}^{\text{II}}Re_3^{IV}]$ system

Adrián Sanchis-Perucho, Carlos Rojas-Dotti, Nicolás Moliner, José Martínez-Lillo

Electronic Supplementary Information (ESI)

Field-induced slow relaxation of the magnetisation in an anionic heterotetranuclear[Zn^{II}Re$^{IV}_3$] system

Adrián Sanchis-Perucho, Carlos Rojas-Dotti, Nicolás Moliner and José Martínez-Lillo*

Instituto de Ciencia Molecular (ICMol)/Departament de Química Inorgànica, Universitat de València, c/ Catedráti n 2, 46980, Paterna, Valencia, Spain.

Table of contents   **page**

Synthesis of 1.

All chemicals were used as received. The precursor $(NBu_4)_2[ReCl_4(ox)]$ was prepared following the literature procedures indicated in the references No. 24 and 25 of the main text.

A solution of $(NBu_4)_2[ReCl_4(ox)]$ (202.5 mg, 0.225 mmol) in a isopropanol/MeCN (15 mL, 9:1, v/v) mixture was added to a solution of $Zn(ClO_4)_2 \cdot 6H_2O$ (27.9 mg, 0.075 mmol) in isopropanol (15 mL) under continuous stirring. The resulting pale green solution was allowed to evaporate at room temperature. Green needles of **1** were grown in one day, were filtered off and washed with cold isopropanol and diethyl ether. Yield: *ca*. 50%. Better crystals of **1** were obtained when a 1:1 Re/Zn molar ratio was used in the synthesis. Anal. Calcd. for $C_{70}H_{144}N_4O_{12}Cl_{12}Re_3Zn$ (**1**): C, 36.80; H, 6.40; N, 2.45. Found: C, 37.30; H, 7.00; N, 2.50. IR (KBr pellet/cm^{-1}): bands associated to the oxalate ligand are observed at 1712m, 1656vs and 812m.

Table S1. Summary of the crystal data for compound 1.

Compound	1
Formula	$C_{70}H_{144}N_4O_{12}Cl_{12}Re_3Zn$
M_r	2283.25
Crystal system	triclinic
Space group	$P\bar{1}$
$a/\text{Å}$	9.813(1)
$b/\text{Å}$	19.331(1)
$c/\text{Å}$	25.223(1)
$\alpha/°$	84.45(1)
$\beta/°$	83.08(1)
$\gamma/°$	81.72(1)
$V / \text{Å}^3$	4684.8(5)
Z	2
$D_c/\text{g cm}^{-3}$	1.619
$\mu(\text{Mo-K}_\alpha)/\text{mm}^{-1}$	4.511
Goodness-of-fit on F^2	0.992
$R_1 [I > 2\sigma(I)]$	0.0195
$wR_1 [I > 2\sigma(I)]$	0.0478
$\Delta\rho_{\text{max, min}}/\text{e.Å}^{-3}$	2.388 and -0.902

2
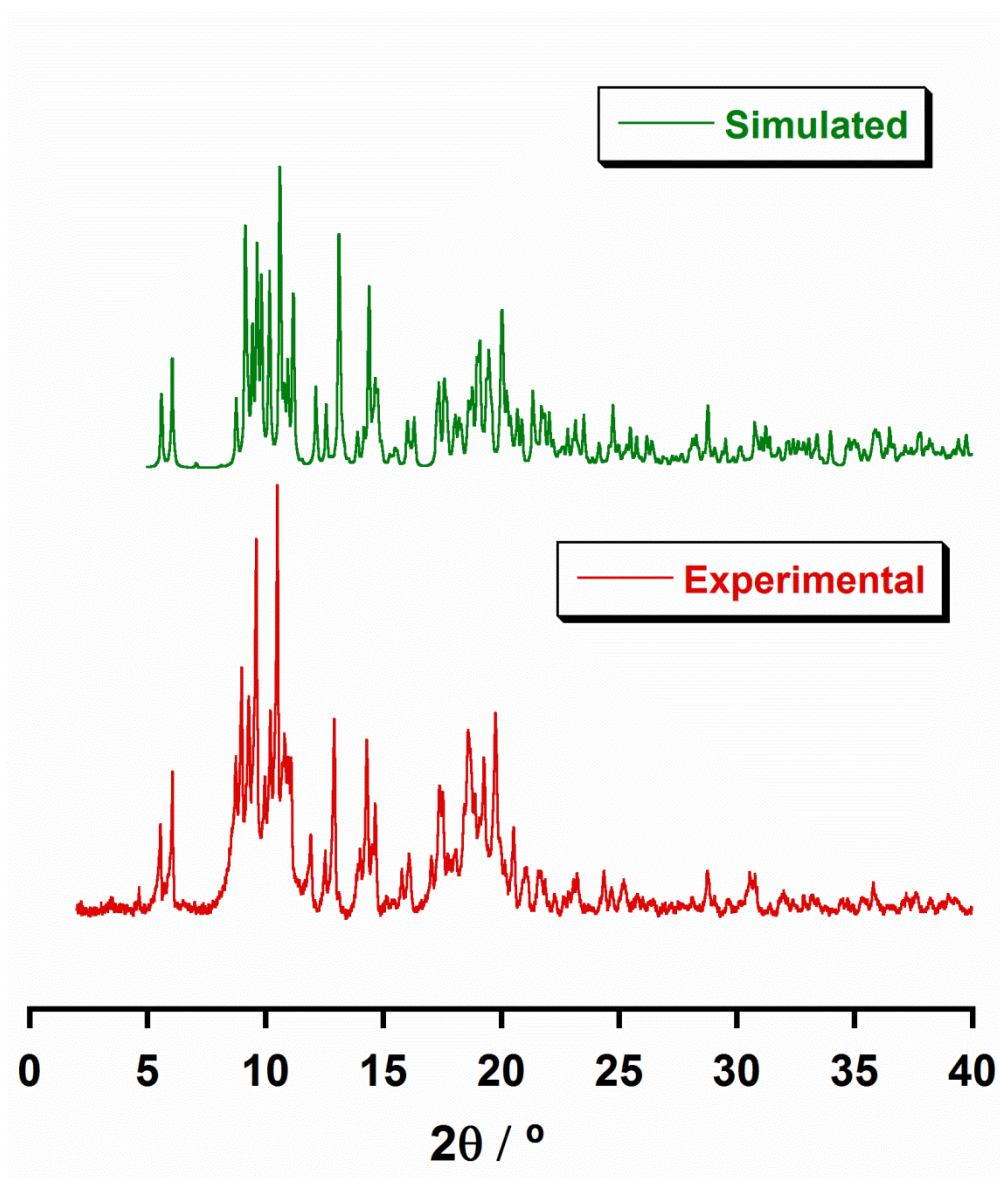
Figure S1. Plot of the simulated (green line) and experimental XRD (red line) patterns profile in the 2θ/° range 0–40° for **1**.

(a)
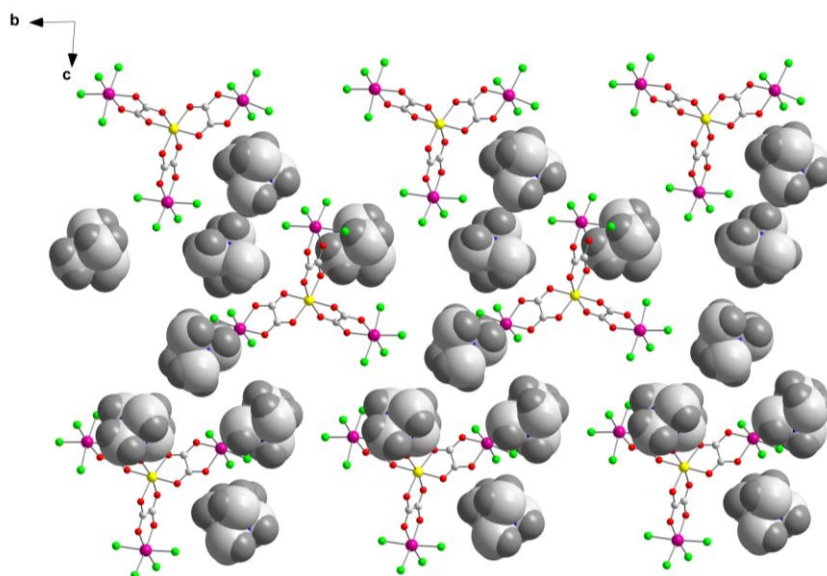
(b)
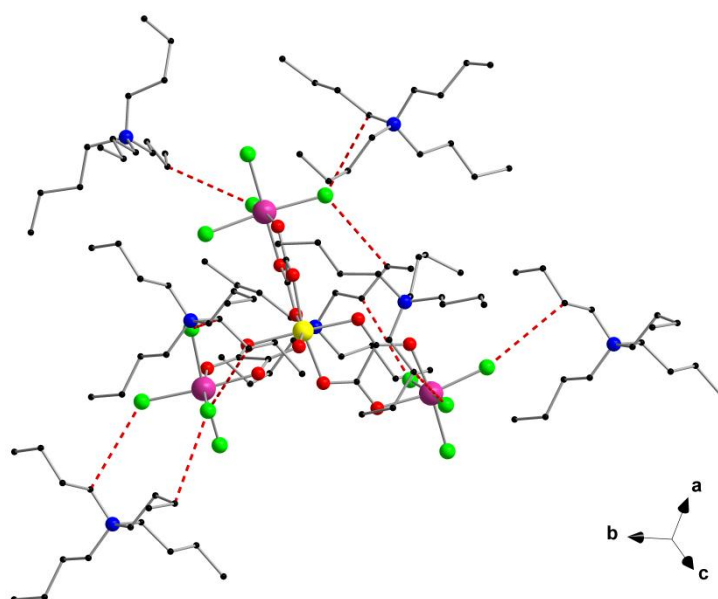
Figure S2. (a) View along the *a* crystallographic axis of the crystal packing of **1** showing the relative arrangement of the tetra-*n*-butylammonium cations (space-filling model) and the $[Zn\{ReCl_4(\mu\text{-ox})\}_3]^{4-}$ anions. For the sake of clarity, only the $N(CH_2)_4$ skeleton of the tetra-*n*-butylammonium cations is shown. Colour code: pink, Re; yellow, Zn; green, Cl; red, O; blue, N; white, C; grey, H. (b) Detail of the weak C···Cl interactions between cations and anions in **1** (red dashed lines) with colour code: pink, Re; yellow, Zn; green, Cl; red, O; blue, N; black, C.

4
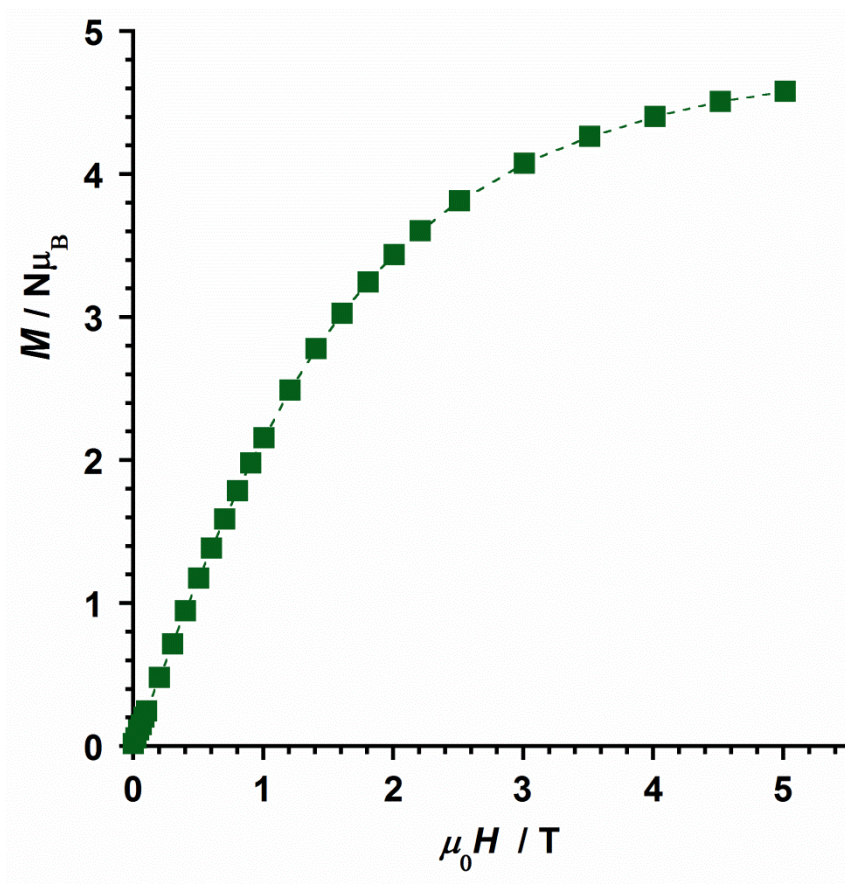
Figure S3. Plot of the variable-field magnetisation *versus* applied field at 2.0 K for **1**.
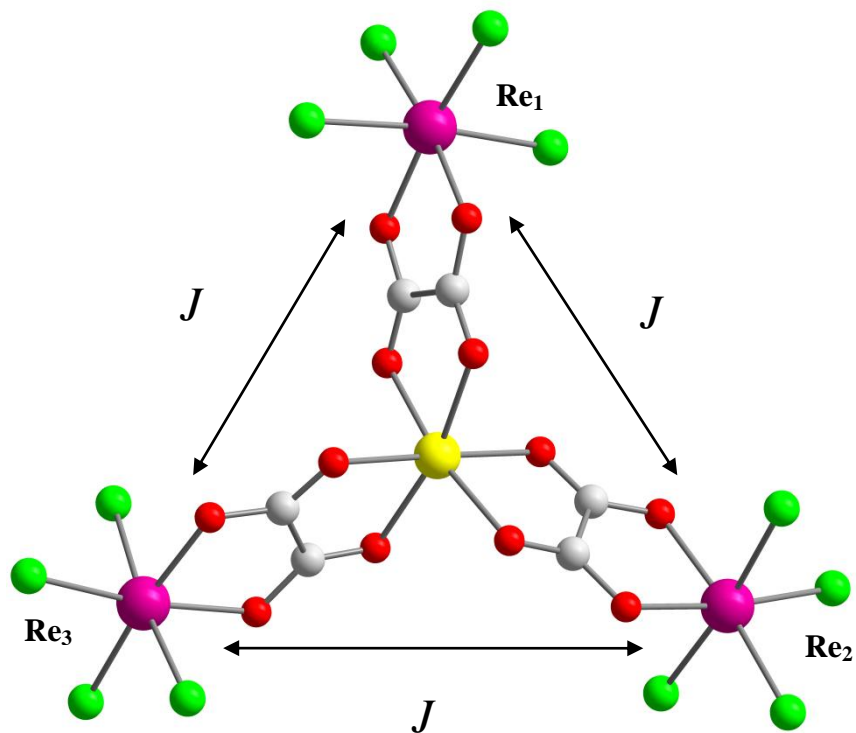
Figure S4. One *J* model employed to fit the experimental magnetic susceptibility data of compound **1**, where *J* is the exchange coupling constant for the intramolecular Re^{IV}–Re^{IV} interactions through the oxalate bridges. It is assumed that $g_{Re} = g_{Re1} = g_{Re2} = g_{Re3}$ and $D_{Re} = D_{Re1} = D_{Re2} = D_{Re3}$. Colour code: pink, Re; yellow, Zn; green, Cl; red, O; blue, N; white, C.

6

(a)
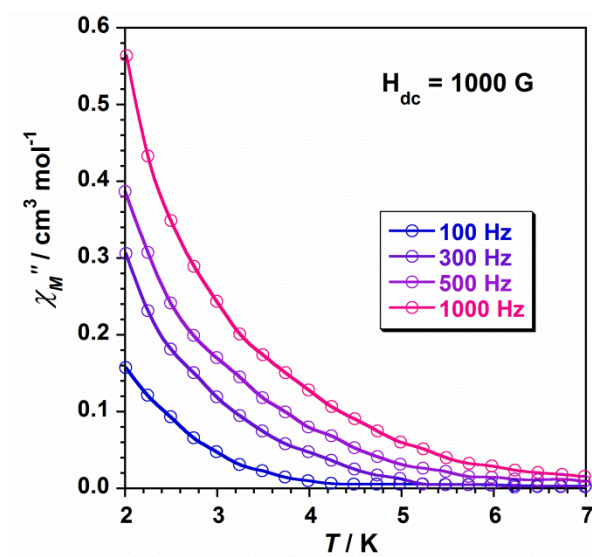
(b)
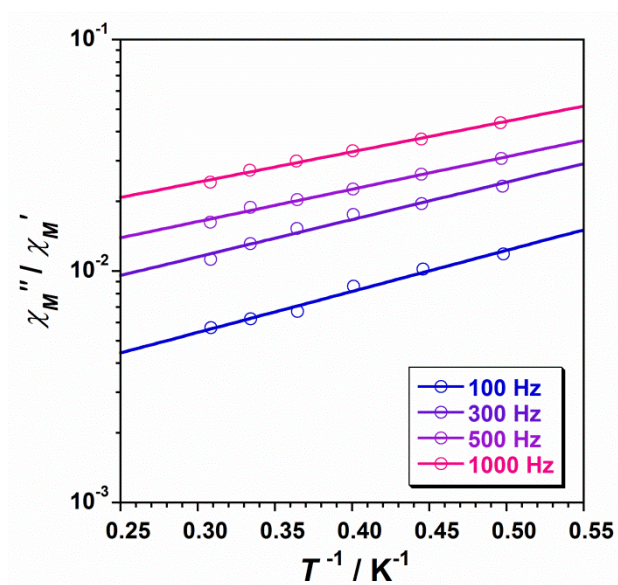
Figure S5. (a) Out-of-phase *ac* susceptibility *versus* temperature plot (χ''_M *vs*. *T*) for **1** at four different frequencies (100-1000 Hz range) under a dc field of 1000 G. (b) χ''_M/χ'_M *vs*. 1/*T* plot for **1**. The solid lines are the best-fit curves.

(a)
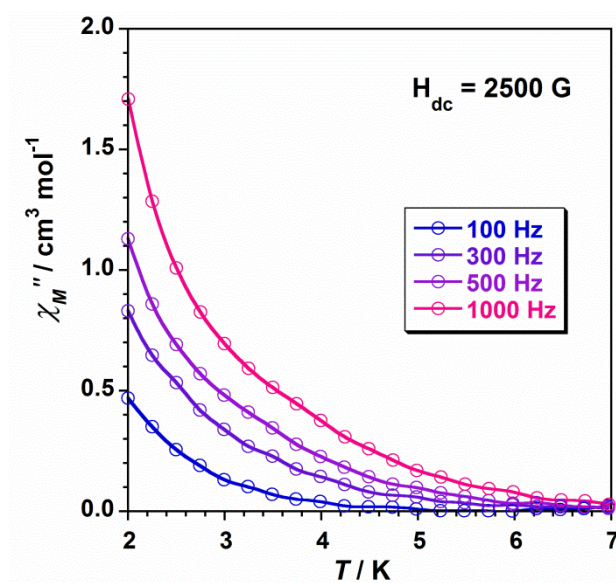
(b)
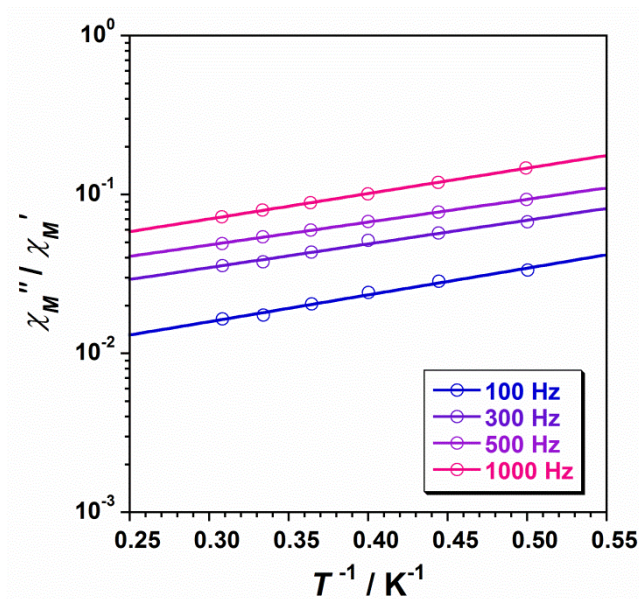
Figure S6. (a) Out-of-phase *ac* susceptibility *versus* temperature plot (χ''_M *vs*. *T*) for **1** at four different frequencies (100-1000 Hz range) under a dc field of 2500 G. (b) χ''_M/χ'_M *vs*. 1/*T* plot for **1**. The solid lines are the best-fit curves.

8

(a)
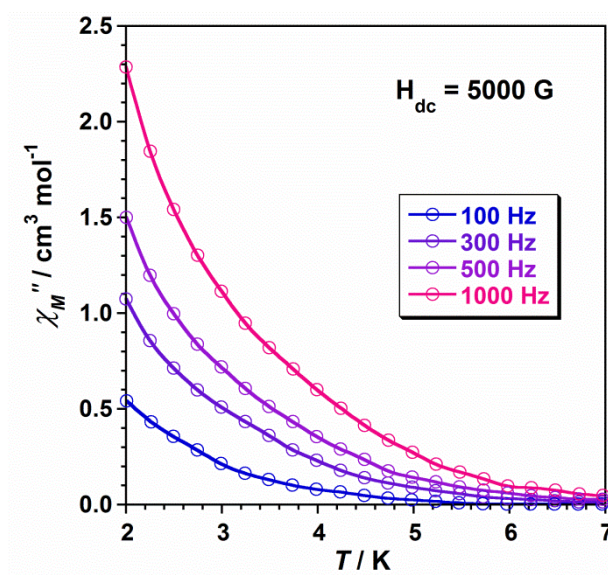
(b)
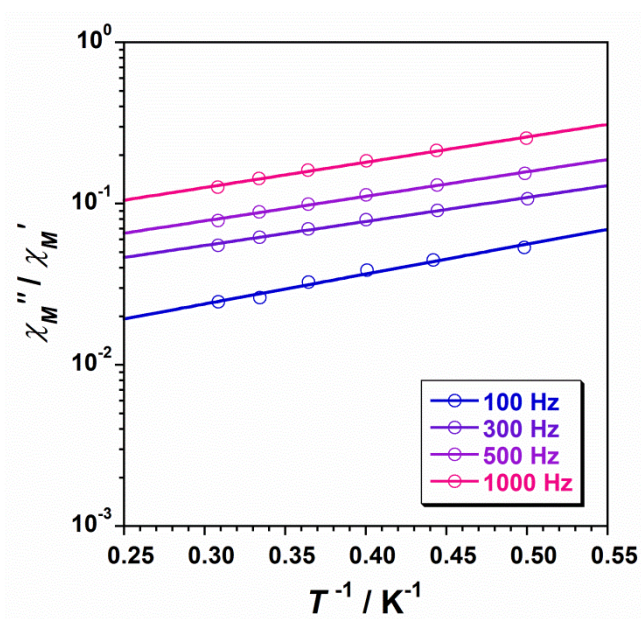
Figure S7. (a) Out-of-phase *ac* susceptibility *versus* temperature plot (χ''_M *vs.* *T*) for **1** at four different frequencies (100-1000 Hz range) under a dc field of 5000 G. (b) χ''_M/χ'_M *vs.* 1/*T* plot for **1**. The solid lines are the best-fit curves.

9
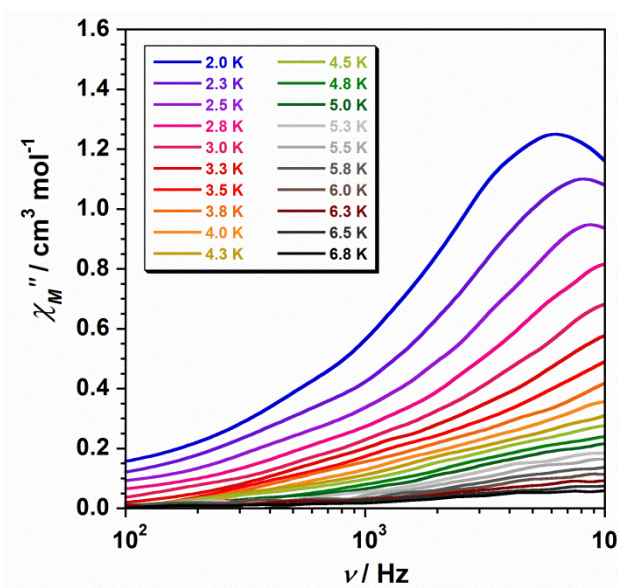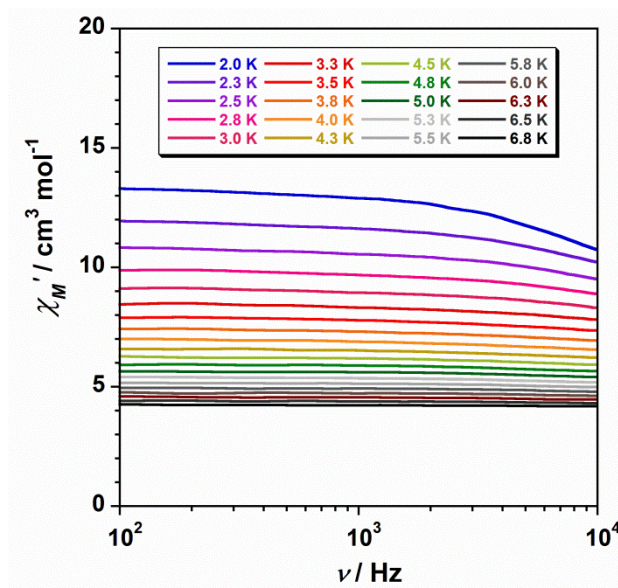
Figure S8. Frequency dependence of the in-phase (top) and out-of-phase (bottom) *ac* susceptibility signals for **1** under a dc field of 1000 G.
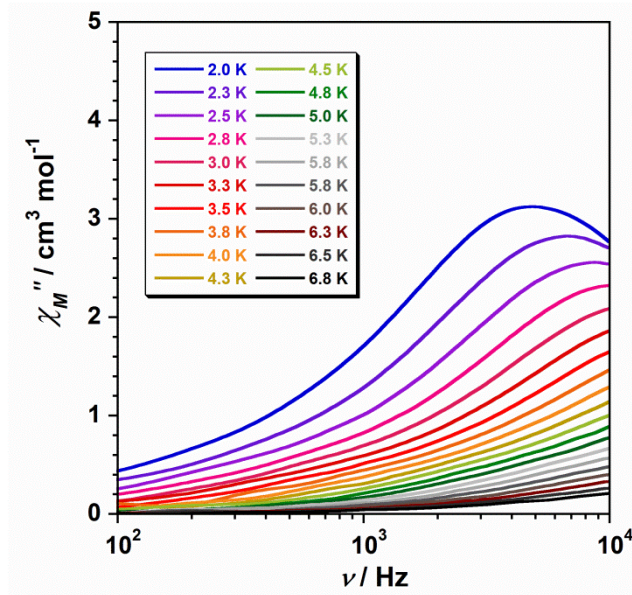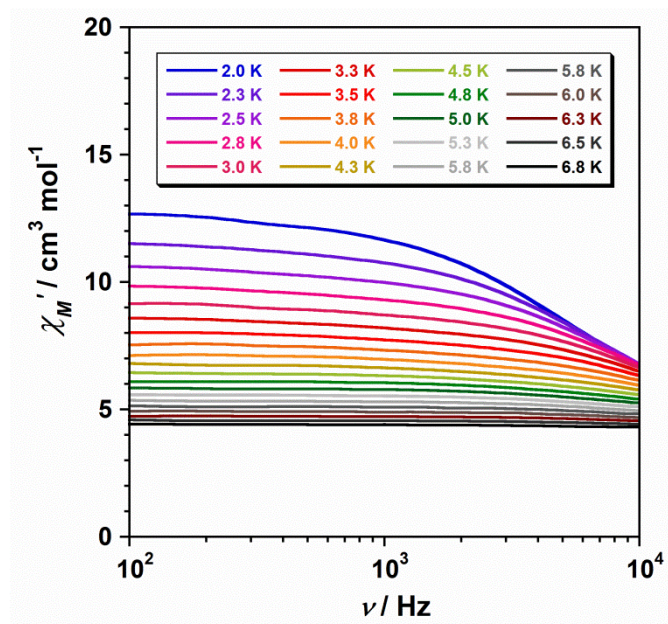
Figure S9. Frequency dependence of the in-phase (top) and out-of phase (bottom) *ac* susceptibility signals for **1** under a dc field of 2500 G.
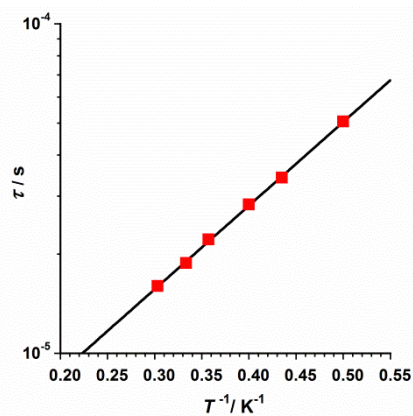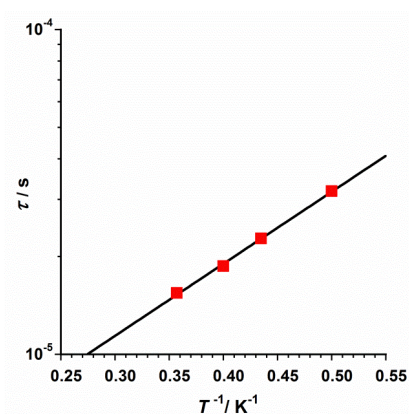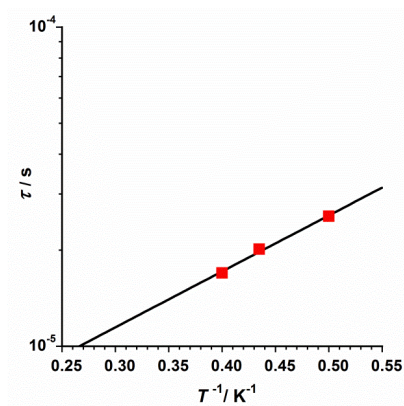
11

Figure S10. Arrhenius best-fit plots for **1** obtained by using the $\tau = \tau_o \exp(E^{\#}/k_BT)$ equation [where τ_o is the pre-exponential factor, τ is the relaxation time, $E^{\#}$ is the barrier to relaxation of the magnetisation and k_B is the Boltzmann constant] and the data from the *ac* measurements of the 1000 (top), 2500 (middle) and 5000 G (bottom) magnetic fields.

Table S2. Values of $E^{\#}$ and τ_0 obtained from different dc applied magnetic fields (H_{dc}) and equations (a and b) for **1**.

H_{dc} / G	$E^{\#}$ (K/cm^{-1}) [a]	τ_0 (x 10^{-6}) [a] / s	$E^{\#}$ (K/cm^{-1}) [b]	τ_0 (x 10^{-6}) [b] / s
1000	3.50 / 2.43	2.02	4.03 / 2.80	3.42
2500	3.70 / 2.57	5.66	5.00 / 3.48	2.68
5000	3.81 / 2.65	7.05	5.84 / 4.06	2.72

[a] Values obtained from the $\chi_M''/\chi_M' = 2\pi\nu\tau_o\exp(E^{\#}/k_BT)$ equation

[b] Values obtained from the $\tau = \tau_o\exp(E^{\#}/k_BT)$ equation

13

Article 8.

Synthesis and characterisation of a novel ferrimagnetic chain based on copper(II) and rhenium(IV)

Full paper/Mémoire

Synthesis and characterisation of a novel ferrimagnetic chain based on copper(II) and rhenium(IV)

Synthèse et caractérisation d'une nouvelle chaîne ferrimagnétique à base de cuivre(II) et de rhénium(IV)

Carlos Rojas-Dotti, Adrián Sanchis-Perucho, Marta Orts-Arroyo, Francesc Lloret, José Martínez-Lillo[*]

Instituto de Ciencia Molecular (ICMol)/Departamento de Química Inorgànica, Universitat de València, c/Catedrático José Beltrán 2, Paterna, Valencia, 46980, Spain

A B S T R A C T

A novel one-dimensional copper(II)—rhenium(IV) coordination polymer of formula $\{[Re^{IV}Br_4(\mu\text{-}ox)Cu^{II}(pyim)_2]\cdot MeCN\}_n$ (**1**) [ox = oxalate anion, pyim = 2-(2′-pyridyl)imidazole] has been prepared and characterised. Powder X-ray diffraction measurements on a sample of **1** support the purity of the bulk sample, whereas single-crystal X-ray diffraction shows that **1** crystallises in the orthorhombic system with space group *Pbca*. The crystal structure of **1** is made up of $[Cu^{II}(pyim)_2]^{2+}$ cations and $[ReBr_4(ox)]^{2-}$ anions linked through bridging bromide and oxalate groups, which generate alternating Cu^{II} and Re^{IV} chains. Variable-temperature magnetic susceptibility measurements performed on **1** reveal an antiferromagnetic coupling between the Cu^{II} and Re^{IV} ions; at lower temperatures, this interaction leads to the occurrence of ferrimagnetic behaviour in **1**. Compound **1** is the first ferrimagnetic compound obtained with the $[ReBr_4(ox)]^{2-}$ precursor.

© 2019 Académie des sciences. Published by Elsevier Masson SAS. All rights reserved.

R É S U M É

Un nouveau polymère de coordination unidimensionnel à base de cuivre(II) et de rhénium(IV), de formule $\{[Re^{IV}Br_4(\mu\text{-}ox)Cu^{II}(pyim)_2]\cdot MeCN\}_n$ (**1**) [ox = anion oxalate, pyim = 2-(2′-pyridyl)imidazole], a été préparé et caractérisé. Les mesures de diffraction des rayons X sur poudre ont confirmé la pureté de l'échantillon, alors que la diffraction des rayons X sur monocristal montre que **1** cristallise dans le système orthorhombique et le groupe d'espace *Pbca*. La structure du composé **1** contient des cations $[Cu^{II}(pyim)_2]^{2+}$ et anions $[ReBr_4(ox)]^{2-}$, lesquels sont connectés par des groupes bromure et oxalate, générant des chaînes de Cu^{II} et Re^{IV} alternés. La susceptibilité magnétique dc de **1** révèle un couplage antiferromagnétique entre ions Cu^{II} et Re^{IV}, mais aussi un comportement typique d'une chaîne ferrimagnétique. **1** est le premier composé ferromagnétique obtenu avec le précurseur $[ReBr_4(ox)]^{2-}$.

© 2019 Académie des sciences. Published by Elsevier Masson SAS. All rights reserved.

---

* Corresponding author.
   E-mail address: f.jose.martinez@uv.es (J. Martínez-Lillo).

1. Introduction

The first one-dimensional systems displaying ferrimagnetic behaviour were designed, prepared and investigated during the decade of the 1980s [1—9], and they certainly helped to stimulate progress in the field of molecular magnetism [10]. Most of these systems were mainly based on Cu^{II} and Mn^{II} metal ions [1—9], although subsequent studies incorporated also organic radicals [11,12].

The magnetic behaviour of ferrimagnetic chains is governed, at least in part, because the antiferromagnetic interaction between distinct spin carriers cannot completely cancel the alternating magnetic moments, thus inducing a short-range magnetic order [11]. Hence, to get this type of systems, it seems a good strategy to make use of the combination of couples of paramagnetic 3d and 5d metal ions exhibiting different magnetic spins.

In this way, in 1999, it was reported the first ferrimagnetic chain based on Cu^{II} (3d^9 ion with $S = 1/2$) and Re^{IV} (5d^3 ion with $S = 3/2$), which was obtained with the [ReCl$_4$(ox)]$^{2-}$ metalloligand (ox = oxalate anion), thus demonstrating that the choice of this pair of 3d/5d ions was a promising synthetic route to get ferrimagnetic systems [13]. Indeed, four studies dealing with ferrimagnetic chains based on Cu^{II} and Re^{IV} were later reported [14—17], by using the building block [ReCl$_4$(ox)]$^{2-}$ and as terminal ligands towards the Cu^{II} ion the organic macrocycles *N-dl*-5,7,7,12,14,14-hexamethyl-1,4,8,11-tetraazacyclotetradeca-4,11-diene [14] and *N-meso*-5,12-Me$_2$-7,14-Et$_2$-[14]-4,11-dieneN$_4$ [15,17], or the 2-(2′-pyridyl)imidazole ligand [16]. In all cases, the alternating Cu^{II} and Re^{IV} ions exhibit antiferromagnetic coupling between them and the thus obtained chains behave as ferrimagnetic compounds at very low temperatures [13—17].

More recently, the bromo derivative [ReBr$_4$(ox)]$^{2-}$ metalloligand has been studied and used to prepare polynuclear complexes with paramagnetic 3d and 4f ions [18—23], some of them behaving as single-molecule magnet [20]. However, no ferrimagnetic chain containing the [ReBr$_4$(ox)]$^{2-}$ precursor has been reported so far.

As a continuation of our investigation on the magnetic properties of rhenium(IV)-based compounds, we report herein the synthesis and magnetostructural characterisation of a novel copper(II)—rhenium(IV) compound of formula {[Re^{IV}Br$_4$(µ-ox)Cu^{II}(pyim)$_2$]·MeCN}$_n$ (**1**) [ox = oxalate anion, pyim = 2-(2′-pyridyl)imidazole]. Compound **1** is the third reported copper(II)—rhenium(IV) complex obtained with the [ReBr$_4$(ox)]$^{2-}$ precursor and the first [ReBr$_4$(ox)]$^{2-}$-containing compound to exhibit magnetic behaviour typical of ferrimagnetic chain.

2. Experimental section

2.1. Materials

All manipulations were performed under aerobic conditions, using chemicals as received from Sigma—Aldrich. Type 4 molecular sieves were used to dry the CH$_3$CN and CH$_3$NO$_2$ solvents before use. The precursor (NBu$_4$)$_2$[ReBr$_4$(ox)] was prepared following the synthetic method described in the literature [18,23].

2.2. Synthesis

2.2.1. {[ReBr$_4$(µ-ox)Cu(pyim)$_2$]·MeCN}$_n$ (**1**)

(NBu$_4$)$_2$[ReBr$_4$(ox)] (53.9 mg, 0.05 mmol) was dissolved in 20 mL of a CH$_3$NO$_2$/CH$_3$CN (4:1, v/v) mixture and was added dropwise to a solution of Cu(NO$_3$)$_2$·3H$_2$O (12.1 mg, 0.05 mmol) and 2-(2′-pyridyl)imidazole (14.5 mg, 0.10 mmol) dissolved in the same solvent mixture (20 mL). The resulting pale green solution was left to evaporate at room temperature. Dark green crystals of **1** were obtained in 2 weeks and were suitable for X-ray diffraction (XRD) studies. Yield: ca. 60%. Found: C, 24.4; H, 1.6; N, 9.4. Calcd for C$_{20}$H$_{17}$N$_7$O$_4$Br$_4$CuRe (**1**): C, 24.3; H, 1.7; N, 9.9%. X-ray microanalysis gave Re/Cu and Re/Br molar ratios of 1:1 and 1:4, respectively. IR peaks (KBr pellets/cm^{-1}): 3358 (m), 3129 (m), 2930 (w), 1704 (vs), 1651 (s), 1619 (m), 1570 (m), 1549 (m), 1500 (m), 1475 (s), 1404 (w), 1366 (s), 1300 (w), 1161 (m), 1098 (m), 1020 (w), 970 (w), 931 (w), 890 (w), 800 (m), 786 (m), 747 (m), 700 (m), 659 (w), 542 (m), 460 (w).

2.3. Physical measurements

Elemental analysis (C, H, N) were performed using a CE Instruments EA 1110 CHNS analyser. Infrared spectra were recorded using a Thermo-Nicolet 6700 FT-IR spectrophotometer in the 4000—400 cm^{-1} region. The Re/Cu and Re/Br molar ratios were analysed using a Philips XL-30 scanning electron microscope equipped with a system of X-ray microanalysis from the Central Service for the Support to Experimental Research at the University of Valencia. Magnetic susceptibility measurements of **1** were carried out with a Quantum Design SQUID magnetometer in the temperature range 1.9—300 K and under an applied magnetic field of 0.1 T. All of the experimental magnetic data were corrected for the diamagnetic contributions of the constituent atoms in **1**, through the Pascal's constants [24], and also for the sample holder.

2.4. Crystallographic data collection and structure determination

Powder XRD measurements were performed using a PANalytical Empyrean diffractometer with a hybrid monochromator (CuK$_{\alpha}$1 radiation), a PIXcel detector and a capillary sample holder. XRD data of a single crystal of **1**, with dimensions 0.42 × 0.18 × 0.15, were collected using a Bruker D8 Venture diffractometer with PHOTON II detector and using monochromatized MoK$_{\alpha}$ radiation (λ = 0.71073 Å). The structure was solved by standard direct methods and subsequently completed by Fourier recycling using SHELXTL [25—28]. The final full-matrix least-squares refinements on F^2, minimising the function $\Sigma w(|F_o| - |F_c|)^2$, reached convergence with values of the discrepancy indices given in Table 1. All non-hydrogen atoms were refined anisotropically. All hydrogen atoms of the MeCN molecule were set in calculated positions and refined as riding atoms. Graphical manipulations were performed using DIAMOND [29]. Main interatomic bond lengths and angles for **1** are given in Table 2. CCDC 1885666 contains the supplementary crystallographic data for compound **1**.

Table 1
Crystal data and structure refinement for {[ReBr$_4$(μ-ox)Cu(pyim)$_2$]·MeCN}$_n$ (**1**).

CCDC	1885666
Formula	C$_{20}$H$_{17}$Br$_4$N$_7$O$_4$CuRe
Formula weight	988.8
Crystal system	Orthorhombic
Space group	*Pbca*
Z	8
a (Å)	18.977(4)
b (Å)	14.282(3)
c (Å)	19.809(5)
α (°)	90
β (°)	90
γ (°)	90
V (Å^3)	5369(2)
D$_c$ (g cm^{-3})	2.449
F(000)	3696
μ (mm^{-1})	11.293
Goodness-of-fit on F^2	1.415
R$_1$ [I > 2σ(I)][a]	0.0831
wR$_2$[b,c]	0.1958

[a] $R_1 = \Sigma ||F_o| - |F_c||/\Sigma|F_o|$.
[b] $wR_2 = \{\Sigma[w(F_o^2 - F_c^2)^2]/[(w(F_o^2)^2)]\}^{1/2}$.
[c] $w = 1/[\sigma^2(F_o^2) + (aP)^2 + bP]$ with $P = [F_o^2 + 2F_c^2]/3$.

Table 2
Selected bond lengths (Å) and angles (°) for **1**.

Re(1)–O(1)	2.052(1)
Re(1)–O(2)	2.057(1)
Re(1)–Br(1)	2.499(1)
Re(1)–Br(2)	2.468(1)
Re(1)–Br(3)	2.458(1)
Re(1)–Br(4)	2.491(1)
Cu(1)–O(4)	2.682(1)
Cu(1)–N(1)	1.995(1)
Cu(1)–N(2)	1.994(1)
Cu(1)–N(4)	2.056(1)
Cu(1)–N(5)	1.941(1)
O(1)–Re(1)–O(2)	78.9(4)
O(1)–Re(1)–Br(2)	92.4(3)
O(2)–Re(1)–Br(2)	171.1(3)
O(1)–Re(1)–Br(3)	172.7(3)
O(2)–Re(1)–Br(3)	93.8(3)
Br(2)–Re(1)–Br(3)	94.9(1)
O(1)–Re(1)–Br(4)	87.5(3)
O(2)–Re(1)–Br(4)	88.5(3)
Br(2)–Re(1)–Br(4)	93.2(1)
Br(3)–Re(1)–Br(4)	92.1(1)
O(1)–Re(1)–Br(1)	89.4(1)
O(2)–Re(1)–Br(1)	85.8(3)
Br(2)–Re(1)–Br(1)	92.2(1)
Br(3)–Re(1)–Br(1)	90.3(1)
Br(4)–Re(1)–Br(1)	173.9(1)
N(5)–Cu(1)–N(2)	99.3(5)
N(5)–Cu(1)–N(1)	166.4(5)
N(2)–Cu(1)–N(1)	83.1(5)
N(5)–Cu(1)–N(4)	82.0(5)
N(2)–Cu(1)–N(4)	157.8(5)
N(1)–Cu(1)–N(4)	100.8(5)
C(3)–N(1)–Cu(1)	132.9(1)
C(7)–N(1)–Cu(1)	113.3(10)
C(8)–N(2)–Cu(1)	110.0(10)
C(10)–N(2)–Cu(1)	145.7(12)
C(11)–N(4)–Cu(1)	126.8(11)
C(15)–N(4)–Cu(1)	113.0(11)
C(16)–N(5)–Cu(1)	111.4(10)
C(18)–N(5)–Cu(1)	140.2(11)
O(4)–C(1)–O(1)	122.8(14)

3. Results and discussion

3.1. Crystal structure of {[ReBr$_4$(μ-ox)Cu(pyim)$_2$]·MeCN}$_n$ (**1**)

Compound **1** crystallises in the orthorhombic system with space group *Pbca* (Table 1). The crystal structure is made up of [Cu(pyim)$_2$]$^{2+}$ cations and [ReBr$_4$(ox)]$^{2-}$ anions, which are mainly linked through alternating oxalato and bromo bridges generating a Cu^{II}–Re^{IV} chain of repeating [ReBr$_4$(μ-ox)Cu(pyim)$_2$] units. A MeCN molecule along with a dinuclear [ReBr$_4$(μ-ox)Cu(pyim)$_2$] complex forms the asymmetric unit in **1**. Although selected bonds lengths and angles are listed in Table 2, a perspective drawing showing the metal-based ions in **1** is given in Fig. 1.

There exist a couple of significant structural differences between **1** and the previously reported [ReCl$_4$(μ-ox)Cu(pyim)$_2$] (**2**) and [ReBr$_4$(μ-ox)Cu(bpy)$_2$] (**3**) compounds that we would like to point out [16,19]. Compounds **2** and **3** crystallise in the monoclinic system with space group *P*2$_1$/*n*, but besides that, **2** and **3** do not contain solvent molecules of crystallisation. Remarkably, the coordination of the oxalate group to the Cu^{II} ion is through the O(1) atom in **2**, whereas it is by means of the O(4) atom in **1** and **3**. Only in **3** there exist short halogen···halogen contacts connecting the adjacent Cu^{II}–Re^{IV} chains [19].

In **1**, rhenium(IV) ion is six-coordinate by four bromide anions and two oxygen atoms in a distorted octahedral geometry. The main cause of such a distortion is the reduced bite angle of the oxalate group [the value of the O(1)–Re(1)–O(2) angle is 78.9(1)°], which exhibits bidentate and monodentate bridging modes towards the Re^{IV} and Cu^{II} ions, respectively. The O(1), O(2), Br(2) and Br(3) set of atoms constitute the best equatorial plane around the Re^{IV} ion, the largest deviation from planarity being 0.070 Å for O(2). The average value of the Re^{IV}–Br [2.479(1) Å] and Re^{IV}–O [2.055(1) Å] bond lengths, and also the bond angles,
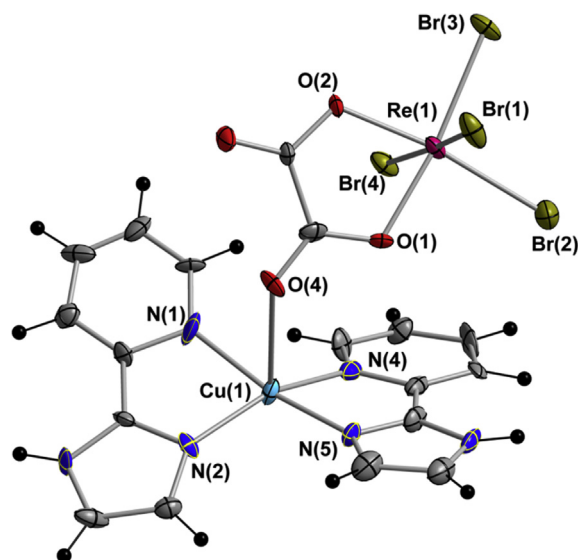
Fig. 1. Molecular structure of the dinuclear [Re^{IV}Br$_4$(μ-ox)Cu^{II}(pyim)$_2$] unit showing the atom numbering of the Cu^{II} and Re^{IV} metal ions along with those of their chromophores in compound **1**. Thermal ellipsoids are drawn at the 50% probability level.

found in **1** are in agreement with those previously reported for complexes containing the anionic $[ReBr_4(ox)]^{2-}$ entity [18–22].

Each Cu^{II} ion in **1** is mainly five-coordinate and bonded to four nitrogen atoms from two pyim molecules and an oxygen atom from the oxalate group of the closer $[ReBr_4(ox)]^{2-}$ anion, in a distorted square pyramidal geometry. The Cu^{II}–O bond length is 2.682(1) Å and the average value of the Cu^{II}–N bond lengths is 1.997(1) Å. Nevertheless, having into account the Br(1a) ion that would occupy a sixth position generating the one-dimensional motif [the Cu(1)···Br(1a) distance is ca. 3.23 Å; (a) = x, 1/2 − y, 1/2 + z], the Cu^{II} ion could also be seen in a very distorted octahedral environment, as previously described in similar chloro-derivative Cu^{II}–Re^{IV} systems [13,16].

The intramolecular Cu^{II}···Re^{IV} distance through the oxalato bridge is 5.457(1) Å, whereas this intermetallic distance through the bromo bridge is somewhat shorter [Cu(1a)···Re(1) distance of 5.263(1) Å; (a) = x, 1/2 − y, 1/2 + z]. The average C–C and C–N bond length values of the pyim ligand show the expected values for this molecule when coordinated to a metal ion [30–67].

In the crystal packing of **1**, the $[ReBr_4(\mu\text{-}ox)Cu(pyim)_2]$ units are arranged helicoidally forming chains that grow along the *c*-axis direction (Fig. 2). These Cu^{II}–Re^{IV} chains are extended to layers, on the crystallographic *bc* plane (Fig. 3), by means of bifurcated hydrogen-bonding interactions between oxalate and N–H groups of coordinated pyim ligands [the N(6)···O(3b) and N(6)···O(4b) distances are 2.87(2) and 2.93(2) Å, respectively; (b) = 3/2 − x, 1 − y, −1/2 + z]. Likewise, π···π type interactions between the aromatic rings of neighbouring pyim ligands connect the Cu^{II}–Re^{IV} chains along the crystallographic *ab* plane (the shortest intercentroid distance being approximately 3.42 Å). The value of the shortest intermolecular Cu^{II}···Re^{IV} distance between adjacent chains is 8.822(2) Å [Cu(1)··· Re(1c), (c) = 3/2 − x, −y, −1/2 + z], whereas the shortest intermolecular Cu^{II}···Cu^{II} and Re^{IV}···Re^{IV} distances are 7.385(3) and 9.161(2) Å [Cu(1)···Cu(1d) and Re(1)···Re(1d), (d) = 3/2 − x, −1/2 + y, z], respectively.

In addition, weak C–H···Br interactions that vary in the range 3.72–3.78 Å link parallel planes and contribute to stabilising the supramolecular structure of **1**.

Finally, the phase purity of the bulk sample of **1** was confirmed through powder XRD patterns (Fig. 4).

3.2. Magnetic properties

Direct current magnetic susceptibility measurements were carried out on a microcrystalline sample of **1** in the 1.9–300 K temperature range and under an external magnetic field of 0.1 T. The $\chi_M T$ versus T plot (χ_M being the molar magnetic susceptibility per $Cu^{II}Re^{IV}$ pair) of **1** is shown in Fig. 5. At room temperature the $\chi_M T$ value is 1.96 cm^3 mol^{-1} K, which is very close to that expected for a pair of uncoupled Cu^{II} (3d^9, $S = 1/2$ with $g = 2.2$) and Re^{IV} (5d^3, $S = 3/2$ with $g = 1.8$) ions [14–18]. Upon cooling, the $\chi_M T$ value decreases slowly with decreasing temperature, more abruptly at approximately 50 K, reaching a minimum value of 0.50 cm^3 mol^{-1} K at 2.0 K. Then, the $\chi_M T$ value increases giving a final value of 0.58 cm^3 mol^{-1} K at 1.9 K. No maximum of the magnetic susceptibility is detected in the χ_M versus T plot. The magnetic behaviour observed at higher temperatures would be because of the large zero-field splitting of the Re^{IV} ion, together with antiferromagnetic interaction between the Re^{IV} and Cu^{II} centres, whereas the final increases in the $\chi_M T$ value at very low temperatures would account for a ferrimagnetic behaviour for **1** [13–16].

The field dependence of the molar magnetisation (*M*) plot for **1** at 2.0 K is given in Fig. 6, which exhibits a continuous increase in *M* with the applied magnetic field and neither saturation nor hysteresis loop was observed. The lack of saturation of *M* at this temperature is likely because the applied magnetic field would overcome the weak intrachain antiferromagnetic interaction [13,16]. The *M* versus *H* plot also supports the presence of antiferromagnetic interactions in **1**, given that the maximum value of *M* per $Cu^{II}Re^{IV}$ pair (ca. 1.19 μ$_B$) is smaller than that of the mononuclear $[ReBr_4(ox)]^{2-}$ complex isolated as its tetra-*n*-butylammonium salt (ca. 1.50 μ$_B$) [23].

$$\chi_{//} = \frac{N\beta^2}{4kT}\left(g_{Cu_{//}}^2 + g_{Re_{//}}^2 \frac{1 + 9\exp(-D/kT)}{1 + \exp(-D/kT)}\right)F_{J_{//}} \qquad (1)$$

$$\chi_{\perp} = \frac{N\beta^2}{4kT}\left(g_{Cu\perp}^2 + g_{Re\perp}^2 \frac{4 + 6kT/D(1 - \exp(-D/kT))}{1 + \exp(-D/kT)}\right)F_{J\perp} \qquad (2)$$
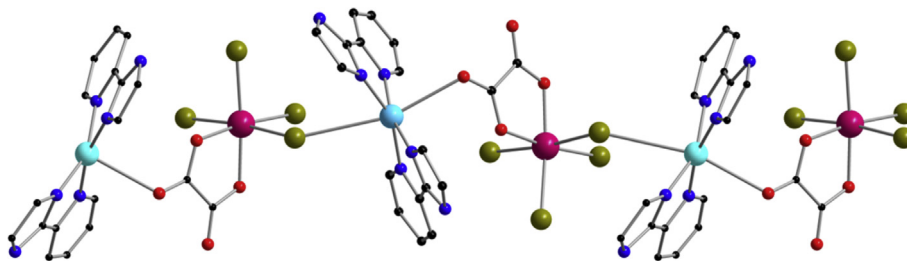
where

Fig. 2. Perspective view showing the one-dimensional motif of **1** along the *a*-axis direction. Hydrogen atoms and MeCN molecules have been omitted for clarity. Colour code: pink, Re; pale blue, Cu; green, Br; red, O; blue, N; black, C.
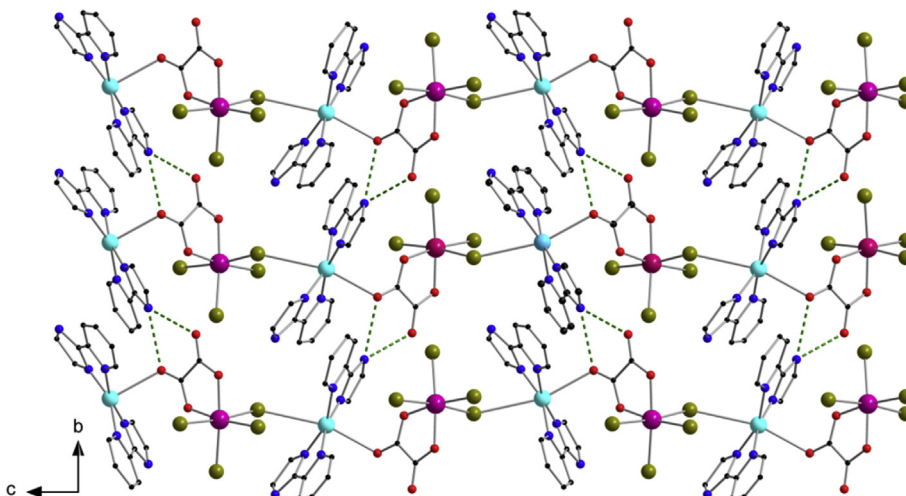
Fig. 3. View along the crystallographic *a* axis of a fragment of the crystal packing of **1** showing the arrangement of $[Cu(pyim)_2]^{2+}$ cations and $[ReBr_4(ox)]^{2-}$ anions linked through oxalato and bromo bridges. Hydrogen atoms and MeCN molecules have been omitted for clarity. Colour code: pink, Re; pale blue, Cu; green, Br; red, O; blue, N; black, C.

$$F_{J_{//}} = \frac{\exp(J_+/kT) + R^2 \exp(-J_+/2kT)}{(1+R^2)\cosh(J_-/2kT)};$$

$$F_{J_\perp} = \frac{2kT}{j} \tan gh\left(\frac{j}{4kT}\right) + \frac{1}{2}\sec h^2\left(\frac{j}{4kT}\right);$$

$$J_\pm = \frac{J\pm j}{2}; \quad g_\pm = \frac{g_{Re}\pm g_{Cu}}{2}; \quad R = \frac{g_-}{g_+}$$

Taking into account both the structural description of **1** (see above) and the presence of a minimum at very low temperature in the $\chi_M T$ versus T plot, we can consider that compound **1** behaves as a ferrimagnetic chain [13–16]. Thus, to analyse the magnetic properties of **1**, the experimental magnetic susceptibility data have been treated through Eqs 1 and 2 and the following spin Hamiltonian (Eq 3):

of **1** in the high temperature region may be described by two contributions: one from the $^4A_{2g}$ term of the Re^{IV} ion and the other from the uncoupled Cu^{II} ion. In the low temperature region it would be described as a chain of $S_{Re} = S_{eff} = 1/2$ with different local g_{Cu} and g_{Re} Landé factors [13–16].

To avoid overparameterisation, we have also assumed that $g = g_{//} = g_\perp$ for the Cu^{II} and Re^{IV} ions. This approach has previously been used for fitting the magnetic data of similar heterometallic Cu^{II}Re^{IV} chains [13–16,58]. A least-squares fit of the experimental data in the 1.9–300 K temperature range afforded the following parameters for **1**: $J = -6.3$, $j = -5.4$, $g_{Cu} = 2.25$, $g_{Re} = 1.87$, and $|D_{Re}| = 64.2$ cm^{-1} with $R = 6.4 \times 1\text{-}0^{-5}$ {R being the agreement factor defined as $\Sigma i [(\chi_M T)_{obs}(i) - (\chi_M T)_{calc}(i)]^2/\Sigma i[(\chi_M T)_{obs}(i)]^2$}. As shown in Fig. 5, the theoretical curve for **1** (red solid line) matches quite well with the experimental magnetic data in the

$$\widehat{H} = \sum_i \left(\begin{array}{l} -J\widehat{S}_{2i-1}^z \cdot \widehat{S}_{2i}^z - j\widehat{S}_{2i}^z \cdot \widehat{S}_{2i-1}^z + g_{Cu//}\beta\widehat{S}_{2i-1}^z H^z + g_{Re//}\beta\widehat{S}_{2i}^z H^z \\ +g_{Cu\perp}\beta\left(\widehat{S}_{2i-1}^x H^x + \widehat{S}_{2i-1}^y H^y\right) + g_{Re\perp}\beta\left(\widehat{S}_{2i}^x H^x + \widehat{S}_{2i}^y H^y\right) + D_{Re}\left[\left(\widehat{S}_{2i}^z\right)^2 - 5/4\right] \end{array} \right) \tag{3}$$

The approach that we have used to fit the experimental data consists in assuming that the magnetic susceptibility is given by that of the $^4A_{2g}$ term (ground state for a d^3 ion in an octahedral environment), including the zero-field splitting, and modulated by a factor predicted from the Ising model of the magnetic exchange with the parameters J and j that would be assigned to the magnetic exchange pathways of the alternating oxalato and bromo bridges, respectively (and defined as indicated in Eqs 1 and 2) [16,17]. This is possible because the magnetic susceptibility

studied temperature range. The values of the J and j magnetic exchanges that we have obtained by this approach are referred to an $S_{eff} = 1/2$ and aiming at comparing them with the D_{Re} value (which is referred to a real $S_{Re} = 3/2$), they should be reduced by a factor of about 3/5 ($3J/5 = -3.8$ cm^{-1} and $3j/5 = -3.2$ cm^{-1}), as previously reported [13,16,58]. The calculated values for the g_{Cu}, g_{Re} and D_{Re} parameters are in agreement with those previously computed for similar one-dimensional Cu^{II}Re^{IV} systems [13–16,58]. The calculated values of the J and j magnetic
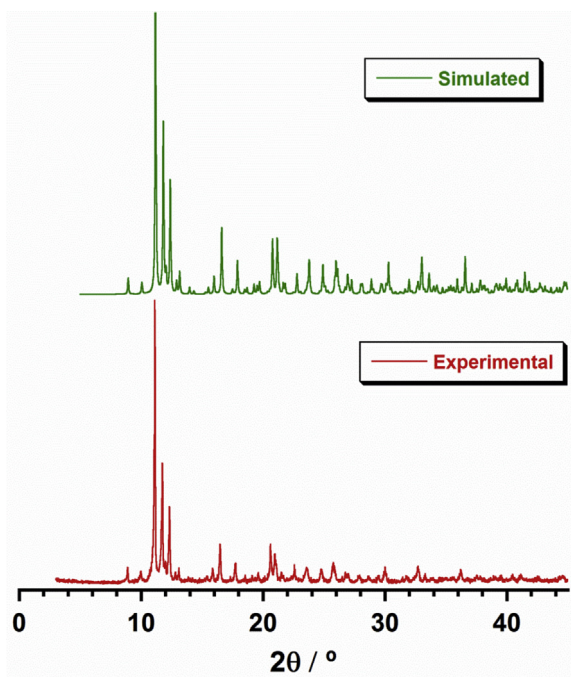
Fig. 4. Plot of the simulated (top) and experimental XRD (bottom) patterns profile in the 2θ/° range 0–45° for **1**.

exchanges support antiferromagnetic interactions between the Re^{IV} and Cu^{II} centres across the two magnetic pathways, that is, through the alternating oxalato and bromo bridges in **1**. According to the orthogonality of the involved magnetic orbitals [e_g for Cu^{II} and t_{2g} for Re^{IV}], a priori, a ferromagnetic exchange would be expected. However, this orthogonality is broken because of the asymmetry of the bridges and the distorted coordination geometry of the Cu(II) ion, resulting in a very poor overlap of the magnetic
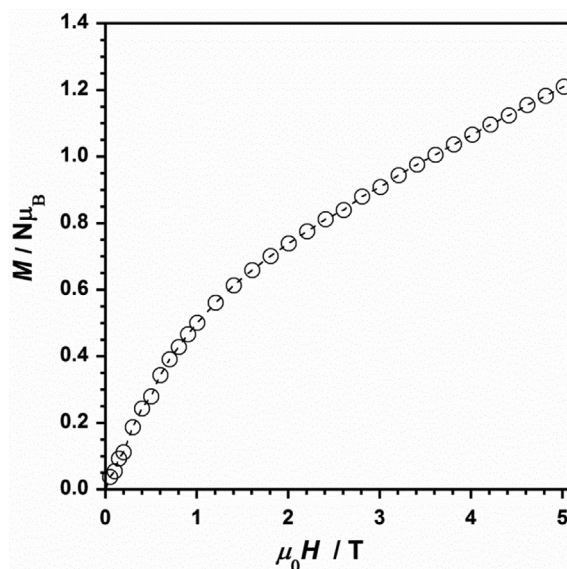
Fig. 6. Plot of the variable-field magnetisation versus applied field at 2.0 K for **1** (see text).

orbitals and, hence, in a weak antiferromagnetic exchange between these metal ions.

Despite showing a chain motif in its crystal structure, compound **3** behaves magnetically as a tetranuclear [$Re^{IV}_2Cu^{II}_2$] species [19]. Compound **3** does not exhibit behaviour of ferrimagnetic chain given that contains in their crystal lattice significant Re–Br···Br–Re interactions (Br···Br separation of ca. 4.8 Å) between adjacent Re^{IV}-Cu^{II} chains. These intermolecular interactions in the rhenium(IV) chemistry are usually very strong and can easily overcome the intramolecular ones, accounting for the magnetic behaviour observed in the $\chi_M T$ versus T variation [68]. Nevertheless, this fact has not been reported for ferrimagnetic chains based on other 5d metal ions [69].

As far as we know, compound **1** is the first system containing the [ReBr$_4$(ox)]$^{2-}$ metalloligand to exhibit magnetic behaviour of ferrimagnetic chain and, therefore, any comparison would be precluded. Nonetheless, we have tried to compare our results with those obtained for the previously studied $Cu^{II}Re^{IV}$ chains based on the chloro-derivative [ReCl$_4$(ox)]$^{2-}$ complex [13–17]. Thus, we have plotted the J values versus the Re^{IV}···Cu^{II} distances and the Re–X–Cu angle (°) (X = Cl and Br) for ferrimagnetic $Cu^{II}Re^{IV}$ chains (Table 3). As shown in Fig. 7, there exists a certain trend in these systems: when the Re···Cu separation shortens and the Re–X–Cu angle decreases, the value of the antiferromagnetic coupling also decreases (red solid line in Fig. 7). Although we cannot talk about a magnetostructural correlation, given that more data of $Cu^{II}Re^{IV}$ systems would be needed to complete the study in detail, this trend could help at least to design new ferrimagnetic $Cu^{II}Re^{IV}$ compounds and similar systems, having into account the high magnetic anisotropy that Re^{IV} ion exhibits [70–75].
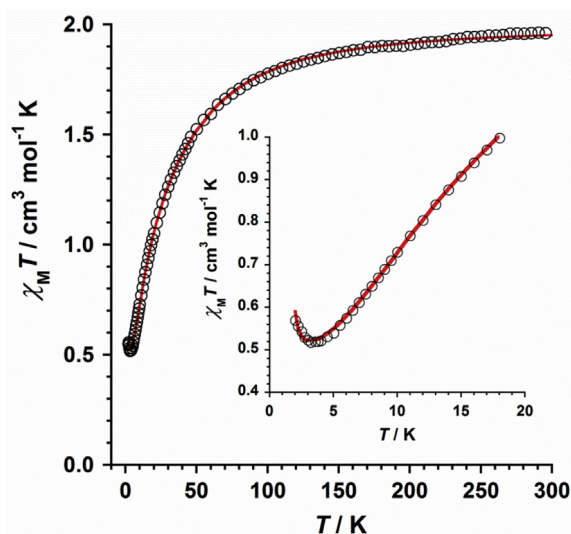

Fig. 5. Thermal variation of the $\chi_M T$ (o) product for **1**. The solid line is the calculated curve and the inset shows a detail of the low temperature range (see text).

Table 3
Selected magnetostructural parameters for ferrimagnetic Re^{IV}–Cu^{II} chains.[a]

Compound	Space group	d(Re⋯M) (Å)	J, j (cm^{-1})	|D| (cm^{-1})	g_{Re}	g_{Cu}	Ref.
[ReCl$_4$(μ-ox)Cu(bpy)$_2$]	P2$_1$/n	4.798, 4.658	−25.0, −13.0	53.0	1.84	2.17	[13]
[ReCl$_4$(μ$_3$-ox)Cu(L$_1$)]	P2$_1$	5.568, 5.870	−3.4, NA	49.6	1.91	2.27	[14]
[ReCl$_4$(μ-ox)Cu(L$_2$)]	P$\bar{1}$	4.684, 4.718	−18.1, −0.7	63.0	1.89	2.20	[15]
[ReCl$_4$(μ-ox)Cu(pyim)$_2$]	P2$_1$/n	4.544, 4.805	−7.8, −6.0	54.8	1.80	2.29	[16]
[ReCl$_4$(μ-ox)Cu(L$_2$)]	P2$_1$/c	6.030, 4.769	−14.2, −8.7	54.5	1.81	2.24	[17]
[ReBr$_4$(μ-ox)Cu(pyim)$_2$]	Pbca	5.457, 5.263	−6.3, −5.4	64.2	1.87	2.25	This work

[a] bpy = 2,2′-bipyridine; pyim = 2-(2′-pyridyl)imidazole; L$_1$ = N-dl-5,7,7,12,14,14-hexamethyl-1,4,8,11-tetraazacyclotetradeca-4,11-diene; L$_2$ = N-meso-5,12-Me$_2$-7,14-Et$_2$-[14]-4,11-dieneN$_4$; NA = not available.
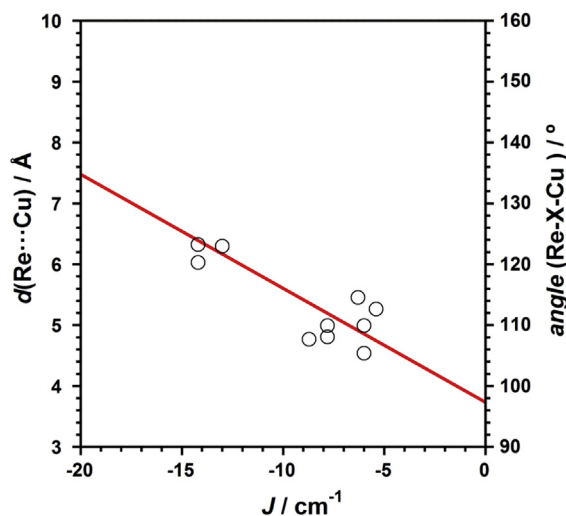
Fig. 7. Dependence of the J parameter (cm^{-1}) on the Re^{IV}⋯Cu^{II} distance (Å) and the Re−X−Cu angle (°) for ferrimagnetic Cu^{II}Re^{IV} chains. The solid line represents the linear best fit.

4. Conclusions

We have reported the synthesis, characterisation and magnetic properties of a novel Cu^{II}Re^{IV} compound of formula {[Re^{IV}Br$_4$(μ-ox)Cu^{II}(pyim)$_2$]·MeCN}$_n$ (**1**) [ox = oxalate anion, pyim = 2-(2′-pyridyl)imidazole]. The analysis of the magnetic properties of **1** through variable-temperature magnetic susceptibility data revealed a magnetic behaviour typical of ferrimagnetic chain, which is consistent with its crystal structure. Remarkably, compound **1** is the first reported copper(II)−rhenium(IV) complex obtained with the [ReBr$_4$(ox)]$^{2-}$ metalloligand that exhibits such a magnetic behaviour.

In addition, by comparing our results with those reported in the literature, we have observed a trend associated with the family of ferrimagnetic Cu^{II}Re^{IV} chains, although more systems would be needed to complete a study that establishes a proper magnetotructural correlation.

Acknowledgements

Appendix A. Supplementary data

Supplementary data related to this article can be found at https://doi.org/10.1016/j.crci.2019.04.004.

References

[1] A. Gleizes, M. Verdaguer, J. Am. Chem. Soc. 103 (1981) 7373.
[2] D. Beltran, E. Escrivá, M. Drillon, J. Chem. Soc., Faraday Trans. 78 (1982) 1773.
[3] M. Verdaguer, M. Julve, A. Michalowicz, O. Kahn, Inorg. Chem. 22 (1983) 2624.
[4] A. Gleizes, M. Verdaguer, J. Am. Chem. Soc. 106 (1984) 3727.
[5] R. Georges, J. Curély, M. Drillon, J. Appl. Phys. 58 (1985) 914.
[6] E. Coronado, M. Drillon, A. Fuertes, D. Beltran, A. Mosset, J. Galy, J. Am. Chem. Soc. 108 (1986) 900.
[7] Y. Pei, O. Kahn, J. Sletten, J. Am. Chem. Soc. 108 (1986) 3143.
[8] Y. Pei, M. Verdaguer, O. Kahn, J. Sletten, J.P. Renard, J. Am. Chem. Soc. 108 (1986) 7428.
[9] Y. Pei, M. Verdaguer, O. Kahn, J. Sletten, J.P. Renard, Inorg. Chem. 26 (1987) 138.
[10] J. Ferrando-Soria, J. Vallejo, M. Castellano, J. Martínez-Lillo, E. Pardo, J. Cano, I. Castro, F. Lloret, R. Ruiz-García, M. Julve, Coord. Chem. Rev. 339 (2017) 17.
[11] A. Caneschi, D. Gatteschi, P. Rey, R. Sessoli, Inorg. Chem. 27 (1988) 1756.
[12] T. Ise, T. Ishida, D. Hashizume, F. Iwasaki, T. Nogami, Inorg. Chem. 42 (2003) 6106.
[13] R. Chiozzone, R. González, C. Kremer, G. De Munno, J. Cano, F. Lloret, M. Julve, J. Faus, Inorg. Chem. 38 (1999) 4745.
[14] A. Tomkiewicz, J. Mroziński, I. Brüdgam, F. Hartl, Eur. J. Inorg. Chem. (2005) 1787.
[15] A. Bieńko, J. Kłak, J. Mroziński, R. Kruszyński, D.C. Bieńko, R. Boča, Polyhedron 27 (2008) 2464.
[16] J. Martínez-Lillo, D. Armentano, G. De Munno, F. Lloret, M. Julve, J. Faus, Dalton Trans. (2008) 40.
[17] A. Bieńko, R. Kruszyński, D. Bieńko, Polyhedron 75 (2014) 1.
[18] R. Chiozzone, A. Cuevas, R. González, C. Kremer, D. Armentano, G. De Munno, J. Faus, Inorg. Chim. Acta 359 (2006) 2194.
[19] R. Chiozzone, R. González, C. Kremer, D. Armentano, G. De Munno, M. Julve, F. Lloret, Inorg. Chim. Acta 370 (2011) 394.
[20] J. Martínez-Lillo, T.F. Mastropietro, G. De Munno, F. Lloret, M. Julve, J. Faus, Inorg. Chem. 50 (2011) 5731.
[21] J. Martínez-Lillo, L. Cañadillas-Delgado, J. Cano, F. Lloret, M. Julve, J. Faus, Chem. Commun. 48 (2012) 9242.
[22] J. Martínez-Lillo, D. Armentano, G. De Munno, M. Julve, F. Lloret, J. Faus, Dalton Trans. 42 (2013) 1687.
[23] J. Martínez-Lillo, T.F. Mastropietro, E. Lhotel, C. Paulsen, J. Cano, G. De Munno, J. Faus, F. Lloret, M. Julve, S. Nellutla, J. Krzystek, J. Am. Chem. Soc. 135 (2013) 13737.
[24] G.A. Bain, J.F. Berry, J. Chem. Educ. 85 (2008) 532.
[25] M. Nardelli, J. Appl. Crystallogr. 28 (1995) 659.
[26] G.M. Sheldrick, Acta Crystallogr. A 64 (2008) 112.
[27] SHELXTL NT−Version 5.1 Copyright, Bruker Analytical X-ray Systems Inc., Madison, Wisconsin, USA, 1998.

[28] SHELXTL-2013/4, Bruker Analytical X-Ray Instruments, Madison, WI, 2013.
[29] DIAMOND 4.5.0, Crystal Impact GbR, CRYSTAL IMPACT, 2018.
[30] J. Carranza, C. Brennan, J. Sletten, F. Lloret, M. Julve, J. Chem. Soc., Dalton Trans. (2002) 3164.
[31] J. Carranza, C. Brennan, J. Sletten, B. Vangdal, P. Rillema, F. Lloret, M. Julve, New J. Chem. 27 (2003) 1775.
[32] G.S. Matouzenko, G. Molnar, N. Brefuel, M. Perrin, A. Bousseksou, S.A. Borshch, Chem. Mater. 15 (2003) 550.
[33] A. Morsali, A. Ramazani, M. Babaee, F. Jamali, F. Gouranlou, H. Arjmandfar, A. Yanovsky, J. Coord. Chem. 56 (2003) 455.
[34] D.-X. Zhu, Y.-Q. Lan, Y.-M. Fu, Z.-M. Su, Acta Crystallogr. E: Struct. Rep. Online 62 (2006) m3479.
[35] T.I.A. Gerber, E. Hosten, P. Mayer, Z.R. Tshentu, J. Coord. Chem. 59 (2006) 243.
[36] H. Mishra, R. Mukherjee, J. Organomet. Chem. 691 (2006) 3545.
[37] K. Pachhunga, B. Therrien, K.A. Kreisel, G.P.A. Yap, M.R. Kollipara, Polyhedron 26 (2007) 3638.
[38] G.S. Matouzenko, M. Perrin, B. Le Guennic, C. Genre, G. Molnar, A. Bousseksou, S.A. Borshch, Dalton Trans. (2007) 934.
[39] F.S. Delgado, F. Lahoz, F. Lloret, M. Julve, C. Ruiz-Perez, Cryst. Growth Des. 8 (2008) 3219.
[40] B.A. Leita, B. Moubaraki, K.S. Murray, J.P. Smith, Polyhedron 24 (2005) 2165.
[41] L. Zhang, Y.-Y. Ge, F. Peng, M. Du, Inorg. Chem. Commun. 9 (2006) 486.
[42] J. Carranza, M. Julve, J. Sletten, Inorg. Chim. Acta 361 (2008) 2499.
[43] J. Martínez-Lillo, D. Armentano, G. De Munno, J. Faus, Polyhedron 27 (2008) 1447.
[44] C. Yuste, D. Armentano, N. Marino, L. Cañadillas-Delgado, F.S. Delgado, C. Ruiz-Perez, D.P. Rillema, F. Lloret, M. Julve, Dalton Trans. (2008) 1583.
[45] Y.-Q. Lan, S.-L. Li, Y.-M. Fu, Y.-H. Xu, L. Li, Z.-M. Su, Q. Fu, Dalton Trans. (2008) 6796.
[46] J. Carranza, J. Sletten, F. Lloret, M. Julve, Polyhedron 28 (2009) 2249.
[47] J. Carranza, J. Sletten, F. Lloret, M. Julve, Inorg. Chim. Acta 362 (2009) 2636.
[48] H.-Y. Zang, Y.-Q. Lan, Z.-M. Su, G.-S. Yang, G.-J. Xu, D.-Y. Du, L. Chen, L.-K. Yan, Inorg. Chim. Acta 363 (2010) 118.
[49] T. Ghosh, S. Das, S. Pal, Polyhedron 29 (2010) 3074.
[50] O. Schott, J. Ferrando-Soria, A. Bentama, S.-E. Stiriba, J. Pasán, C. Ruiz-Pérez, M. Andruh, F. Lloret, M. Julve, Inorg. Chim. Acta 376 (2011) 358.
[51] C.-J. Li, J.-M. Lu, F. Tu, J.-Y. Chen, Y.-J. Li, Acta Crystallogr. E: Struct. Rep. Online 67 (2011) m269.

[52] G. Yuan, K.-Z. Shao, D.-Y. Du, X.-L. Wang, Z.-M. Su, Solid State Sci. 13 (2011) 1083.
[53] S. Yue, N. Li, J. Bian, T. Hou, J. Ma, Synth. Met. 162 (2012) 247.
[54] F.R. Fortea-Pérez, J. Vallejo, M. Inclán, M. Deniz, J. Pasán, E. García-España, M. Julve, J. Coord. Chem. 66 (2013) 3349.
[55] T. Hou, J. Bian, X. Yue, S. Yue, J. Ma, Inorg. Chim. Acta 15 (2013) 394.
[56] W. Hou, J. Guo, Z. Wang, Y. Xu, J. Coord. Chem. 66 (2013) 2434.
[57] G.-X. Liu, X.-F. Wang, H. Zhou, J. Solid State Chem. 199 (2013) 305.
[58] J. Martínez-Lillo, J. Kong, W.P. Barros, J. Faus, M. Julve, E.K. Brechin, Chem. Commun. 50 (2014) 5840.
[59] W. Hou, J. Guo, X. Xu, Z. Wang, D. Zhang, H. Wan, Y. Song, D. Zhu, Y. Xu, Dalton Trans. 43 (2014) 865.
[60] G. Hu, Y. Dong, X. He, H. Miao, S. Zhou, Y. Xu, Inorg. Chem. Commun. 60 (2015) 33.
[61] H. Miao, G. Hu, J. Guo, H. Wan, H. Mei, Y. Zhang, Y. Xu, Dalton Trans. 44 (2015) 694.
[62] Y.-H. Luo, B. Li, X.-Y. Yu, C.-M. Han, X.-X. Lu, H. Zhang, X. Chen, Polyhedron 85 (2015) 705.
[63] Z. Setifi, F. Setifi, B.M. Francuski, S.B. Novakovic, H. Merazig, Acta Crystallogr. E: Struct. Rep. Online 71 (2015) 346.
[64] M. López-Jorda, M. Giménez-Marques, C. Desplanches, G. Mínguez-Espallargas, M. Clemente-León, E. Coronado, Eur. J. Inorg. Chem. (2016) 2187.
[65] M.-G. Alexandru, D. Visinescu, S. Shova, W.X.C. Oliveira, F. Lloret, M. Julve, Dalton Trans. 47 (2018) 6005.
[66] M.-G. Alexandru, D. Visinescu, S. Shova, M. Andruh, F. Lloret, M. Julve, Eur. J. Inorg. Chem. 360 (2018).
[67] X.-Q. Wei, Q. Pi, F.-X. Shen, D. Shao, H.-Y. Wei, X.-Y. Wang, Dalton Trans. 47 (2018) 11873.
[68] J. Martínez-Lillo, J. Faus, F. Lloret, M. Julve, Coord. Chem. Rev. 289–290 (2015) 215.
[69] H. Zhou, K. Wu, C. Chen, R. Dong, Y. Liu, X. Shen, Eur. J. Inorg. Chem. (2017) 3946.
[70] D. Armentano, J. Martínez-Lillo, Inorg. Chim. Acta 380 (2012) 118.
[71] J. Martínez-Lillo, D. Armentano, G. De Munno, N. Marino, F. Lloret, M. Julve, J. Faus, CrystEngComm 10 (2008) 1284.
[72] J. Martínez-Lillo, A.H. Pedersen, J. Faus, M. Julve, E.K. Brechin, Cryst. Growth Des. 15 (2015) 2598.
[73] D. Armentano, J. Martínez-Lillo, RSC Adv. 5 (2015) 54936.
[74] D. Armentano, J. Martínez-Lillo, Cryst. Growth Des. 16 (2016) 1812.
[75] C.H. Woodall, G.A. Craig, A. Prescimone, M. Misek, J. Cano, J. Faus, M.R. Probert, S. Parsons, S. Moggach, J. Martínez-Lillo, M. Murrie, K.V. Kamenev, E.K. Brechin, Nat. Commun. 7 (2016) 13870.

Conclusions and Perspectives

This PhD Thesis has developed a deep research on the field of the Molecular Magnetism, specifically, on systems based on Mn(III) and Re(IV) metal ions, which present interesting magnetic properties. This research also involves the potential application in nanoscale devices of some of the obtained complexes.

In what Mn(III)-based systems concerns, six new members of the family of oxime-based [Mn$_6$] complexes have been synthesised and magnetostructurally characterized. All of these compounds are reported in three publications and display a magnetic behavior consistent with the single-molecule magnet (SMM) phenomenon. Particularly, the energy barrier value to the relaxation of the magnetization (U$_{eff}$) for the cationic compound obtained using dmf as a coordinating solvent, and reported in the first work included in this memory, is the highest reported U$_{eff}$ so far for cationic oxime-based [Mn$_6$]$^{2+}$ systems. Furthermore, due to their cationic character, these singular SMMs could be used as suitable building blocks for preparing new magnetic materials, just by replacing the anion by another anionic species exhibiting an additional functionality, namely, conductivity or luminescence. Additionally, in the second work present here, the crystal structure of the first example of Mn-based complex containing 5-phenyltetrazole was reported.

To complete this work, and also as the highlight of the Section A of this Thesis, the 3-(acetylthio)propionic and 6-(acetylthio)hexanoic derivatized [Mn$_6$] SMMs have been reported. These structures have also been the first reported complexes containing the 3-(acetylthio)propionate (3-atpa) and 6-(acetylthio)hexanoate (6-atha) ligands. Such features, together with their relative stability, make them suitable SMMs to be studied on devices in the field of molecular spintronics. Given that, a future perspective of this line of work is to investigate the obtained [Mn$_6$] systems as molecular connectors in junction devices. Furthermore, aiming in the same direction, another perspective work is to functionalise [Mn$_6$] molecules with other thioester-type ligands, that is, molecules presenting longer aliphatic chains and other functional sulphur-based groups which are key for connecting the complexes to the junction devices.

The second part of the present PhD Thesis, dedicated to the study on Re(IV)- based complexes, summarizes a huge contribution to the knowledge and the understanding of such systems.

Hence, the crystal structures and magnetic properties of four novel hexahalogen Re(IV) salts, based on cations of different nature, have been reported in two publications. In the former, the two of the compounds exposed, which are those based on 9H-adenine-1,7-diium, present the organic cations and the inorganic anions self-assemble into novel supramolecular structures through a combination of hydrogen and halogen bonds. The latter are responsible for propagating relatively strong intermolecular antiferromagnetic exchange interactions between the Re(IV) ions through short Re–X···X–Re contacts. Given that the two of the compounds are isostructural, exhibiting the same value of the

Conclusions and Perspectives

shortest X···X distance, we can directly observe the effect of changing the halide ligand on the magnetic exchange. As evidenced by our results, the larger diffuse character of the 4p orbitals of the bromide ligands when compared to the 3p orbitals of chloride ligands would account for the enhancement of the magnetic exchange observed in the bromide based analogous.

In addition, the two reported Fe(II)–Re(IV) compounds display a behaviour typical of isolated paramagnetic centers with high values of zero-field splitting of the involved metal ions. The large separation that exists among $[Fe(dmf)_6]^{2+}$ cations and $[ReX_6]^{2-}$ anions in the solid accounts for the lack of any significant through-space magnetic coupling between the Fe(II) and Re(IV) ions. Remarkably, these are the first examples of paramagnetic salts based on the $[Fe(dmf)_6]^{2+}$ cation that have been magnetostructurally characterized.

A future perspective work should be focused on completing this research on the Re(IV) hexahalogen-mononuclear species. Herein, we present the perspective of studding the magnetic properties of structurally isolated $[ReX_6]^{2-}$ anions (X = Cl, Br, I) for what bulky cautions, such as tetrabutylammonium and tetraphenylphosphonium, would be employed.

In the attempt of exploring new strategies of synthesis to perform ligand substitutions on Re(IV)-based mononuclear species, two novel mononuclear complexes have been synthesized and magnetostructurally characterized. They were prepared from the well-known cis-$[ReCl_4(MeCN)_2]$ precursor, by means of ligand substitution reactions upon heating in the employed solvent. Remarkably, the complex of formula cis-$[ReCl_4(dma)_2]$ is the first example of crystal structure containing N,N-dimethylacetamide (dma) molecules coordinate to a paramagnetic 5d metal ion.

Finally, the crystal structure and magnetic properties of two heteropolynuclear complexes of formula $(NBu_4)_4[Zn\{ReCl_4(\mu-ox)\}_3]$ and $\{[ReBr_4(\mu-ox)Cu(pyim)_2]\cdot MeCN\}_n$ [NBu_4^+ = tetra-n-butylammonium cation, ox = oxalate anion and pyim = 2-(2'-pyridyl)imidazole] have been reported. The former is an unusual Zn(II)–Re(IV) system and the first example of an oxalato-bridged Zn(II) complex coordinated to a 5d metal ion that exhibits slow relaxation of magnetisation, and, in addition, given the diamagnetic nature of the Zn(II) ion, this compound has enabled us to obtain for the first time the J value of the magnetic interaction between Re(IV) ions linked through oxalate ligands. The latter complex is a novel Cu(II)-Re(IV) monodimensional compound which has revealed a magnetic behaviour typical of ferrimagnetic chain, which is consistent with its crystal structure. This is the first reported Cu(II)-Re(IV) complex obtained with the $[ReBr_4(ox)]^{2-}$ metalloligand that exhibits such a magnetic behaviour.